A thesis entitled

THEORY, MANUFACTURE AND PERFORMANCE OF HOLOGRAPHIC X-RAY GRATINGS

by

ROBERT LAWRENCE JOHNSON

submitted for the degree of

Doctor of Philosophy

in the University of London

Department of Physics

Imperial College of Science and Technology

London SW7 2BZ

DECEMBER 1975

ABSTRACT

The aim of the work described in this thesis is to improve the performance of grazing incidence grating spectrometers and spectrographs used in the soft x-ray wavelength region 5 Å to 150 Å.

In recent years a considerable amount of interest has developed in the application of soft x-rays in such diverse fields as high temperature plasma diagnostics, x-ray astronomy, valence band analysis, light element analysis, long wavelength x-ray diffraction and x-ray microscopy.

During the course of the present work, diffraction gratings, suitable for use in the soft x-ray region, have been examined in collaboration with several grating manufacturers. The results of some of these examinations will be described; however, the most significant advance in the past three years has been the development of highly efficient holographically-formed diffraction gratings for use in the soft x-ray region.

The holographic method opens up new design possibilities for spectrographs and some of these are investigated theoretically in this work. The processes used in the manufacture of holographic gratings are described. Finally, the performance of the present generation of holographic gratings is discussed.

CONTENTS

PREFACE

This thesis describes some of the more important work performed by the author while supported by an S.R.C. CAPS research studentship in conjunction with I.C. Optical Systems Ltd. in the period 1972 - 1975.

The research programme is concerned with diffraction gratings for use at grazing incidence in the soft x-ray region and continues the work performed in this laboratory by Dr. J.M. Bennett (1967-71). The research has involved successful collaboration with grating producers in America, France, Germany and U.K. Grating calibrations have also been performed for users in other parts of the world. Since the importance of the soft x-ray region of the spectrum has only recently been realised, it is to be expected that the international collaboration and importance of the grating test facility at Imperial College will increase in the future.

Although the subject of the research programme has been "soft x-ray diffraction gratings", the work has involved a large number of disciplines including optics, solid state physics, electronics, computer science, and some mechanical engineering.

I am very grateful to the experts at Imperial College who have advised me in these fields and in particular my supervisor, Dr. R.J. Speer. The financial support of the S.R.C. is gratefully acknowledged.

Most of the units have been expressed in S.I. form except for vacuum pressure (expressed throughout in torr $\equiv 1.33 Nm^{-2}$) and wavelengths (expressed in Angstrom $\equiv 0.1nm$).

In the soft x-ray region it is convenient to specify the grazing angle of incidence measured between the incident ray and the surface rather than the usual angle of incidence measured between the incident ray and the normal. In this work the grazing angle of incidence has been denoted by, α, and the grazing angle of diffraction by, β.

It should be noted that the term "classical grating" as used in this thesis means any grating whose rulings would be equispaced straight lines when projected onto the tangent plane at the pole of the grating. Such gratings are produced by a conventional ruling engine and may also be formed by recording the interference fringes from two plane waves.

Gratings produced by recording the interference fringes formed with light from a laser in a photosensitive medium have been termed both "interference" (or more formally "interferographic") and "holographic" gratings. The concept of gratings formed using laser light as holograms is more general than considering them as interferograms. The term "holographic grating" avoids any possible confusion with the wavefront interferograms produced when optically testing gratings and also avoids confusion with the interferometric control system used on modern ruling engines. The term "holographic grating" has been used throughout this work since it is unambiguous and also because concepts from holography allow the properties of focussing gratings to be more easily understood.

CHAPTER 1

INTRODUCTION

1.1 HISTORICAL REVIEW OF THE DEVELOPMENT OF HOLOGRAPHIC GRATINGS

The history of the ruled grating has been extensively reviewed in the literature and a most comprehensive description has been given by Stroke (1). The history of the holographic grating is much less well known, even though it is shorter than that of the ruled grating.

The concept of the holographic grating can be traced back one hundred years to Cornu (68) who realised the relationship between interference fringes and the rulings of a grating. Cornu showed that gratings with a systematically varying spacing would have focussing properties and he demonstrated these focussing properties experimentally with two photographs of interference fringes. This important work is considered in greater detail in Chapter 2, section 3.

Lord Rayleigh considered photographic reduction as a method for producing gratings but concluded it was impossible for practical reasons, however, he showed that it was possible to photograph gratings ruled on glass by contact printing (134). In 1927 Michelson (2) suggested that it would be possible to make a grating by photographing standing wave interference fringes. However, it was not until 1958 that Burch (3) at NPL succeeded in making gratings for measuring purposes photographically by this method using Kodak Maximum Resolution emulsion and light from a high intensity Hg lamp. These gratings had little spectroscopic value because of the granularity of the emulsion and its instability; however, they made gratings of considerable size and with frequencies up to 2240mm^{-1}. Also in 1958

Ritschl and Polze (4) reported photographing interference fringes to produce a grating. In 1962 Denisyuk (5) reported the possibility of using Lippman emulsions for recording diffraction gratings. Labeyrie (6) suggested various methods for recording the interference fringes produced by two coherent laser light beams; however, they required the use of photosensitive materials which were not sufficiently stable for the production of high-quality gratings.

In 1967 Rudolph and Schmahl (7) in Germany demonstrated that gratings could be made holographically by recording two beam interference fringes from an argon ion laser in a photoresist layer coated on an optical flat. They also showed that gratings produced by this method had sufficient dimensional stability and diffraction efficiency to make them useful for spectroscopic purposes. Also in 1967 the prototype commercial holographic gratings were produced at the firm of Jobin-Yvon in France (8).

In America, Shankoff of Bell Laboratories received a patent (9) on the production of relief gratings to obtain blaze qualities, and a patent on the technique of imparting focussing properties to a flat holographic grating is held by Brooks and Haflinger of TRW Inc. (10).

In 1968 Sheridon (11) described a method for producing "blazed" holographic gratings and in 1969 Rudolph and Schmahl (12) published a full description of the processes they used and also how they produced gratings in metallic form with no photoresist present in the final grating. In 1969 Rudolph and Schmahl also spelled out the special advantages of the holographic method:

1) size only limited by the optics used to produce the light beams

2) completely ghost-free spectra with very low stray light

3) the possibility of introducing focussing properties when constructing the grating.

Since 1970 several groups have been working in this field and the performance of holographic gratings in the visible to UV region has been investigated by several authors (13 - 20). The major commercial supplier of holographic gratings is Jobin-Yvon so that most of the reports published discuss the properties of their gratings. However, it was clear that although holographic gratings would not entirely replace classically ruled gratings, they immediately earned a place in spectroscopic instrumentation and were generally considered to be complementary to classically ruled gratings in the visible and UV regions.

Because the efficiency of classical ruled gratings was very low in the soft x-ray region (typically $\sim$1-2%), the potential gains in efficiency which could be achieved by using the holographic method to make soft x-ray gratings were much higher than any possible improvements which could be obtained in the visible region where ruled gratings had already nearly attained the maximum theoretical efficiency. Furthermore, the holographic technique offered the possibility of correcting the aberrations which limited the performance of classical grazing incidence systems. If efficient holographic gratings for use at soft x-ray wavelengths could be produced, a new era in grazing incidence instrument design would begin.

1.2 THE FIRST EFFICIENCY MEASUREMENTS OF HOLOGRAPHIC GRATINGS IN THE SOFT X-RAY REGION

Our early measurements on the efficiency of holographic gratings in 1972 showed that they had a useable efficiency in the soft x-ray region, see Fig. 1 and 2. The efficiency of the 1200 1/mm holographic grating produced by Jobin-Yvon compares very favourably with a typical Bausch and Lomb 1200 1/mm shallow blazed grating when it is considered that the holographic grating is only a first prototype. A comparison of the spectra shows the stray light to be lower for the holographic grating.

The N.P.L. holographic gratings and Jobin-Yvon gratings shown in Fig. 1 are both resist gratings coated with respectively aluminium and gold, and both have a sinusoidal profile. Since photoresist is an easily degradable organic material, it seemed that the method developed by Rudolph and Schmahl for producing gratings with an all-metallic structure would be preferable for use in the soft x-ray region. The efficiency of the first grating made for us at Göttingen is shown in Fig. 2. Although the absolute efficiency is no better than that of the other early holographic grating types, it is an important result since the zero order curve shows evidence of phase cancellation, i.e. the grating is behaving like a phase grating. Since the manufacturing process used at Göttingen was intended to produce a laminar profile on the grating surface, this result was to be expected.

However, this was the first holographic grating which we had examined with other than a sinusoidal profile. It is to be noted that we had asked for the grating to be made with a groove depth of 160 Å and

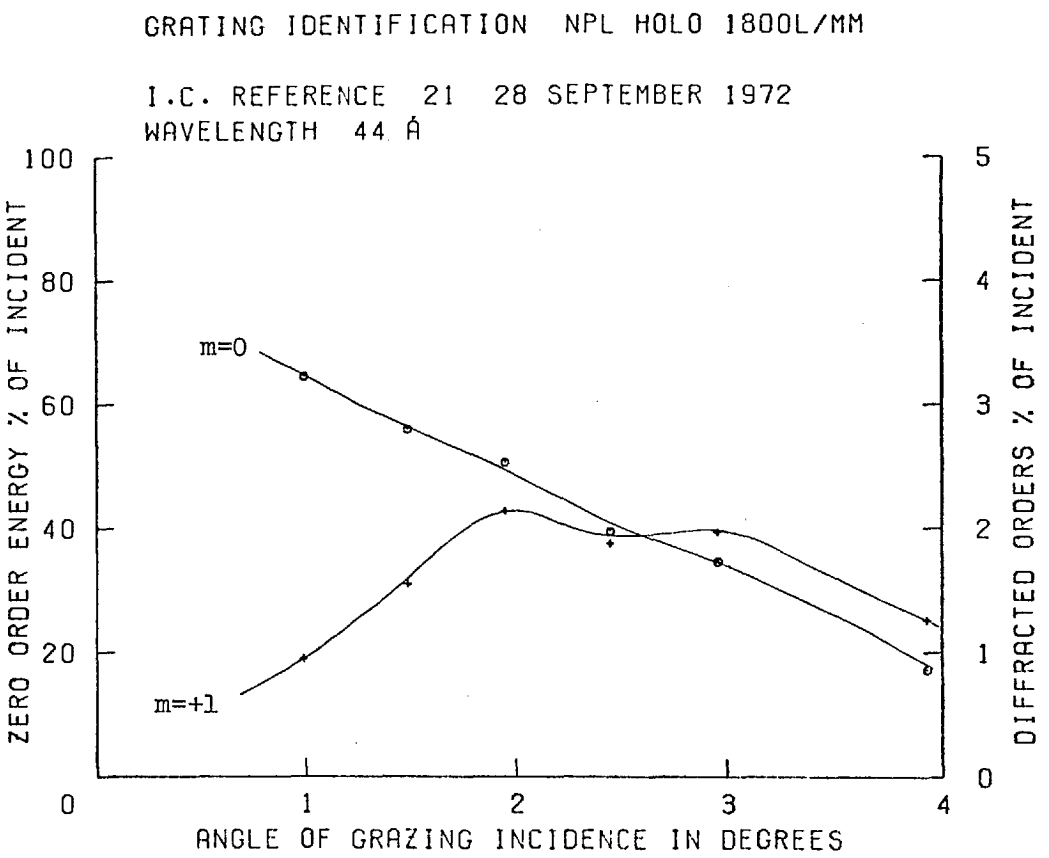
GRATING IDENTIFICATION NPL HOLO 1800L/MM
I.C. REFERENCE 21 28 SEPTEMBER 1972
WAVELENGTH 44 Å
ZERO ORDER ENERGY % OF INCIDENT
DIFFRACTED ORDERS % OF INCIDENT
m=0
m=+1
ANGLE OF GRAZING INCIDENCE IN DEGREES

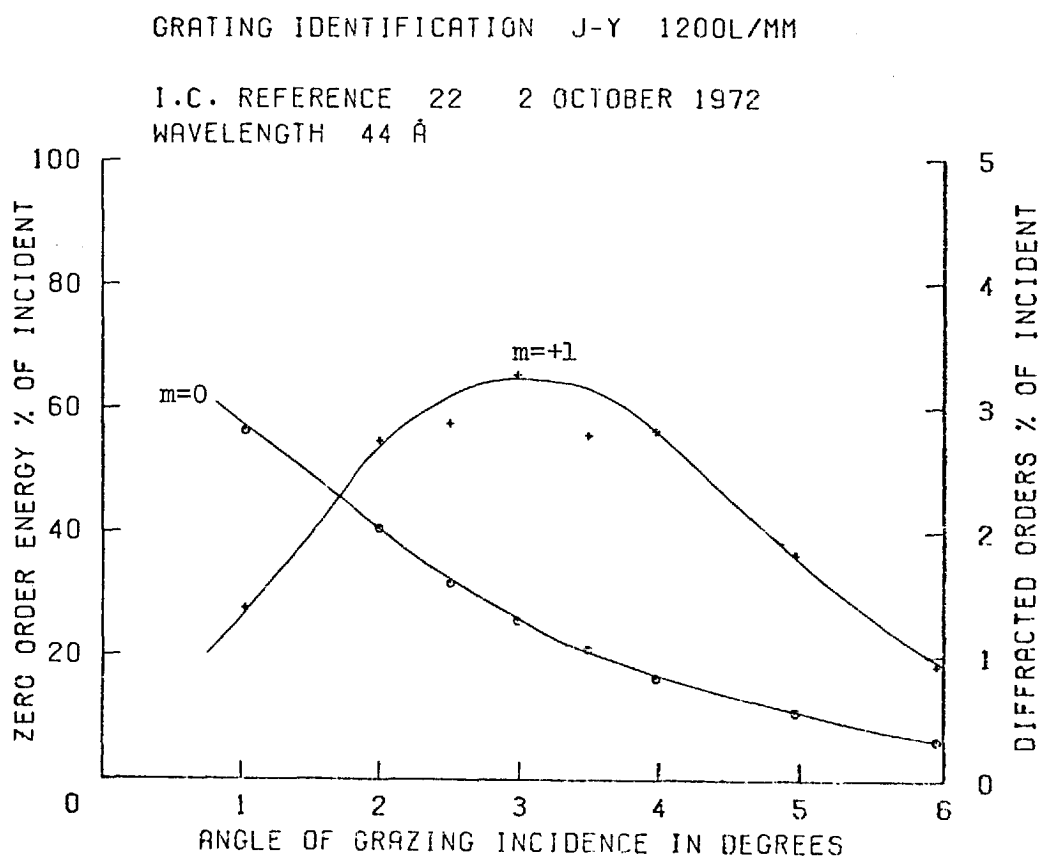
GRATING IDENTIFICATION J-Y 1200L/MM
I.C. REFERENCE 22 2 OCTOBER 1972
WAVELENGTH 44 Å
ZERO ORDER ENERGY % OF INCIDENT
DIFFRACTED ORDERS % OF INCIDENT
m=+1
m=0
ANGLE OF GRAZING INCIDENCE IN DEGREES

FIG. 1

EFFICIENCY AT 44 ANGSTROMS vs GRAZING ANGLE.

GÖTTINGEN HOLOGRAPHIC GRATING.

600 l/mm, PLANE, DEPTH 150-200 Å, GOLD COATED 100 Å.

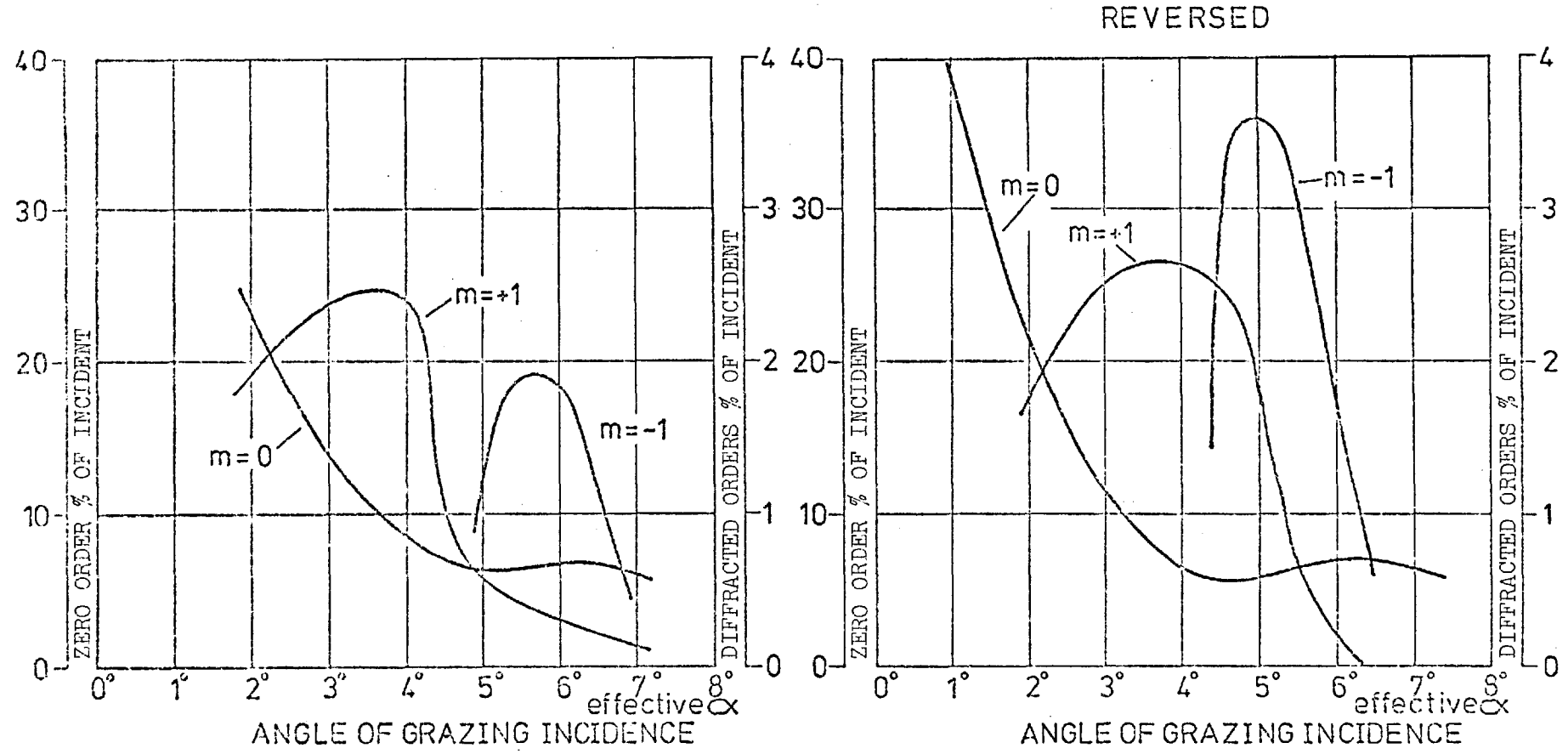

FIG. 2

the position of the diffraction maxima showed that the groove depth was in fact 160 Å. Since the Göttingen group was also particularly interested in the development of soft x-ray gratings and had already done a lot of work on zone plates for soft x-ray use (21), a joint collaborative research program was set up to develop the holographic grating for use in the soft x-ray region.

The results of the collaboration with the Grating Laboratory of the University of Göttingen and my work there form the basis of this thesis. The Group at National Physical Laboratory under Dr. A. Franks has also done some very important work recently on holographic or interference gratings for x-ray use and this work will also be reviewed.

CHAPTER 2

THE THEORY OF THE HOLOGRAPHIC X-RAY GRATING

2.1 THE THEORY OF THE CONCAVE GRATING

From Rowland's time to the present day, the theory of the concave grating has been treated extensively in the literature (52, 53, 54, 55, 60, 62) and particularly notable are the papers by Beutler (56) and Namioka (57, 58). In order to introduce the notation and make the foundations for later discussions, the theory of the concave grating will be briefly reviewed.

It is conventional to use a Cartesian coordinate system when describing the theory of the diffraction grating. The origin of the coordinate system, O, is taken as the centre of the grating and we will take the x-axis parallel to the rulings and the z-axis as the normal to the surface at O. The grating surface is defined by its equation in Cartesian coordinates or may, in general, be described by a series expansion. The groove shape is ignored in the treatment of the aberrations of the grating but it is of course extremely important in calculations of the intensity distribution in the spectrum.

An incident ray from point A (x_A, y_A, z_A) to point P (x,y,z) on the grating surface is diffracted towards point B (x_B, y_B, z_B). The optical path length is the sum of the two straight lines AP and PB. By expanding the optical path length as a power series in terms of the grating pupil coordinates and applying Fermat's principle, the spectral image formation and aberrations of the concave grating can be examined.

For a classical ruled grating the rulings are the intersections

with the grating surface of planes spaced equally a distance d apart parallel to the yz-plane. In order that rays from different grooves reinforce one another, the optical path length for the two rays can only differ by an integral number of wavelengths. Therefore, following Beutler (56) and Namioka (57), the characteristic light path function, F, can be defined:

$$F = \langle AP \rangle + \langle BP \rangle + (y/d)\, m\lambda$$

According to Fermat's principle, point B is located so that the light path function will have a stationary value for any point, P, on the grating surface. For focussing of light from points along x on the grating surface the partial derivative of F with respect to x must be zero.

$$\partial F/\partial x = 0$$

Similarly for perfect focussing of light from points on the grating surface along y:

$$\partial F/\partial y = 0$$

For a spherical grating $\partial F/\partial x$ and $\partial F/\partial y$ are functions of x and y and cannot be made zero for all points, P. The partial derivatives of the light path function have the significance of the difference in the direction cosines between the diffracted ray and the line from P to B. Thus the partial derivatives can be directly related to the aberrations observed.

The light path function, F, can in general be written as a power series and each of the terms in the series can be associated

with a particular form of aberration. Since there is normally only a plane of symmetry in spectrographs instead of the axial symmetry encountered in lens design, the characteristic function is more complex than that of centred systems. The most comprehensive description of the terms of the light path function for a concave grating has been given by Werner (75). The treatment by Beutler and Namioka was restricted to the Rowland circle and the vicinity of the meridian plane because of certain approximations. By using a transformed pupil coordinate system Werner was able to define a general focussing condition in his more complete formulation of the concave grating theory. Recently, Danielsson and Lindblom (55) have extended Namioka's treatment of the light path function so that it is valid for all values of x and valid to the fourth order in y and z.

The complete expression for the terms of the light path function will not be reproduced here. Instead we will present only the first few terms.

Using cylindrical coordinates for the object and image points (see Fig. 3)

$$F = \langle AP \rangle + \langle PB \rangle + y \frac{m\lambda}{d}$$

$$= r\left[1 + \frac{x_A^2}{r^2}\right]^{\frac{1}{2}} + r'\left[1 + \frac{x_B^2}{r'^2}\right]^{\frac{1}{2}}$$

$$+ y\left[\frac{m\lambda}{d} - \left[1 + \frac{z_A^2}{r^2}\right]^{-\frac{1}{2}} \sin\alpha - \left[1 + \frac{x_B^2}{r'^2}\right]^{-\frac{1}{2}} \sin\beta\right]$$

THE GRATING COORDINATE SYSTEM

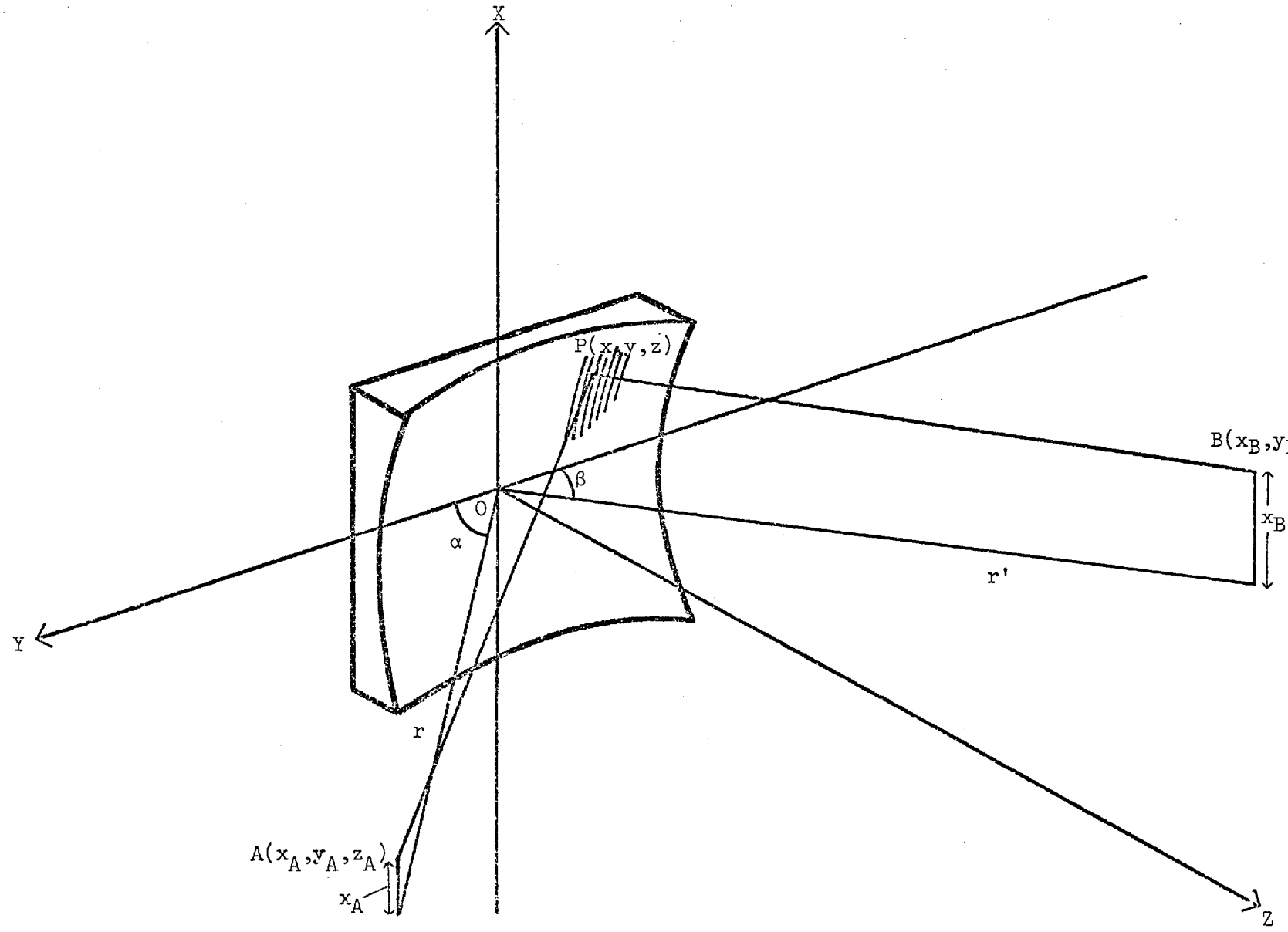

FIG. 3

$$- x\left[\frac{x_A}{r}\left(1+\frac{x_A}{r^2}\right)^{-\frac{1}{2}} + \frac{x_B}{r'}\left(1+\frac{x_B}{r'^2}\right)^{-\frac{1}{2}}\right] +$$

$$\frac{1}{2}y^2\left[\left(1+\frac{x_A^2}{r^2}\right)^{-\frac{3}{2}}\left(\frac{\cos^2\alpha}{r} - \frac{\cos\alpha}{R} + \frac{x_A^2}{r^2}\left(\frac{1}{r} - \frac{\cos\alpha}{R}\right)\right)\right.$$

$$\left. + \left(1+\frac{x_B^2}{r^2}\right)^{-\frac{3}{2}}\left(\frac{\cos^2\beta}{r'} - \frac{\cos\beta}{R} + \frac{x_B^2}{r'^2}\left(\frac{1}{r'} - \frac{\cos\beta}{R}\right)\right)\right]$$

$$+ \frac{1}{2}x^2\left(\frac{1}{r} - \frac{\cos\alpha}{R}\left(1+\frac{x_A^2}{r^2}\right)\right)\left(1+\frac{x_A^2}{r^2}\right)^{-\frac{3}{2}}$$

$$+ \left(1+\frac{x_B^2}{r'^2}\right)^{-\frac{3}{2}}\left(\frac{1}{r'} - \frac{\cos\beta}{R}\left(1+\frac{x_B^2}{r'^2}\right)\right)$$

$$- xy\left(1+\frac{x_A^2}{r^2}\right)^{-\frac{3}{2}}\frac{x_A\sin\alpha}{r^2} + \left(1+\frac{x_B^2}{r'^2}\right)^{-\frac{3}{2}}\frac{x_B\sin\beta}{r'^2}$$

$$+ \ldots\ldots$$

In general the light path function F can be written as:

$$F = F_{000} + xF_{100} + yF_{010} + \frac{1}{2}x^2F_{200} + xyF_{110} + \frac{1}{2}y^2F_{020} + \ldots$$

where the subscripts correspond to the indices in x, y and z.

Although the series expansions given by Beutler, Namioka and Werner are somewhat cumbersome, it is convenient to examine them term by term. Since the expressions contain successively higher inverse powers of R, r, and r', which are normally large compared to the grating dimensions, the terms rapidly decrease in magnitude. Each term of the series expansion also has a physical significance in that each can be associated with image formation or a particular form of aberration.

Application of Fermat's principle to the first-order terms of the expansion gives the well known grating equations. The second-order terms yield the general image equation of a diffraction grating which provides the Rowland Circle and Wadsworth mounting as solutions. The higher order terms can be associated respectively with astigmatism, coma, spectrum line curvature and spherical aberration.

In the soft x-ray region it is usual to use spherical gratings in the grazing incidence Rowland circle mounting. In this mounting the terms, F_{020}, F_{030} and F_{040} of the light path function become identically zero and spherical aberration remains with some higher order terms to limit resolution in the meridian plane.

For the Rowland circle mounting the spherical aberration term is given by:

$$\frac{y^4}{8R^3}\left(\frac{\cos^2\alpha}{\sin\alpha}+\frac{\cos^2\beta}{\sin\beta}\right)$$

Hence, as the width of the grating is increased the spherical aberration rapidly becomes larger. Thus there exists an optimum

grating width for the attainment of maximum resolution which was derived by Mack, Stehn and Edlén (59) from a physical optics approach and is given by:

$$W_{opt} = 2.36 \left\{ \frac{4\lambda R^3}{\pi(\cot\alpha \cos\alpha + \cot\beta \cos\beta)} \right\}^{\frac{1}{4}}$$

As pointed out by MacAdam (76) this result is only a factor of 1.06 greater than that obtained by applying Rayleigh's criterion and it may be questioned whether the introduction of the generalised criterion of resolution is of any real significance in this case. However, the calculations of Mack, Stehn and Edlén show that the simple criterion can be safely applied in practice.

Fig. 4 shows a series of curves produced by the above equation for wavelengths up to 100 Å at various angles of incidence onto a 600 l/mm grating. The three scales on the vertical axis correspond to 1m, 2m, and 5 m radii of curvature.

The maximum resolving power for a grating illuminated with a point source was given by Mack, Stehn and Edlén to be:

$$\text{Optimum Resolution} = 0.92\ W_{opt}\ m/d$$

for a grating of optimum width and for a grating much wider than the optimum width

$$\text{Resolution} = 0.75\ W_{opt}\ m/d.$$

However, it must be remembered that normally the resolution of spectrographs used in the grazing incidence region is limited by the

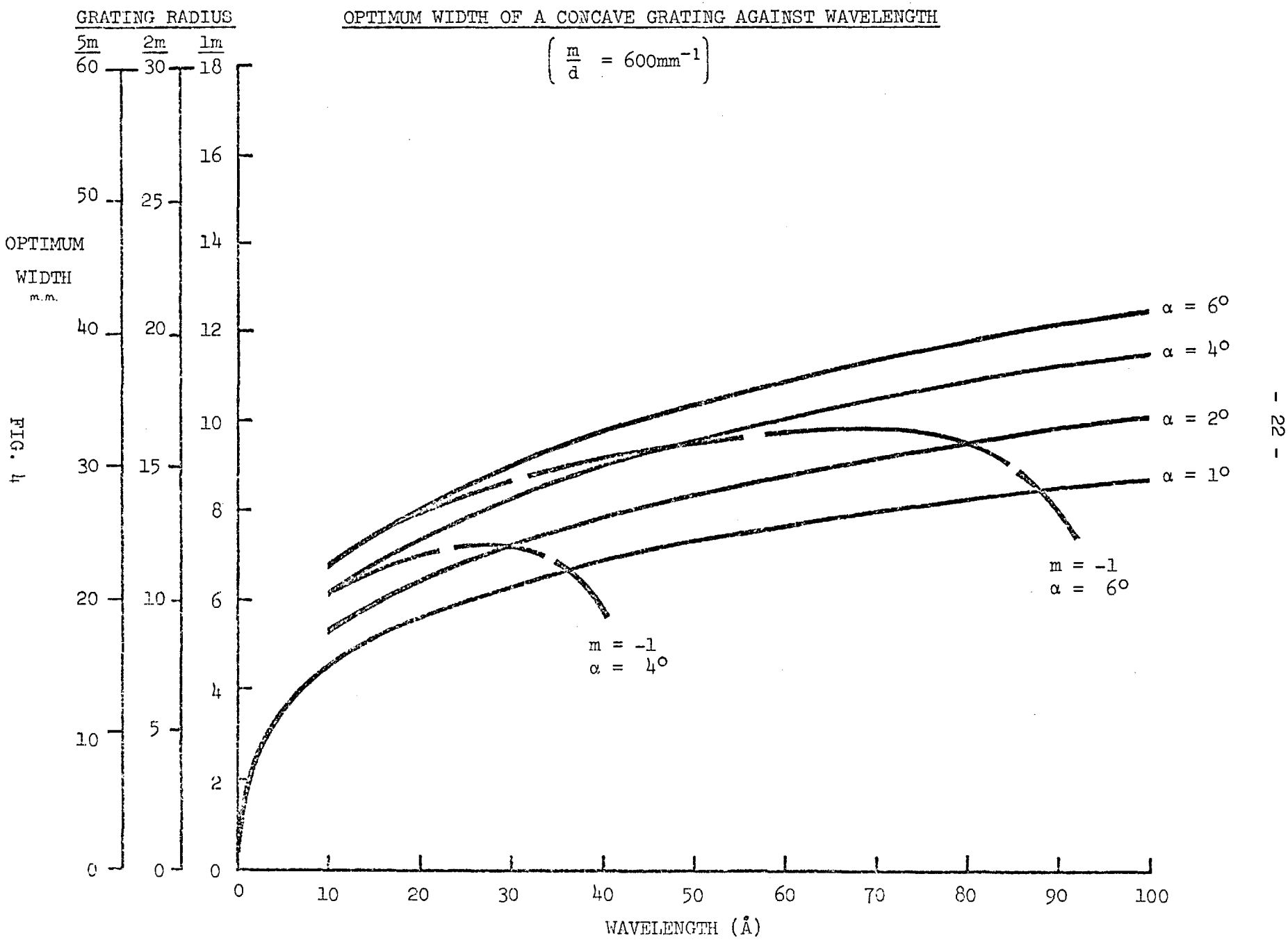
GRATING RADIUS
5m
2m
1m
OPTIMUM WIDTH OF A CONCAVE GRATING AGAINST WAVELENGTH
$\left(\frac{m}{d} = 600mm^{-1}\right)$
OPTIMUM WIDTH m.m.
60
50
40
30
20
10
0
30
25
20
15
10
5
0
18
16
14
12
10
8
6
4
2
0
α = 6°
α = 4°
α = 2°
α = 1°
m = -1
α = 6°
m = -1
α = 4°
0
10
20
30
40
50
60
70
80
90
100
WAVELENGTH (Å)

FIG. 4

width of the entrance slit. The maximum resolution for a spectrograph with entrance slit width s limited by the slit width is given by:

$$R_{slit} = 0.91\ R\lambda m/sd$$

Thus, it is only when the slit resolution is greater than the resolving power of the grating that the theory of the grating developed for an infinitesimal slit can be strictly applied. For a grating of optimum width the resolution will be determined by the slit width provided

$$s > R\lambda/W_{opt}$$

For a 5m grating at an angle of 5^{o} with a width of 40mm at 100 Å, the resolution will be slit width limited for entrance slit widths of 1.25μm or greater. Since the production of slits narrower than 1μm is difficult and the use of such slits in practical soft x-ray spectroscopy often nearly impossible, it is not surprising that most grazing incidence spectrographs are slit width limited. For this example the projected width of the entrance slit on the plate is given by s/sinβ which is equal to 8.9μm. Since the best photographic emulsions for use in the soft x-ray region have a resolution of 10μm quoted by the manufacturers even if slits as narrow as 1μm can be employed, the resolution may be limited by the photographic plate rather than by the grating. Provided a grating of optimum width is employed in a correctly adjusted spectrograph with an entrance slit width of one micron resolution of the order of 20,000 should be attainable at 100 Å on the basis of the theory proposed by Mack, Stehn and Edlén. However, in practice it is rare for the resolution to exceed 5,000.

At shorter wavelengths when smaller angles of incidence also have to be used to ensure sufficient reflectivity the optimum width decreases rapidly. For example for a 600 l/mm 5m grating used at a grazing angle of 1° the optimum width for 10 Å radiation is only 15.5mm. Thus, the resolution and luminosity of the grating have both decreased. For this example the resolution will be slit width limited for all practical cases and for a 1μm slit the resolution will be 2730.

Since the optimum width is determined by the spherical aberration the optimum width can be increased if the spherical aberration is reduced. In determining the optimum width Mack, Stehn and Edlén (59) effectively applied the aberration tolerance that the spherical aberration should not exceed 0.309λ. This tolerance is only slightly greater than Rayleigh's quarter wavelength rule. Rayleigh (77) showed that for a system with primary spherical aberration provided the wavefront in the exit pupil departs from the Gaussian reference sphere by less than $\lambda/4$, the intensity at the Gaussian focus is diminished by less than 20%. However, it is well known (Born and Wolf 78) that in the presence of a small amount of primary spherical aberration the diffraction focus is situated midway between the paraxial and marginal foci. Under this condition the required tolerance for primary spherical aberration is that the maximum deviation of the wavefront from the Gaussian reference sphere must be less than 0.94λ.

Substituting this value in the aberration integral yields an increase in the optimum width.

$$W'_{opt} = 3.312 \left(\frac{\lambda R^3}{\cos\alpha \cot\alpha + \cos\beta \cot\beta} \right)^{\frac{1}{4}}$$

instead of

$$W_{opt} = 2.5069 \left(\frac{\lambda R^3}{\cos\alpha \cot\alpha + \cos\beta \cot\beta} \right)^{\frac{1}{4}}$$

Bowen (65) first established that an increase in grating width and resolution was possible by allowing either or both the slit or plate to be slightly displaced from the Rowland Circle. In general by allowing displacements of the entrance slit and plate terms in y^2 and y^3 are introduced into the aberration polynomical which were zero for the Rowland circle case. By setting the y^3 term to zero and for a grating extending from $y = -Y$ to $+Y$ setting the coefficient of y^2 to $-Y^2$ times the coefficient of the y^4 term, the maximum value of the aberration is reduced to a quarter of its value without the offset from the Rowland circle. Hence, Bowen determined that it was possible to keep the aberration below a certain value over a range of $y\sqrt{2}$ times as great as without the offset. Bowen gave the optimum grating width to be

$$W_{opt\ (Bowen)} = 3.55 \left(\frac{\lambda R^3}{\cos\alpha \cot\alpha + \cos\beta \cot\beta} \right)^{\frac{1}{4}}$$

Bowen also applied geometrical optics to determine the distances of the ray intersections from the Rowland circle. He discovered that the displacement of the entrance slit introduced a dissymmetry in the image. However, he pointed out that this dissymmetry could materially decrease the width of the image on the plate when the angle between the extreme rays is comparable to the angle between the incident principal ray and the plane of the plate.

From geometrical optics (79) it is known that in the presence of primary spherical aberration the position of sharpest focus, or circle of least confusion, is located at three quarters the distance from the Gaussian to marginal focus. At this position the image has one quarter the width it would have at the Gaussian focus. Thus for an entrance slit on the Rowland circle the best image is formed at a distance $\Delta r'$ beyond the Rowland circle given by:

$$\Delta r' = \frac{3}{4}\left(\frac{\cos\alpha\,\cot\alpha + \cos\beta\,\cot\beta}{8R}\right) W^2$$

where W is the grating width.

By differentiation of the focus term, F_{020}, for small departures of the entrance slit from the Rowland circle, Δr:

$$(\sin^2\alpha/r^2)\Delta r + (\sin^2\beta/r'^2)\Delta r' = 0$$

Hence, in the vicinity of the Rowland circle $\Delta r = -\Delta r'$. Thus either the entrance slit or the plate may be moved outside the Rowland circle to improve focussing or the grating radius may be altered.

The limitation of plate resolution and its effect on the optimum grating width was also considered by Bowen. He gave the width of the lines on the photographic plate to be

$$c = \frac{(\cos\alpha\,\cot\alpha + \cos\beta\,\cot\beta)}{4R^2\sin\beta}\, y^3$$

Thus, if c is the resolution of the plate then the optimum grating width is given by

$$W_{opt\ (Plate)} = \left\{ \frac{32cR^2 \sin\beta}{\cos\alpha \cot\alpha + \cos\beta \cot\beta} \right\}^{\frac{1}{3}}$$

Fig. 5 shows a series of curves drawn from the above equation for various angles of incidence for a plate resolution of 10μm. For practical cases it can be seen that there is little difference between the optimum width as calculated by Mack, Stehn and Edlén and the optimum width derived from the limitation of plate resolution.

Kozlenkov (64) used geometrical optics to establish the form of the aberrations in a spectrograph in the presence of adjustment errors. The errors considered were displacements of the entrance slit towards the centre of the grating and displacement of the detector along the diffracted chief ray. Kozlenkov essentially generalised and expanded Bowen's earlier treatment dealing more comprehensively with displacements of the entrance slit off the Rowland circle. He showed that the gain in resolution by displacing the entrance slit off the Rowland circle was practically the same as the gain in resolution by displacing the detector. Kozlenkov also showed that corresponding to the maximum optimum width there is a maximum permissible offset given by

$$\Delta r' = \left\{ \frac{\lambda R}{2} (\cos\alpha \cot\alpha + \cos\beta \cot\beta) \right\}^{\frac{1}{2}}$$

The maximum optimum width is $\sqrt{2}$ times the optimum width on the Rowland circle. If the offset is increased beyond this value the

PLATE LIMITED OPTIMUM WIDTH OF A CONCAVE GRATING AGAINST WAVELENGTH FOR A PLATE RESOLUTION OF 10μm

$(m/d = 600mm^{-1})$

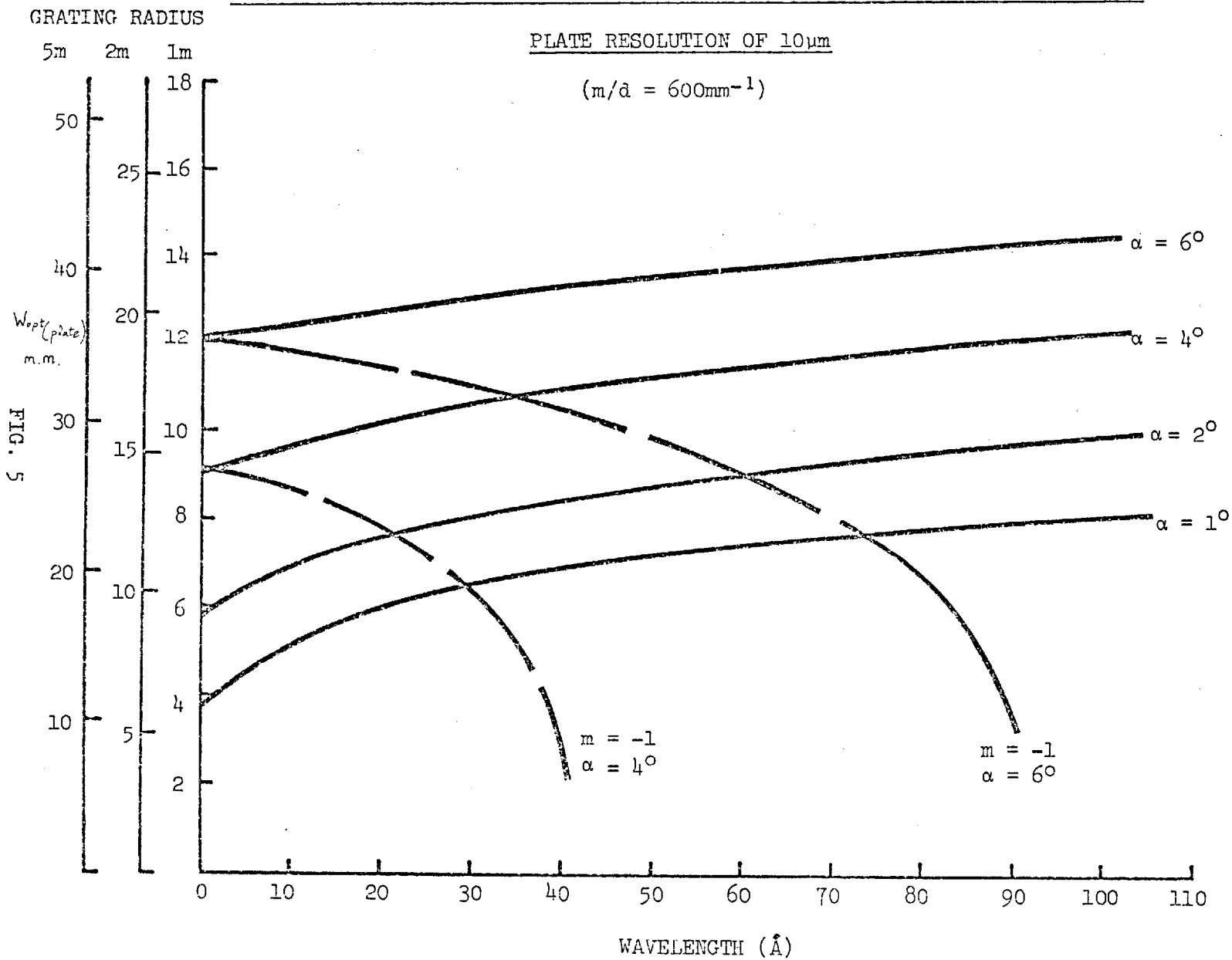

FIG. 5

integral over the wavefront becomes greater than $\lambda/4$ and the resolution will decrease.

In practice the situation is somewhat more complex than considered above because the finite size of the entrance slit must be considered as well as the grating aperture. If the disturbances are nearly in phase the best focus will be half way between the paraxial and marginal foci. However, if phase differences exceeding 2π are involved and the aberrations are large the energy will tend to travel along the ray paths causing the best focus to move to three quarters the way from the paraxial to marginal foci.

Recently Fellner-Feldegg (80) has extended the theory of Mack, Stehn and Edlén using Cornu's method in a numerical approach to obtain quantitative information about the influence on line shape, resolution, and intensity of ghosts for slight departures from the Rowland circle condition. In agreement with Bowen it was found that there is an optimum signal to noise ratio if either the detector is displaced outside the Rowland circle or a grating of slightly smaller radius than the instrument circle diameter is used. Significant gains in peak intensity and resolution were found typically of the order of 25 to 50% and an even greater increase in signal to noise ratio - typically a factor of two - was found for gratings having the optimum width. For gratings larger than optimum there is an increase in intensity but the signal to noise ratio remains practically unaltered and the intensity and signal to noise ratio become more dependent on r making adjustment more critical. All the above results were obtained by only considering effects in the plane of the Rowland circle assuming a coherent point source. If finite slit widths are considered the computations become

much more complex because the phase distribution at each point on the grating must be calculated for each point on the entrance slit.

It is interesting to note that the optimum radius for a 5m grating in a spectrograph in which the entrance slit and detector are accurately set on the Rowland circle is typically 1mm less than 5m in order to obtain optimum signal to noise ratio. Since spherical blanks are usually worked for a tolerance at best of $\lambda/20$ it can be easily calculated that for a typical grating blank of 50mm width the radius can be in error by up to 2mm. Thus it is essential that some adjustment is provided on a spectrograph to compensate for this uncertain source of error.

It is clear that optimum focussing will only be obtained if either or both the entrance slit and plate are adjusted to lie slightly outside the Rowland circle. Since the adjustments are small - typically less than a millimeter - the usual method of setting up a spectrograph is to adjust photographically until the optimum focus is found. With a new high resolution spectrograph used in this work the facility for displacing the entrance slit from the Rowland circle in a controlled way is incorporated. Experiments have been performed in an attempt to determine the optimum offset correction, however, the spectral lines of the source used were too broad to allow any precise determination to be carried out. Further details of this work are described in Chapter 7 (Practical X-Ray Spectroscopy).

The astigmatism of the grazing incidence mounting is determined by the terms F_{200} and F_{400} in the light path function. As shown by Kayser (54), and others (56, 60) for a concave grating in a Rowland circle mounting the length of the astigmatic focal line divided by the length of the rulings illuminated by a point source in the meridian plane is given by:

$$\sin\beta \left(\frac{\cos^2\alpha}{\sin\alpha} + \frac{\cos^2\beta}{\sin\beta} \right)$$

For a typical 1cm length of rulings of a 600 l/mm grating illuminated with 100 Å radiation at a grazing angle of 4° the length of the astigmatic focal lines will be 2.83cm. For a cylindrical grating the corresponding length of the focal lines would be 2.86cm. Thus, it can be seen that the vertical focussing effect of the concave grating is negligible at grazing incidence.

The astigmatism causes a large loss in light intensity and also causes a broadening of the spectral lines because of spectrum line curvature.

There are two forms of spectrum line curvature. The first occurs when the entrance slit has a finite length because principal rays incident on the grating from outside the meridian plane are deviated by different amounts to the chief ray in the meridian plane. This aberration was called "enveloping curvature" by Beutler. The second form of line curvature occurs for a point source in the meridian plane and is due to the term F_{210} in the light path function. This aberration

which becomes significant in the presence of large astigmatism was termed "astigmatic curvature" by Beutler. The effects of astigmatic curvature and enveloping curvature have been described by Welford (60) and he concluded that sharp lines can only be obtained by using a short slit to minimise the effect of enveloping curvature. In this work the effect of using entrance slits of finite lengths on the imaging of spectral lines has been analysed by exact ray tracing. The results of this research are given in Chapter 3.

2.2 ASPHERIC GRATINGS

In order to obtain a reduction of the astigmatism of the concave grating several authors have proposed the use of toric or ellipsoidal grating blanks. The theory of the torus grating has been described by Haber (61) using an approach similar to that of Beutler. He showed that if a grating blank has radii of curvature at the origin of R in the meridian (y-z) plane and ρ in the sagittal (x-z) plane, the condition for stigmatic focus on the Rowland circle is

$$\sin \alpha \sin \beta = \rho/R$$

Thus, for a given angle of grazing incidence α there are two stigmatic points on the Rowland circle corresponding to angles of diffraction β and $-\beta$. For other angles of diffraction the tangential and sagittal focal lines will not coincide and the sagittal focus will lie either inside or outside the Rowland circle. Thus a "quasi-stigmatic" range can be found over which the astigmatism is less than a certain value. For the torus grating Haber showed that the astigmatic length of the focal lines was given by

$$A = \frac{L}{\rho \sin \alpha} (\sin \alpha + \sin \beta) (\rho - R \sin \alpha \sin \beta)$$

where L is the length of rulings illuminated by a point source.

Haber also solved this equation for $\sin \beta$ so that the limits of angular range of the spectrum for the astigmatism to be less than a certain value can be calculated.

$$\sin \beta = \left[\frac{\rho - R \sin^2\alpha}{2R \sin \alpha} + \frac{(\rho - R \sin^2\alpha)^2}{4R^2 \sin^2\alpha} + \frac{\rho}{R} \left[1 \pm \frac{A}{L} \right] \right]^{\frac{1}{2}}$$

Haber pointed out that the largest quasi-stigmatic wavelength range was obtained for images formed around the grating normal. In his treatment he determined equations for secondary astigmatism, coma, inclination and curvature of the spectral lines and finally the toric aberrations which impose limitations on the grating aperture which may be employed.

Under Rowland circle conditions the toric aberration is given by

$$\left(\frac{\cos^2\alpha}{\sin\alpha} + \frac{\cos^2\beta}{\sin\beta}\right)\left(\frac{y^4}{8R^3} + \frac{y^2x^2}{4R^2\rho}\right) + \frac{(\sin\alpha + \sin\beta)(\rho - R\sin\alpha\sin\beta)x^4}{8R\rho^3\sin\alpha\sin\beta}$$

The limitations which should be applied to the grating aperture can be found by applying the aberration tolerance that the toric aberration should be less than 0.25λ.

From the equation for the toric aberration, considering the meridian plane $x = 0$, it can be seen that the maximum width of the grating should be limited to the same optimum width as a corresponding spherical grating. For a stigmatic point the second term vanishes and for $y = 0$ there is no limitation on the length of ruling. However, the term in y^2x^2 can cause significant broadening to the image and this term becomes equal to the usual spherical aberration of a spherical grating if

$$x_{max}^2 = \frac{y_{max}^2\rho}{2R}$$

Hence, the resolution attainable with a torus grating is less than that which can be obtained with a spherical grating. The broadening of

spectral images due to the toric aberration may be calculated from:

$$\Delta_{TORIC} = \left(\frac{\cos^2\alpha}{\sin\alpha} + \frac{\cos^2\beta}{\sin\beta}\right)\left(\frac{y^3}{2R^2} + \frac{yx^2}{2R\rho}\right)$$

The image broadening due to coma for a stigmatic image in the meridian plane was given by Haber to be

$$\Delta_{COMA} = \left[\left(\frac{\cos\alpha}{\sin^2\alpha}\right)\left(\rho - R\sin^2\alpha\right) + \left(\frac{\cos\beta}{\sin^2\beta}\right)\left(\rho - R\sin^2\beta\right)\right]\frac{x^2}{2R\rho}$$

$$+\left[\left(\frac{\cos^2\alpha}{\sin^3\alpha}\right)\left(\rho - R\sin^2\alpha\right) + \left(\frac{\cos^2\beta}{\sin^3\beta}\right)\left(\rho - R\sin^2\beta\right)\right]\frac{x^2y}{R^2\rho}$$

For the torus grating the coma term can contribute significantly to the broadening of the spectral images and as in the case of the spherical grating the term corresponding to spectrum line curvature requires that the size of the light source is restricted. It should be noted that the coma terms are also reduced by decreasing the illuminated lengths of the rulings.

The magnitude of the broadening due to coma has been calculated for a practical grazing incidence toroid with the following parameters:

$R = 2000$ mm $\quad \rho = 5.65$ mm $\quad \alpha = 2.408 \quad \lambda = 23$ Å

$x = 0.75 \quad y = 5.0 \quad \frac{1}{d} = 600$ l/mm

and yields a value of $\Delta_{COMA} = 13.4\mu m$. The magnitude of the broadening due to the toric aberration for the above case is given by $\Delta_{TORIC} = 5.4\mu m$. Whereas for a spherical grating in the same geometry the line width

would be only 0.6μm measured as the transverse aberration. The reason for this large difference is that for a spherical grating due to the large astigmatism fans of rays with given azimuthal angle originating from a point source are imaged at separate points on the parabolically curved focal line. If the astigmatism is reduced the curvature of the focal line will become a broadening of the image which will cause a reduction in the resolution of the grating.

Theoretically, therefore, it can be seen that the torus grating offers a useful reduction in astigmatism at the expense of resolution. In order to investigate the properties of the torus grating more thoroughly extensive analysis by means of exact ray tracing has been performed. The results of the ray tracing will be compared in Chapter 3 with the experimentally observed images formed by a prototype holographic toroidal grating.

Very few examples of the use of aspheric gratings have been reported in the literature and this can be attributed to the technical difficulty of optically working aspheric surfaces to sufficient accuracy and the problems of ruling gratings on such surfaces. Greiner and Schäffer (81) in 1959 showed how the radii of the torus grating should be chosen to minimise astigmatism over a given wavelength range and described the design of a spectrograph using a torus grating. The torus described by Greiner and Schäffer had only a slight difference between the two radii since it was to be used at the usual angles of incidence and diffraction for the Seya-Namioka type mountings.

More recently Schönheit (82) successfully used a toroidal grating to reduce astigmatism in a Seya-Namioka monochromator. The grating used in this case had 1150 l/mm ruled on a blank with primary and secondary radii of curvature of 489 mm and 330 mm respectively. Similar work has been described by Strezhev and Andreeva (83) who made several toroidal gratings for a Seya-Namioka monochromator and a spectrograph to cover several spectral ranges.

At grazing incidence it has been more popular to use a toroidal mirror as a condenser in front of a grazing incidence spectrograph to remove astigmatism at one wavelength and reduce it in the vicinity of that wavelength. Rense and Violett (84) used such a system in a rocket-borne spectrograph to perform solar spectroscopy and recorded wavelengths down to 84Å. A similar system has also been used by Cantù and Tondello (85) to increase intensity when performing laboratory soft x-ray absorption spectroscopy. The analysis of such systems has been described by Ishii et al (86) and Shchepetkin (87). It should be noted that in the design

of such systems it is essential that the aberrations of the total system are considered with respect to the geometry, source size and slit widths employed in order to obtain optimum performance.

It is well known that an ellipsoidal mirror can theoretically produce a perfect image of a point source located at one of the foci. The general optical characteristics of concave gratings ruled on ellipsoidal blanks has been described by Namioka (58), and he has also applied the theory to the grazing incidence mounting (88). By expanding the equation of the ellipsoid as a series Namioka derived the light path function with terms up to the fourth degree in grating aperture. Application of Fermat's principle yielded the locus of minimum aberration for horizontal focus to be a circle in the y-z plane with diameter b^2/c analagous to the Rowland circle (where a, b and c are the semi-axes in respectively the x, y, and z directions). The condition for vertical focus is the same as for a toroid and can be written in terms of the semi-axes as

$$\frac{a^2}{b^2} = \sin\alpha \cdot \sin\beta$$

Provided the width of grating is restricted to the optimum the astigmatic length of the images for a point source is the same as that for a toroid. However, if a larger grating width is considered the image will become larger due to comatic elongation and the length of the images will be given by

$$A' = L \sin\beta \left\{ \left[\operatorname{cosec}\alpha - \frac{b^2}{a^2}\sin\alpha \right] \left[\frac{b^2/c - y\cot\beta}{b^2/c - y\cot\alpha} \right] + \operatorname{cosec}\beta - \frac{b^2}{a^2}\sin\beta \right\}$$

provided $yc/b^2\tan\beta < 1$ and $yc/b^2\tan\alpha < 1$

The optimum value of a/b can be calculated over a range of angles of diffraction for a given angle of incidence by minimising the astigmatic aberration term. The full equation for the optimum ratio given by Namioka will not be given here; instead an approximate expression is given:

$$\frac{a}{b} = \frac{1}{2}\left[\sin\alpha.\frac{\{2(\beta_1-\beta_2)+\sin2\beta_2-\sin2\beta_1\}}{\cos\beta_2-\cos\beta_1}\right]^{\frac{1}{2}}$$

The grazing angle of incidence is α and the grazing angle of diffraction lies between β_1 and β_2.

The width of an ellipsoidal grating must be restricted as in the case of a spherical grating to limit the term corresponding to spherical aberration. For the ellipsoidal grating this term is given by:

$$\frac{y^4c^3}{8\,b^6}\left(\frac{1}{\sin\alpha}+\frac{1}{\sin\beta}-\frac{b^2}{c^2}(\sin\alpha+\sin\beta)\right)$$

From this expression it can be seen that by proper choice of the semi-axes a larger optimum width may be employed than for a corresponding spherical grating.

The optimum width considering only the first Huyghens zone on the grating is given by:

$$W_{opt} = 2\left[2\,\frac{\lambda b^6}{c^3}\,\frac{\sin\alpha\,\sin\beta}{(\sin\alpha+\sin\beta)(1-\frac{b^2}{c^2}\sin\alpha\,\sin\beta)}\right]^{\frac{1}{4}}$$

For b = c the above equation yields the result for a spherical grating but leaves the value of a to be chosen to reduce astigmatism. In the spectral region where $|1-(b^2/a^2)\sin\alpha \sin\beta| < |1-\sin\alpha \sin\beta|$ the astigmatism can be reduced and also the optimum width increased by using an ellipsoidal grating with semi-axes a and c equal.

Namioka gave an example for an angle of grazing incidence of 5° with angles of diffraction of 6.5° and 15° corresponding to the wavelength range 44-505 Å. With a ratio of semi-axes of a/b = 0.1344 the astigmatism was reduced to about 25% of that of a spherical grating. However, Namioka concluded that the combination of a toroidal mirror and spherical grating is more efficient at reducing astigmatism than the ellipsoidal grating.

Although the properties of the ellipsoidal grating look very promising it should be remembered that the ellipsoidal mirror suffers severely from coma for off-axis object points. This restricts the applicability of ellipsoidal mirrors, however, a system using an ellipsoid-hyperboloid mirror combination has been described by Chase and Silk (89) for x-ray imaging of radiation from laser fusion pellets. The configuration is a natural modification of the paraboloid-hyperboloid mirrors used for high resolution x-ray astronomy. It was shown by ray tracing that this system would be capable of spatial resolution 1-3μm over a field of a few hundred microns and would have a collecting area greater than 10^3 times that of the pinhole cameras often used for x-ray imaging. However, it was pointed out that the tolerance for making such mirror systems for use with finite conjugates at sec of arc resolution would be between one-half to one-tenth those for a

typical x-ray telescope. Thus the performance of the mirror system will be limited by the accuracy with which the surfaces can be figured and the degree of surface perfection which can be attained.

The imaging properties of a grating formed on a section of an elliptical cylinder can be analysed using the formulae given by Namioka. Although a grating on a blank of this form produces no vertical focussing by appropriate choice of the semi-axes for the wavelength region of use, the width of grating and hence luminosity and resolution may be increased considerably over that of a spherical grating. The ratio of the optimum width of an elliptical grating to that of a spherical grating is given by

$$\frac{W_{opt(ellipse)}}{W_{opt(sphere)}} = \left(\frac{1-\sin\alpha \sin\beta}{|1-(b^2/c^2)\sin\alpha \sin\beta|} \right)^{\frac{1}{4}}$$

The dependence of this function on wavelength is shown in Fig. 6 and 7 for two ratios of the semi-axes, b/c. It can be seen from these curves that the optimum width may be doubled over a wavelength range of 10 - 20 Å about the design wavelength depending on the grating frequency and angle of incidence. If a narrower spectral range can be employed the gain can be even greater. For the case shown in Fig. 8 the optimum width may be increased by a factor of 5 over that of a spherical grating for wavelengths ±0.3 Å either side of the design wavelength. However, this is a rather extreme case yet use of an elliptical grating can give an increase in optimum width over a wide spectral range as can be seen from the curves in Fig. 7. The example

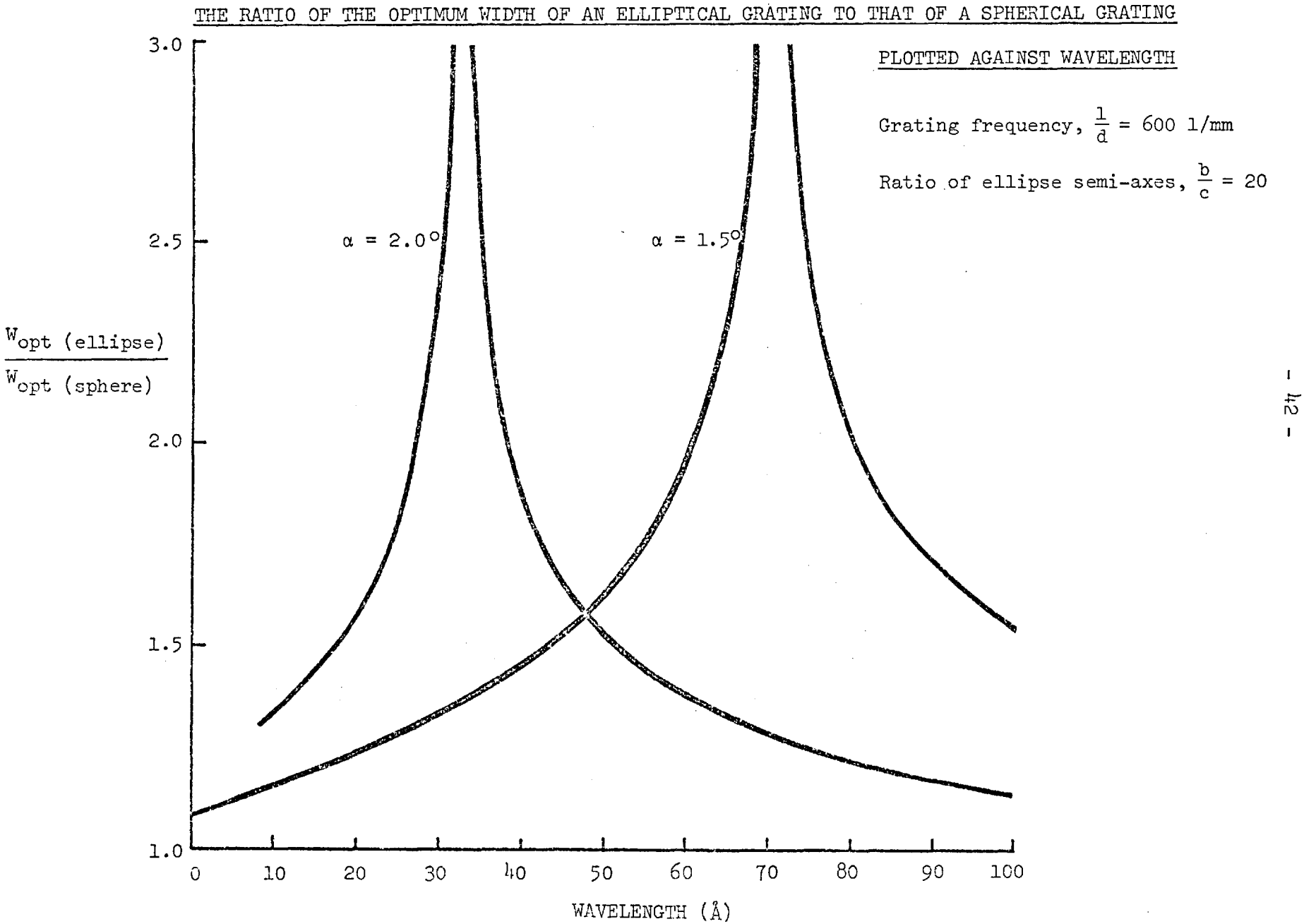
THE RATIO OF THE OPTIMUM WIDTH OF AN ELLIPTICAL GRATING TO THAT OF A SPHERICAL GRATING
PLOTTED AGAINST WAVELENGTH
Grating frequency, 1/d = 600 l/mm
Ratio of ellipse semi-axes, b/c = 20
α = 2.0°
α = 1.5°
W opt (ellipse) / W opt (sphere)
3.0
2.5
2.0
1.5
1.0
0
10
20
30
40
50
60
70
80
90
100
WAVELENGTH (Å)

FIG. 6

THE RATIO OF THE OPTIMUM WIDTH OF AN ELLIPTICAL GRATING TO THAT OF A SPHERICAL GRATING AGAINST WAVELENGTH

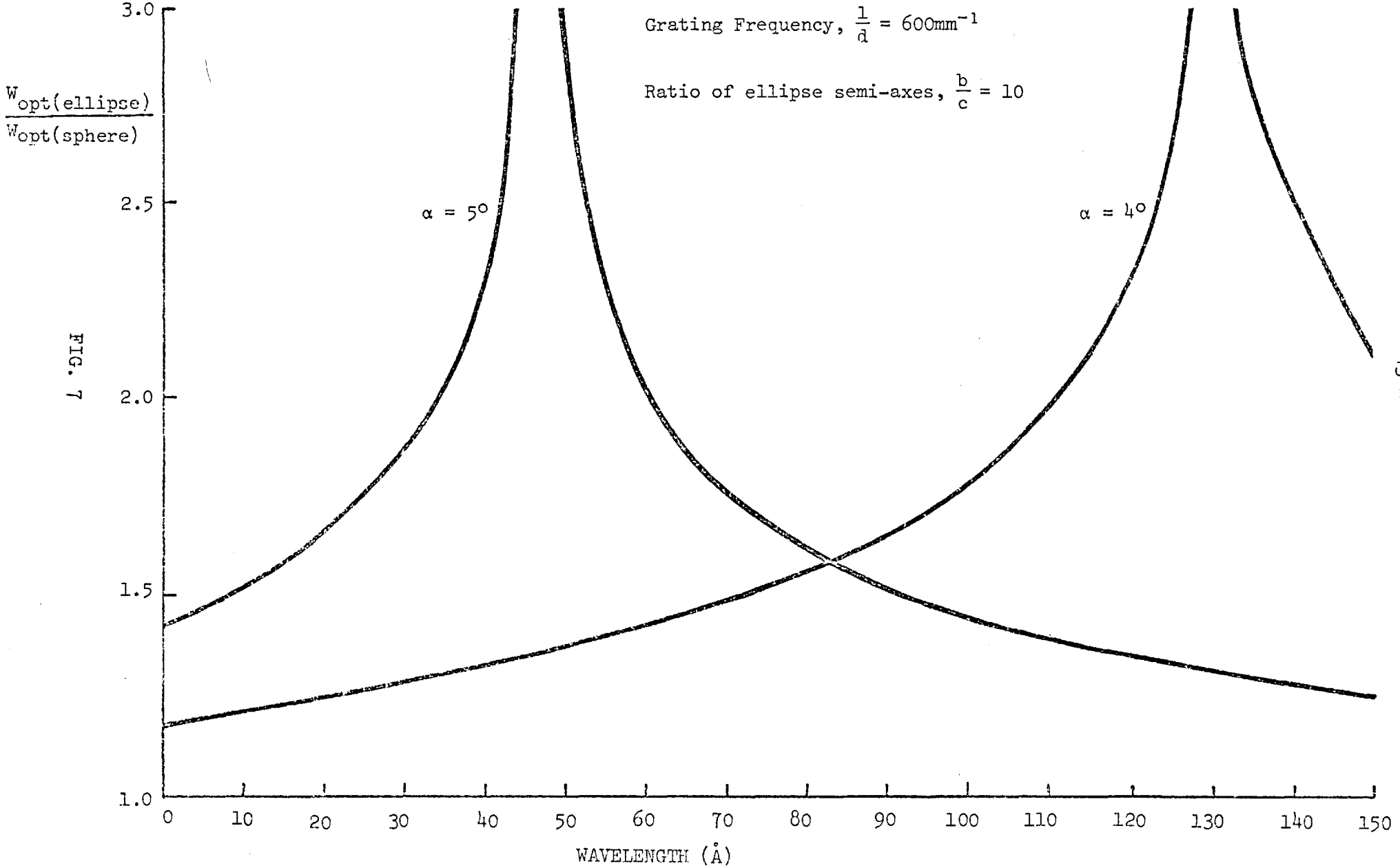

FIG. 7

THE RATIO OF THE OPTIMUM WIDTH OF AN ELLIPTICAL GRATING TO THAT OF A SPHERICAL GRATING FOR A PRACTICAL CASE

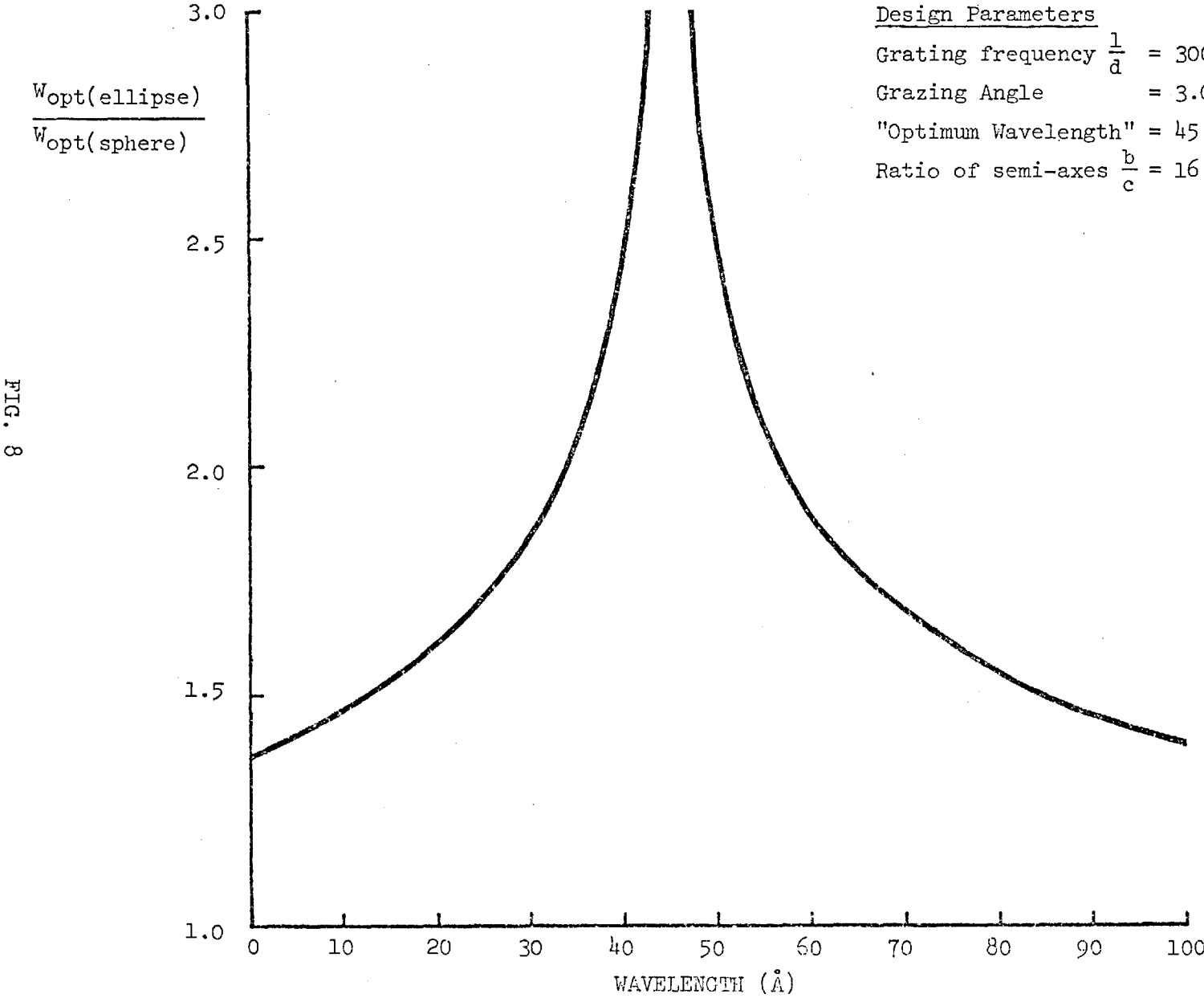

FIG. 8

COMPARISON OF OPTIMUM WIDTH FOR AN ELLIPTICAL GRATING AND A SPHERICAL GRATING AGAINST WAVELENGTH

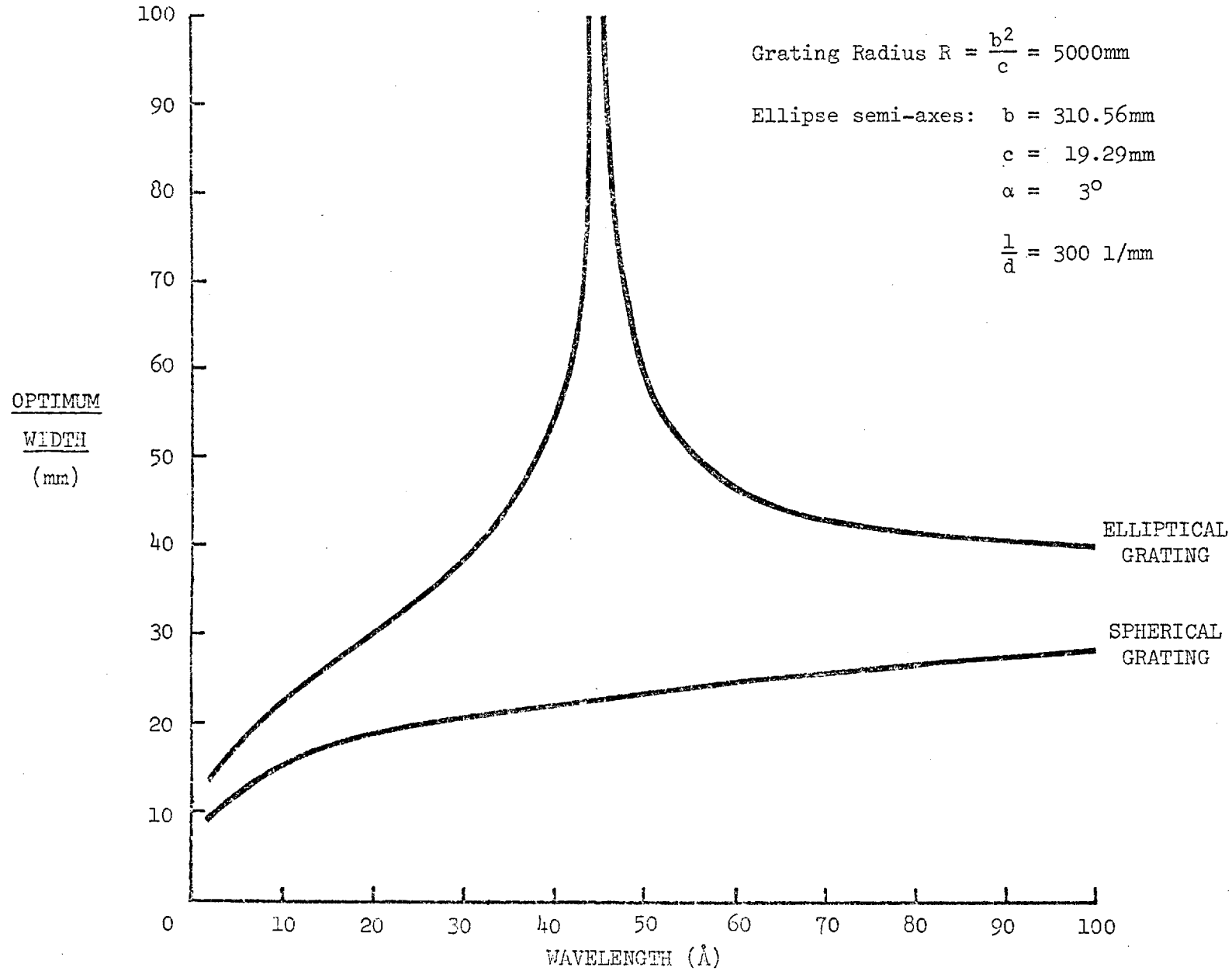

FIG. 9

shown in Fig. 9 illustrates the improvement which can be gained with an elliptical grating, compared to a spherical grating for a practical case in the soft x-ray region. It can be seen that if one is interested in spectra in the wavelength range 30 - 100 Å, use of an elliptical grating permits an increase in grating width from about 20mm as required for a spherical grating to nearly 40mm.

Thus, elliptical gratings can be used in existing spectrographs to enhance resolution over a restricted wavelength range and provide improved performance over spherical gratings over a wide wavelength range. The large possible gains in resolution and luminosity by using elliptical gratings means that they are ideally suited to applications in monochromators.

In view of all the theoretical advantages in using elliptical gratings, it is surprising that they are not widely used in the grazing incidence region. However, it is generally thought that the production of aspheric surfaces to the required accuracy and surface finish is very difficult and that the ruling of gratings on such surfaces is also very difficult. Hence, as far as I am aware no successful elliptical or ellipsoidal gratings have been made until recently.

It is well known that aspheric surfaces can be formed by deforming a glass blank. Toroidal surfaces have been made in this way and Bennett and Turner (71) have described the design procedure for making elliptical mirrors by bending suitably shaped flats. Since it is relatively easy to obtain a good surface finish and flatness on a plane rather than an aspheric surface, it is possible to satisfy the exacting requirements of soft x-ray reflection by this method. The effects of bending the mirror to the desired curvature were examined on a Twyman-Green

interferometer and it was found that some astigmatism was introduced. However, since the astigmatism of this system is already large it should not cause image degradation.

The author has successfully produced several elliptical mirrors of this type and elliptical diffraction gratings have been formed on five of them holographically. A photograph of an elliptical mirror is shown in Fig. 10. All the elliptical gratings produced so far have had a frequency of 300 l/mm on an area 5 cm long by 1 cm wide which corresponds to the central area of the mirrors which has the correct surface figure. The efficiency of the elliptical gratings has been measured and as was to be expected it was the same as that of typical plane and concave gratings produced by the holographic technique. The efficiency was typically about 10% at 45 Å.

The visible light imaging properties of the elliptical mirrors formed by bending have been investigated and no significant additional aberrations were found. Similarly images in the zero order at 45 Å showed no excessive broadening or scattered light. Since an x-ray tube with a graphite anode was used for the initial tests no definite conclusions could be made about the resolution of the gratings because the C_K radiation from graphite has a rather large wavelength spread about 44.8 Å. However, it can be said that the results were most encouraging and further tests are being performed with a more suitable line source so that a true comparison between the resolution of elliptical and spherical gratings can be made.

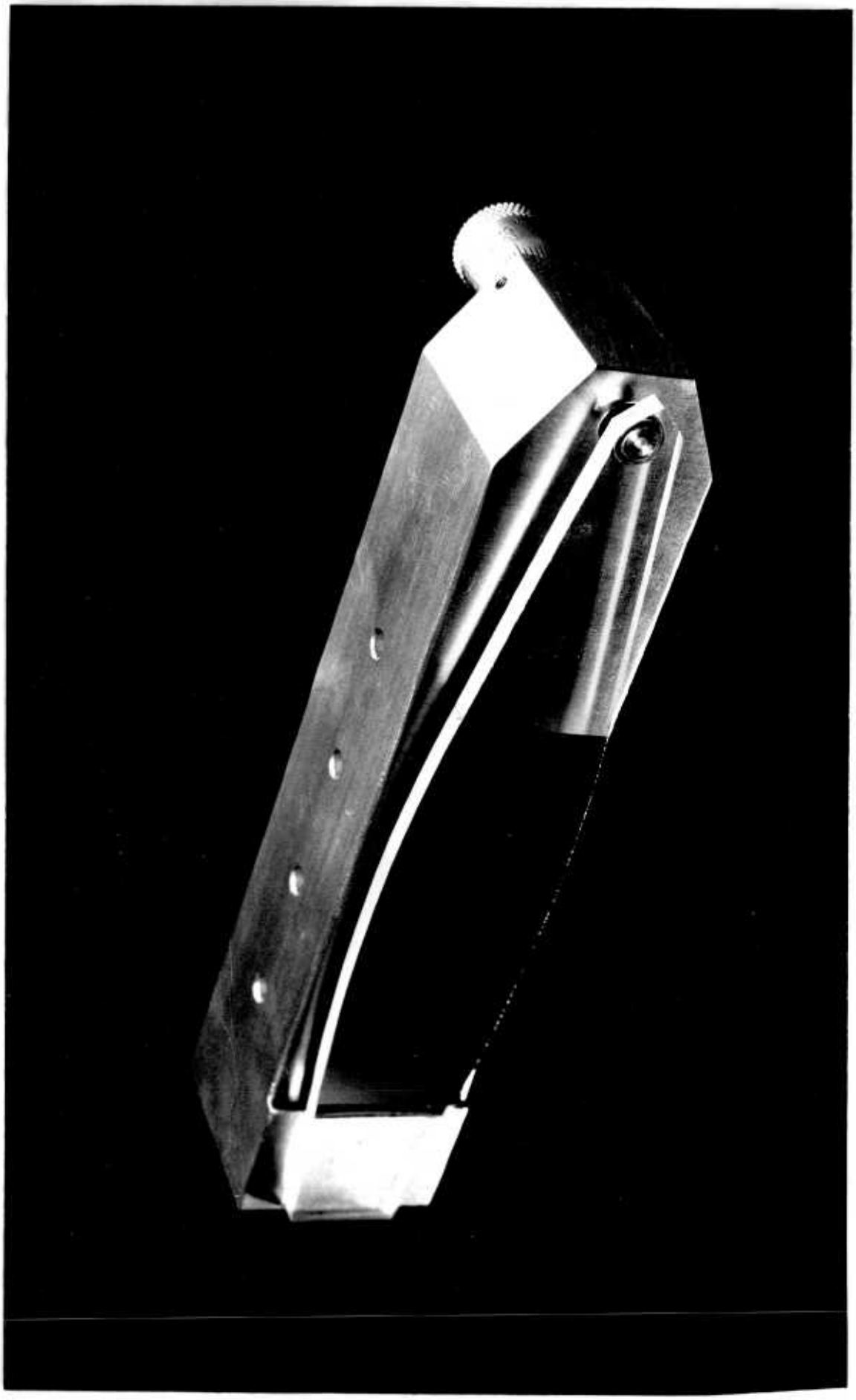

FIG. 10 AN ELLIPTICAL MIRROR

2.3 THE VARIABLE FREQUENCY GRATING

It has been known for a hundred years that a systematic variation in the spacing of the lines on a grating can impart focussing properties to a plane grating. In 1875 Cornu (68) demonstrated the correspondence between the interference fringes formed between two surfaces and the pattern of rulings on a diffraction grating which gives it focussing properties. It is well known that if a shallow convex spherical surface is placed in contact with an optical flat concentric interference fringes called Newton's rings can be observed about the point of contact. The interference fringes formed in this way are due to the superposition of two spherical waves. If R is the radius of the spherical surface and is large the thickness of the air gap, d, at a distance r from the point of contact is

$$d = \frac{r^2}{2R}$$

Since there is a phase change of π on reflection at the lower surface, when illuminated with monochromatic radiation of wavelength λ', dark fringes are formed at radii of

$$r^2 = n\lambda' R$$

Thus the squares of the radii of successive dark rings are proportional to the natural numbers.

By a geometrical approach Cornu was able to show that this was also the law by which the rulings on a grating must be separated in order to bring a cylindrical wave emanating from a slit

parallel to the rulings to a focus. Cornu combined the equations for imaging from a diffraction grating and the equation for interference fringes to yield

$$\frac{1}{u} + \frac{1}{v} = \frac{2}{R}\,\frac{k\,\lambda}{\lambda'}$$

which he realised was identical to the classical lens formula with object and image distances u and v. Thus he was able to state that for a plane grating, whose straight or circular rulings are separated in the same law as the interference fringes formed at normal incidence between a plane surface and a cylinder or a sphere of radius R, has the properties of a cylindrical or a spherical lens. The grating has a series of real or virtual foci lying on a straight line through the centre of the grating at distances from the grating which are sub-multiples of positive or negative integers corresponding to the different orders of diffraction.

The first order primary focal length of the grating for monochromatic light of wavelength λ' used to produce the grating is equal to half the radius R. For light of another wavelength λ the focal length is altered by the ratio λ'/λ.

Cornu noted that these focussing properties would remain if only a part of the pattern were illuminated. Hence, if a grating were ruled with a uniform systematic error over part of the area it would have focussing properties. Such properties had been observed for apparently good plane gratings by Mascart and it was found that, in accordance with Cornu's theory, real foci were formed for positive orders of diffraction and virtual foci for negative orders.

Cornu verified his theoretical work experimentally by obtaining photographs of interference fringes formed between a flat surface and a quartz plate slightly curved with weights. He noted that elliptical fringes were first formed which became straight lines before changing to hyperbolic fringes. From two small photographs of the straight fringes Cornu measured the spacing of the fringes and found that the theoretical focal length was close to that measured directly using sodium light.

Although earlier work had been performed on zone plates or circular gratings (67), I believe Cornu's work to have been the first to be published about the variable frequency grating and the first to describe the formation of interference, or holographic gratings.

Rowland (66) included the case of the variable frequency grating in his extensive analysis of the imaging properties of concave gratings. He was able to show that the definition of a grating may be very good even when the error of run is considerable provided it is linear. Since gratings of spectroscopic value could only be produced on ruling engines at that time, he did not consider the variable frequency grating in great depth. However, he gave equations to calculate the distribution of light intensity for gratings with lines at variable distances. He pointed out that the effect of variable frequency would be to give the grating a different focus according to the angle and order of diffraction and that this effect often appeared in gratings. He noted that at any given angle the same effect can be produced by variations of the ruled surface from the ideal shape. He also stated that a theoretically perfect grating for one position of the slit and eyepiece can be ruled on any surface.

After the activity concerning diffraction gratings at the end of the last century, no significant progress was made in the field of variable frequency gratings until 1966 when Gale (73) communicated "The theory of the variable spacing grating". In this paper a physical optics approach is used to assess theoretically the behaviour of plane and aspherical gratings in which the spacings of the rulings are unequal. Since reference is made to the possible use of such gratings for wavelengths from 50 - 500 Å this paper is particularly relevant to the present work.

Gale applied the Kirchhoff diffraction integral and obtained an equation for the scattered amplitude in terms of the Fresnel integrals. After applying several simplifying approximations it was shown that to obtain maximum intensity the rulings must be positioned so that the optical path length increases by $m\lambda$ from one ruling to the next, i.e. the waves diffracted by all the rulings are in phase at the focus. Once the ruling pattern has been chosen for a given wavelength and geometry it is not possible to obtain the maximum intensity for another wavelength. Instead it is necessary to choose object and image coordinates such that the variation in maximum intensity is minimised for each new wavelength. Considering only the meridian plane Gale expanded the optical path length as a power series in grating width, y, up to the fourth power. He obtained equations for the positions of the rulings in terms of the coefficients of the power series and the optical path length for the coordinates at a different wavelength. In the meridian plane there are four coordinate parameters which means that three of the coefficients of the

expansion of the optical path length can be removed. However, since this would entail two possibly complex motions, Gale does not consider this case any further. Instead the locus of maximum diffracted intensity is given for which the second order term is zero. Gale then goes on to consider the optimum number of rulings for focussing plane gratings. He points out that plane focussing gratings with a large number of rulings produce a rapidly varying intensity for wavelengths in the vicinity of the design wavelength, λ. Such behaviour would make comparison of spectra difficult and Gale goes on to consider a relaxation of the ideal focussing condition in which the grating spacing increases linearly with y. He calls this grating a quadratic plane grating and it has the same focal curve as the focussing plane grating but without the singularity in the optimum number of rulings. The diffracted intensity distribution was calculated numerically and it was found to be asymmmetrical with a peak displacement of typically 0.04 minutes of arc. If the number of rulings was increased above the optimum the intensity profile became much more complex and the maximum intensity decreased rapidly.

Finally, Gale derived an expression for the optical path length function for unequally spaced rulings on a slightly aspherical surface. Gale realised that the problem of increasing the optimum number of rulings of a spherical grating could be solved by appropriate choice of ruling parameters and aspheric coefficients so that the fourth and higher order terms of the optical path length function would be made zero.

He analysed the expressions in the optical path length function and showed that it was possible to obtain a focussing curve independent of the angle of diffraction. The third order term could also be made to vanish but the fourth order term could not be made zero independent of the angle of diffraction. Hence, the fourth order term can only be made zero for one particular wavelength for a given ruling pattern and geometry. However, Gale concluded that no improvement in the focussing properties of a concave spherical grating can be obtained by any choice of ruling pattern or asphericity. It can be seen that without further qualification this statement is obviously incorrect. However, it is interesting to observe that although there are theoretical advantages in using both aspheric and variable frequency gratings for certain applications in the soft x-ray region, no improvement in horizontal focussing over that of the concave spherical grating has been demonstrated experimentally to date.

By means of the present research programme in the near future we intend to show experimentally that not only resolution but also luminosity can be considerably increased by suitable design of diffraction gratings for use in the soft x-ray region.

Gratings with unequal groove spacings have been successfully ruled by Gerasimov et al (104) and Harada (105). There are many problems in ruling such gratings; however, this method allows the possibility of ruling patterns which cannot be achieved holographically and also allows the high efficiency of present ruled blazed gratings in the visible and UV regions to be retained.

However, for soft x-ray use holographic gratings now have a higher efficiency than ruled gratings and the holographic method enables cer-

tain types of variable frequency grating to be easily produced. Furthermore, the holographic method enables gratings to be formed on steeply curved substrates upon which it would be exceedingly difficult to rule a grating. Thus, although we accept that variable frequency gratings can be made on a ruling engine we have attempted to find holographic solutions applicable to the soft x-ray grazing incidence geometry.

The aberrations of a grating with imaging properties can be minimised in a given wavelength region by optimal choice of substrate curvature and surface variation of spatial frequency.

In 1960 Murty (90) showed that a zone plate imposed on a spherical surface forms an aplanatic system free from spherical aberration and coma if the object and image points are inverse points with respect to the circle which lies in the spherical surface. The line joining the object and image points is divided harmonically internally and externally by the circle and this circle is known as the circle of Apollonius (see Fig. 11).

If a reflection hologram is formed on the spherical surface by the interference of light wavelength λ_0 with one wave converging on point B and a second coherent wave diverging from point A; when it is reilluminated with polychromatic radiation from source point A, according to the holographic principle, a perfect image will be formed at B of light wavelength λ_0. In addition it can be shown (91) that radiation of wavelength $\lambda_0/(M+1)$ is focussed at the centre O of the sphere and that radiation of wavelength $2\lambda_0/(M+1)$ is focussed back at A free from spherical aberration. Similarly if the polychromatic

THE CIRCLE OF APOLLONIUS

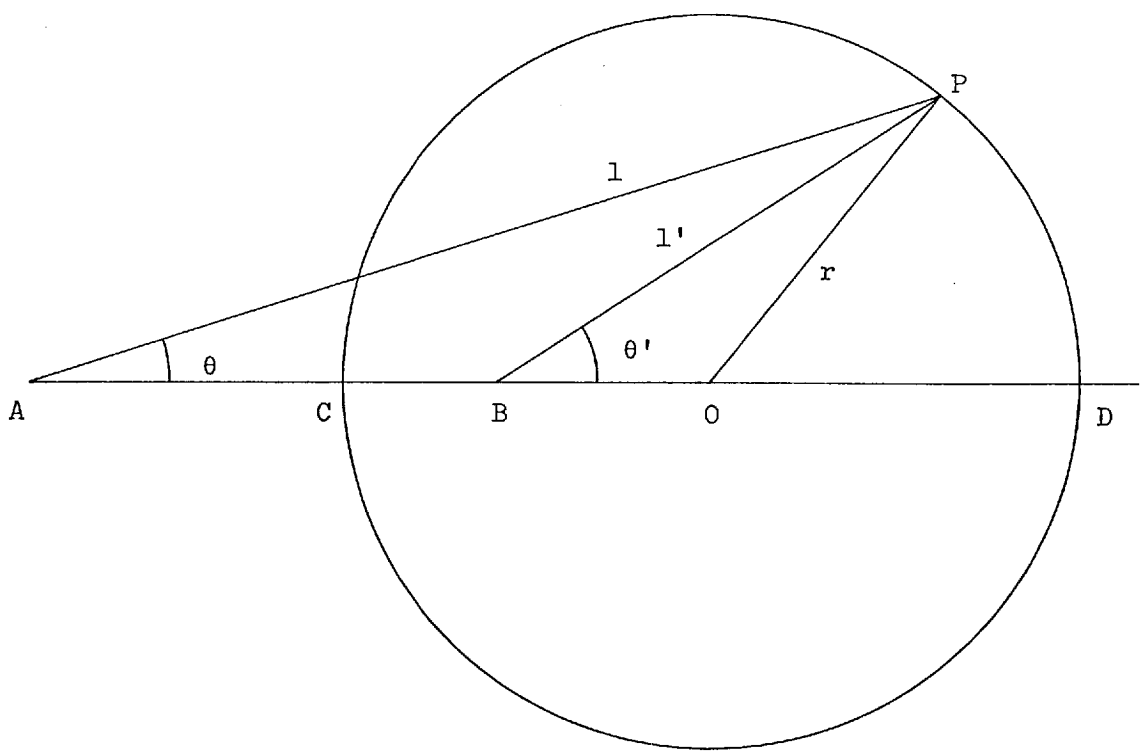

P lies on a circle diameter CD where C and D divide AB harmonically internally and externally such that:

$$\frac{AC}{CB} = \frac{AD}{DB} = \frac{l}{l'} = M \text{ (constant)}$$

Hence $OA.OB = r^2$ and $M = \frac{OA}{OB}$

FIG. 11

source is positioned at B wavelength λ_0 is focussed at A, wavelength $M\lambda_0/(M+1)$ is focussed at the centre and wavelength $2M\lambda_0/(M+1)$ is focussed back at B. Thus to make a given grating there are three points at which the two recording sources may be located. Once a grating has been formed a source may be placed at any of the three points to provide stigmatic images at the other two points.

It has been suggested (92) that the grating formed by the interference of waves from a point source located at the centre of curvature of the grating and a point source located on the opposite side of the grating could be used in the x-ray domain. For this case a point source at A forms a stigmatic image with wavelength λ_0 at O and a stigmatic image with wavelength $(1-M)\lambda_0$ at B. As $M \to 1$ the wavelength imaged at B becomes small and points A and B come close to the grating sphere. Murty and Das (91) have examined the spherical aberration for this type of system and found that it varied considerably between the zero aberration positions. They found that the variation was least for M values of 2 or 0.5. Values of M from 0-1 signify that point A is outside the circle and point B inside the circle; M-values from $1-\infty$ correspond to A inside and B outside the circle. Thus interchanging A and B changes M to 1/M.

The general properties of stigmatic spherical gratings have been described by Labeyrie (93). The locus of a spectrum from this type of grating - which has been classified as "Type III" by Jobin-Yvon - is obtained by setting the coefficient of Y^2 to zero in the optical path length function. The locus is a curve which has three intersections with the revolution axis of the system. The three intersections are

the stigmatic points and the revolution axis is the locus of sagittal focus. The aberrations of the zone plate type holographic grating on a spherical surface have thus been extensively examined in the literature. Recently, from general isoplanatism considerations Welford (95) proposed a similar system for a hologram lens (96) and showed how the ray tracing equation for holography and the isoplanatism theorem enable the effect of a change in the reconstruction geometry to be calculated.

The general method for calculating the aberrations of holographic gratings has been outlined by Cordelle et al (94). They gave the basic expressions for the light path function for holographic gratings and obtained a series expansion up to third order for a grating recorded on a spherical surface. They also mentioned that because of the large number of possible combinations (including the possible use of correcting lenses during recording) and the many different needs, grating imaging would probably develop as a distinct field in optical computing.

It is only in the last two years that the theory of the holographic grating has been established, with the same rigor as that of the classical ruled grating, by Namioka, Noda and Seya (98, 100). The theory of the holographic diffraction grating is the subject of the thesis of Dr. H. Noda (99).

In this treatment of the theory of the holographic grating the light path function for the classical grating is extended to include terms containing the coordinates of the recording point sources. The meridian plane is defined by the origin of the grating and the two coherent point sources C and D. Points A, B and P are an object

point, the corresponding image point and a point on the grating surface. Assuming the distances of C and D from the origin is an integer number of wavelengths and positive-working photoresist is used so that a groove is formed at the origin; using laser light of wavelength λ_0 the n^{th} groove will be formed according to:

$$n\,\lambda_0 = (\langle CP\rangle - \langle DP\rangle) - (\langle CO\rangle - \langle DO\rangle)$$

This relation may be substituted in the usual expression for the light path function and expanded as a power series. The series expansion then contains terms corresponding to the classical ruled grating plus additional terms which are unique to holographic gratings.

Application of Fermat's Principle to the power series yields the grating equation, magnification, and horizontal and vertical curves in a similar way as in the treatment of the classical ruled grating.

In order to be able to choose the recording parameters to reduce the residual aberrations over a given wavelength range the geometry in which the grating is to be used must be determined. The most widely used mountings are those based on the Rowland circle, hence, it is convenient to design holographic gratings having a horizontal focal curve which lies on the Rowland circle. The alternative is to abandon the Rowland circle and to find another horizontal focal curve of which the lemniscate focal curve of Jobin-Yvon Type III stigmatic gratings is a good example.

On the Rowland circle the first and third terms of the light path function for a classical grating are zero thus the corresponding

terms for the holographic grating must also be made zero. These terms can be made zero for three possible recording geometries. The first possibility is to set the recording point sources at infinity so that plane waves are used to produce equispaced fringes in the tangent plane to the grating surface. Gratings of this sort have been classified as Type I by Jobin-Yvon and have a groove pattern identical to classical ruled gratings.

The second possibility is to locate the point sources on the Rowland circle. The Rowland circle conditions with the requirement for a given frequency at the centre of the grating only leave one degree of freedom in choosing the coordinates of the recording sources. This degree of freedom may be used to make one of the succeeding terms in aberration polynomial zero at a given wavelength and so eliminate astigmatism or coma-type aberration. If the grating frequency is also a free parameter both astigmatism and coma-type aberration may be eliminated for one wavelength.

The third possibility is to use the special solutions for stigmatic imaging corresponding to the Jobin-Yvon type III gratings which can have a similar ruling law to the variable frequency mechanically ruled gratings proposed by Sakayanagi (103) and Gerasimov (104). Unfortunately, none of the well-known solutions can be applied to the grazing incidence region since the grating efficiency decreases with increasing frequency. The design options for holographic gratings are also restricted by the usable range of available laser wavelengths.

Namioka et al have thoroughly investigated the design possibilities for holographic gratings for use in the Seya-Namioka monochromator (97, 98, 99, 101, 102). The results of this comprehensive research

programme have been to demonstrate that the performance of Seya-Namioka monochromators can be improved by the use of aberration-reduced holographic concave gratings. They found theoretically that although reduction of astigmatism was possible rather large coma-type terms were produced by this reduction. They concluded that it was preferable to reduce the coma-type aberration and verified this conclusion experimentally by producing both coma-reduced and astigmatism-reduced holographic gratings. They also produced spot diagrams by ray tracing in order to evaluate the imaging characteristics of the holographic gratings designed and found that they corresponded to the images obtained experimentally Thus further gratings can be safely designed and tested using a digital computer rather than producing and testing them experimentally.

In the grazing incidence region the limitations on the design parameters for holographic gratings are most severe. We have already seen that the two most significant aberrations, astigmatism and spherical aberration, severely limit the luminosity and resolution of grazing incidence instruments. We have also seen that the astigmatism may be greatly reduced over a small wavelength range by using a toroidal substrate but that coma-type aberration tends to dominate and cause a loss of resolution in this case. Alternatively by employing an elliptically figured cylindrical substrate the spherical aberration may be reduced over a restricted wavelength range so increasing usable grating width and resolution. Thus, we have two conflicting requirements which depend on wavelength. Either we can

reduce astigmatism and accept a loss in resolution or we can neglect astigmatism and obtain an increase in resolution over that of a spherical grating.

In order to be able to design a practical holographic grating the application, requirements and physical constraints of use must be known. These facts together with an understanding of the limitations of the holographic process should enable the optimum grating to be designed for the purpose. Unfortunately many grating users' needs are of a general nature and they require gratings which have a high efficiency and permit high resolution to be achieved over a wide wavelength range. Such general requirements are incompatible with the properties of aberration-corrected holographic gratings used at grazing incidence. However, for certain specialised applications it may be possible to find useful solutions.

Since the grating width and hence resolution of grazing incidence spectrographs is limited by spherical aberration it would be useful to investigate whether some particular variation of grating frequency could be employed to reduce spherical aberration over a useful wavelength range. By a geometrical approach it can be easily understood that for a single wavelength in a given geometry the variation of grating frequency can in theory be chosen in such a way that all rays from the source point striking the grating are diffracted to the same image point. However, when such a grating is illuminated with a polychromatic source only one wavelength will be imaged perfectly and the other wavelengths will be aberrated to varying degrees. Thus in order to design gratings of this type it is necessary

to apply an aberration tolerance and calculate numerically the aberrations of various systems. Since the phase errors for moderate aperture grazing incidence systems are large the Strehl type of tolerance (106) cannot be applied but instead a modified quality factor, as suggested by Pouey (107), can be used. Rather than calculate aberrations by using approximate series expansions we have concentrated on using exact ray tracing to give numerical values for the transverse aberrations and direction cosines of diffracted rays. This work resulted from a natural extension of the ray tracing program used for the classical grating to the variable frequency case. The analysis we have performed is therefore not limited by any holographic restrictions imposed by using two recording point sources as in the approach suggested by Noda et al (46).

From the analysis performed it became clear that variable frequency gratings are not suited for use in spectrographs but may be usefully employed in scanning monochromators or spectrometers. In Fig. 12 are shown curves of the frequency variation in the meridian plane to give zero spherical aberration for the case (A) with object point on the Rowland circle and (B) with the object point outside the Rowland circle. These curves indicate that for a grating whose frequency varies linearly with y there exists a locus for object and image points which lies outside the Rowland circle. By expressing the local angles of incidence and diffraction as power series in the pupil coordinate, y, Speer (108) has shown that the object and image points are located on the circle which is the continuation of the grating surface. This result was checked by ray tracing and it was noticed that there was a systematic discrepancy which increased with

GRATING FREQUENCY AS A FUNCTION OF Y TO CORRECT THE ABERRATIONS OF A SPHERICAL GRATING IN THE MERIDIAN PLANE

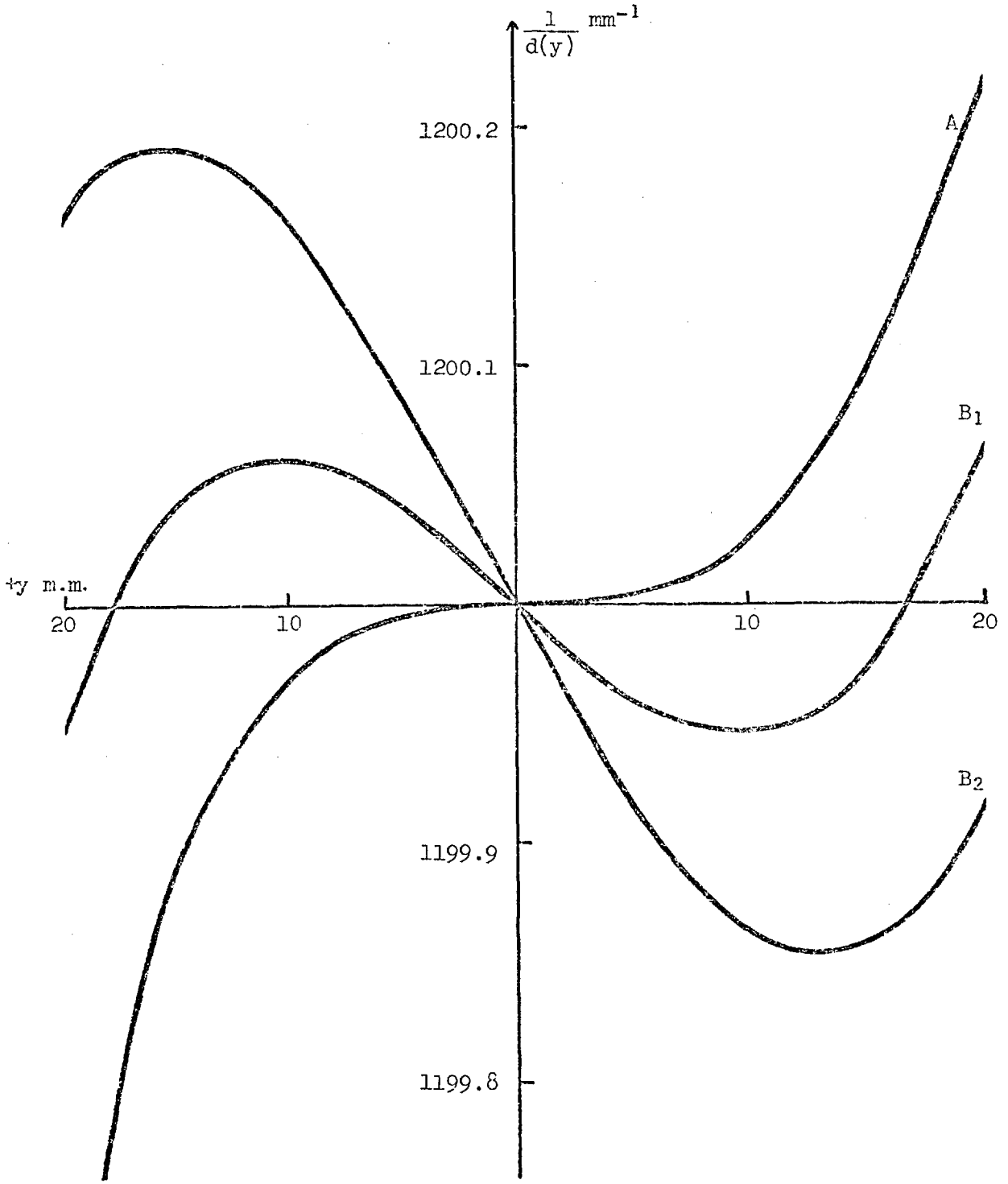

Parameters	R = 5000mm λ = 50 Å α = 2.0° Order (m) = +1	
	Frequency at centre of grating 1/do = 1200 mm^{-1}	
Curve A :	Object point on Rowland Circle	Δr=0
Curve B_1 :	Object point optimum distance outside Rowland Circle	Δr=1.116mm
Curve B_2 :	Object point further outside Rowland circle	Δr=2.233mm

FIG. 12

grating pupil coordinate.

In order to resolve this discrepancy it was decided to derive the grating frequency law which would give zero spherical aberration for object and image points located on the continuation of the grating surface. From general considerations it was evident that this problem could best be treated using polar coordinates rather than rectangular coordinates. The derivation of the grating frequency law has been described by Turner (70) and the elements of this derivation are described in the following section.

2.4 DERIVATION OF SPEER-TURNER GRATING FREQUENCY LAW

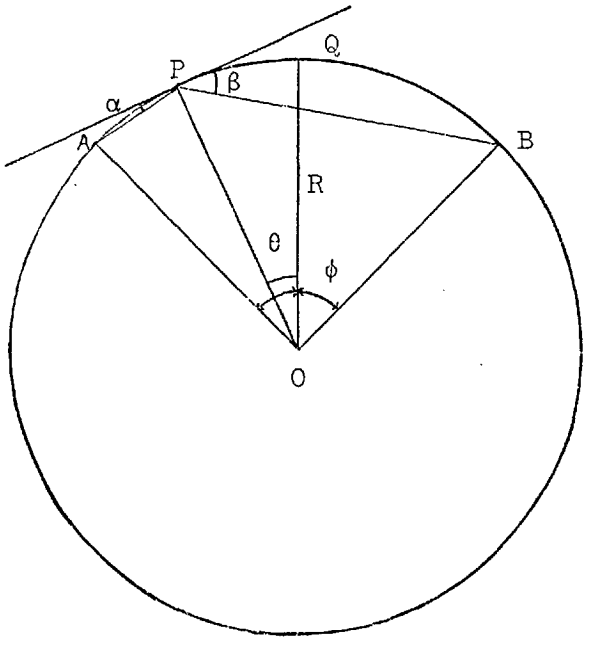

FIG. 13

The object and image points are to lie on a circle which is the continuation of the grating surface. Considering only the plane of the circle let θ be the angle subtended at the centre of the circle by the arc PQ where P is any point on the grating circle and Q is the centre of symmetry of the grating. The source position A is defined by the angle ϕ which is the angle subtended by AQ at the origin.

Let the grating frequency be a function of θ only

$$N = f(\theta)$$

so that the frequency is zero at Q.

By geometry:

$$\text{Grazing angle of incidence} \quad \alpha = \frac{\phi-\theta}{2}$$

For all diffracted rays to pass through B:

$$\text{Grazing angle of diffraction} \quad \beta = \frac{\phi+\theta}{2}$$

Substitution of these values in the grating equation for grazing incidence yields:

$$N = \frac{1}{d} = \frac{\cos(\phi/2-\theta/2)-\cos(\phi/2+\theta/2)}{m\lambda}$$

$$= \frac{2\sin\phi/2 \sin\theta/2}{m\lambda}$$

$$N = K \sin\theta/2 \qquad \text{where} \quad K = \frac{2\sin\phi/2}{m\lambda}$$

The value of K is fixed when the grating is made. The wavelength λ focussed is chosen by calculating the angular position ϕ of the source from:

$$\phi = 2 \sin^{-1} \frac{m\lambda K}{2}$$

The image is then formed at the point on the circle given by the angle $-\phi$.

Thus by varying the angular position of the source a range of wavelengths may be focussed. However, only one wavelength will be perfectly focussed at the circle for each angular setting. The other

wavelengths are focussed with varying amounts of spherical aberration on the line which joins the perfect focus B to the centre of symmetry of the grating, Q.

If the grating surface includes the zero frequency position Q radiation reflected from this point will also be present in the focus. Since this is not normally wanted the grating length must be restricted to exclude this point. The grating length is also limited by the object position at the shortest wavelength to be focussed by the grating. The angle θ must also be less than 90° otherwise the grating frequency becomes too high for useful diffraction to take place.

A possible design for a grating of this type for use in the soft x-ray region could be specified by the following typical parameters:

Minimum wavelength of use	23 Å
Radius of curvature	2500 mm
Length of grating	200 mm
K-value	50846 mm^{-1}

The grating frequency varies from 183 mm^{-1} at one end of the grating to 2217 mm^{-1} at the other end of the grating.

For such a grating the angle of incidence to the centre of the grating for 23 Å would be 2° and for 45 Å it would be 5°. Thus the angle of incidence increases with wavelength in a similar way to the critical angle of reflection.

A grating whose frequency at each point on the surface varies linearly with the sine of half the angle subtended at the centre of the circle between the point and the centre of symmetry of the grating

may be used in a scanning monochromator. This possibility is covered by a British Patent (72), however, there are difficulties in realising this solution practically. The most cogent arguments against this invention are found by considering the rapid variation of grating frequency across the surface. In the Patent it is suggested that gratings of this type may be fabricated using the interference properties of coherent laser beams. However, a rapid variation of grating frequency means that the recording laser beams must intersect the substrate at rapidly changing angles which can pose serious exposure problems. Furthermore, no simple combination of point sources has been found which produces the necessary grating frequency law when using existing lasers suitable for holographic purposes. It is conceivable that this grating frequency law can be achieved by using suitably deformed wavefronts, however, consideration must be made of the accuracy with which the grooves must be positioned. Consideration must also be made of the accuracy with which the reflectometer-type linkages necessary for this type of monochromator can be made. It is generally acknowledged that the adjustment of grazing incidence spectrographs based on the Rowland circle geometry is difficult. However, it can be envisaged that the adjustment of a scanning monochromator using a variable frequency grating for soft x-ray use will be much more difficult. Finally, even if such a grating can be realised, since the diffraction efficiency diminishes with increasing grating frequency, it is possible that the higher frequency zones of the grating will contribute little useful energy to the focus. Thus, although this solution offers potential theoretical

advantages over Rowland circle mountings for monochromators, at present due to technical limitations, there may be little advantage in employing this type of variable frequency grating.

The variable frequency grating described above may be used to form a stigmatic image if the grating is made on the surface which is formed by rotating an arc of the circle about the line joining A and B. It can be seen that in this case the rulings will be circles about the axis AB and that the frequency distribution will be the same for all planes passing through A and B. Thus a variable frequency grating on this type of toroidal surface can produce geometrically perfect imaging at one wavelength. However, it can be seen that imposing the condition for vertical focus precludes the possibility of scanning in wavelength. It would be possible to image a small range of wavelengths using a grating of this type provided that the system is so designed that the aberrations are less than a certain tolerance. The performance of a grating of this type would also be severely limited by any manufacturing imperfections. This example is of interest since it represents a limiting case for grating design and also introduces a second form of toroidal surface.

The type of toroid considered by Haber generated by rotating a circle of radius ρ about a circle of radius R has been designated "Type A" in order to differentiate it from the second type of toroid which has been designated "Type B". The differences between these two surfaces can be readily appreciated by referring to Fig. 14. The imaging properties of these two types of toroidal gratings have been investigated by ray tracing and are described in Chapter 3.

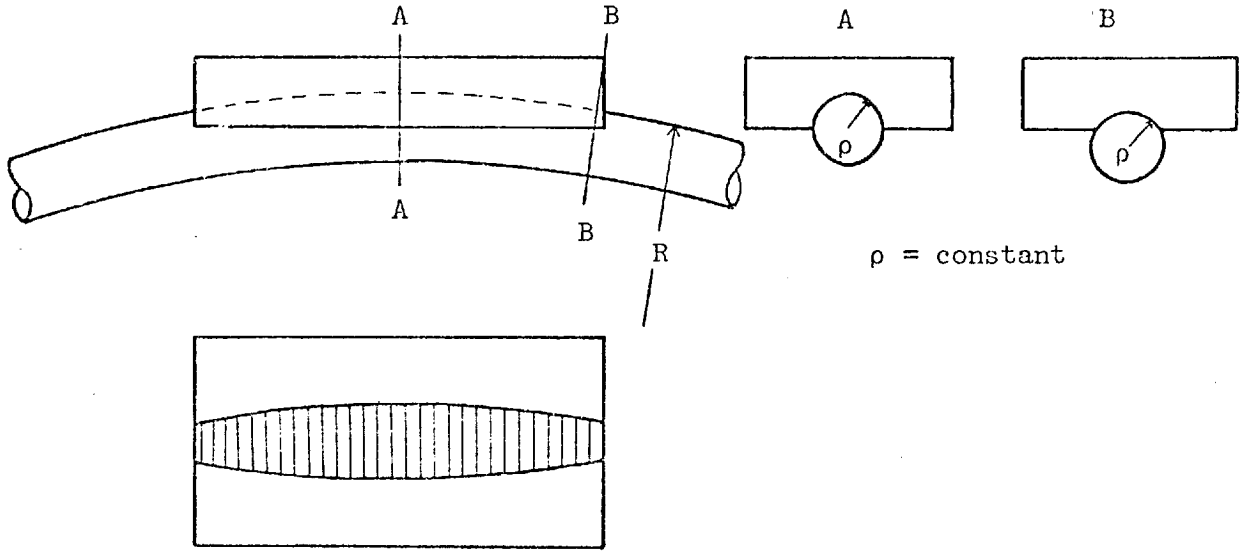

THE "TYPE A" TOROID

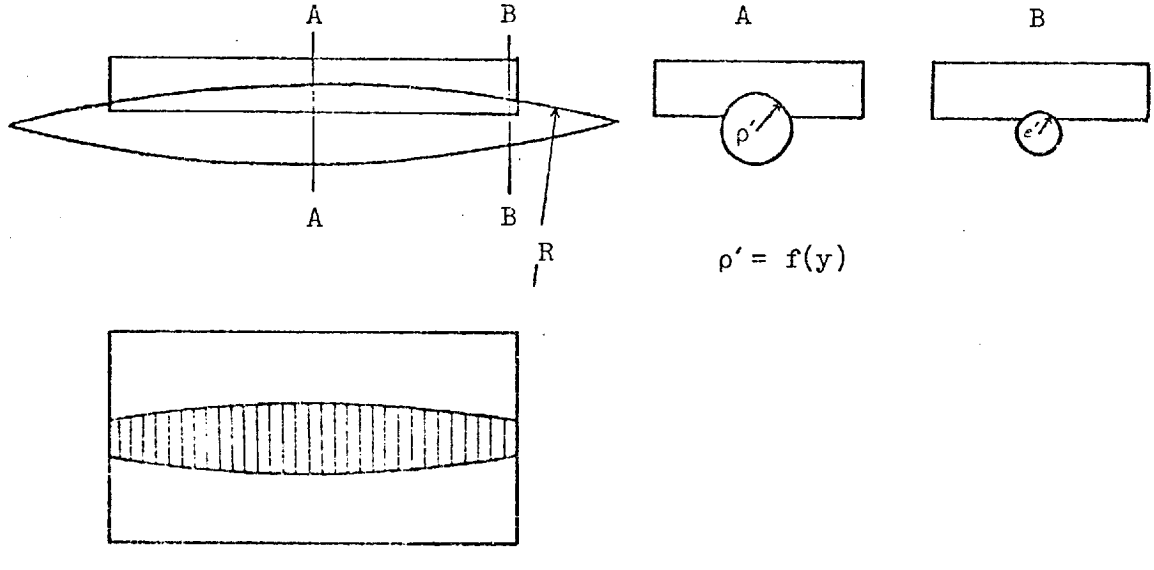

THE "TYPE B" TOROID

FIG. 14

2.5 GRATING EFFICIENCY IN THE SOFT X-RAY REGION

It has long been known that the calculation of the diffraction efficiency of gratings is one of the most important problems in optics. However, it is only recently that this problem has been rigorously solved for gratings having finite conductivity (109). The present theory gives very good agreement with experiment in the visible and ultra-violet regions, but for wavelengths below 1000 Å, where λ/d is generally small, the numerical computations require large amounts of computer time. In order to formulate a satisfactory approach for the soft x-ray region solutions of the integral equations for the field and its normal derivative on the grating surface must be found. The integral equations may be obtained by applying Green's theorem (110). The problem is to find numerical methods of solution which converge rapidly. Alternative solutions may be found by using a differential method, or even semi-analytic methods. However, unless the grating surface profile can be properly characterised and the material constants known accurately, no exact numerical calculations of grating efficiency can be performed.

Even though it is not rigorously or generally applicable, scalar diffraction theory has been used for many years and can be applied to the case of diffraction gratings in the soft x-ray region. Calculations of grating efficiency were performed in 1955 by Sprague, Tomboulian and Bedo (111) using a greatly simplified model for a grating. They also performed experimental photometric determinations of grating efficiency and obtained efficiency values of 5.4% and 1.5% in first and second orders at 110 Å from a lightly-ruled glass grating with 1181 l/mm at

a grazing angle of 4.64°. Lukirskii and Savinov (112) performed experimental determination of the performance of gratings and "echelettes", or blazed gratings, with 600 l/mm at several wavelengths in the soft x-ray region and compared the results with theoretical predictions. The experimentally observed efficiencies were considerably less than the calculated theoretical values. The discrepancy was attributed to deviations of the grating profile from the ideal form assumed in the calculations. They concluded that it was necessary to determine the diffraction efficiency experimentally but that the optimum blaze angle could be calculated. They found the efficiency of blazed gratings to be similar to that of "scratched" gratings in the wavelength region below 60 Å, but that for wavelengths >100 Å the efficiency of the blazed gratings was higher.

It has been shown by Sayce and Franks (113) that laminar phase gratings have a high efficiency in the x-ray region. The theory of this type of grating has been described by Bennett (30) who also performed experimental measurements on five laminar gratings. The agreement between theory and experiment was adequate but it was not possible to predict accurately the absolute efficiency of a grating. The significance of theory is that it enables the design parameters for a laminar grating to be chosen in order to provide the best possible results. The theory is of fundamental importance to all manufacturers of laminar gratings for use in the soft x-ray region and the salient features of the theory will therefore be described.

The grating profile is assumed to be as shown in Fig. 15. Three cases can be considered depending on whether the grating

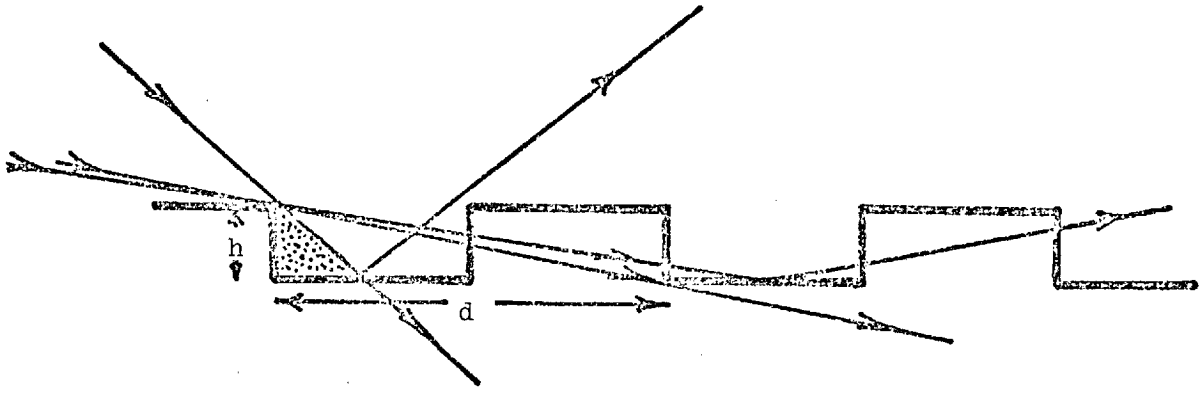

Partial Masking

THE LAMINAR GRATING

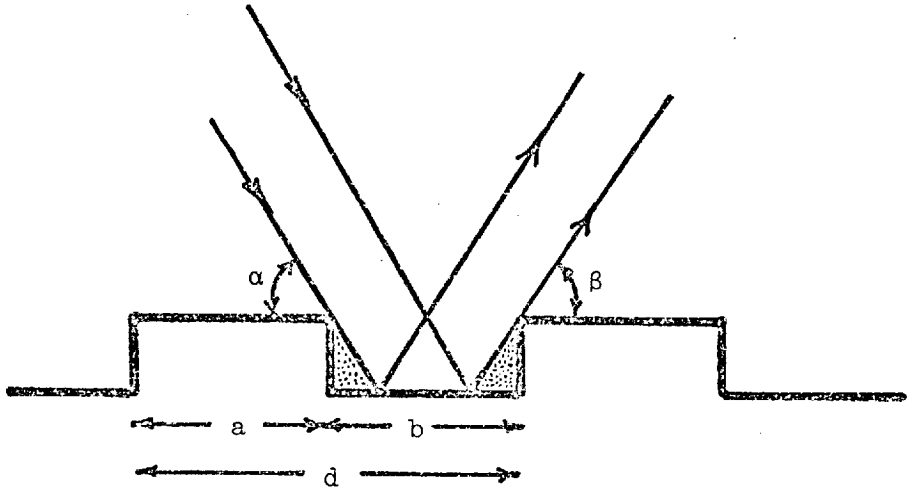

Full Masking

FIG. 15

material is non-absorbent, partially absorbent or totally absorbent. The method is identical for all cases and is a straight-forward application of the Fresnel-Kirchhoff diffraction integral to the case of Fraunhofer diffraction. Radiation is assumed to be only scattered by the lands and the bottoms of the grooves of the grating. The phase difference between the radiation scattered by the lands and the grooves is given by:

$$\delta = \frac{2\pi}{\lambda} h (\sin\alpha + \sin\beta)$$

Performing the integrations for equal land and groove widths yields the percentage of the incident radiation diffracted in order m to be:

$$E_m = 100 \frac{\sin^2(m\pi/2)}{(m\pi/2)^2} \cos^2\left(\frac{\delta + m\pi}{2}\right)$$

Thus only odd orders are diffracted from gratings with equispaced lands and grooves and the absolute efficiency (percent) is given by:

$$E_{m=odd} = \frac{400}{m^2\pi^2} \sin^2 \frac{\delta}{2}$$

The percentage of the incident radiation reflected in the zero order is given by:

$$E_{m=o} = 100 \cos^2 \frac{\delta}{2}$$

The typical oscillatory behaviour of these functions is shown in Fig. 16 for practical grazing incidence cases.

THEORETICAL DIFFRACTION EFFICIENCY OF A PHASE GRATING (NO MASKING)

Groove Depth (Å)				Frequency mm^{-1}
A	B	C	D	
100	200	400	400	300
50	100	200	200	600

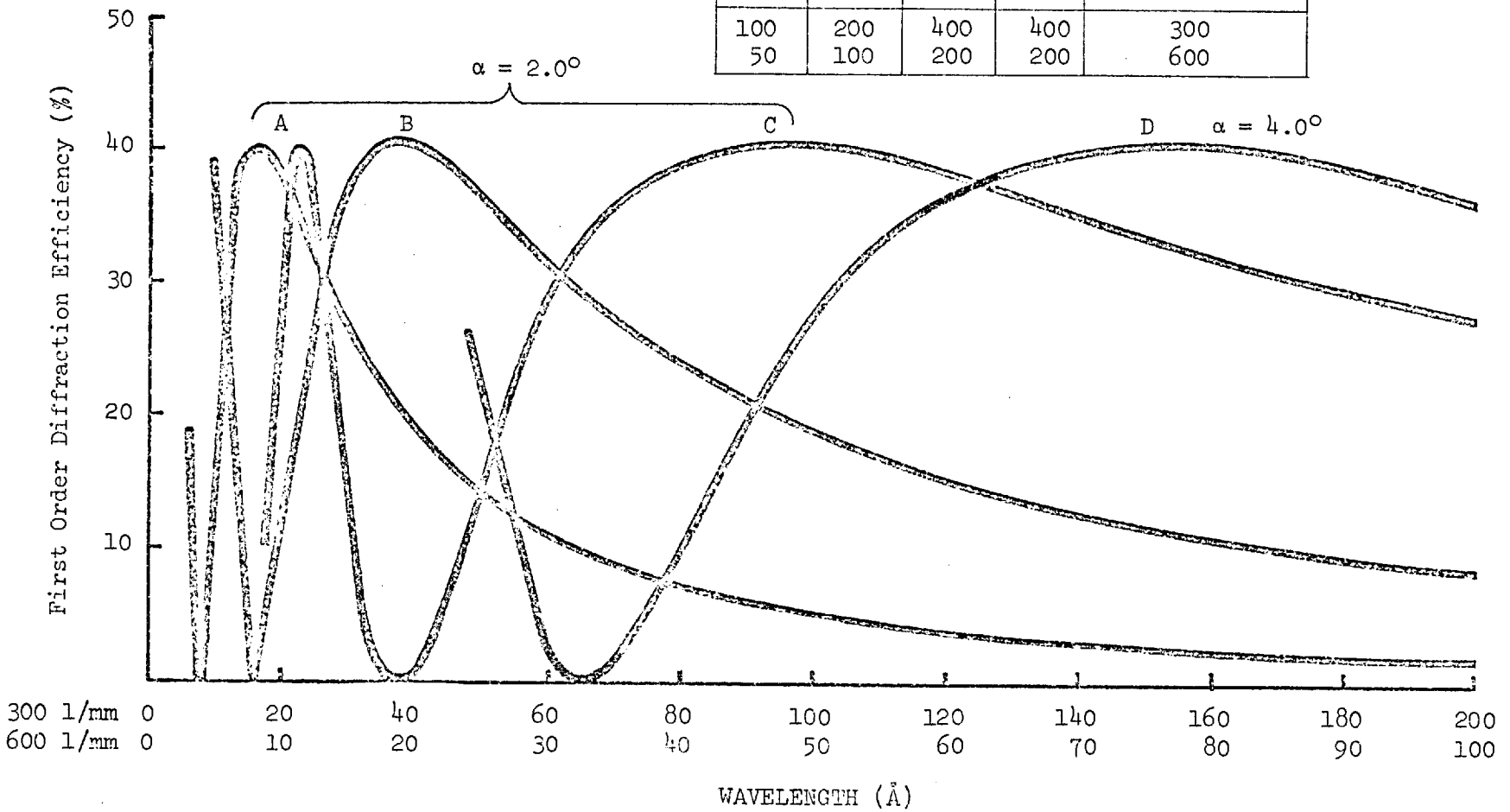

FIG. 16

The theoretical maximum efficiency of a phase grating is four times greater than that of an amplitude grating which has a theoretical maximum efficiency of $1/\pi^2$. Theoretically, the first order maxima of efficiency should be displaced to slightly longer wavelengths than the zero order minima but, associated with each maximum of first order efficiency, there is a minimum in the zero order efficiency.

For a grating with a given groove depth the wavelength diffracted at maximum efficiency increases with increasing angle of incidence. Thus a laminar phase grating may be used over a range of wavelengths with high efficiency if the angle of incidence is adjusted accordingly. At a fixed angle of incidence the wavelength diffracted with maximum efficiency increases with increasing groove depth. The largest wavelength range of high efficiency is achieved for large λ/d; therefore, the grating frequency should be as high as possible. However, shadowing effects become more important for higher frequency gratings.

The effects of shadowing and absorption of radiation in the grating material are described by Bennett in his extensions of the basic theory. If the absorption of radiation by the grating material is small, radiation incident on any part of the grating surface at angles greater than the critical angle will be refracted into the grating surface and will propagate through the grating. This situation is described by the "partial masking model" which should be applicable to laminar gratings at x-ray wavelengths less than 10 Å. Referring to Fig. 15 it can be seen that as the angle of incidence is decreased radiation passing through the side of a groove will either pass into

the bulk of the grating material or it will pass through the land and can be reflected off the bottom of the next groove. It can be seen that neglecting refraction, radiation may pass through a land and be reflected from second groove if

$$\tan\alpha < h/d$$

For a 600 l/mm grating with a groove depth of 100 Å radiation may be reflected from a second groove if the angle of grazing incidence is less than 20 minutes. Such small grazing angles are only encountered in the shortest wavelength region for x-ray spectroscopy at about 1 Å. Thus the "partial masking model" only represents an extreme case and will not be considered in further detail. The equations for grating efficiency taking into account the effects of absorption and phase changes in the grating material have been given by Bennett. However, he only found qualitative agreement between the theory and experimental results at 1.54 Å.

If complete absorption takes place for radiation incident on the grating surface at angles larger than the critical angle the grooves will only contribute to the diffracted intensity when they are directly illuminated and when the diffracted radiation is not obstructed by the following land. The fraction of the groove shadowed is given by:

$$(\cot\alpha + \cot\beta)\ h/b$$

Neglecting the material properties of the grating the percentages of incident radiation in the zero order and in the diffracted orders

are given by Bennett as:

$$E_{m=o} = 25 \left[1+\left(1-\frac{2h}{b}\cot\alpha\right)^2 + 2\left(1-\frac{2h}{b}\cot\alpha\right)\cos\left(\frac{4\pi h}{\lambda}\sin\alpha\right)\right]$$

$$E_{m=odd} = \frac{100}{m^2\pi^2}\left[1+\sin^2\left[\frac{m\pi}{2}\left(1-\frac{h}{b}(\cot\alpha+\cot\beta)\right)\right]\right.$$

$$\left.-2(-1)^{\frac{m+1}{2}}\cos\left[\frac{m\pi}{2}\left(2+\frac{h}{b}(\cot\alpha-\cot\beta)\right)+\delta\right].\sin\left[\frac{m\pi}{2}\left(1-\frac{h}{a}(\cot\alpha+\cot\beta)\right)\right]\right]$$

$$E_{m=even} = \frac{100}{m^2\pi^2}\sin^2\frac{m\pi}{2}\left(1-\frac{h}{a}(\cot\alpha+\cot\beta)\right)$$

The above equations which take into account the shadowing effects for a grating with equispaced lands and grooves would seem to be adequate to represent the geometrical conditions applicable to laminar gratings used in the soft x-ray region. In practice the grating will have a profile differing from the ideal laminar profile and the material properties of the grating surface will also modify the distribution of energy in the diffracted orders.

The scalar theory can be readily expanded to describe the case of non-equal land and groove areas. If the parameter f is defined as the ratio of the land width, a, to the grating spacing, d, it can be shown that the first order efficiency for a laminar grating, neglecting shadowing, is given by:

$$E_{m=1} = \frac{100}{\pi^2}\left[\sin^2 f\pi+\sin^2(1-f)\pi+2\cos(\pi+\delta)\sin f\pi.\sin(1-f)\pi\right]$$

The maximum intensity in the first order is achieved for equal land and groove areas. When the effect of shadowing is considered it

is evident that for the highest diffraction efficiency to be achieved from a phase grating, the amplitudes of the waves from the lands and grooves should be equalised. Thus the land to groove ratio should be optimised so that the land and groove areas contributing to the diffracted radiation are equal.

In order to design a laminar grating for use at a given wavelength, λ, and at a given angle of grazing incidence, α, the groove depth, h, should be calculated from:

$$h = \frac{\lambda}{2(\sin\alpha + \sin\beta)}$$

Once the optimum groove depth has been calculated, the ratio, f, of the land width to grating spacing can be calculated from:

$$f = \frac{a}{d} = \frac{1}{2} - \frac{h}{2d}(\cot\alpha + \cot\beta)$$

Alternatively, the land to groove ratio may be calculated from:

$$\frac{a}{b} = \frac{1 - \frac{h}{d}(\cot\alpha + \cot\beta)}{1 + \frac{h}{d}(\cot\alpha + \cot\beta)}$$

It can be seen that when the grooves of a laminar grating are completely shadowed it cannot function as a phase grating. Thus depending on the groove depth and conditions of use there is a maximum grating frequency for which a laminar grating can still function as a phase grating.

Complete shadowing of the grooves occurs for:

$$b = h(\cot\alpha + \cot\beta)$$

Thus a laminar grating, having equal lands and groove widths, with a groove depth of 150 Å used at a grazing angle of 2^{o} will no longer function as a phase grating for radiation of wavelength 50 Å if the grating frequency is higher than 862 l/mm. The effect of shadowing of the grooves must therefore be carefully considered when designing laminar gratings and a reduction in grating efficiency is to be expected for grating spacings, d, when:

$$4h\cot\alpha > d > 2h\cot\alpha$$

It is to be expected that the efficiency of laminar gratings will decrease with increasing grating frequency simply due to the effects of shadowing and absorption and that the efficiency will become identical to a comparable amplitude grating. Since the efficiency of an amplitude grating is a maximum for equal land and groove widths it is to be expected that high frequency laminar gratings will have maximum efficiency for equal land and groove areas.

The effects of these parameters on the performance of laminar holographically-formed x-ray gratings with nominal frequencies of 300, 600 and 1200 l/mm, with systematically varying land to groove ratios, and groove depths, have been investigated experimentally.

The results of this work and a more complete discussion are the subject of Chapter 7.

CHAPTER 3

RAY TRACING

3.1 INTRODUCTION

Ray tracing is a well-established technique for examining the performance of optical systems; however, until recently this method has seldom been used in the grazing incidence region. With the advent of holographic gratings new design opportunities became possible and a reliable means of image evaluation was essential. Hence, we have been using exact computer ray tracing to explore some of the new design possibilities opened up by the holographic method and also to examine quantitatively the aberrations of complete grazing incidence systems.

The computer programs used in this work are based on the method proposed by Welford (40) for straight rulings but incorporating the vector equations suggested by Spencer and Murty (41). This approach enables rays to be traced through gratings on any surface and with any variation of frequency provided the coordinates of the point of incidence and the direction cosines of the normal and tangent to the rulings and the frequency can be calculated. The method is equivalent to that used by Kastner and Neupert (42) who considered elemental plane gratings in the tangent plane at each point on the spherical grating surface. Naturally, the results obtained from ray tracing are only valid provided the conditions for the geometrical optics approximation are satisfied. Fortunately, this is generally the case in the soft x-ray region.

3.2 DESCRIPTION OF THE RAY TRACING METHOD

The usual system to be analysed in the grazing incidence region consists of three surfaces.

The first surface is the object plane which will usually contain the entrance slit to a spectrograph and we can consider the object point to be a self-luminous point on the entrance slit. The second surface is the grating and the third surface the image surface which will normally be the Rowland cylinder in the case of spectrographs and will be a plane for spectrometers.

In order to trace a ray through the system we must calculate the direction cosines of a ray from an object point to a point on the grating surface. Then from the calculated direction cosines, the co-ordinates of the point on the grating and the grating parameters at that point the direction cosines of a ray of given wavelength diffracted in a given order must be calculated. This operation is analagous to the "refraction process" used when ray tracing through lenses and may be called the diffraction operation. When the direction cosines of the diffracted ray have been calculated, the point at which the ray meets the image surface must be found. This corresponds to the transfer operation in ordinary ray tracing. Thus to trace a ray through the complete system we must apply a transfer operation from the object point to a point on the grating surface, then apply the diffraction operation and finally apply a transfer operation to calculate the co-ordinates of the ray intersection with the image surface. These three operations are described in the following sections. However, we must first define the coordinate systems to be used. It is often convenient to associate a coordinate system with each surface.

Starting from the origin in the object coordinate system we trace a reference, or chief ray, a distance, d, along the z-axis to the centre of the grating where it makes a given angle of incidence, i, with the normal at the pole of the grating. We then define a second coordinate system centred on the grating pole with the z-axis along the normal. The diffraction operation to determine the direction cosines of the diffracted chief ray is performed in this coordinate system. Finally, we define a third coordinate system on the chief diffracted ray, a distance d' from the grating pole in order to measure the transverse aberrations with respect to the chief ray.

When the chief ray has been traced, a uniform mesh of skew rays is generated over the surface of the grating from the object point. At each point on the grating the normal to the surface and the direction of the vector along the rulings are calculated. The direction cosines of the diffracted rays are then calculated from given values of the local grating frequency. The intersections of the diffracted rays with the image plane are then calculated and a spot diagram is drawn. The above process can be repeated for many object points to simulate a finite sized object.

3.3 THE TRANSFER OPERATION FROM OBJECT COORDINATE SYSTEM TO GRATING COORDINATE SYSTEM

To represent the physical situation it is required to generate a set of rays emanating from a point A (x'_A, y'_A, z'_A) representing a uniformly divergent pencil. Each ray is specified by the position of A (α, d, h) and the direction cosines (a'_1, a'_2, a'_3) in the coordinate systems O'X'Y'Z. See Fig. 17.

The coordinates of A in OXYZ are given by

$$x_A = h \qquad y_A = d\cos\alpha \qquad z_A = d\sin\alpha$$

$$\underline{AP} = (x-h)\underline{\hat{x}}+(y-d\cos\alpha)\underline{\hat{y}}+(z-d\sin\alpha)\underline{\hat{z}}$$

The direction cosines of the incident ray are:

$$a_1 = \frac{-(x-h)}{\langle AP\rangle} \qquad a_2 = \frac{-(y-d\cos\alpha)}{\langle AP\rangle} \qquad a_3 = \frac{-(z-d\sin\alpha)}{\langle AP\rangle}$$

The components of AP in O'X'Y'Z' are given by applying the rotation matrix

$$R = \begin{pmatrix} 1 & 0 & 0 \\ 0 & \cos\psi & \sin\psi \\ 0 & -\sin\psi & \cos\psi \end{pmatrix} \qquad \text{where } \psi = 90+\alpha$$

Since: $\cos(90+\alpha) = -\sin\alpha \qquad \sin(90+\alpha) = \cos\alpha$

$$(\underline{AP})' = (x-h)\underline{\hat{x}}+(z\cos\alpha-y\sin\alpha)\underline{\hat{y}}+(d-y\cos\alpha-z\sin\alpha)\underline{\hat{z}}$$

TRANSFER OPERATION FROM OBJECT TO GRATING COORDINATE SYSTEM

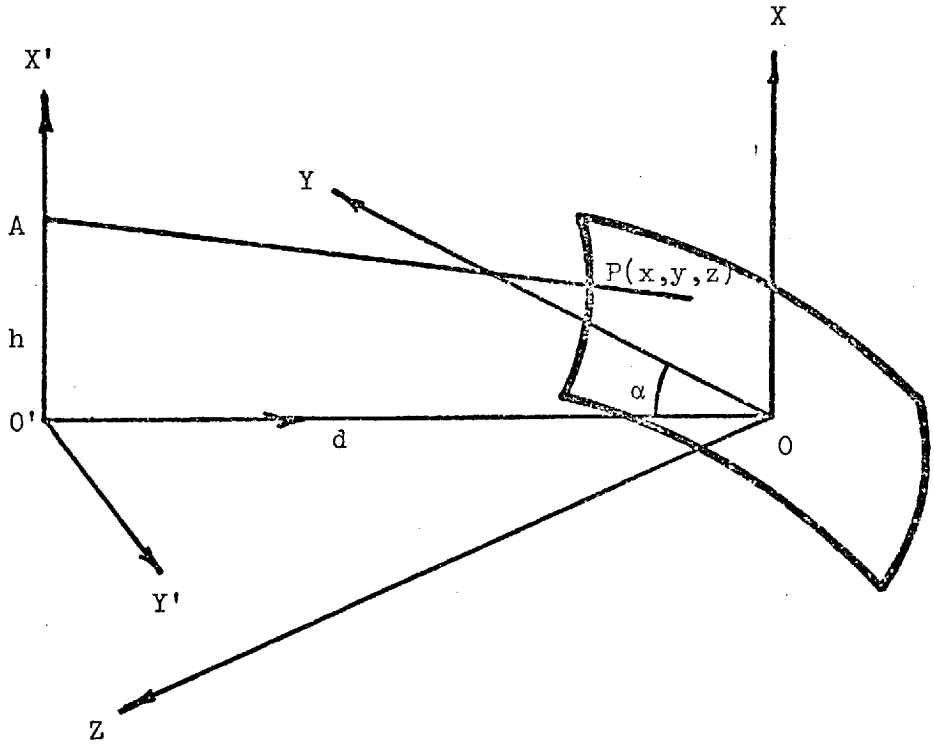

FIG. 17

$$\text{Now } \frac{a_1'}{a_2'} = \frac{x - h}{z\cos\alpha - y\sin\alpha} = f \qquad \frac{x - h}{d - y\cos\alpha - z\sin\alpha} = \frac{a_1'}{a_3'} = g$$

$$\therefore \quad x - h = f\,z\cos\alpha - f\,y\sin\alpha \tag{1}$$

$$x - h = dg - g\,y\cos\alpha - g\,z\sin\alpha$$

$$y = \frac{dg - z\,(f\cos\alpha - g\sin\alpha)}{g\cos\alpha - f\sin\alpha} \tag{2}$$

The coordinates of the point of intersection of the ray with the surface can be found by iteration using equations (1) and (2) and the equation of the surface. Choosing z, = 0 as a first approximation equation (2) gives a value of y, which can be substituted in equation (1) to give a value of x, which can be substituted in the equation of the surface to give a new value of z_2 which can be used to repeat the process until a sufficient accuracy is reached.

Alternatively, a mesh of points on the x-y tangent plane at the centre of the grating may be specified and the values of the x and y coordinates substituted in the equation for the surface to yield the z coordinates and hence the direction cosines for the rays incident on the surface.

The first method enables a uniformly divergent fan of rays to be projected onto the grating which will normally resemble the physical conditions of illimination closely. However, by careful choice of the mesh of rays in the second method, an equally accurate representation can be achieved and the iteration process avoided. Both methods have been used in the programs employed in this work.

3.4 NOTATION FOR GRATING COORDINATE SYSTEM

In the grating coordinate system with origin O in the grating surface, the z-axis is normal to the grating surface and the x-axis and y-axis are tangents to the surface. A point of incidence of a ray on the grating surface is denoted by P (x, y, z), a point on the incident ray is denoted by A (x_A, y_A, z_A), and a point on the diffracted ray from P of wavelength λ is denoted by B (x , y, z). We associate with the grating at point P a right triple of unit vectors $\hat{q}$, $\hat{p}$ and $\hat{r}$ where $\hat{q}$ is a vector parallel to the rulings, $\hat{p}$ is a vector normal to the rulings and $\hat{r}$ is a vector normal to the grating surface. The directions of the incident and diffracted rays are represented by unit vectors $\hat{a}$ and $\hat{b}$.

THE GRATING COORDINATE SYSTEM

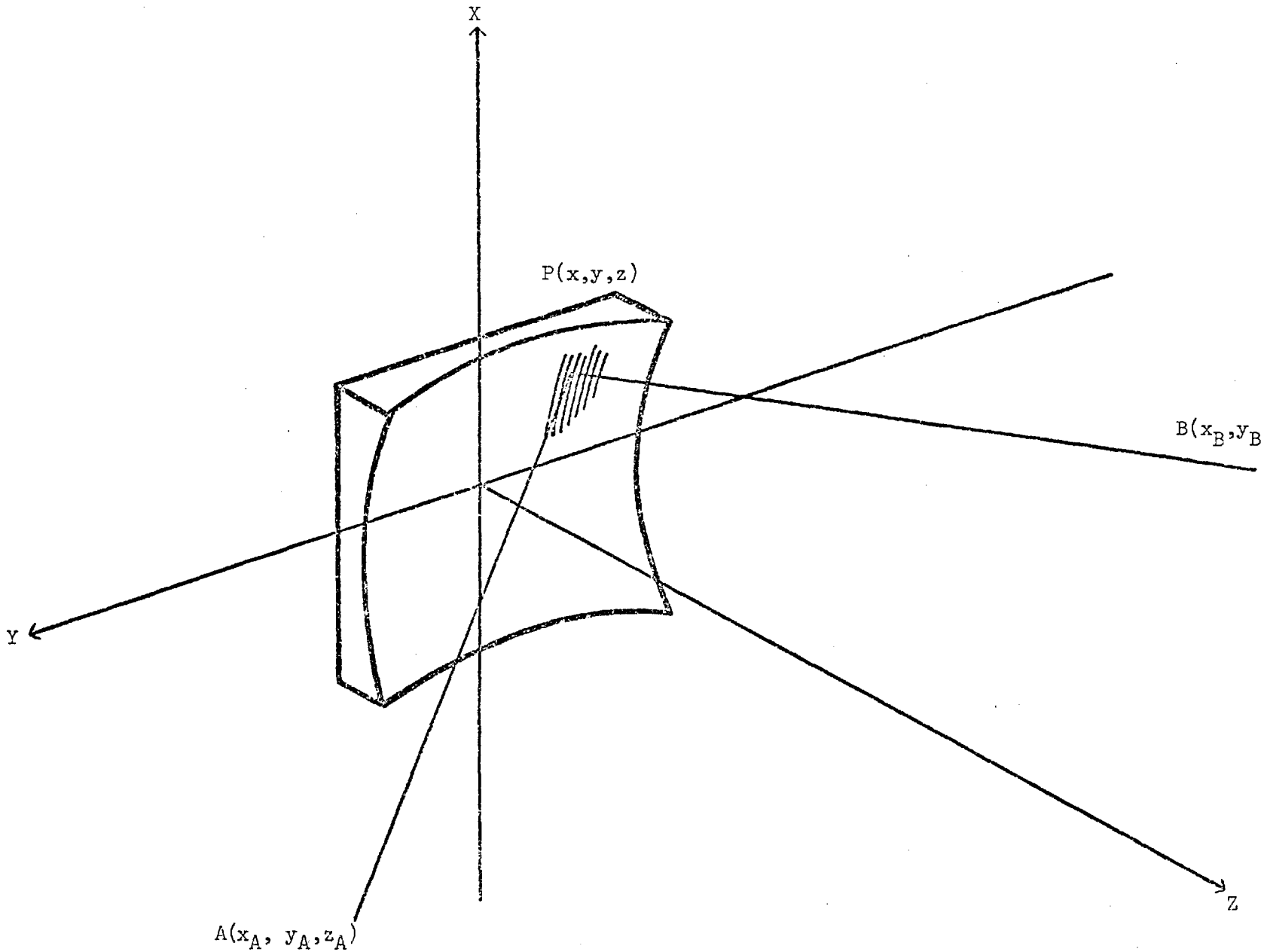

FIG. 18

3.5 THE DIFFRACTION OPERATION

The diffraction equation which gives the relation between the directions of the incident and diffracted rays from a grating may be written vectorially for the general case as:

$$n' \underline{b} \times \underline{\hat{r}} = n \underline{\hat{a}} \times \underline{\hat{r}} + \frac{m \lambda}{d} \underline{\hat{q}} \qquad (1)$$

where n is the refractive index in the medium in which the ray is incident and n' is the refractive index in the medium in which the ray is diffracted. λ is the vacuum wavelength of the incident radiation.

In the soft x-ray region we are primarily interested in reflection gratings used in vacuum which allows the above equation to be simplified to:

$$- \underline{b} \times \underline{\hat{r}} = \underline{\hat{a}} \times \underline{\hat{r}} + \frac{m \lambda}{d} \underline{\hat{q}} \qquad (2)$$

$$\underline{\hat{r}} \times \underline{b} = \underline{\hat{a}} \times \underline{\hat{r}} + \frac{m \lambda}{d} \underline{\hat{q}}$$

when n = -1 as is conventional in optical design where no formal distinction is made between formulae applying to reflecting and refracting surfaces.

It can be seen that equation (2) becomes the familiar grating equation in the meridian plane when $\underline{\hat{q}}$ is perpendicular to the meridian plane

$$\sin i' + \sin i = \frac{m \lambda}{d}$$

where i and i' have equal signs when on the same side of the surface normal and opposite sides when on opposite sides.

In this case the vectors $\hat{a}$ and $\hat{b}$ are directed towards the object and image points respectively.

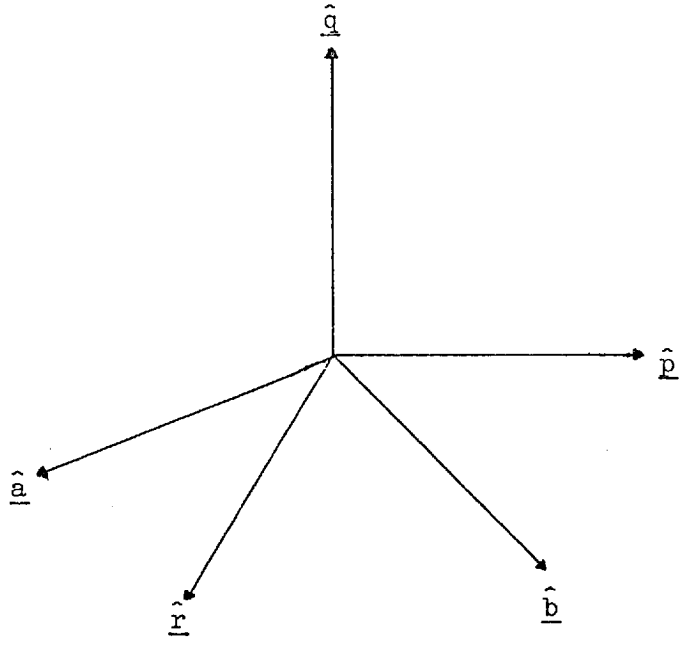

FIG. 19

The above equation is similar to that given by Spencer and Murty (41) however, they have observed the convention that n' = 1 on reflection which means that the image space behind a reflecting surface is represented as the mirror image of the actual image space. This technique is useful since it enables complex mirror systems to be folded apart, however, the standard convention will be observed in this work.

The method for solving the diffraction equation in order to find the direction cosines of the diffracted ray was first outlined by Spencer and Murty and all subsequent authors have followed their approach.

Substituting $\hat{q} = -\hat{p} \times \hat{r}$ in equation (2) gives

$$\left\{ \hat{a} \times \hat{b} - \frac{m \lambda}{d} \hat{p} \right\} \times \hat{r} = 0 \qquad (4)$$

which is satisfied by any vector of the form

$$\underline{b} = -\underline{a} + \frac{m\lambda}{d}\hat{p} + Q\underline{r} \qquad (5)$$

where Q is a scalar parameter; $\underline{r}$ need not have unit magnitude since the multiplier Q will renormalise it.

The above equation is the same as that originally derived by Welford (40) and recently derived by Noda (45) for holographic gratings by application of Fermat's principle to the light path function.

The physical significance of the scalar parameter, Q, can be understood by taking the vector product of (1) with $\hat{r}$.

$$\hat{r} \times (n'\underline{b} \times \hat{r}) = \hat{r} \times (n\hat{a} \times \hat{r}) + \frac{m\lambda}{d}\ \hat{r} \times \hat{q}$$

Hence:

$$n'b' - (\hat{r}.n'\underline{b})\hat{r} = n\hat{a} - (\hat{r}.n\hat{a}).\hat{r} - \frac{m\lambda}{d}\ \hat{p}$$

$$\cos i = \hat{r}.\hat{a} \qquad \cos i' = \hat{r}.\underline{b}$$

where i is the angle the incident ray makes with the normal and i' is the angle between the diffracted ray and the normal.

$$n'\underline{b} = n\hat{a} + (n' \cos i' - n \cos i)\,\hat{r} - \frac{m\lambda}{d}\ \hat{p} \qquad (6)$$

Thus, as pointed out by Welford, Q corresponds to the normalised value of the generalised power. For the case of reflection at a mirror Q becomes -2 cos i.

The technique for solving equation (5) is to square it which yields

a quadratic equation in Q

$$Q^2 + 2Q\left(\frac{m\lambda}{d}\,\hat{\underline{p}}.\hat{\underline{r}} - \hat{\underline{a}}.\hat{\underline{r}}\right) + \left(\frac{m\lambda}{d}\right)^2 - \frac{2m\lambda}{d}\,\hat{\underline{a}}.\hat{\underline{p}} = 0$$

since $\hat{\underline{p}}.\hat{\underline{r}} = 0$

$$Q^2 - 2Q\,\hat{\underline{a}}.\hat{\underline{r}} - \frac{2m\lambda}{d}\,\hat{\underline{a}}.\hat{\underline{p}} + \left(\frac{m\lambda}{d}\right)^2 = 0 \qquad (7)$$

Hence

$$Q = \hat{\underline{a}}.\hat{\underline{r}} \pm \left((\hat{\underline{a}}.\hat{\underline{r}})^2 - \left(\frac{m\lambda}{d}\right)^2 - \frac{2m\lambda}{d}\,\hat{\underline{a}}.\hat{\underline{p}}\right)^{1/2} \qquad (8)$$

When m = 0 either Q = 0 or Q = 2 $\hat{\underline{a}}.\hat{\underline{r}}$. The first solution corresponds to a transmission grating when the ray passes undeviated and the second solution to a reflection grating. Thus the larger value of Q is the solution we require and the direction cosines of the diffracted ray may be found by substituting this value in equation (5).

An alternative method, which has been used in our computer programs, for obtaining the direction cosines of the diffracted ray is to take the scalar product of equation (6) with $\hat{\underline{q}}$ and $\hat{\underline{p}}$

$$\underline{b}.\hat{\underline{q}} = -\hat{\underline{a}}.\hat{\underline{q}} = c_1 \qquad (9)$$

$$\underline{b}.\hat{\underline{p}} = -\hat{\underline{a}}.\hat{\underline{p}} + \frac{m\lambda}{d} = c_2 \qquad (10)$$

$$\underline{b}.\underline{b} = 1 \qquad (11)$$

where c_1 and c_2 are known scalar parameters.

Therefore we have three equations from which we can calculate the three direction cosines of the diffracted ray. The following equations were used to perform the diffraction operation in the computer programs.

Taking the component equations of (9), (10) and (11)

$$q_1 b_1 + q_2 b_2 + q_3 b_3 = c_1 \qquad (12)$$

$$b_1 p_1 + b_2 p_2 + b_3 p_3 = c_2 \qquad (13)$$

$$b_1^2 + b_2^2 + b_3^2 = 1 \qquad (14)$$

Eliminating b_2 between (12) and (13)

$$(p_2 q_1 - q_2 p_1) b_1 + (p_2 q_3 - q_2 p_3) b_3 = p_2 c_1 - q_2 c_2$$

Let $d_1 = p_2 q_1 - q_2 p_1 \quad d_2 = p_2 q_3 - q_2 p_3 \quad d_3 = p_2 c_1 - q_2 c_2$

$$b_1 = \frac{d_3}{d_1} - \frac{d_2}{d_1} b_3$$

Let $f_1 = \frac{d_3}{d_1} \qquad f_2 = \frac{d_2}{d_1}$

Then $b_1 = f_1 - f_2 d_3 \qquad (15)$

Eliminating b_1 between (12) and (13)

$$(p_1 q_2 - p_1 p_2) b_2 + (p_1 q_3 - q_1 p_3) b_3 = p_1 c_1 - q_1 c_2$$

Let $e_1 = p_1 q_2 - q_1 p_2 \quad e_2 = p_1 q_3 - q_1 p_3 \quad e_3 = p_1 c_1 - q_1 c_2$

$$b_2 = \frac{e_3}{e_1} - \frac{e_2}{e_1} b_3$$

Let:

$$f_3 = \frac{e_3}{e_1} \qquad f_4 = \frac{e_2}{e_1}$$

$$b_2 = f_3 - f_4 b_3 \tag{16}$$

Substituting (15) and (16) in (14) yields:

$$(1+f_2^2+f_4^2)b_3^2-(2f_1f_2+2f_3f_4)b_3+f_1^2+f_3^2-1 = 0$$

We obtain a quadratic equation for b_3. In order to decide upon the required solution we consider the case when $m = 0$ which must give a solution which satisfies the law of reflection. Once b_3 has been calculated its value is substituted in equations (15) (16) to yield values of b_1 and b_2.

3.6 TRANSFER OPERATION FROM GRATING SURFACE TO IMAGE SURFACE

From the point P (x, y, z) on the grating surface we now know the direction cosines of the diffracted ray and wish to calculate the coordinates of the ray intersection with the image surface. There are two image surfaces of importance in the grazing incidence region; the first is a plane surface perpendicular to the chief ray a distance d' from the grating pole and the second is a cylinder which touches the grating surface tangentially at the grating pole and has a radius equal to half the grating radius. The plane image surface is generally more useful because the image is specified in terms of the familiar transverse aberrations used by optical designers. However, specifying the Rowland cylinder as the image plane can be most useful when evaluating refocussing conditions for spectrographs. Hence both cases will be treated.

In order to evaluate the transverse aberrations we define a new coordinate system whose origin is a distance d' along the chief ray and whose z-axis lies along the chief ray. Hence, the z-axis has been rotated by an angle $\psi = 90 - \beta$ and translated a distance d'.

Referring to the diagram the coordinates of P are defined by the vector $\underline{x}$, and the direction cosines of the diffracted ray by the unit vector $\underline{b}$. In the rotated coordinate system

$$\underline{x}' = R(\underline{x}) \qquad \underline{b}' = R(\underline{b})$$

where R is the rotation matrix with $\psi = 90 - \beta$.

In the image coordinate system after rotation and translation the equation of the diffracted ray is

$$\underline{x}'' = \underline{x}' + s.\underline{b}$$

TRANSFER OPERATION FROM GRATING TO IMAGE COORDINATE SYSTEM

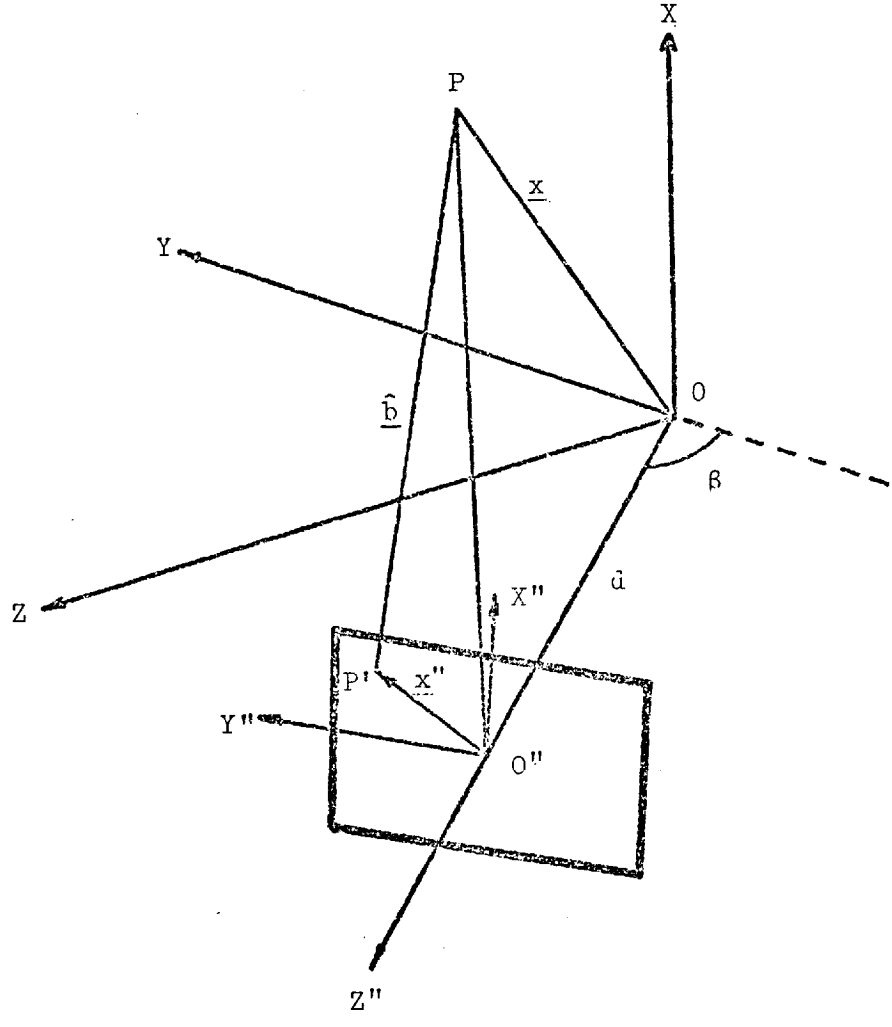

FIG. 20

where s is the distance from point P to a general point on the image plane and $\underline{x}'' = \underline{x}' - tr\ (0, 0, d)$ in matrix notation.

Since $(x'')_3 = 0$ on the image plane

$$s = - \frac{(x')_3}{b_3}$$

Hence, the above equation gives the transverse aberrations directly.

The following transformation equations were used in the computer program:

$$x' = x$$

$$y' = y \sin \beta + z \cos \beta$$

$$z' = -y \cos \beta + z \sin \beta - d$$

$$b_1' = b_1$$

$$b_2' = b_2 \sin \beta + b_3 \cos \beta$$

$$b_3' = -b_2 \cos \beta + b_3 \sin \beta$$

$$s = - z'/b_3'$$

$$x'' = x' + s\, b_1'$$

$$y'' = y' + s\, b_2'$$

3.7 TO FIND THE INTERSECTION OF THE DIFFRACTED RAY WITH THE ROWLAND CYLINDER

The equation of the Rowland cylinder is:

$$y^2 + z^2 - Rz = 0 \quad \text{where R = grating radius} \tag{1}$$

The equation of the diffracted ray is:

$$\underline{x} = \underline{x_1} + s.\underline{b} \tag{2}$$

which can be written in component form as:

$$x = x_1 + s\, b_1 \tag{3}$$

$$y = y_1 + s\, b_2 \tag{4}$$

$$z = z_1 + s\, b_3 \tag{5}$$

Substituting equations (4) and (5) into equation (1) yields a quadratic equation in s:

$$s^2(b_2^2+b_3^2)+s(2y_1b_2+2z_1b_3-Rb_3)+y_1^2+z_1^2-Rz_1 = 0$$

The value of s with the larger magnitude is the required value on the Rowland circle since s is the distance from the point on the grating to the image point. Substitution of the calculated value of s yields the coordinates of the ray intersection with the Rowland cylinder.

In a spectrograph which uses photographic plates as the recording medium the plates are bent to lie on the Rowland cylinder in order to record the images but the plates are subsequently measured flat.

Hence, in order to simulate the images recorded in a spectrograph we must transfer the coordinates (x_B, y_B, z_B) of the ray intersection on the Rowland cylinder into distances measured along the surface from the chief ray intersection. It is convenient to consider a cylindrical coordinate system centred on the centre of the Rowland circle with coordinates (R/2, θ, x)

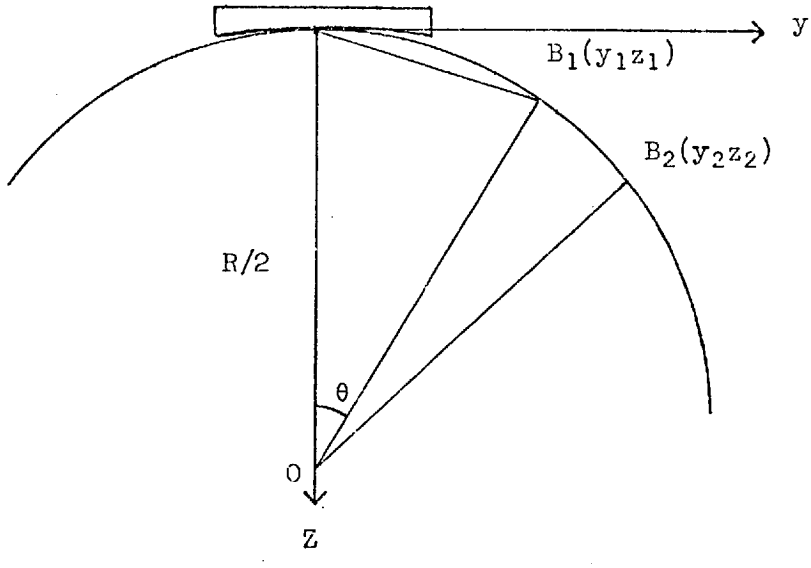

FIG. 21

From the diagram it can be seen that the required distance is the arc $B_1\ B_2$ where B_1 represents the chief ray intersection point and B_2 any other ray intersection point.

$$\text{arc}\ \ B_1\ B_2 \ = \ R\left[\tan^{-1}\frac{z_2}{y_2} \ - \ \tan^{-1}\frac{z_1}{y_1}\right]$$

where R is the grating radius

Naturally, the x coordinate remains unchanged during this transformation.

The preceeding methods for obtaining the coordinates of the ray intersections with the image plane have avoided the unnecessarily powerful extended matrix method introduced by Kastner and Neupert (42) and recently used by Noda (45, 46). Although the general matrix method is valid for all surfaces, it is felt that for the simple image surfaces generally encountered alternative computation methods are more efficient.

3.8 SPECIFICATION OF GRATING VECTORS FOR CLASSICAL GRATINGS

We can associate with each point on the grating surface three unit vectors which specify the normal to the surface $\hat{\underline{r}}$, the direction of the tangent to the rulings $\hat{\underline{q}}$ and the normal to the rulings $\hat{\underline{p}}$, and also a local value of the grating frequency. These quantities depend on the grating surface and the method by which the rulings were generated.

Most gratings in use today were produced on ruling engines which generate rulings which are the intersections of the grating surface with essentially parallel planes. Hence, the rulings are straight and equispaced on a plane surface neglecting any ruling errors. We shall refer to these as classical-type gratings.

For the classical grating $\hat{\underline{q}}$ has no component in the y direction since it is directed along a line on the xz plane. Hence:

$$q_1 = -(\hat{\underline{p}}\times\hat{\underline{r}})_1 = r_2p_3 - r_3p_2 = 0$$

$$\underline{p}\cdot\underline{r} = p_1r_1+p_2r_2+p_3p_3 = 0$$

$$\underline{p}\cdot\underline{p} = p_1p_1+p_2p_2+p_3p_3 = 1$$

$$p_1 = 1/\left|1+r_1^2/(r_2^2+r_3^2)\right|^{\frac{1}{2}}$$

$$p_2 = -r_1r_2p_1/(r_2^2+r_3^2)$$

$$p_3 = -r_1r_3p_1/(r_2^2+r_3^2)$$

Since the generating planes intersect the surface obliquely, the local grating frequency is given by:

$N = N_p\ \underline{j}\cdot\underline{p}$ where $\underline{j}$ is the unit normal to the generating planes

where $N_p = \frac{1}{d_p}$ where d_p = grating spacing

More generally following the method of Ludwig (44), we can define a grating generation vector $\underline{G}$ which is normal to the parallel planes ruled in the classical case. The grating ruling vector $\underline{\hat{q}}$ is given by:

$$\underline{q} = \underline{G} \times \underline{r}$$

The grating ruling separation vector $\underline{\hat{p}}$ normal to the rulings on the surface is given by:

$$\underline{\hat{p}} = \underline{\hat{q}} \times \underline{\hat{r}}$$

3.9 SPECIFICATION OF THE GRATING VECTORS AND SPATIAL FREQUENCY OF HOLOGRAPHIC GRATINGS

Holographic gratings are produced by recording the interference pattern from two coherent beams of light. In general the two beams will originate from two point sources C and D. If points C and D are located at infinity, the interference pattern is that of two plane waves which are straight fringes corresponding to the classical ruling case.

We define vector $\underline{C}$ as the vector from point P (x, y, z) on the grating surface to source point C (x_C, y_C, z_C) and vector $\underline{D}$ as the vector from the same point to source point D (x_D, y_D, z_D).

$$\hat{q}' = \hat{C} \times \hat{D}$$

where $\hat{q}'$ is a vector analagous to $\hat{q}$ but not necessarily on the surface.

Then:

$$\hat{p} = \hat{r} \times \hat{q}$$

defines the tangent plane along which the spatial frequency is calculated.

Since the geometrical optics approximation allows the laws governing the propagation of a plane wave across an infinite plane boundary to be applied to the propagation of a vanishingly thin pencil of light across a local region of a nonplanar boundary, we can consider two rays originating from the point sources C and D and intersecting at point P to be plane waves incident upon a plane surface.

The two waves can be represented by:

$$\phi_1 (x,y) = a_1(x,y)e^{-i\delta_1} e^{i\omega t}$$

$$\phi_2 (x,y) = a_2(x,y)e^{-i\delta_2} e^{i\omega t}$$

where δ_1 and δ_2 are phase constants and for monochromatic waves $e^{i\omega t}$ is a common factor and can be omitted.

Superposing the two coherent waves yields the resultant complex amplitude:

$$\phi = a_1e^{-i\delta_1} + a_2e^{-i\delta_2}$$

The resultant intensity is:

$$I = \phi\phi^* = a_1^2 + a_2^2 + a_1a_2\left[e^{i(\delta_2-\delta_1)} + e^{-i(\delta_2-\delta_1)}\right]$$

$$= a_1^2 + a_2^2 + 2a_1a_2\cos(\delta_2-\delta_1)$$

For $a_1 = a_2$ $\qquad I = 4a^2\cos^2\left[\frac{\delta_2-\delta_1}{2}\right]$

The intensity distribution will have maxima when $\delta_2 - \delta_1$ is an even multiple of π and minima when an odd multiple of π. The resultant intensity is thus dependent upon the phase difference or the difference in optical path length between the two beams and not upon any absolute value of phase or optical path length provided the waves are truly monochromatic.

Referring to Fig. 22 it can be seen that the optical path difference between the rays C'P'D' and C P D is

$$\frac{2\pi}{\lambda} (a + b)$$

$$a = d \cos \alpha$$

$$b = d \cos \beta$$

If the intensity at P is a maximum then the intensity at P' will be a maximum if

$$\frac{2\pi}{\lambda} (a + b) = 2\pi n$$

$$d (\cos \alpha + \cos \beta) = n \lambda$$ where d is the fringe spacing.

The above equation may be used to calculate the spatial frequency at each point on the surface of the holographic grating provided the fringe spacing is very small compared to the radius of curvature of the surface and to the source distances. However, this will be true for most practical cases.

The following equations were used in the computer program:

$$\cos \alpha = \underline{\hat{c}} \cdot \underline{\hat{p}}$$

$$\cos \beta = \underline{\hat{d}} \cdot \underline{\hat{p}}$$

$$\text{Spatial frequency} = \frac{1}{d} = \frac{\cos \alpha + \cos \beta}{\lambda c}$$

where λc is the wavelength of the laser.

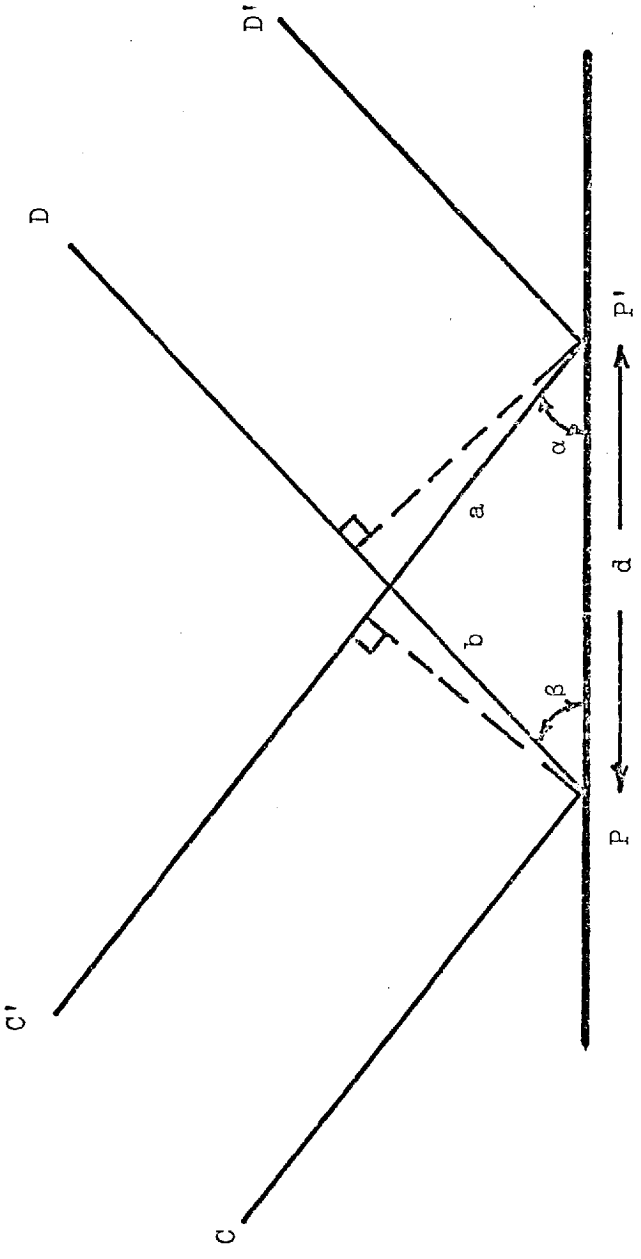

FIG. 22

The method proposed by Ludwig (44) to calculate the local grating spacing by finding the point on the optical surface whose optical path differs by one wavelength from the first point on the surface, agrees with the method described above for the case of plane waves incident upon an elemental plane grating. However, the iteration equations described by Ludwig are unnecessary since if we apply the geometrical optics approximation and treat each point on the grating as an elemental plane grating and the incident rays as plane waves, all the parameters are explicitly defined. If we do not apply the geometrical optics approximation then the other equations given by Ludwig are incorrect and we should not apply ray tracing methods. In this light it is easy to understand how Ludwig can state: "One recalculation is usually sufficient to reduce the error to the computer noise level." If one considers a plane grating with a linear variation of frequency, it can be seen that the iteration method described by Ludwig will yield different values for the grating spacing depending on the direction of the iteration. However, if the grating spacing is large compared to the change in grating spacing, this effect will be insignificant.

We can define a grating generating vector G

$$\underline{G} = \underline{C} \times \underline{D}$$

directed from source point C to source point D.

For light diverging from C and D it can be seen that the intensity will be a maximum for light of wavelength λ_c at any point whose distances from C and D differ by $n\lambda_c$. The locus of the point of maximum in-

tensity is a hyperboloid of revolution having C and D as foci (since a hyperboloid may be defined as the surface generated by a point which moves in such a way that the difference between its distances from two fixed points is a constant). The interference field produced by two beams converging on C and D is naturally the same.

The superposition of one divergent beam with one convergent beam yields an interference field which can be described as a family of ellipsoids of revolution with foci C and D. In the plane perpendicular to G the loci of the interference maximum are circles about G in the familiar zone plate pattern.

This concludes the theoretical aspects of the ray tracing methods used during this work.

3.10 RAY TRACING RESULTS AND DISCUSSIONS

During the course of the present work the aberrations of numerous grating systems have been examined by ray-tracing. It is not possible to give the numerical results from all these calculations because they would take up too much space. Instead the aberrations of several representative grating systems are presented in the form of spot diagrams.

It is generally accepted that spot diagrams give a very useful impression of the geometrical image quality of optical systems. Line profiles may be derived from spot diagrams and these can yield the optical transfer function (OTF) for the system by applying the Fourier transformation. Thus the usual techniques of optical design may be applied using aberration tolerances based on the OTF or some geometrical criterion. However, it must be realised that the spot diagram and OTF only give information about the image at one focal position. In order to be able to determine the effects of refocussing the directions of the rays must also be specified. To design a grating system the designer must have a thorough understanding of the aberrations and a flexible program to calculate numerically the transverse aberrations and direction cosines in the image plane. Once a system has been designed spot diagrams may then be used to indicate the imaging properties.

Geometrically the light intensity in the image is determined by the density of ray intersections in the image plane. However, the recorded images will depend on the detector response which will usually be non-linear as is the case for photographic emulsions.

It is not generally possible to include the effects of plate response directly in the calculations of imaging in spectrographs since the properties of plates for use in the soft x-ray region are variable and depend strongly upon age, storage conditions and development conditions. Little work has been performed on the properties of soft x-ray plates, or films, although Niemann (114) has described the properties of three films suitable for use in zone plate experiments in the soft x-ray region. If the characteristics of the photographic plates, or films, are determined experimentally, the spot diagrams may be interpreted to yield the image expected in practice. If the efficiency of the grating is also known in the spectral region concerned, the entire properties of a spectrograph may be calculated.

In order that the numerical calculations described in this chapter are of practical significance, the geometrical conditions have been chosen to correspond to two grazing incidence spectrographs available commercially. The first is the popular 2m instrument described by Gabriel (115) and the second is a new prefocussed 5m instrument as described by Speer and Turner (116). Since the latter instrument has been designed specifically to be able to take advantage of all the developments in soft x-ray gratings and optics, most of the examples will be based on this instrument.

Spot diagrams showing the aberrations of a 600 1/mm 5m spherical grating illuminated with 50 Å radiation by a point source in the meridian plane on the Rowland circle are given in Fig. 23. The effect of increasing the illuminated grating width from 10mm to 40mm

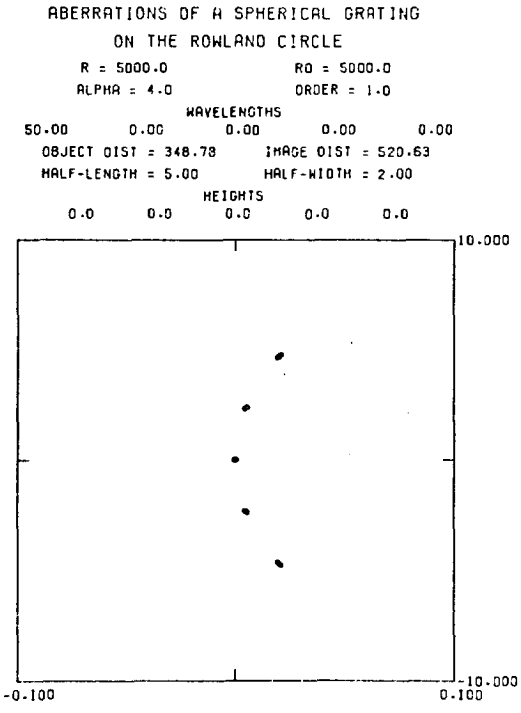
ABERRATIONS OF A SPHERICAL GRATING
ON THE ROWLAND CIRCLE
R = 5000.0
RO = 5000.0
ALPHA = 4.0
ORDER = 1.0
WAVELENGTHS
50.00 0.00 0.00 0.00 0.00
OBJECT DIST = 348.78
IMAGE DIST = 520.63
HALF-LENGTH = 5.00
HALF-WIDTH = 2.00
HEIGHTS
0.0 0.0 0.0 0.0 0.0
10.000
-10.000
-0.100
0.100

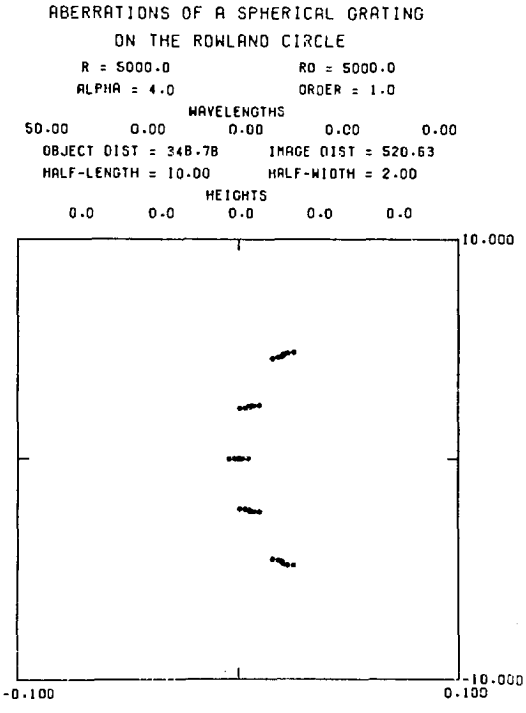
ABERRATIONS OF A SPHERICAL GRATING
ON THE ROWLAND CIRCLE
R = 5000.0
RO = 5000.0
ALPHA = 4.0
ORDER = 1.0
WAVELENGTHS
50.00 0.00 0.00 0.00 0.00
OBJECT DIST = 348.78
IMAGE DIST = 520.63
HALF-LENGTH = 10.00
HALF-WIDTH = 2.00
HEIGHTS
0.0 0.0 0.0 0.0 0.0
10.000
-10.000
-0.100
0.100

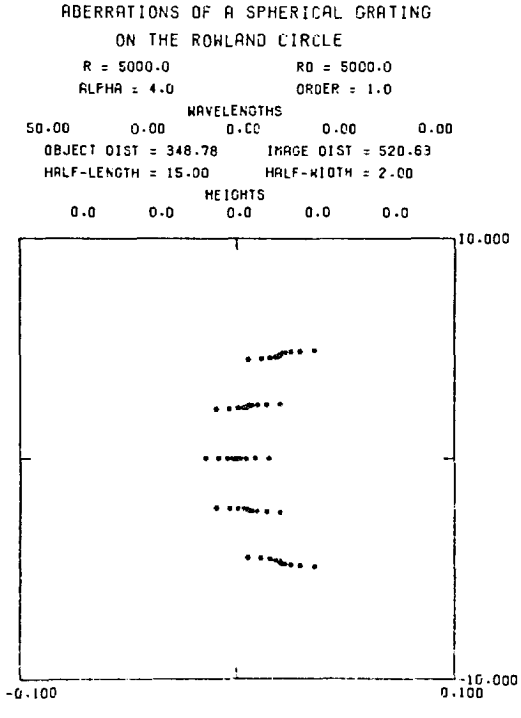
ABERRATIONS OF A SPHERICAL GRATING
ON THE ROWLAND CIRCLE
R = 5000.0
RO = 5000.0
ALPHA = 4.0
ORDER = 1.0
WAVELENGTHS
50.00 0.00 0.00 0.00 0.00
OBJECT DIST = 348.78
IMAGE DIST = 520.63
HALF-LENGTH = 15.00
HALF-WIDTH = 2.00
HEIGHTS
0.0 0.0 0.0 0.0 0.0
10.000
-10.000
-0.100
0.100

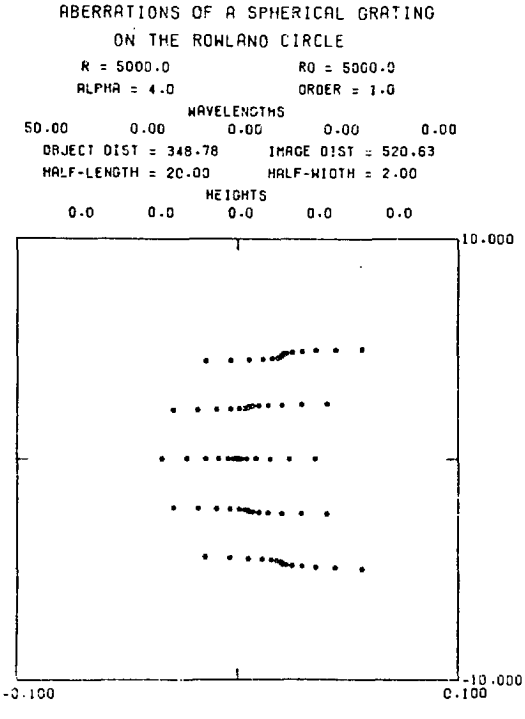
ABERRATIONS OF A SPHERICAL GRATING
ON THE ROWLAND CIRCLE
R = 5000.0
RO = 5000.0
ALPHA = 4.0
ORDER = 1.0
WAVELENGTHS
50.00 0.00 0.00 0.00 0.00
OBJECT DIST = 348.78
IMAGE DIST = 520.63
HALF-LENGTH = 20.00
HALF-WIDTH = 2.00
HEIGHTS
0.0 0.0 0.0 0.0 0.0
10.000
-10.000
-0.100
0.100

FIG. 23

is shown (i.e. the half-width of the grating increases from 5mm to 20mm). It should be noted that the dimensions on all the spot diagrams are in millimetres apart from the wavelengths which are expressed in Angstroms. The vertical scale on the spot diagrams is 100x greater than the horizontal scale. The large difference in scales is necessary in order to show the image structure in the presence of the large astigmatism of a spherical grating at grazing incidence. The second largest aberration is the astigmatic curvature which gives the characteristic parabolic shape to the spectral lines. This curvature is not generally significant in grazing incidence spectra since normally only the central section of the astigmatic image is recorded on the photographic plate.

The most important observation to be made from this series of spot diagrams is the dramatic increase in the line width as the illuminated width of the grating is increased. The increase in line width is due to spherical aberration which varies as the third power of the pupil coordinate. For a spherical grating under the conditions specified in the spot diagrams the optimum grating width as calculated by Mack, Stehn and Edlen is 31.95mm which corresponds to the third spot diagram. It is evident that under these conditions it is possible to obtain a higher resolution on a geometrical basis by using a slightly smaller optimum width than that recommended by Mack et al. It is also clear that for a given detector resolution or exit slit width in spectrometers and monochromators the grating width should be optimised and that there is little to be gained from increasing the optimum width above that recommended by Mack et al. However, the

calculations of Mack et al only apply on the Rowland circle and do not allow for refocussing which is essential to obtain the best imaging in the presence of spherical aberration.

From geometrical optics it is known that the "circle of least confusion" is formed at three-quarters the distance from the paraxial to the marginal focus and that this represents the best focus in the presence of spherical aberration. The position of the marginal focus is dependent on the width of the grating which means that the best focus will shift as the grating width is increased. To compensate for this shift of focus it is possible to move the photographic plate, or detector slit, outside the Rowland circle, to increase the curvature of the grating blank, or to offset the entrance slit outside the Rowland circle. Since the 5m instrument has the facility for displacing the entrance slit in a controlled manner inside and outside the Rowland circle, only refocussing by moving the entrance slit will be considered. Fig. 24 shows the effect of moving a point source out from the Rowland circle along the chief ray to the centre of the grating. The first diagram shows two just resolved lines at 50.00 and 50.01 Å with the entrance slit on the Rowland circle; the subsequent diagrams are for offset distances of 0.57mm, 0.64mm and 0.72mm from the Rowland circle which correspond to correction formulae given by Pouey, De Velis, and the geometrical formula, as described by Speer (117). It is clear that offsetting the entrance slit produces a marked improvement in the geometrical imaging. However, it can be imagined that in the case of spectral lines on the threshold of photographic recording resolution may be higher if the offset is slightly less than that from the geometrical formula. It would be

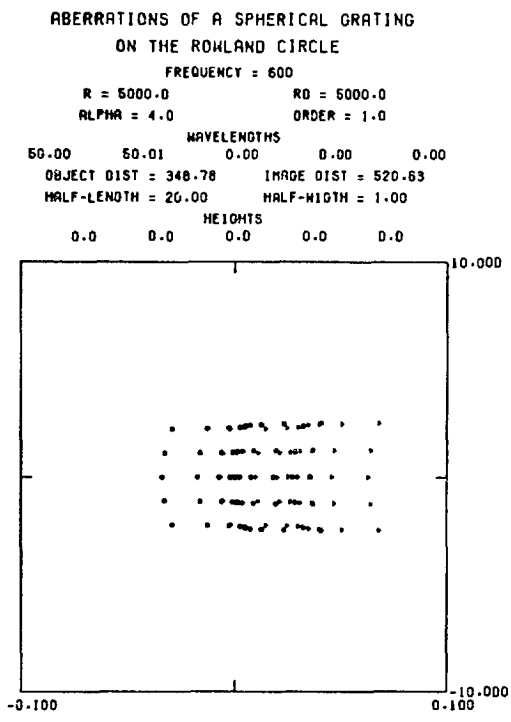
ABERRATIONS OF A SPHERICAL GRATING
ON THE ROWLAND CIRCLE
FREQUENCY = 600
R = 5000.0
RO = 5000.0
ALPHA = 4.0
ORDER = 1.0
WAVELENGTHS
50.00 50.01 0.00 0.00 0.00
OBJECT DIST = 348.78
IMAGE DIST = 520.63
HALF-LENGTH = 20.00
HALF-WIDTH = 1.00
HEIGHTS
0.0 0.0 0.0 0.0 0.0
10.000
-10.000
-0.100
0.100

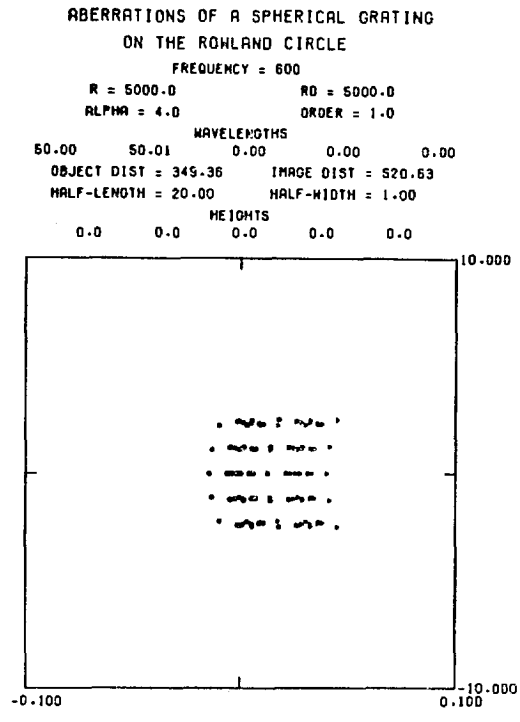
ABERRATIONS OF A SPHERICAL GRATING
ON THE ROWLAND CIRCLE
FREQUENCY = 600
R = 5000.0
RO = 5000.0
ALPHA = 4.0
ORDER = 1.0
WAVELENGTHS
50.00 50.01 0.00 0.00 0.00
OBJECT DIST = 349.36
IMAGE DIST = 520.63
HALF-LENGTH = 20.00
HALF-WIDTH = 1.00
HEIGHTS
0.0 0.0 0.0 0.0 0.0
10.000
-10.000
-0.100
0.100

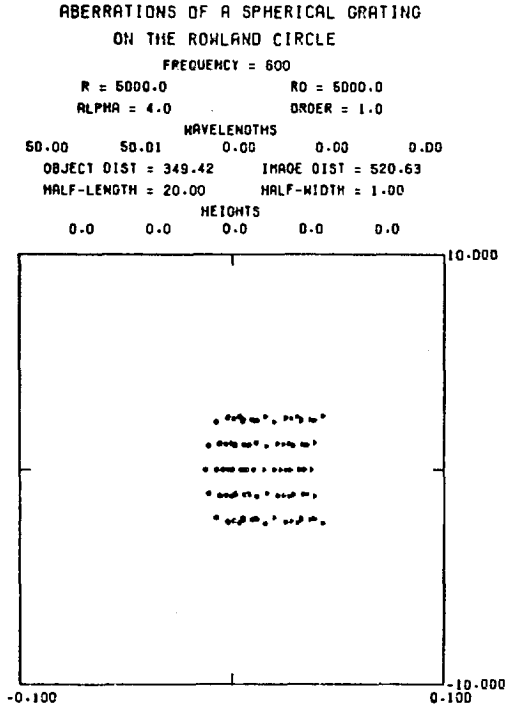
ABERRATIONS OF A SPHERICAL GRATING
ON THE ROWLAND CIRCLE
FREQUENCY = 600
R = 5000.0
RO = 5000.0
ALPHA = 4.0
ORDER = 1.0
WAVELENGTHS
50.00 50.01 0.00 0.00 0.00
OBJECT DIST = 349.42
IMAGE DIST = 520.63
HALF-LENGTH = 20.00
HALF-WIDTH = 1.00
HEIGHTS
0.0 0.0 0.0 0.0 0.0
10.000
-10.000
-0.100
0.100

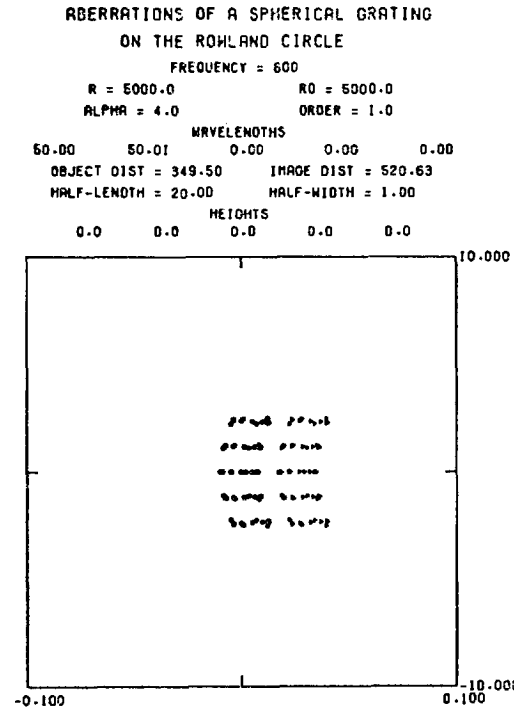
ABERRATIONS OF A SPHERICAL GRATING
ON THE ROWLAND CIRCLE
FREQUENCY = 600
R = 5000.0
RO = 5000.0
ALPHA = 4.0
ORDER = 1.0
WAVELENGTHS
50.00 50.01 0.00 0.00 0.00
OBJECT DIST = 349.50
IMAGE DIST = 520.63
HALF-LENGTH = 20.00
HALF-WIDTH = 1.00
HEIGHTS
0.0 0.0 0.0 0.0 0.0
10.000
-10.000
-0.100
0.100

FIG. 24

necessary to perform some careful experimentation in order to verify this conclusion.

Since most grazing incidence spectrographs are used with entrance slits, it is important to consider the effect of the finite length of the entrance slit on the images. Rays which are incident on the centre of the grating from outside the meridian plane will be deviated by different amounts from the chief ray in the meridian plane. This gives rise to a curvature of spectrum lines called "enveloping curvature" by Beutler which makes the lines concave towards longer wavelengths. The effect of the finite length of an infinitely narrow entrance slit is simulated in the computer program by moving the illuminating point source to various heights above the meridian plane. It can be seen from Fig. 25 that the effect of the finite length of the entrance slit is to cause a slight broadening of the spectral lines. In practice this broadening is usually negligible since it is much less than the spherical aberration and plate resolution for the lengths of entrance slits normally used on spectrographs. For very high resolution work at grazing incidence the length of the entrance slit must be restricted to about 5mm otherwise the spot diagrams show image broadening as in Fig. 26.

It has been found by ray-tracing that the optimum grating width as defined by Mack et al generally corresponds for soft x-ray wavelengths to total geometrical line width of about 25 - 50μm as measured on the Rowland circle. Photographic plates for soft x-ray use can have a resolution of 10μm and the smallest practical slit widths in spectrographs yield geometrical widths projected on the plate of somewhat

ABERRATIONS OF A SPHERICAL GRATING
ON THE ROWLAND CIRCLE

FREQUENCY = 600

R = 5000.0 RO = 5000.0

ALPHA = 4.0 ORDER = 1.0

WAVELENGTHS

100.00 0.00 0.00 0.00 0.00

OBJECT DIST = 348.78 IMAGE DIST = 648.09

HALF-LENGTH = 20.00 HALF-WIDTH = 5.00

HEIGHTS

0.0 1.0 2.0 -1.0 -2.0

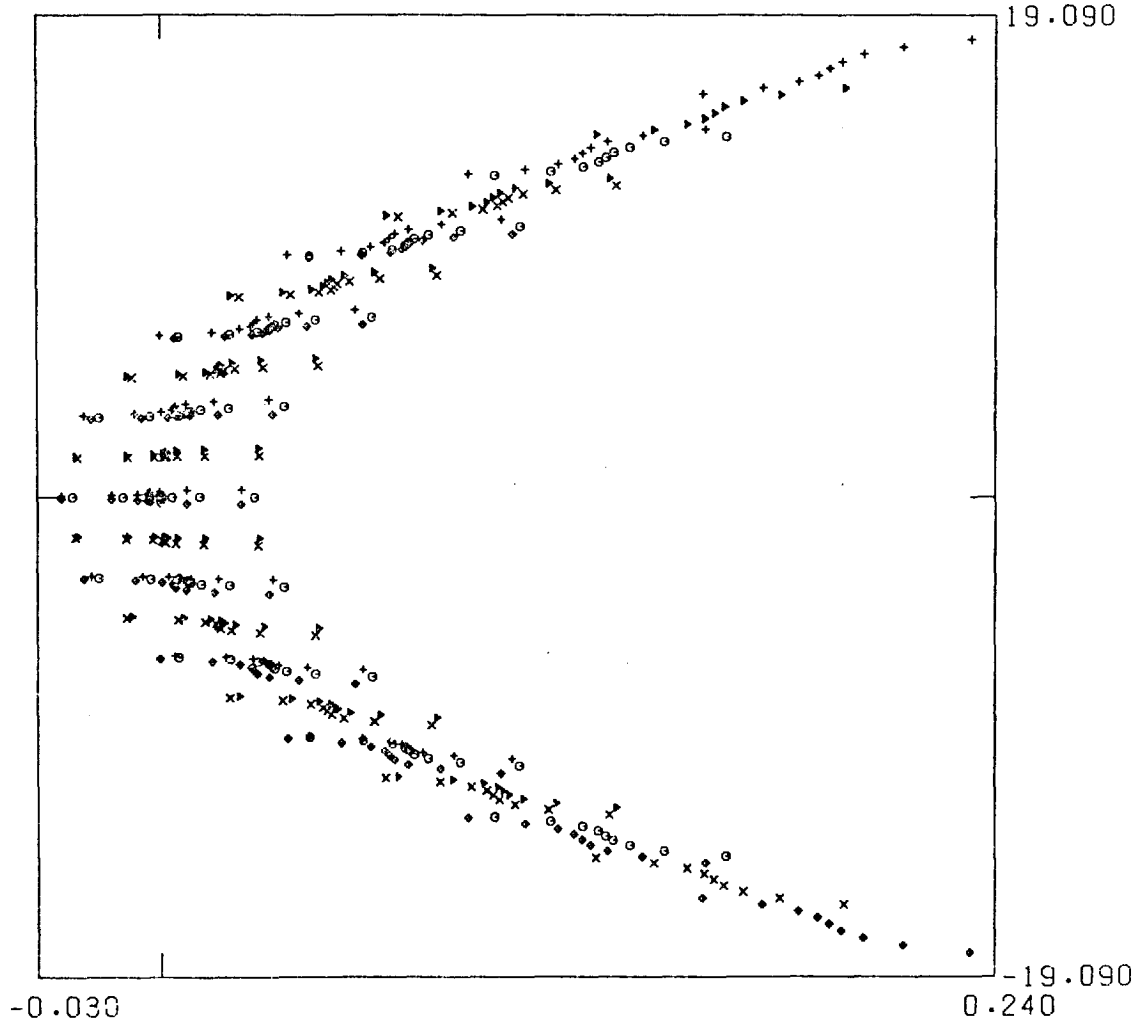

FIG. 25

ABERRATIONS OF A SPHERICAL GRATING
ON THE ROWLAND CIRCLE

FREQUENCY = 600

R = 5000.0 RO = 5000.0

ALPHA = 4.0 ORDER = 1.0

WAVELENGTHS

100.00 0.00 0.00 0.00 0.00

OBJECT DIST = 348.78 IMAGE DIST = 648.09

HALF-LENGTH = 20.00 HALF-WIDTH = 5.00

HEIGHTS

0.0 2.5 5.0 -2.5 -5.0

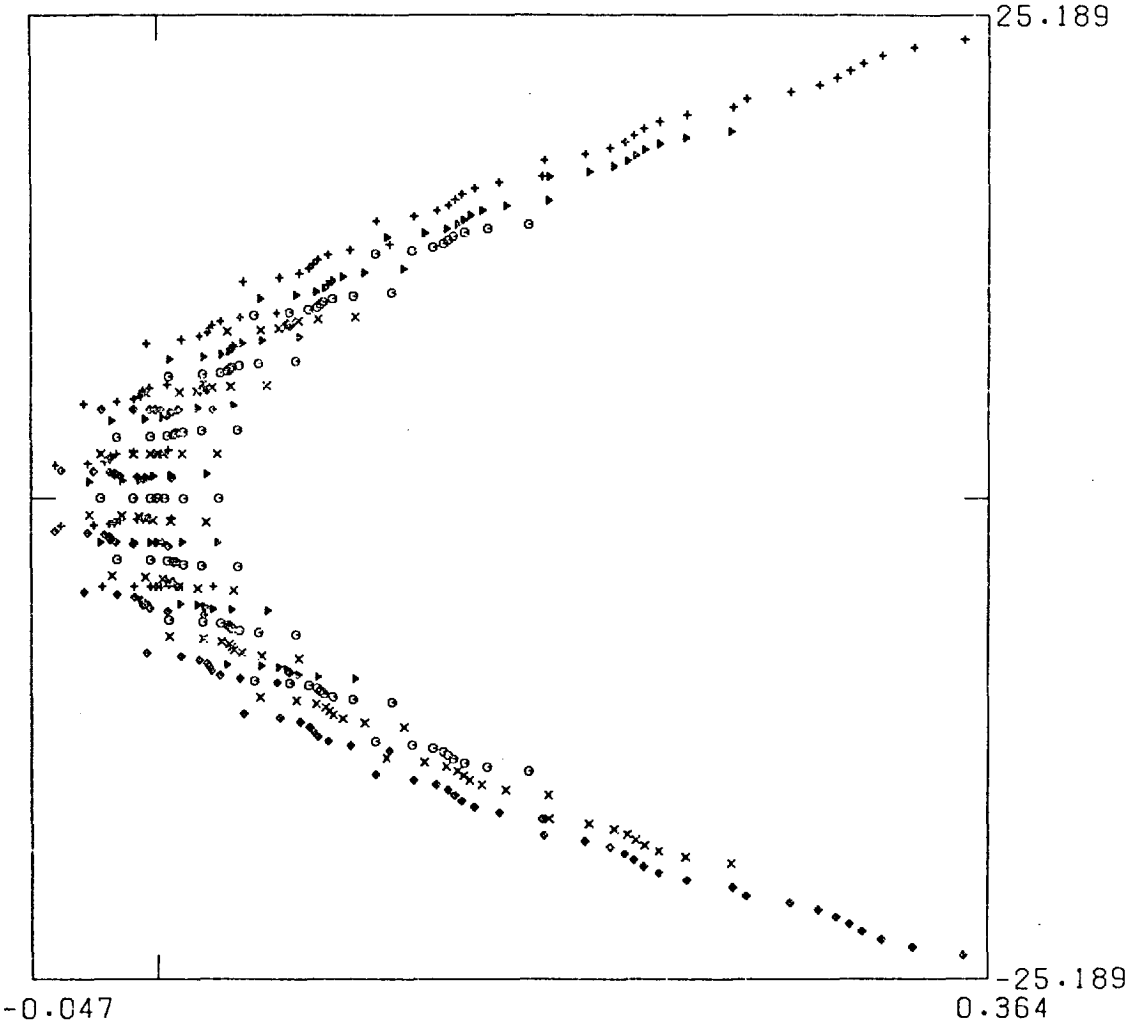

FIG. 26

less than 20μm. It can be seen that the grating width suggested by Mack et al is not only the optimum width from the point of view of theoretical resolution but is also usually the optimum width from a practical point of view considering plate resolution and mechanical limitations. Since few spectra in the soft x-ray region have lines of equal intensity it cannot be expected that the resolution formulae given by Mack, Stehn and Edlén, based on the premise that the spectral lines are of equal intensity, will be satisfied experimentally. In order to obtain the highest resolution for spectral lines having greatly differing intensities, it is necessary to reduce the spherical aberration so that it does not cause any resolvable broadening of the geometrical image of the entrance slit. Thus experimentally it may be possible to attain higher resolutions with grating widths less than the optimum width as defined by Mack et al.

In optical design it is usual to display in spot diagrams the transverse aberrations which are measured in the plane perpendicular to the chief ray. This method was also employed in the first ray tracing programs, however, when studying the aberrations of spectrographs it is preferable to examine the aberrations on the focal surface. If only transverse aberrations are considered in the grazing incidence region one can easily be misled. For example spot diagrams of the transverse aberrations for a spherical grating with a large aperture show a pronounced asymmetry which would lead one to expect that imaging would be improved by masking the grating asymmetrically. However, as can be seen from Fig. 27 this asymmetry

TRANSVERSE ABERRATIONS
OF A SPHERICAL GRATING

FREQUENCY = 600.0000

R = 5000.0 RO = 5000.0

ALPHA = 4.0 ORDER = 1.0

WAVELENGTHS

50.00 49.00 51.00 0.00 0.00

OBJECT DIST = 348.78 IMAGE DIST = 520.63

HALF-LENGTH = 20.00 HALF-WIDTH = 5.00

HEIGHTS

0.0 0.0 0.0 0.0 0.0

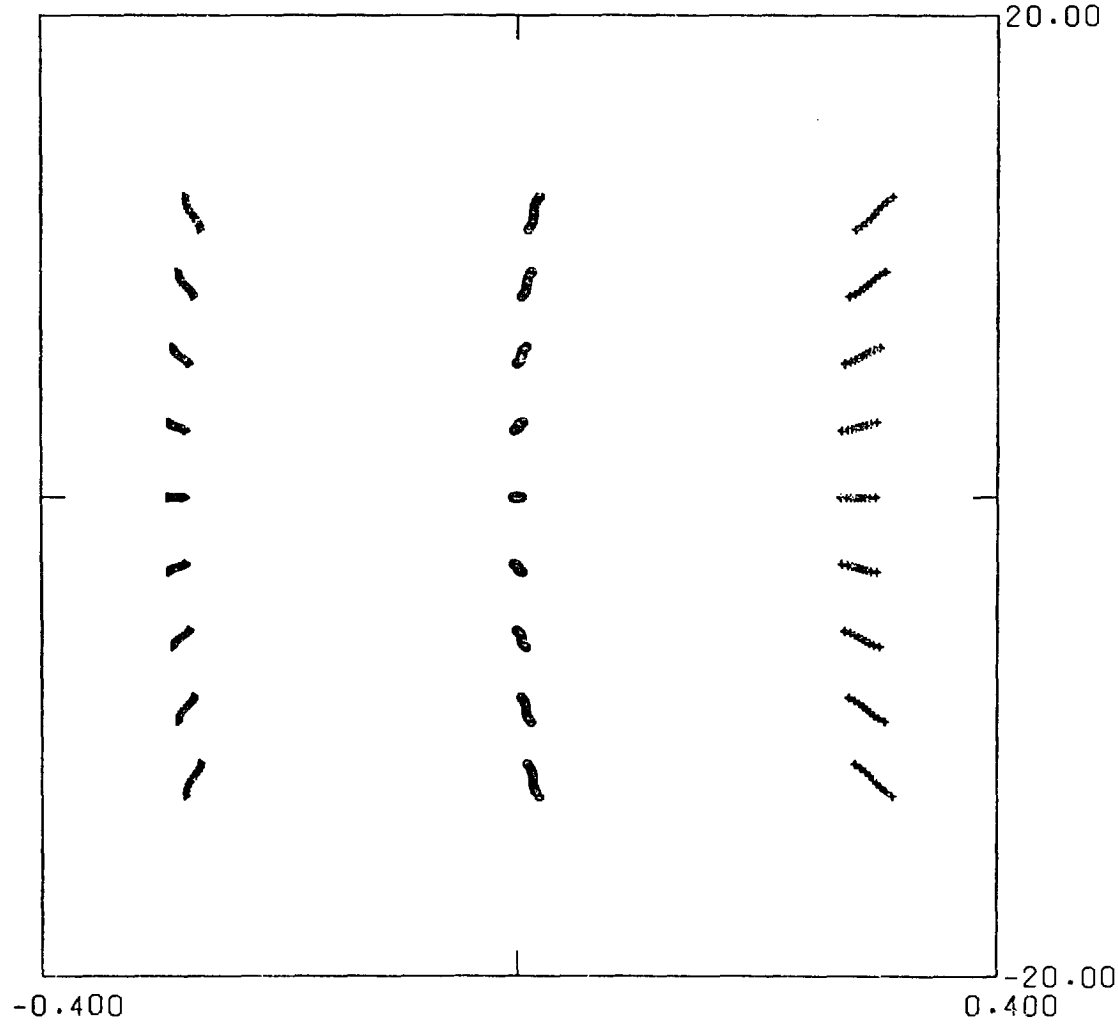

FIG. 27 (a)

ABERRATIONS OF A SPHERICAL
GRATING ON THE ROWLAND CIRCLE

FREQUENCY = 600.0000

R = 5000.0 RO = 5000.0

ALPHA = 4.0 ORDER = 1.0

WAVELENGTHS

50.00 49.00 51.00 0.00 0.00

OBJECT DIST = 348.78 IMAGE DIST = 520.63

HALF-LENGTH = 20.00 HALF-WIDTH = 5.00

HEIGHTS

0.0 0.0 0.0 0.0 0.0

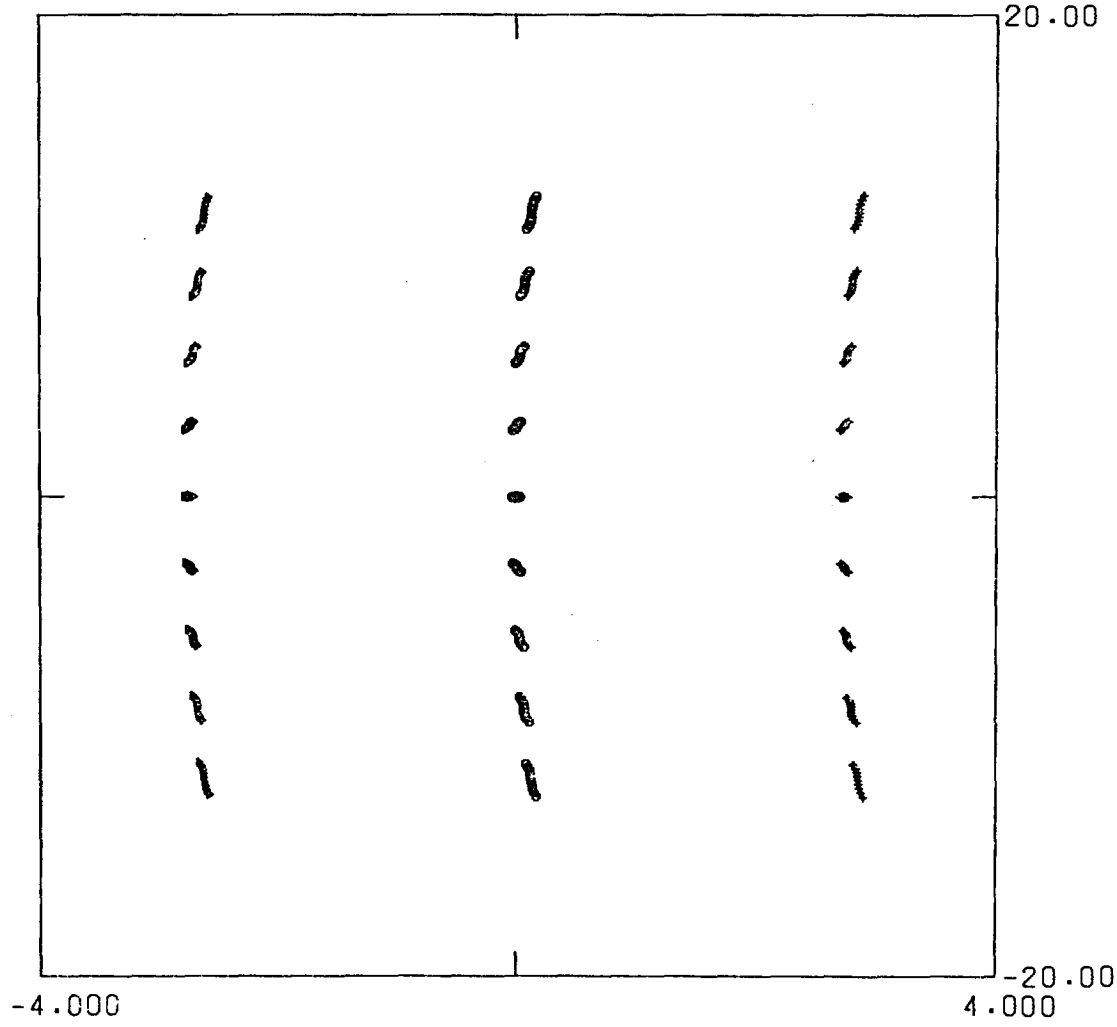

FIG. 27 (b)

disappears when the aberrations are measured on the Rowland circle. The great difference in magnitude between the aberrations measured transverse to the chief ray and along the focal curve means that transverse aberrations which at first appear to be insignificant can be large when projected on the Rowland cylinder. This effect is illustrated in Fig. 28 which shows spot diagrams at wavelengths of 10.00 and 10.01 Å with aberrations measured transversely and on the Rowland cylinder from a 600 l/mm spherical grating in the upper diagrams and a 1200 l/mm grating in the lower diagrams. It is important to note the increase in the horizontal scale from 20μm for the transverse aberrations to 200μm for the aberrations measured along the cylinder. Both methods for representing the aberrations have advantages in certain cases and both methods have been employed in this work.

A final example of the aberrations of a spherical grating as measured along the Rowland cylinder is shown in Fig. 29. The upper spot diagrams show images formed at wavelengths 50.00 and 50.01 Å incident at a grazing angle of 2.0° onto a 600 l/mm and a 1200 l/mm grating. For the 600 l/mm case it can be seen that the marginal rays from one side of the grating for one wavelength fall near the paraxial focus for the other wavelength. Under these conditions it cannot be said that the two lines will always be resolved but they may be depending on the intensities of the lines and the characteristics of the detector. The diagram for the 1200 l/mm grating shows that the two lines are now separated but that they are considerably broadened by spherical aberration. Hence, contrast could be increased by reducing

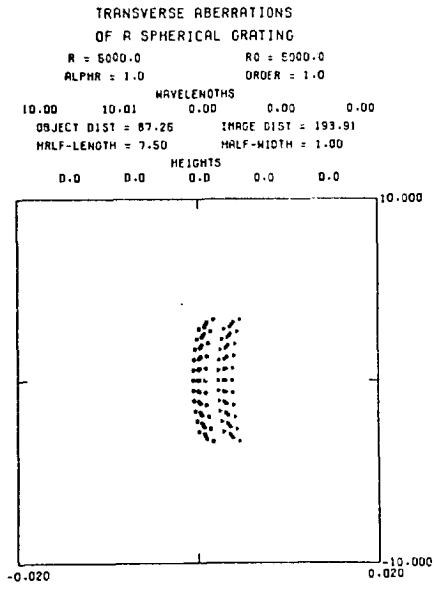
TRANSVERSE ABERRATIONS
OF A SPHERICAL GRATING
R = 5000.0
RO = 5000.0
ALPHA = 1.0
ORDER = 1.0
WAVELENGTHS
10.00 10.01 0.00 0.00 0.00
OBJECT DIST = 87.26
IMAGE DIST = 193.91
HALF-LENGTH = 7.50
HALF-WIDTH = 1.00
HEIGHTS
0.0 0.0 0.0 0.0 0.0
10.000
-10.000
-0.020
0.020

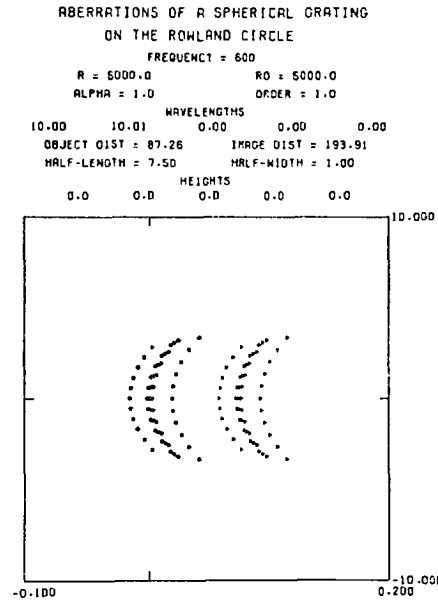
ABERRATIONS OF A SPHERICAL GRATING
ON THE ROWLAND CIRCLE
FREQUENCY = 600
R = 5000.0
RO = 5000.0
ALPHA = 1.0
ORDER = 1.0
WAVELENGTHS
10.00 10.01 0.00 0.00 0.00
OBJECT DIST = 87.26
IMAGE DIST = 193.91
HALF-LENGTH = 7.50
HALF-WIDTH = 1.00
HEIGHTS
0.0 0.0 0.0 0.0 0.0
10.000
-10.000
-0.100
0.200

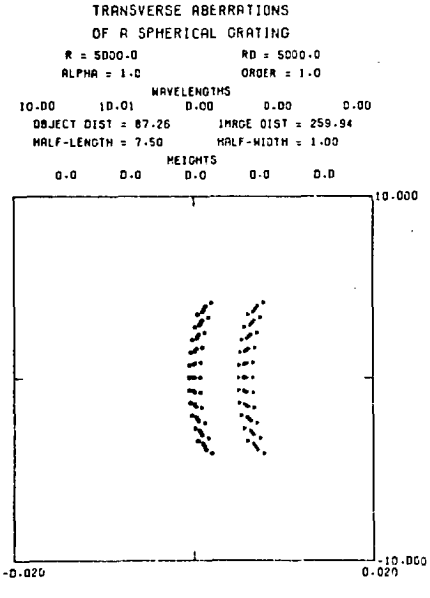
TRANSVERSE ABERRATIONS
OF A SPHERICAL GRATING
R = 5000.0
RO = 5000.0
ALPHA = 1.0
ORDER = 1.0
WAVELENGTHS
10.00 10.01 0.00 0.00 0.00
OBJECT DIST = 87.26
IMAGE DIST = 259.94
HALF-LENGTH = 7.50
HALF-WIDTH = 1.00
HEIGHTS
0.0 0.0 0.0 0.0 0.0
10.000
-10.000
-0.020
0.020

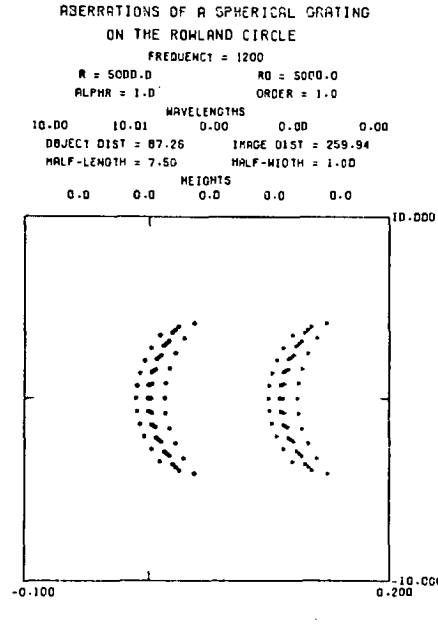
ABERRATIONS OF A SPHERICAL GRATING
ON THE ROWLAND CIRCLE
FREQUENCY = 1200
R = 5000.0
RO = 5000.0
ALPHA = 1.0
ORDER = 1.0
WAVELENGTHS
10.00 10.01 0.00 0.00 0.00
OBJECT DIST = 87.26
IMAGE DIST = 259.94
HALF-LENGTH = 7.50
HALF-WIDTH = 1.00
HEIGHTS
0.0 0.0 0.0 0.0 0.0
10.000
-10.000
-0.100
0.200

FIG. 28

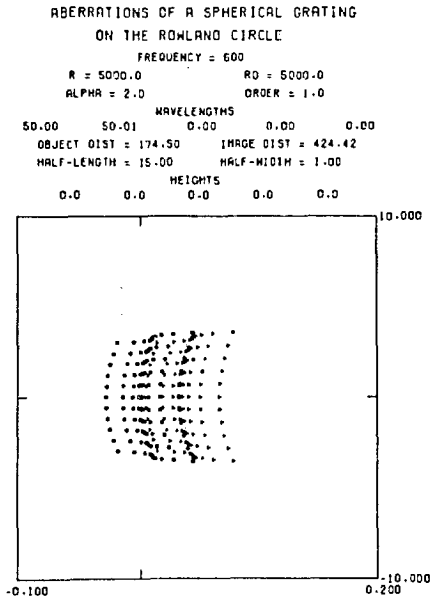
ABERRATIONS OF A SPHERICAL GRATING
ON THE ROWLAND CIRCLE
FREQUENCY = 600
R = 5000.0
RO = 5000.0
ALPHA = 2.0
ORDER = 1.0
WAVELENGTHS
50.00 50.01 0.00 0.00 0.00
OBJECT DIST = 174.50
IMAGE DIST = 424.42
HALF-LENGTH = 15.00
HALF-WIDTH = 1.00
HEIGHTS
0.0 0.0 0.0 0.0 0.0
10.000
-10.000
-0.100
0.200

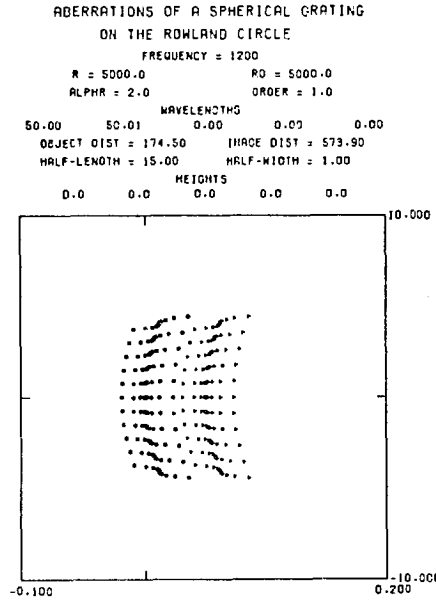
ABERRATIONS OF A SPHERICAL GRATING
ON THE ROWLAND CIRCLE
FREQUENCY = 1200
R = 5000.0
RO = 5000.0
ALPHA = 2.0
ORDER = 1.0
WAVELENGTHS
50.00 50.01 0.00 0.00 0.00
OBJECT DIST = 174.50
IMAGE DIST = 573.90
HALF-LENGTH = 15.00
HALF-WIDTH = 1.00
HEIGHTS
0.0 0.0 0.0 0.0 0.0
10.000
-10.000
-0.100
0.200

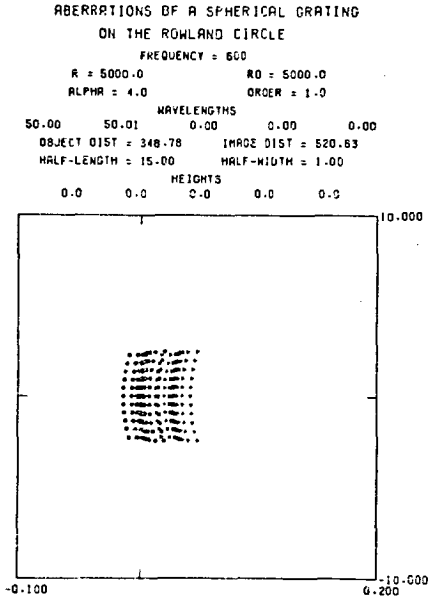
ABERRATIONS OF A SPHERICAL GRATING
ON THE ROWLAND CIRCLE
FREQUENCY = 600
R = 5000.0
RO = 5000.0
ALPHA = 4.0
ORDER = 1.0
WAVELENGTHS
50.00 50.01 0.00 0.00 0.00
OBJECT DIST = 348.78
IMAGE DIST = 520.63
HALF-LENGTH = 15.00
HALF-WIDTH = 1.00
HEIGHTS
0.0 0.0 0.0 0.0 0.0
10.000
-10.000
-0.100
0.200

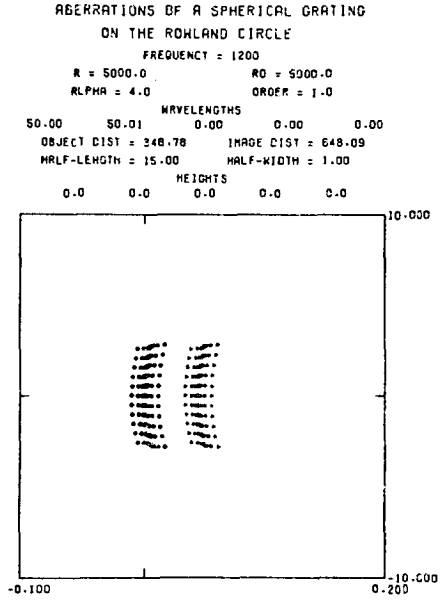
ABERRATIONS OF A SPHERICAL GRATING
ON THE ROWLAND CIRCLE
FREQUENCY = 1200
R = 5000.0
RO = 5000.0
ALPHA = 4.0
ORDER = 1.0
WAVELENGTHS
50.00 50.01 0.00 0.00 0.00
OBJECT DIST = 348.78
IMAGE DIST = 648.09
HALF-LENGTH = 15.00
HALF-WIDTH = 1.00
HEIGHTS
0.0 0.0 0.0 0.0 0.0
10.000
-10.000
-0.100
0.200

FIG. 29

the width of the grating.

In the lower diagram the angle of grazing incidence has been increased to 4°. For the 600 l/mm grating, which also has the optimum width of Mack et al, it can be seen that the extreme rays for the two wavelengths are just overlapping which means that it should be possible to resolve these two lines under all conditions irrespective of line intensity provided that it is above detector threshold.

The maximum resolution of a concave grating is defined by two lines of equal intensity being just resolved when the wavelength difference between them is such that the minimum total intensity between the lines is $8/\pi^2$ times as great as the total intensity of both at the central maximum of either of the lines. In addition to this criterion which has the usual validity of the Rayleigh criterion it is possible to define a "worst-case" resolution applicable to lines of all intensities and defined by the first minimum of one line falling on the minimum of the other line. For a plane grating this "worst-case" resolution would be half that from the Rayleigh criterion but for a concave grating the angular half-wdiths of the lines are greater and the resolution will be correspondingly less. From ray tracing the geometrical line width is immediately obtained and this can be used to define the "worst-case" resolution. From the spot diagram for the 600 l/mm grating it can be seen that the two lines have marginal rays just overlapping which yields a "worst-case" resolution of 5000. This means that a minimum resolution of 5000 should be attainable at this wavelength from a

correctly adjusted spectrograph using a grating under these conditions provided the entrance slit is sufficiently narrow. The maximum theoretical resolution for a grating under these conditions from the formula of Mack, Stehn and Edlén is 16,600 and in practice a resolution lying between these two values should be achieved.

Since resolution is proportional to grating frequency, increasing the grating frequency to 1200 l/mm as in the fourth spot diagram in Fig. 29 doubles the resolution and makes resolution in excess of 10,000 at 50 A a practical proposition. Finally it can be seen that higher resolution is attainable with a grazing angle of 4° than with 2° which illustrates the point made by Mack, Stehn and Edlén that for high resolution it is not desirable to use smaller grazing angles of incidence or diffraction than are necessary for sufficient reflection.

Ray tracing has already enabled us to understand the aberrations of spherical gratings important in the soft x-ray region. This understanding is not based on approximations but on concrete numerical examples. Since the computer used works to 15 significant digits, provided the programs and input data are correct, the results will always be reliable. Hence we have a most powerful method for analysing grazing incidence systems and since all the parameters can be readily adjusted it is possible to speedily calculate the various effects of manufacturing tolerances, focussing errors, etc. A discussion of the tolerances on a grazing incidence spectrograph will not be made here since such a discussion must relate to a specific instrument designed for a specific application. Instead some of the

new possibilities of aspheric and variable frequency gratings for use in the soft x-ray region will be discussed and analysed by ray tracing.

The properties of cylindrical gratings with circular grooves have been described by Singh and Majumder (118) and Woodgate (119) has compared the aberrations of cylindrical and spherical gratings. Since spectrographs usually have cylindrical symmetry it is immediately evident that use of a cylindrical grating would simplify the geometry because all planes parallel to the meridian plane would become equivalent. It is to be expected, therefore, that the aberrations for rays outside the meridian plane will be less for a cylindrical grating than for a spherical grating. Spot diagrams of the images produced by spherical and cylindrical gratings under the same conditions are shown in Fig. 30 and 31. The conditions correspond to a Rowland circle geometry with a 4mm long entrance slit illuminating at 100 Å an area of the grating 10mm x 40mm ruled with 600 l/mm. It can be seen that the astigmatic length of the images for the cylindrical grating is slightly increased but the total width of the line is decreased from 270μm in the case of the spherical grating to 106μm for the cylindrical grating. Since only the central area of the image is recorded in spectrographs, the actual gain in resolution afforded by employing a cylindrical grating is small, however, for special cases when long entrance slits must be used the cylindrical grating has advantages over the spherical grating. Woodgate has suggested that the cylindrical grating would be useful in cases where the need for imaging and high flux necessitates the use of non-spherical grazing incidence optics prior to the entrance slit. The

ABERRATIONS OF A SPHERICAL
GRATING ON THE ROWLAND CIRCLE

FREQUENCY = 600

R = 5000.0 RO = 5000.0

ALPHA = 4.0 ORDER = 1.0

WAVELENGTHS

100.00 0.00 0.00 0.00 0.00

OBJECT DIST = 348.78 IMAGE DIST = 648.09

HALF-LENGTH = 20.00 HALF-WIDTH = 5.00

HEIGHTS

0.0 1.0 2.0 -1.0 -2.0

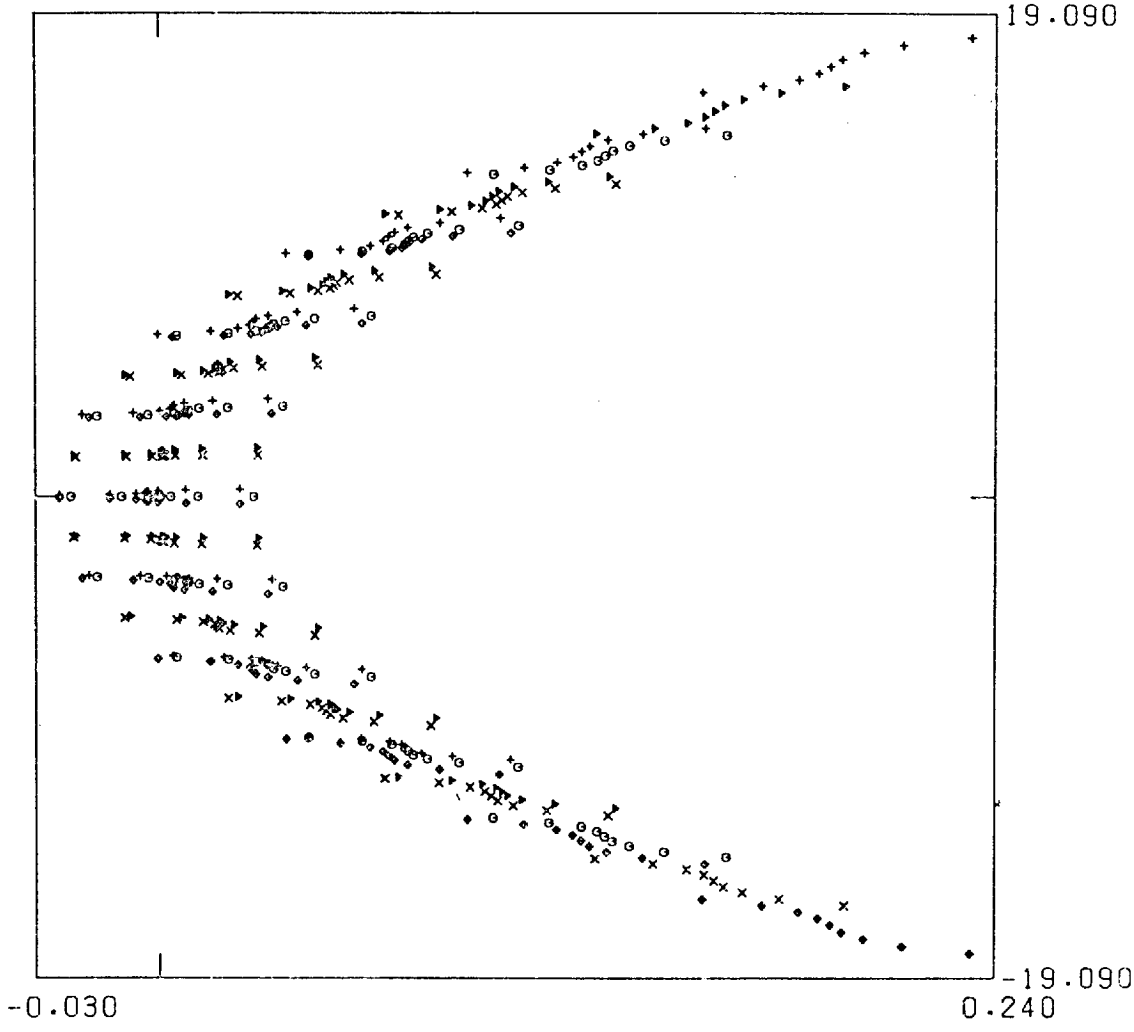

FIG. 30

ABERRATIONS OF A CYLINDRICAL
GRATING ON THE ROWLAND CIRCLE

FREQUENCY = 600.0000

R = 999999999.0 RO = 5000.0

ALPHA = 4.0 ORDER = 1.0

WAVELENGTHS

100.00 0.00 0.00 0.00 0.00

OBJECT DIST = 348.78 IMAGE DIST = 648.09

HALF-LENGTH = 20.00 HALF-WIDTH = 5.00

HEIGHTS

0.0 1.0 2.0 -1.0 -2.0

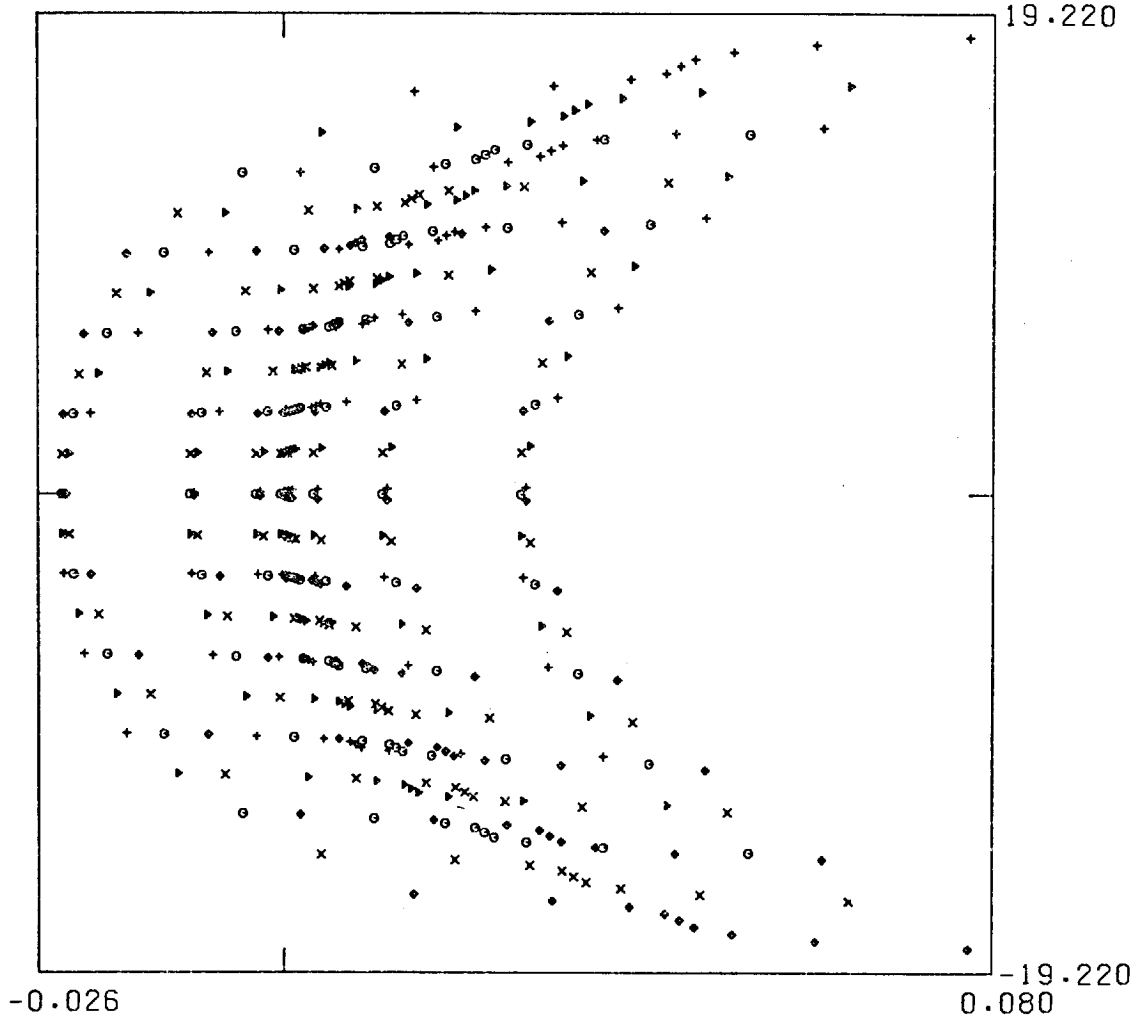

FIG. 31

optimal design of such multi-element systems cannot be achieved by considering the aberrations of each element individually since the aberrations tend to interact. Instead it is necessary to follow modern optical design techniques and optimise the system with regard to a specified quality factor. Even though a cylindrical surface is a simple aspheric, it is not an easy matter to obtain the accuracy of figuring and surface quality required in the soft x-ray region. Careful consideration of the manufacturing tolerances and testing procedures must be made when specifying design tolerances, otherwise designs can become purely hypothetical. However, in recent years significant advances in optical working and testing have taken place which should enable grazing incidence optical systems, incorporating aspheric elements, to be more readily fabricated.

During the course of the present work two types of aspheric grating for use in the soft x-ray region have been made and tested experimentally. Both types of grating have been formed holographically with a laminar profile to yield an all-metallic structure. The first type of aspheric grating has been formed on a toroidal blank and the second type on an elliptical cylinder formed by bending a suitably shaped optical flat.

The toroidal grating blanks were made with a primary radius of 2000mm so that they are compatible with the 2m spectrograph mentioned previously. The secondary radius was chosen to be 5.65mm in order to produce a stigmatic image under Rowland circle geometry at 44.5 Å with an angle of grazing incidence of 2° from a 600 l/mm grating. On such a steeply curved blank it would be practically impossible to mechanically rule a grating, but the fabrication of

A TOROIDAL DIFFRACTION GRATING

FOR USE IN THE SOFT X-RAY REGION

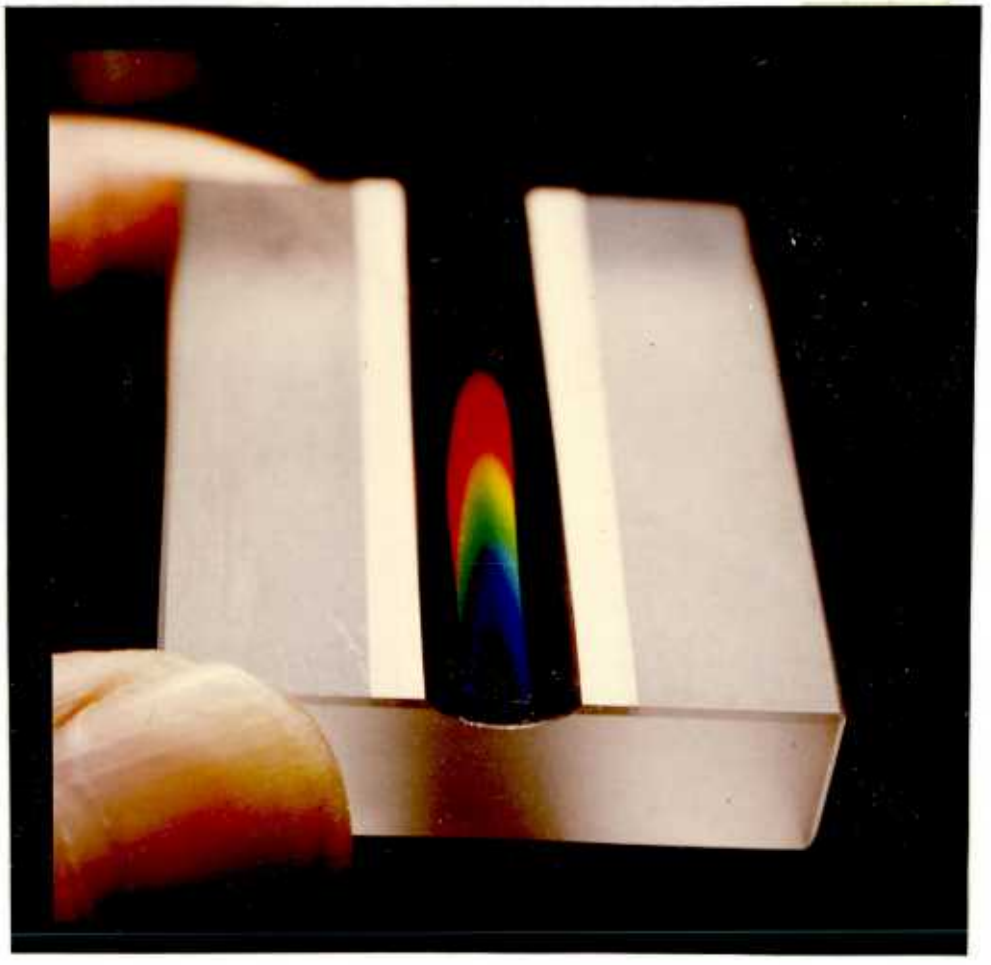

Grating Frequency = 600mm^{-1}

Primary Radius = 2000mm Secondary Radius 5.65mm

With secondary radius chosen to produce a stigmatic image at λ = 44.5 A

for a grazing angle of incidence of 2°

FIG. 32

this grating was successfully accomplished using the holographic technique. The production of the toroidal grating is not only interesting from a theoretical point of view but it has demonstrated that technically it is now possible to form efficient high-quality diffraction gratings on almost any surface on which an interference fringe system can be located. The design possibilities for grating systems have therefore been enormously increased by the advent of the holographic method for manufacturing gratings.

From the stigmatic equation for the toroidal grating a stigmatic image in the zero order is obtained from a toroid with the above radii if the angle of grazing incidence is 3.046° and the object and image distances are those of the Rowland circle geometry. Thus it is possible to examine the zero order aberrations of a toroidal grating, designed for use at soft x-ray wavelengths, under grazing incidence conditions using light of any wavelength. The aberrations of the toroidal blanks were investigated using visible white light before the gratings were formed on them. The optical system employed and typical images obtained are shown in Fig. 33 and Fig. 34.

It was immediately apparent that the toroidal blanks produced large aberrations which could only be reduced by restricting the aperture. However, it was not known whether the aberrations were intrinsic to toric surfaces of this type or were due to manufacturing imperfections. In order to establish the origin of the aberrations found in the white light images from the toroidal blanks spot diagrams were produced to simulate the zero order images.

Spot diagrams showing the effect of increasing the illuminated aperture of the toroid under the same conditions as used for the white

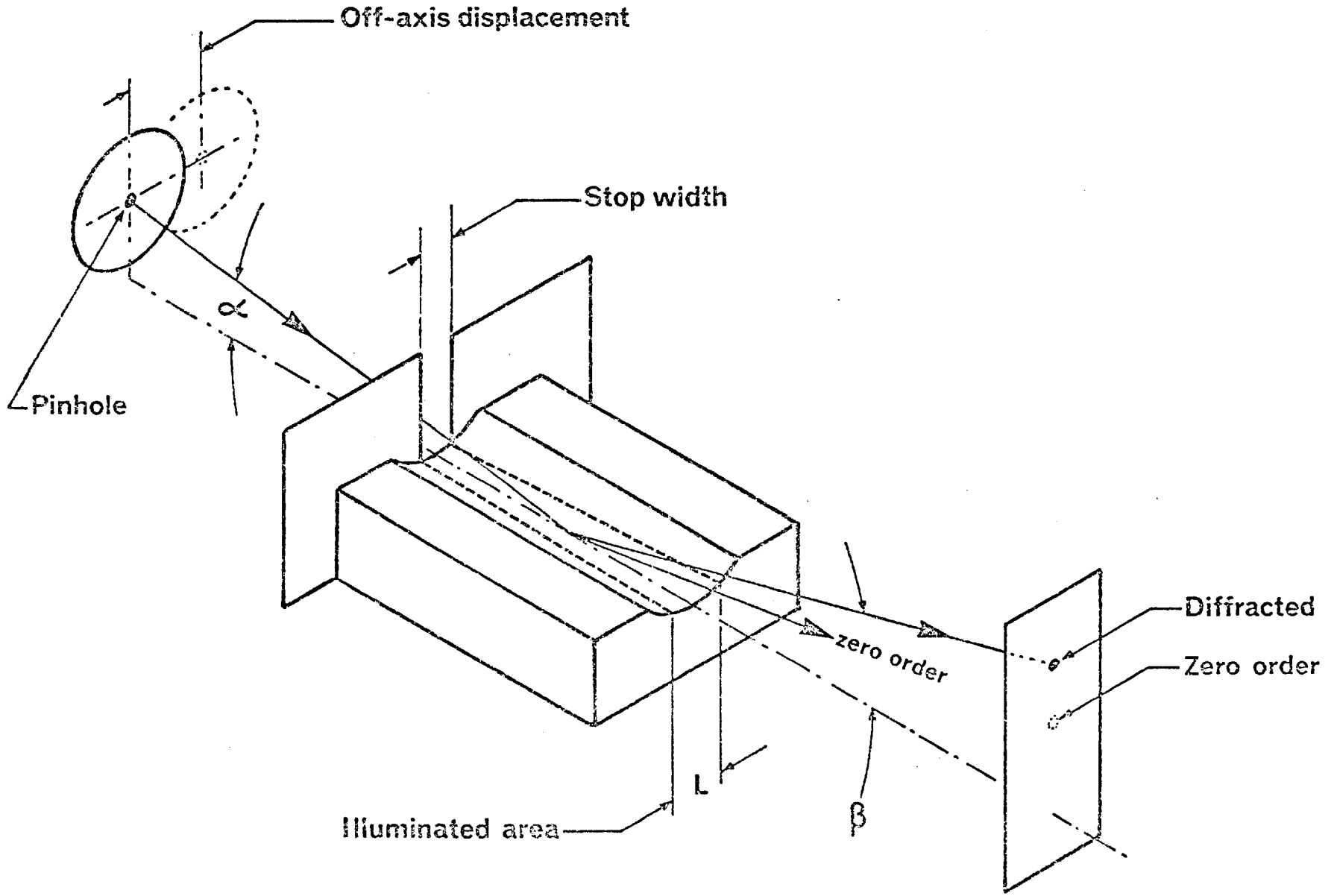
Off-axis displacement
Stop width
α
Pinhole
zero order
Diffracted
Zero order
L
β
Illuminated area

FIG. 33

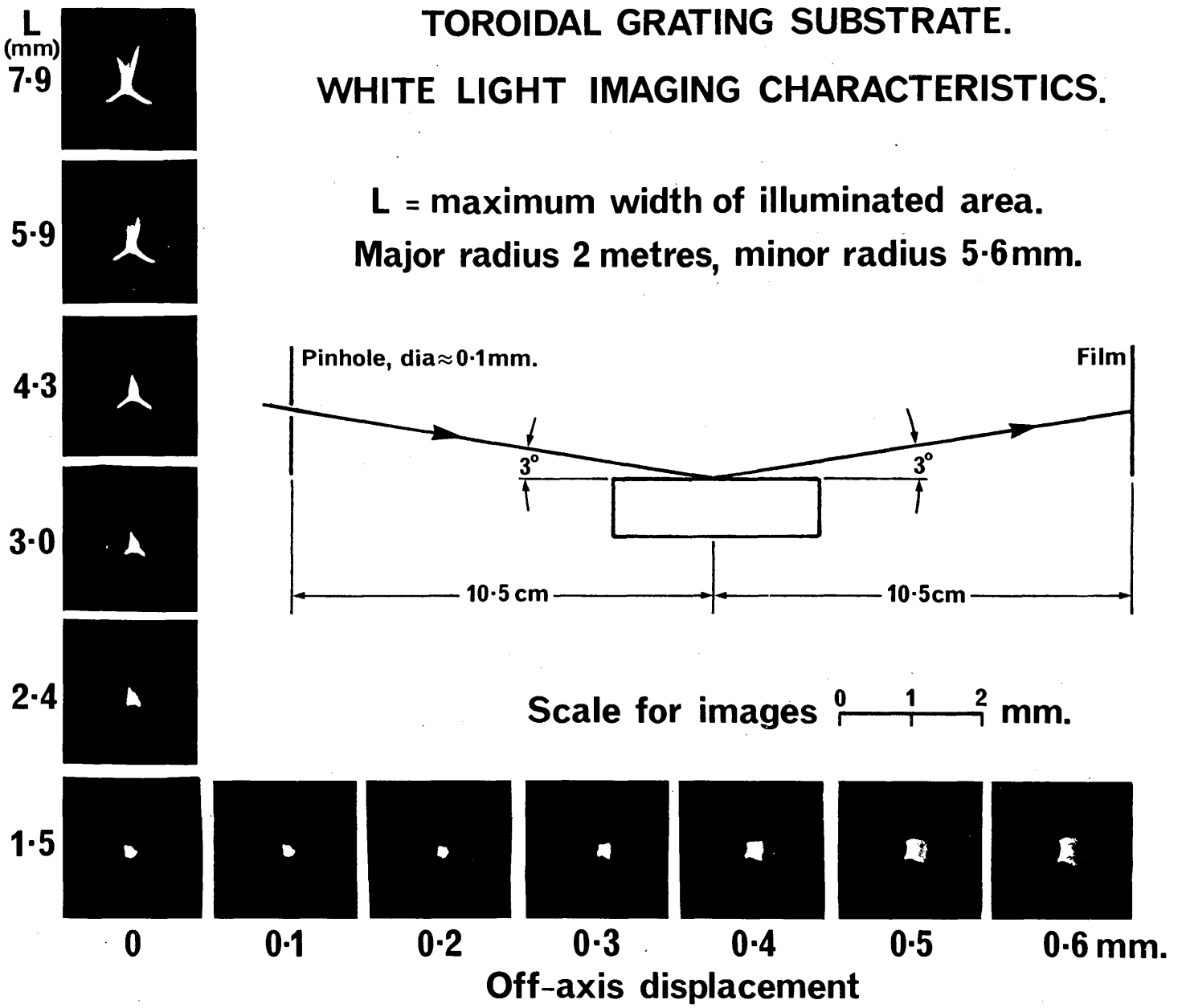
TOROIDAL GRATING SUBSTRATE.
WHITE LIGHT IMAGING CHARACTERISTICS.
L = maximum width of illuminated area.
Major radius 2 metres, minor radius 5·6mm.
L (mm)
7·9
5·9
4·3
3·0
2·4
1·5
Pinhole, dia≈0·1mm.
Film
3°
3°
10·5 cm
10·5cm
Scale for images 0 1 2 mm.
0
0·1
0·2
0·3
0·4
0·5
0·6 mm.
Off-axis displacement

FIG. 34

light images in Fig. 34 are given in Fig. 35. The correlation between the computed images and those obtained experimentally is exceedingly high both in shape and magnitude. Since the experimental results were obtained before the theoretical results, there is no possibility of a psychological bias and it can be safely stated that the aberrations observed are inherent to toric surfaces of this type.

The effect of varying the secondary radius has been investigated by ray tracing and it was found that, since the aberrations are so large, errors in radius of several percent can be tolerated without appreciably altering the aberrations. Thus the fabrication of such toroidal gratings need not be accomplished with such high precision as was initially thought necessary.

The off-axis aberrations for an illuminated area of 1.5mm x 40mm on the back plane of the toroid (i.e. a rectangular entrance pupil 1.5mm x 2.1mm) recorded using white light are shown in Fig. 34 and the corresponding computed spot diagrams are given in Fig. 36. Again the correlation between the spot diagrams and actual images is good when the effects of photographic recording and the ray densities in the spot diagrams are considered. However, the magnitude of the off-axis aberrations is such that it would not be possible to use this type of toroid to produce images from extended objects. This result was to have been expected because a single mirror used at grazing incidence can never be aplanatic. If an aplanatic system is required; that is one free from coma so that near axial points will be focussed in the Airy disc, it is necessary to use two mirror systems with aspheric surfaces such as those given by Wolter (120).

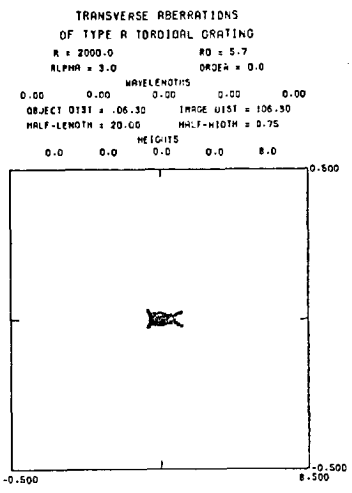
TRANSVERSE ABERRATIONS
OF TYPE A TOROIDAL GRATING
R = 2000.0
RO = 5.7
ALPHA = 3.0
ORDER = 0.0
WAVELENGTHS
0.00 0.00 0.00 0.00 0.00
OBJECT DIST = .06.30
IMAGE DIST = 106.30
HALF-LENGTH = 20.00
HALF-WIDTH = 0.75
WEIGHTS
0.0 0.0 0.0 0.0 8.0
0.500
-0.500
-0.500
8.500

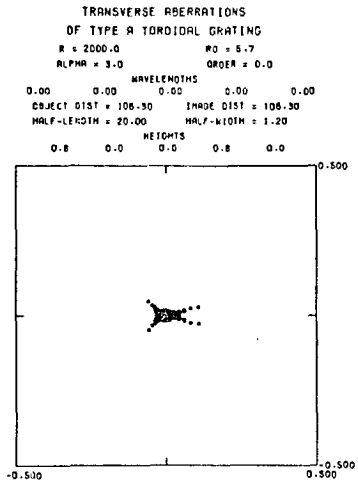
TRANSVERSE ABERRATIONS
OF TYPE A TOROIDAL GRATING
R = 2000.0
RO = 5.7
ALPHA = 3.0
ORDER = 0.0
WAVELENGTHS
0.00 0.00 0.00 0.00 0.00
OBJECT DIST = 106.30
IMAGE DIST = 106.30
HALF-LENGTH = 20.00
HALF-WIDTH = 1.20
WEIGHTS
0.8 0.0 0.0 0.8 0.0
0.500
-0.500
-0.500
0.300

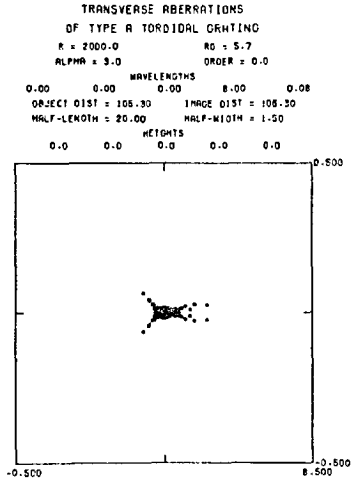
TRANSVERSE ABERRATIONS
OF TYPE A TOROIDAL GRATING
R = 2000.0
RO = 5.7
ALPHA = 3.0
ORDER = 0.0
WAVELENGTHS
0.00 0.00 0.00 8.00 0.00
OBJECT DIST = 106.30
IMAGE DIST = 106.30
HALF-LENGTH = 20.00
HALF-WIDTH = 1.50
WEIGHTS
0.0 0.0 0.0 0.0 0.0
0.500
-0.500
-0.500
8.500

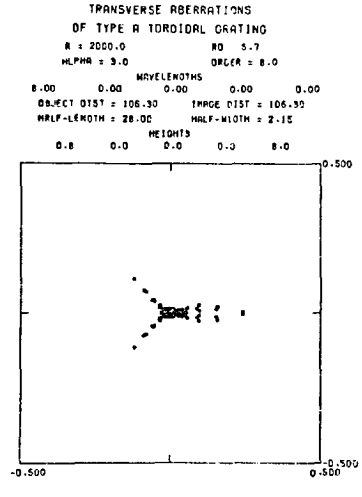
TRANSVERSE ABERRATIONS
OF TYPE A TOROIDAL GRATING
R = 2000.0
RO 5.7
ALPHA = 3.0
ORDER = 8.0
WAVELENGTHS
8.00 0.00 0.00 0.00 0.00
OBJECT DIST = 106.30
IMAGE DIST = 106.30
HALF-LENGTH = 28.00
HALF-WIDTH = 2.15
WEIGHTS
0.8 0.0 0.0 0.0 8.0
0.500
-0.500
-0.500
0.500

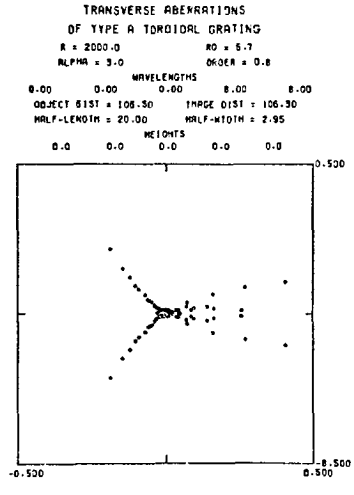
TRANSVERSE ABERRATIONS
OF TYPE A TOROIDAL GRATING
R = 2000.0
RO = 5.7
ALPHA = 3.0
ORDER = 0.8
WAVELENGTHS
0.00 0.00 0.00 8.00 8.00
OBJECT DIST = 106.30
IMAGE DIST = 106.30
HALF-LENGTH = 20.00
HALF-WIDTH = 2.95
WEIGHTS
0.0 0.0 0.0 0.0 0.0
0.500
-0.500
-8.500
8.500

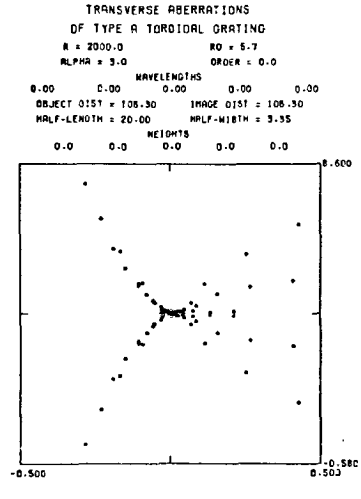
TRANSVERSE ABERRATIONS
OF TYPE A TOROIDAL GRATING
R = 2000.0
RO = 5.7
ALPHA = 3.0
ORDER = 0.0
WAVELENGTHS
0.00 0.00 0.00 0.00 0.00
OBJECT DIST = 106.30
IMAGE DIST = 106.30
HALF-LENGTH = 20.00
HALF-WIDTH = 3.35
WEIGHTS
0.0 0.0 0.0 0.0 0.0
8.600
-0.500
-0.580
8.503

FIG. 35

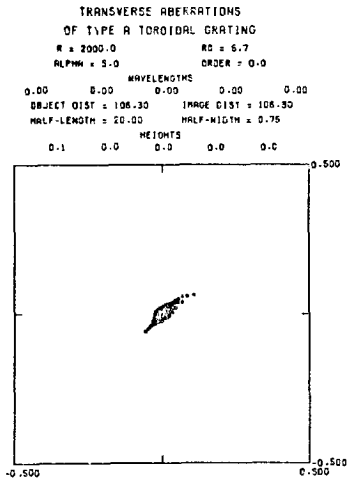
TRANSVERSE ABERRATIONS
OF TYPE A TOROIDAL GRATING
R = 2000.0 RO = 5.7
ALPHA = 5.0 ORDER = 0.0
WAVELENGTHS
0.00 0.00 0.00 0.00 0.00
OBJECT DIST = 106.30 IMAGE DIST = 106.30
HALF-LENGTH = 20.00 HALF-WIDTH = 0.75
HEIGHTS
0.1 0.0 0.0 0.0 0.0
0.500
-0.500
-0.500
0.500

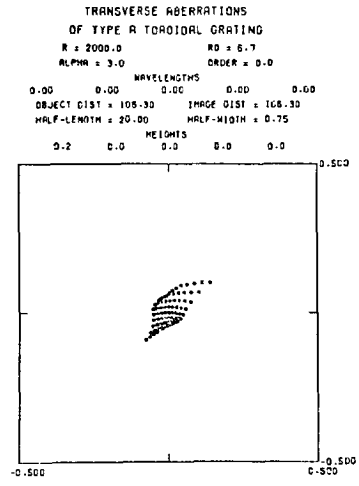
TRANSVERSE ABERRATIONS
OF TYPE A TOROIDAL GRATING
R = 2000.0 RO = 5.7
ALPHA = 3.0 ORDER = 0.0
WAVELENGTHS
0.00 0.00 0.00 0.00 0.00
OBJECT DIST = 106.30 IMAGE DIST = 106.30
HALF-LENGTH = 20.00 HALF-WIDTH = 0.75
HEIGHTS
0.2 0.0 0.0 0.0 0.0
0.500
-0.500
-0.500
0.500

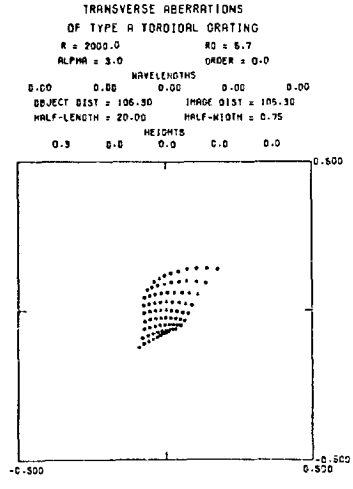
TRANSVERSE ABERRATIONS
OF TYPE A TOROIDAL GRATING
R = 2000.0 RO = 5.7
ALPHA = 3.0 ORDER = 0.0
WAVELENGTHS
0.00 0.00 0.00 0.00 0.00
OBJECT DIST = 106.30 IMAGE DIST = 106.30
HALF-LENGTH = 20.00 HALF-WIDTH = 0.75
HEIGHTS
0.3 0.0 0.0 0.0 0.0
0.500
-0.500
-0.500
0.500

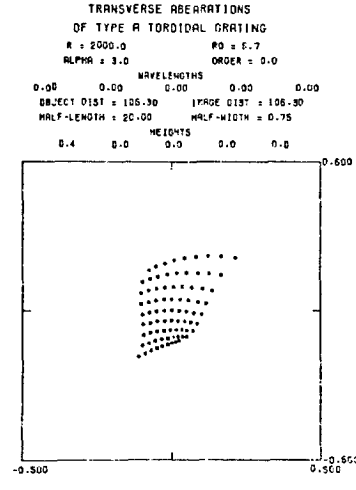
TRANSVERSE ABERRATIONS
OF TYPE A TOROIDAL GRATING
R = 2000.0 RO = 5.7
ALPHA = 3.0 ORDER = 0.0
WAVELENGTHS
0.00 0.00 0.00 0.00 0.00
OBJECT DIST = 106.30 IMAGE DIST = 106.30
HALF-LENGTH = 20.00 HALF-WIDTH = 0.75
HEIGHTS
0.4 0.0 0.0 0.0 0.0
0.500
-0.500
-0.500
0.500

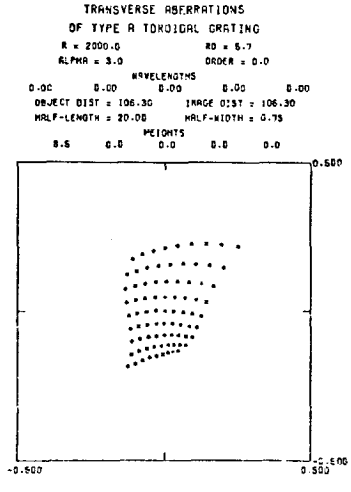
TRANSVERSE ABERRATIONS
OF TYPE A TOROIDAL GRATING
R = 2000.0 RO = 5.7
ALPHA = 3.0 ORDER = 0.0
WAVELENGTHS
0.00 0.00 0.00 0.00 0.00
OBJECT DIST = 106.30 IMAGE DIST = 106.30
HALF-LENGTH = 20.00 HALF-WIDTH = 0.75
HEIGHTS
0.5 0.0 0.0 0.0 0.0
0.500
-0.500
-0.500
0.500

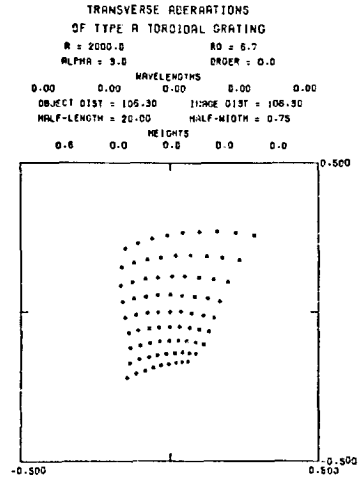
TRANSVERSE ABERRATIONS
OF TYPE A TOROIDAL GRATING
R = 2000.0 RO = 5.7
ALPHA = 3.0 ORDER = 0.0
WAVELENGTHS
0.00 0.00 0.00 0.00 0.00
OBJECT DIST = 106.30 IMAGE DIST = 106.30
HALF-LENGTH = 20.00 HALF-WIDTH = 0.75
HEIGHTS
0.6 0.0 0.0 0.0 0.0
0.500
-0.500
-0.500
0.500

FIG. 36

Holographic gratings were formed on the toroidal blanks and the efficiency and imaging properties of the gratings were measured at soft x-ray wavelengths using the grating testing apparatus. The efficiency was measured using the usual photomultiplier detector system and it was found that the efficiency was typically ~3% which was also about the same as the efficiency of a plane grating produced by the same technique. Thus, the efficiency of holographic gratings appeared to be independent of substrate curvature.

In order to investigate the imaging properties of the toroidal gratings, the grating test apparatus was modified to incorporate photographic recording. Since it was only possible to obtain the best focus by trial, a camera assembly was developed which enabled several separate images to be recorded on one plate. A toroidal grating was carefully set up on the optical bench, in the test apparatus, using a laser and a white light source to correctly position the 100μm pinhole which served as the object, and the 2mm diameter diaphragm in front of the grating which restricted the grating aperture. When the system had been correctly adjusted using white light, the light source was replaced by the x-ray source and the chamber was evacuated. The experimental procedure was to first record the zero order focus to check the alignment and then to adjust the geometry using the calibrated controls and take several exposures at a series of image distances in order to find the best focus. Some typical x-ray images from the toroidal grating are shown in Fig. 37, 38. The images were recorded with the photographic plate set perpendicular to the incident x-ray beam.

TOROIDAL GRATING. Imaging properties at 44Å

Major radius 2 metres. Minor radius 5·6mm. Lamellar profile, 600 lines per mm.

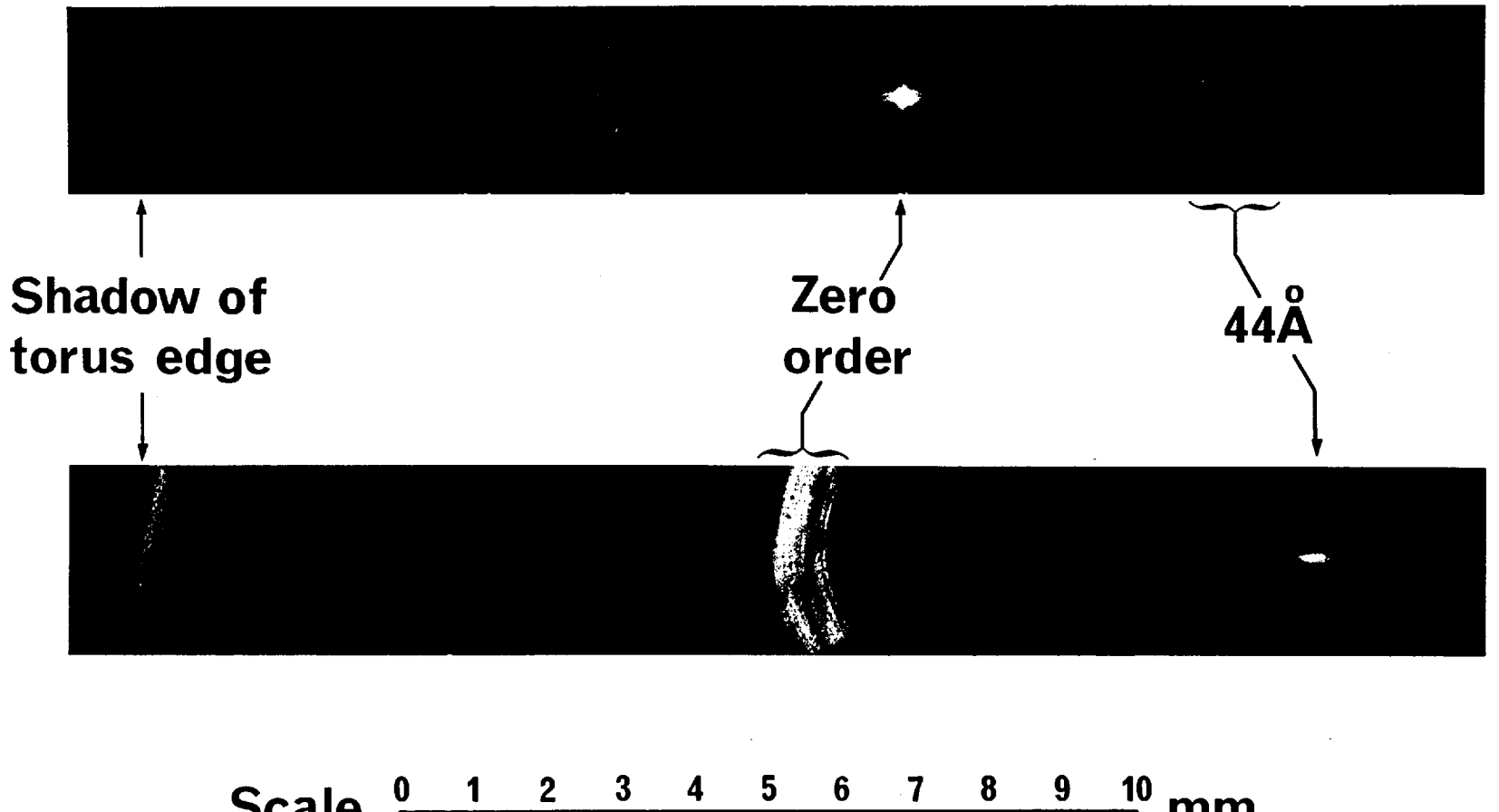

FIG. 37

AN X-RAY IMAGE FORMED AT 23 A FROM

THE TOROIDAL GRATING

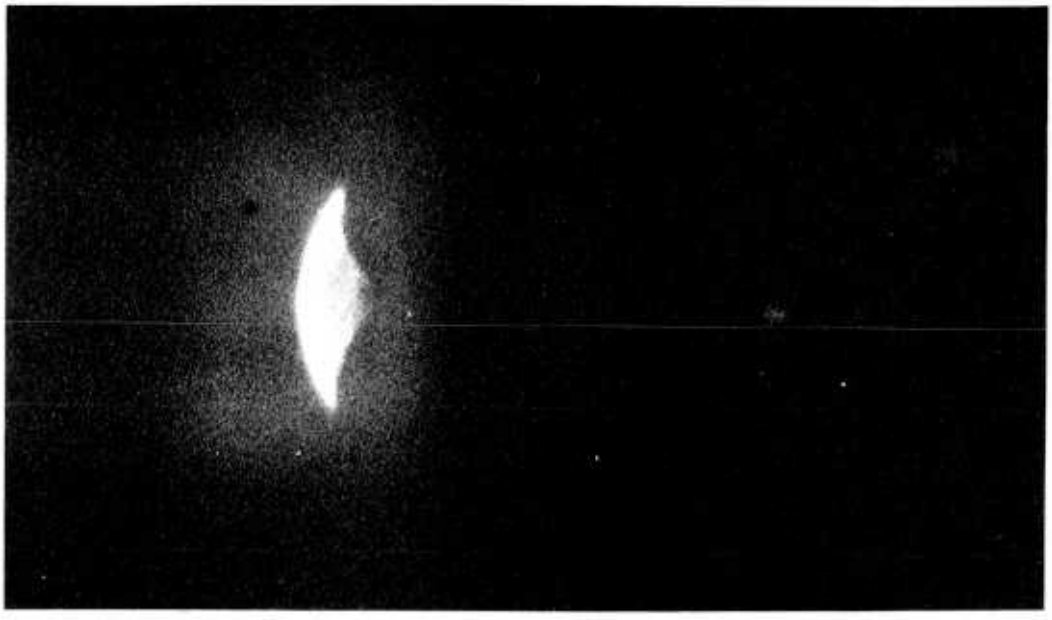

Zero Order (out of focus)

23 A Stigmatic Image

SCALE 0 1 2 3 4 5 mm

Angle of grazing incidence = 2.4°

Image recorded on an Ilford Q2 plate set perpendicular to the incident x-ray beam. The print is to the same scale as Fig. 37.

FIG. 38

The experimental investigation of the imaging properties of the toroidal diffraction grating at 45 Å and 23 Å demonstrated conclusively that it was possible to fabricate stigmatic gratings for use in the soft x-ray region by forming the gratings holographically on an aspheric surface. The experimental results also indicated that for most practical purposes the gratings which had been constructed were not ideal. However, the method had been demonstrated, the technology proved, and the path now lay open for all kinds of grating systems to be designed.

Before proceeding to the design of other systems it was necessary to thoroughly understand the aberrations of the toroidal grating so that these defects could be avoided in future. Fig.39 shows the aberrations of a spherical grating with 600 l/mm, radius 2m and the same dimensions as the toroidal grating, under Rowland circle conditions illuminated by a point source, on axis, emitting 21 Å, 23 Å and 25 Å. It can be seen that the lines are broadened by spherical aberration. The transverse aberrations for the same conditions are shown in Fig. 40 and it can be seen that instead of the 21 Å line becoming out of focus at the image distance for 23 Å in fact the ray bundle becomes narrower. The reason for this is that the grating width is very much greater than the optimum and should be reduced to 11.7mm on the Mack, Stehn and Edlén criterion. Fig. 41 shows the greatly reduced transverse aberrations when the grating width is reduced to 10mm. The transverse aberrations of a toroidal grating under the same conditions as the spherical grating in Fig. 40 are shown in Fig. 42. The large reduction in astigmatism has enabled the vertical scale for the spot diagrams from the toroidal

ABERRATIONS OF A SPHERICAL GRATING
ON THE ROWLAND CIRCLE

R = 2000.0 RO = 2000.0

ALPHA = 2.4 ORDER = 1.0

WAVELENGTHS

23.00 21.00 25.00 0.00 0.00

OBJECT DIST = 84.03 IMAGE DIST = 134.48

HALF-LENGTH = 20.00 HALF-WIDTH = 0.75

HEIGHTS

0.0 0.0 0.0 0.0 0.0

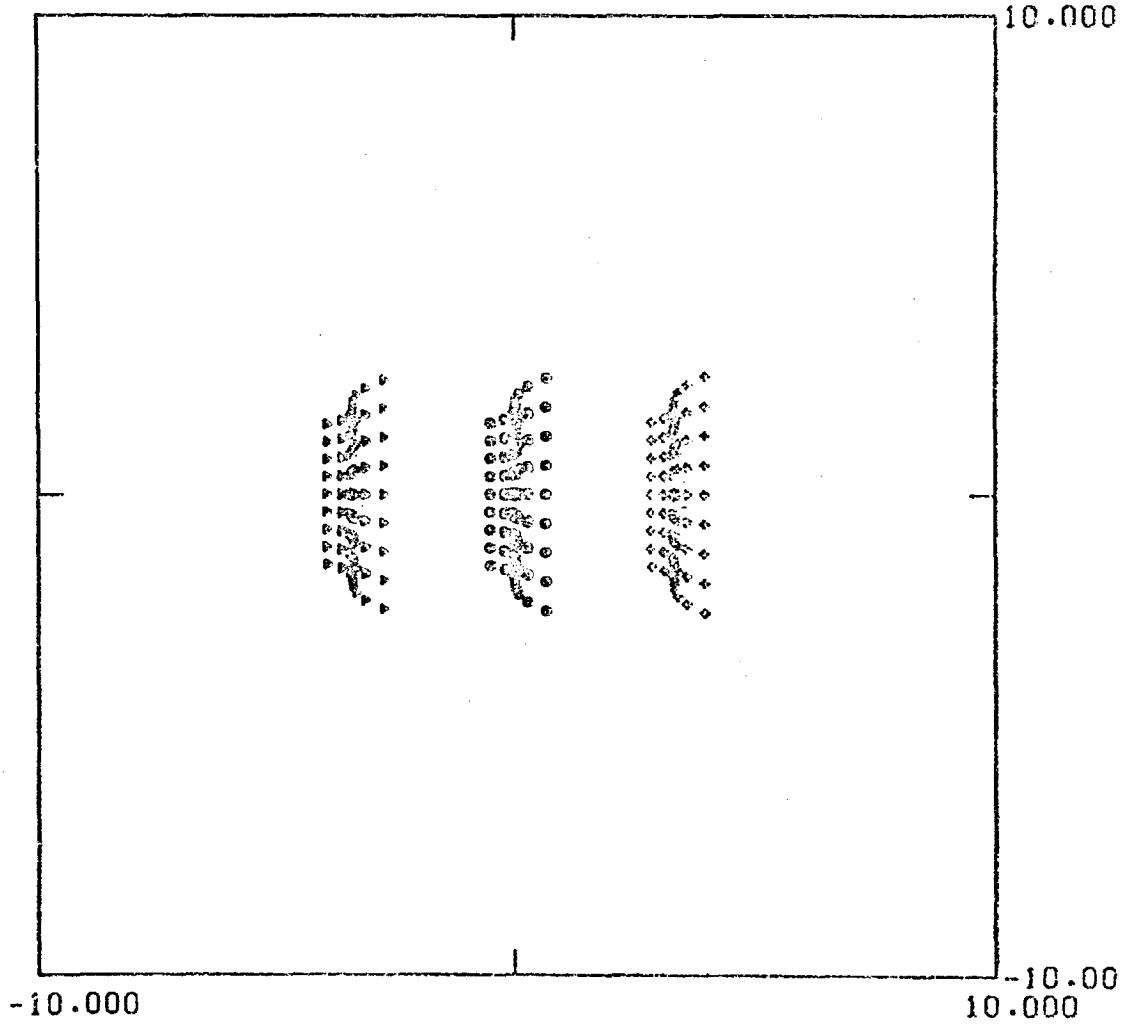

FIG. 39

TRANSVERSE ABERRATIONS
OF A SPHERICAL GRATING

R = 2000.0 RO = 2000.0

ALPHA = 2.4 ORDER = 1.0

WAVELENGTHS

23.00 21.00 25.00 0.00 0.00

OBJECT DIST = 84.03 IMAGE DIST = 134.48

HALF-LENGTH = 20.00 HALF-WIDTH = 0.75

HEIGHTS

0.0 0.0 0.0 0.0 0.0

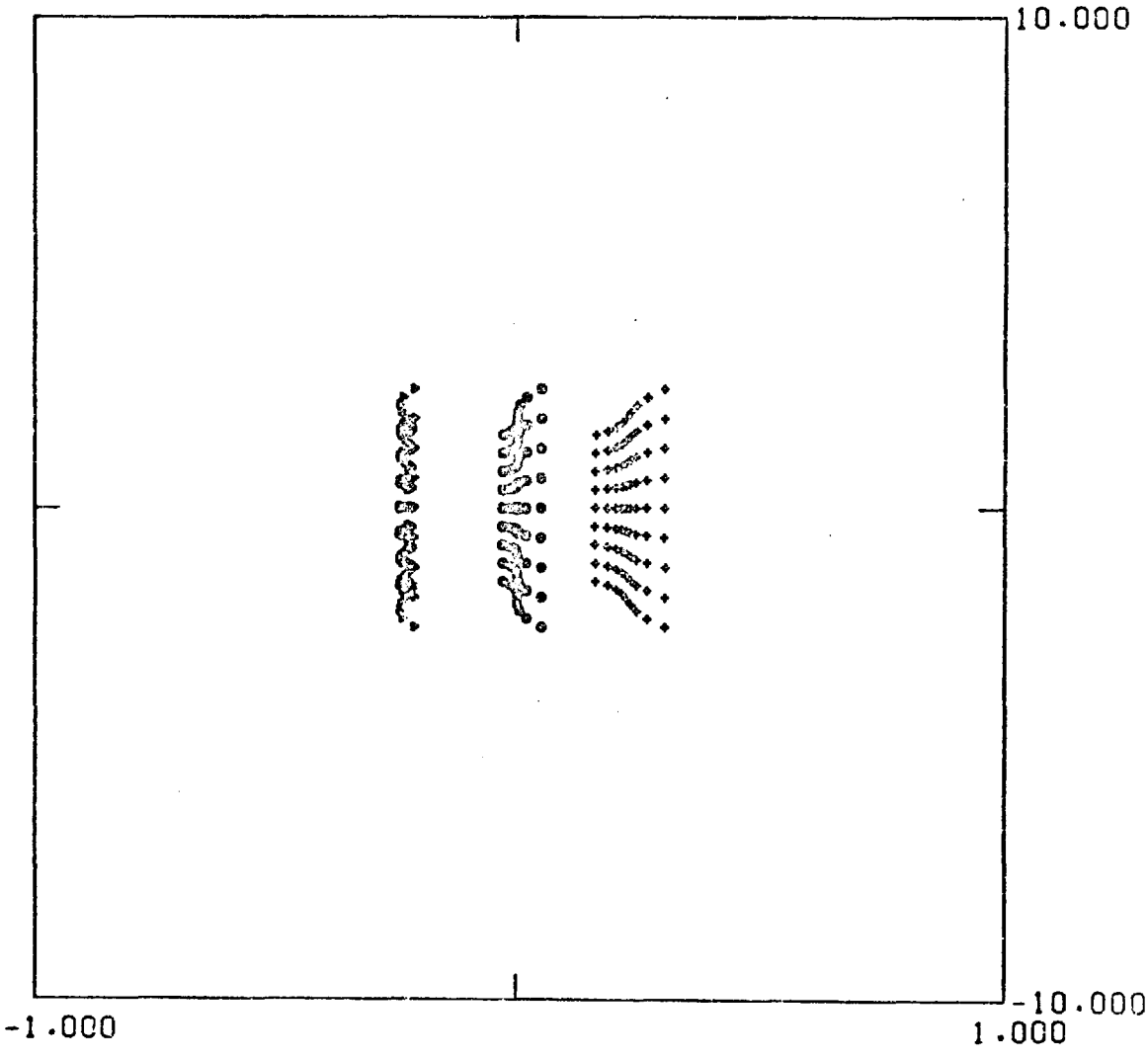

FIG. 40

TRANSVERSE ABERRATIONS
OF A SPHERICAL GRATING

R = 2000.0 RO = 2000.0

ALPHA = 2.4 ORDER = 1.0

WAVELENGTHS

23.00 21.00 25.00 0.00 0.00

OBJECT DIST = 84.03 IMAGE DIST = 134.48

HALF-LENGTH = 5.00 HALF-WIDTH = 0.75

HEIGHTS

0.0 0.0 0.0 0.0 0.0

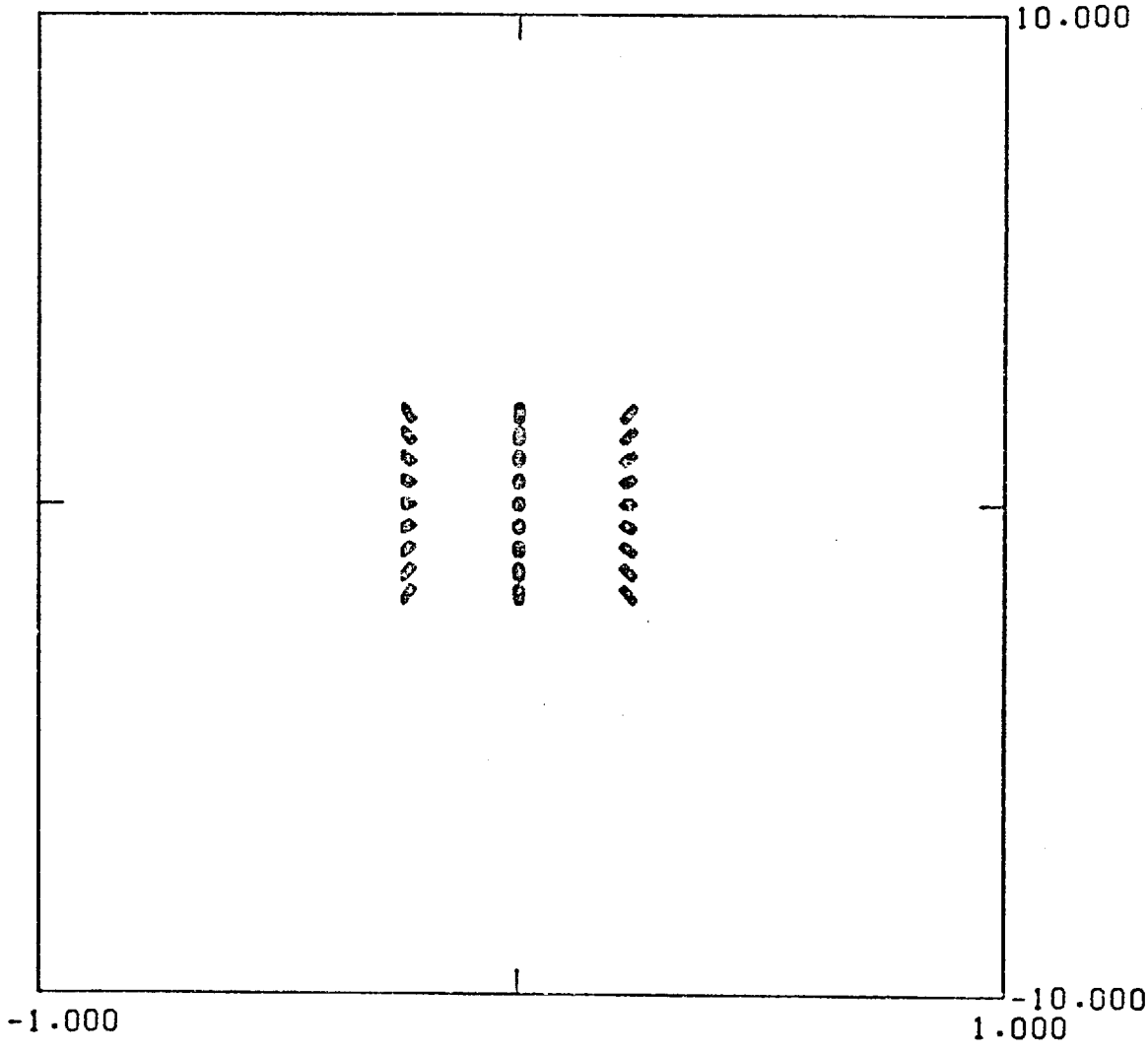

FIG. 41

TRANSVERSE ABERRATIONS
OF TYPE A TOROIDAL GRATING

R = 2000.0 RO = 5.7

ALPHA = 2.4 ORDER = 1.0

WAVELENGTHS

23.00 21.00 25.00 0.00 0.00

OBJECT DIST = 84.03 IMAGE DIST = 134.48

HALF-LENGTH = 20.00 HALF-WIDTH = 0.75

HEIGHTS

0.0 0.0 0.0 0.0 0.0

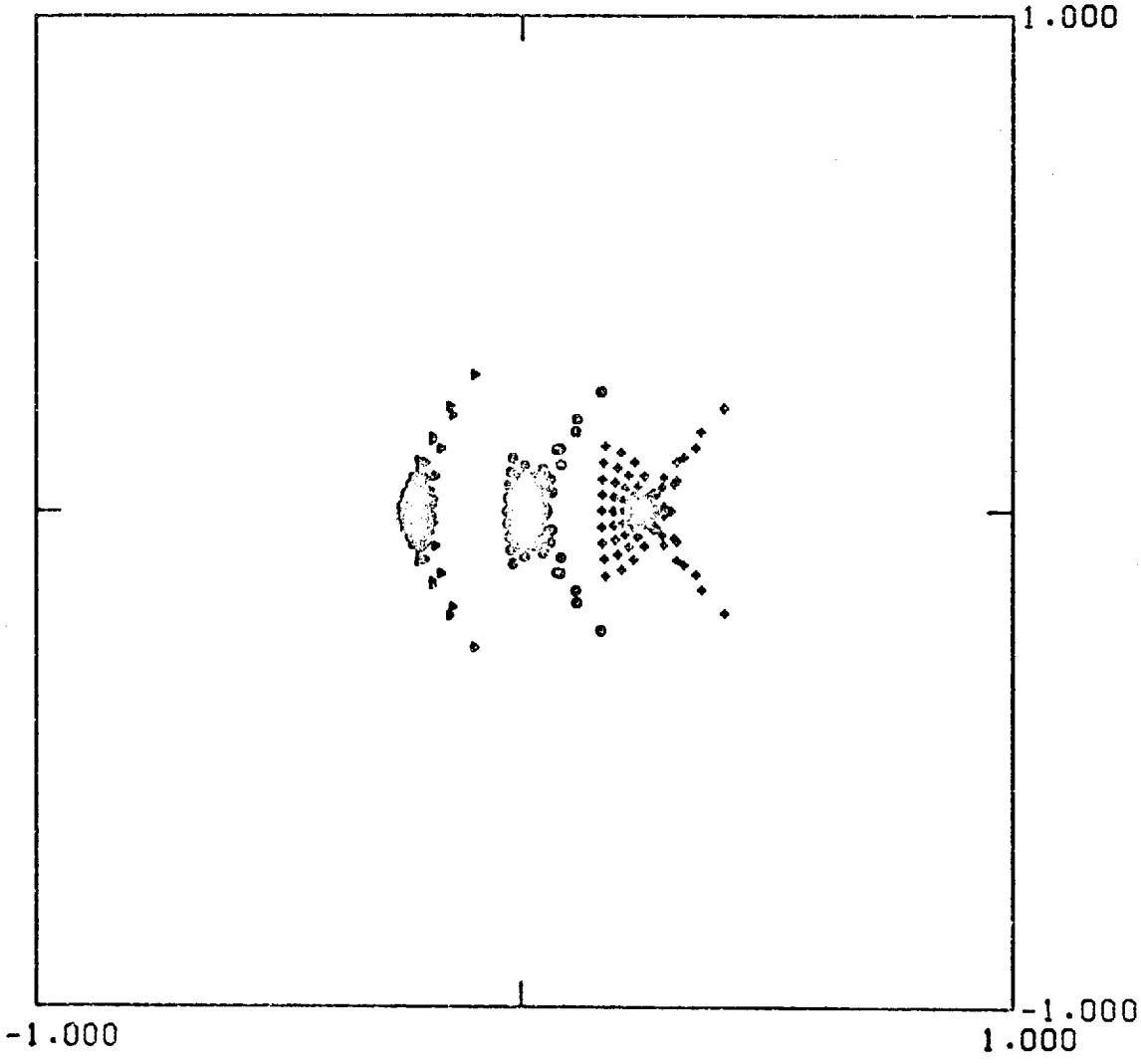

FIG. 42

grating to be increased by a factor of 10 so that both horizontal and vertical sides are equal. However, the images have become broadened and "wings" have appeared. If the width of the toroid is reduced to the optimum width for the spherical grating as in Fig. 43, it can be seen that the "wings" disappear and the images become much more symmetrical in shape. However, it should be noted that images from the toroidal grating are considerably broader than those from a corresponding spherical grating and that the geometrical centre of the images from the toroid have been shifted towards longer wavelengths by the coma-type aberration. Finally, at these wavelengths, in Fig. 44 are shown images produced by three point sources; one on axis and one 0.2mm above and one 0.2mm below the meridian plane (corresponding to a field angle of 16 arc minutes). The off-axis points are afflicted with coma, however, it can be seen that both spatial and spectral resolution can be achieved simultaneously by this system at x-ray wavelengths provided the field angle and grating aperture are restricted.

The ray tracing analysis of the imaging from the toroidal grating has also been performed at wavelengths of 40 A, 44.5 A and 49 A. The structure of the image is clearly shown in Fig. 45 in which the whole width of the grating is illuminated and the improvement obtained by reducing the grating width is shown in Fig. 46. Similarly, the off-axis images for the full grating width and optimum width are shown in Fig. 47 and Fig. 49. Finally the spot diagram showing the aberration at three wavelengths - 40 A, 44.5 A and 49 A - and for three object points - on axis, 0.2mm above and 0.2mm below the meridian plane - is given in Fig. 49. This result again demonstrates that for a restricted wavelength range and a

TRANSVERSE ABERRATIONS
OF TYPE A TOROIDAL GRATING

R = 2000.0 RO = 5.7

ALPHA = 2.4 ORDER = 1.0

WAVELENGTHS

23.00 21.00 25.00 0.00 0.00

OBJECT DIST = 84.03 IMAGE DIST = 134.48

HALF-LENGTH = 5.00 HALF-WIDTH = 0.75

HEIGHTS

0.0 0.0 0.0 0.0 0.0

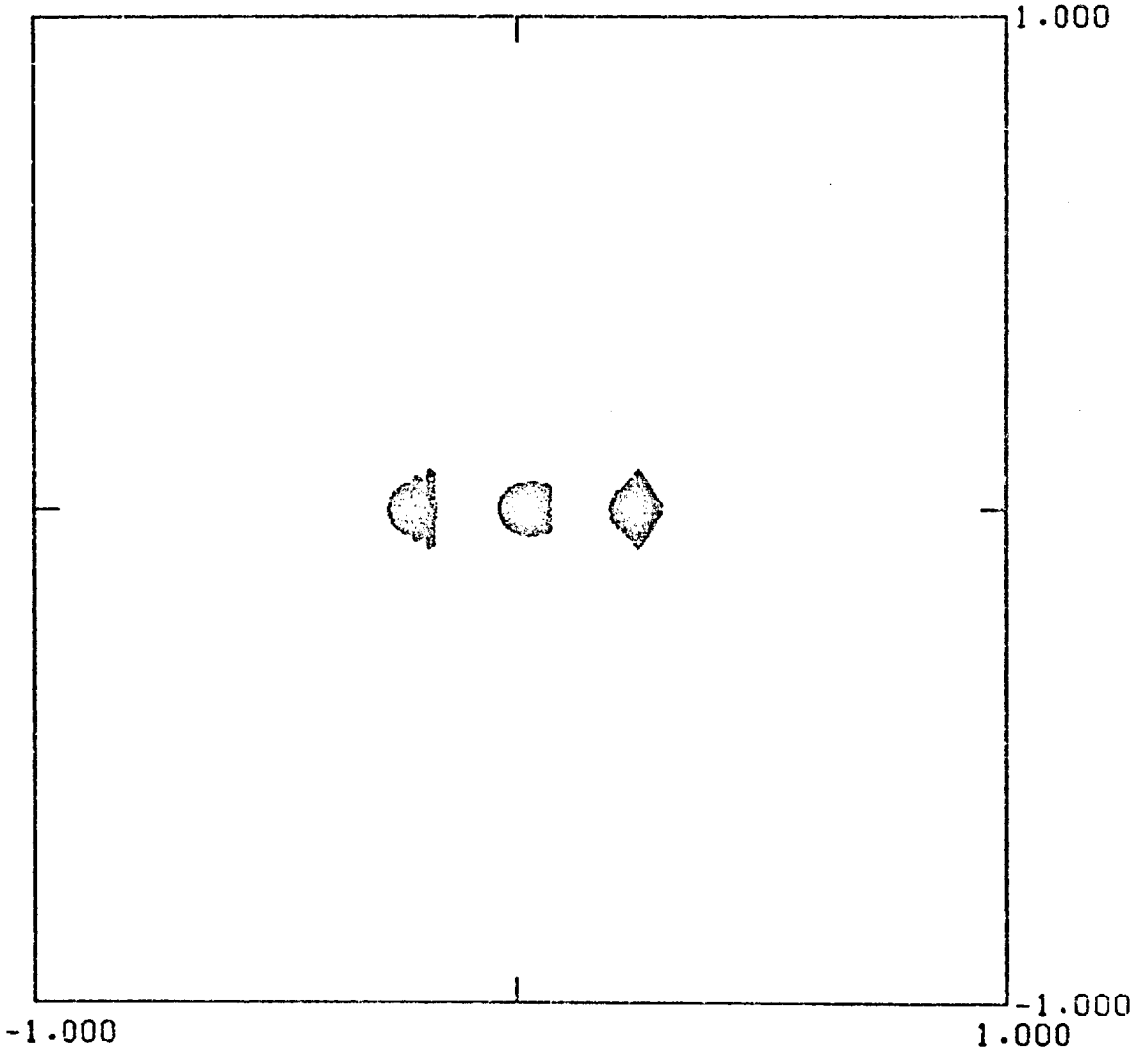

FIG. 43

TRANSVERSE ABERRATIONS
OF TYPE A TOROIDAL GRATING

R = 2000.0 RO = 5.7

ALPHA = 2.4 ORDER = 1.0

WAVELENGTHS

23.00 21.00 25.00 0.00 0.00

OBJECT DIST = 84.03 IMAGE DIST = 134.48

HALF-LENGTH = 5.00 HALF-WIDTH = 0.75

HEIGHTS

0.0 0.2 -0.2 0.0 0.0

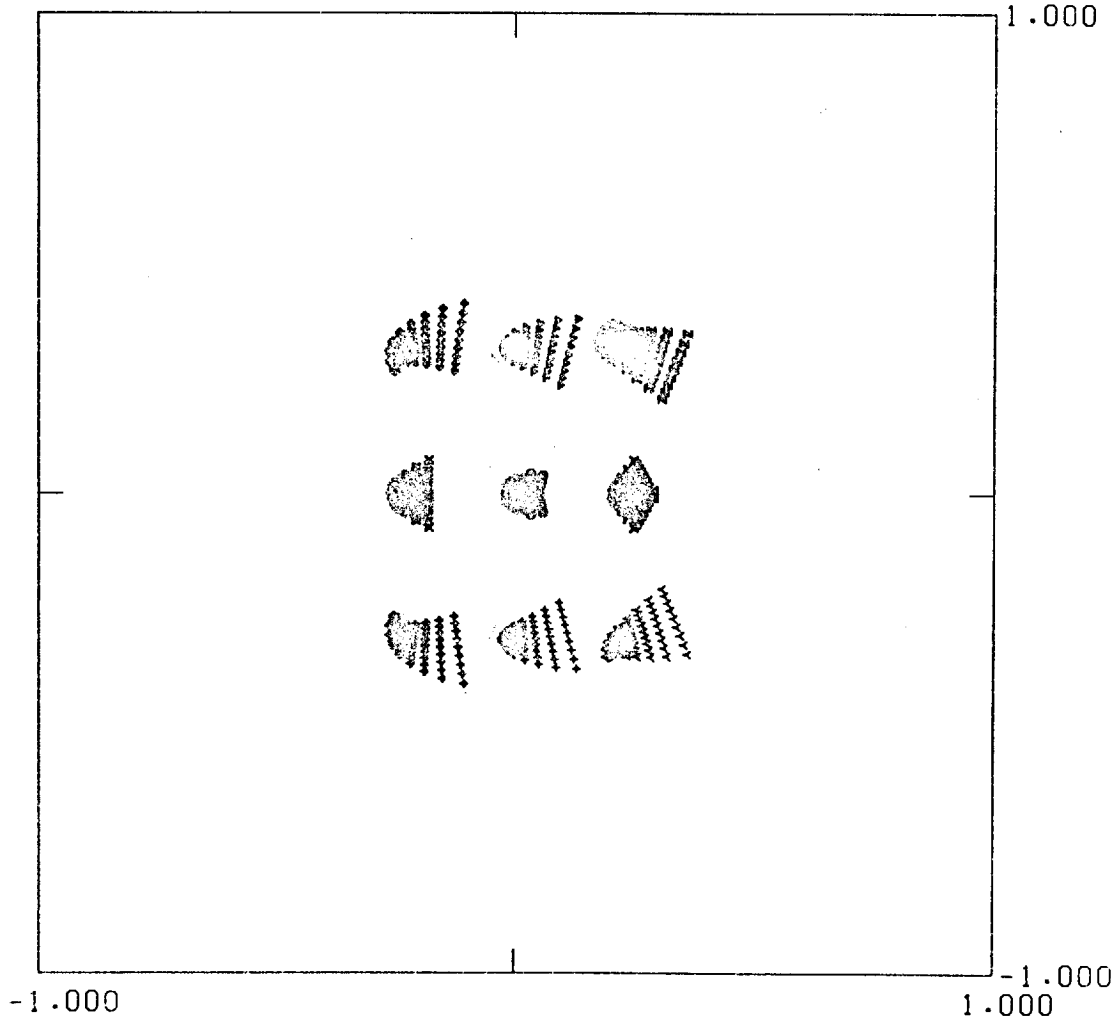

FIG. 44

TRANSVERSE ABERRATIONS
OF TYPE A TOROIDAL GRATING

R = 2000.0 RO = 5.7

ALPHA = 2.0 ORDER = 1.0

WAVELENGTHS

44.50 40.00 49.00 0.00 0.00

OBJECT DIST = 69.82 IMAGE DIST = 161.84

HALF-LENGTH = 20.00 HALF-WIDTH = 0.75

HEIGHTS

0.0 0.0 0.0 0.0 0.0

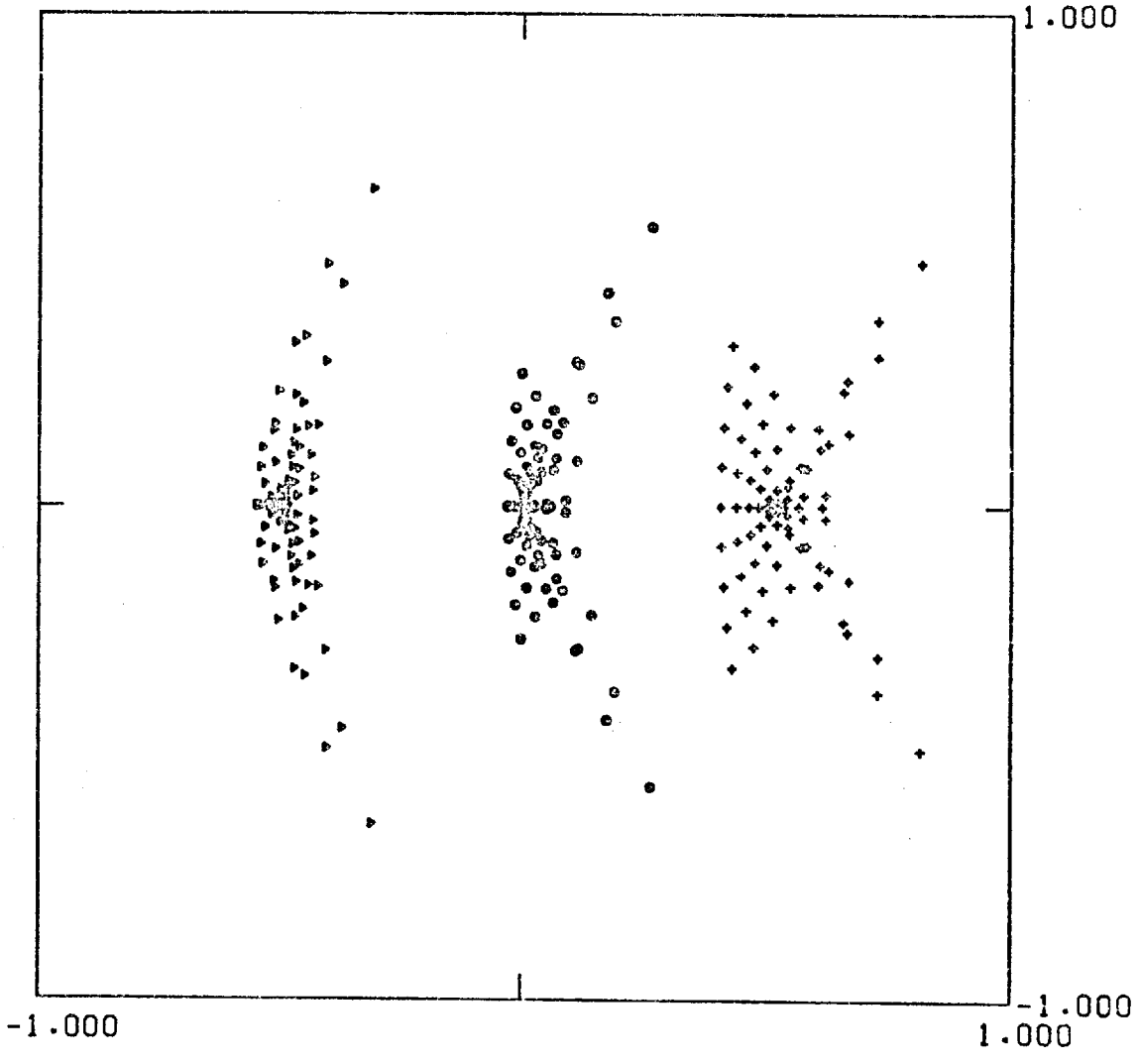

FIG. 45

TRANSVERSE ABERRATIONS
OF TYPE A TOROIDAL GRATING

R = 2000.0 RO = 5.7

ALPHA = 2.0 ORDER = 1.0

WAVELENGTHS

44.50 40.00 49.00 0.00 0.00

OBJECT DIST = 69.82 IMAGE DIST = 161.84

HALF-LENGTH = 5.00 HALF-WIDTH = 0.75

HEIGHTS

0.0 0.0 0.0 0.0 0.0

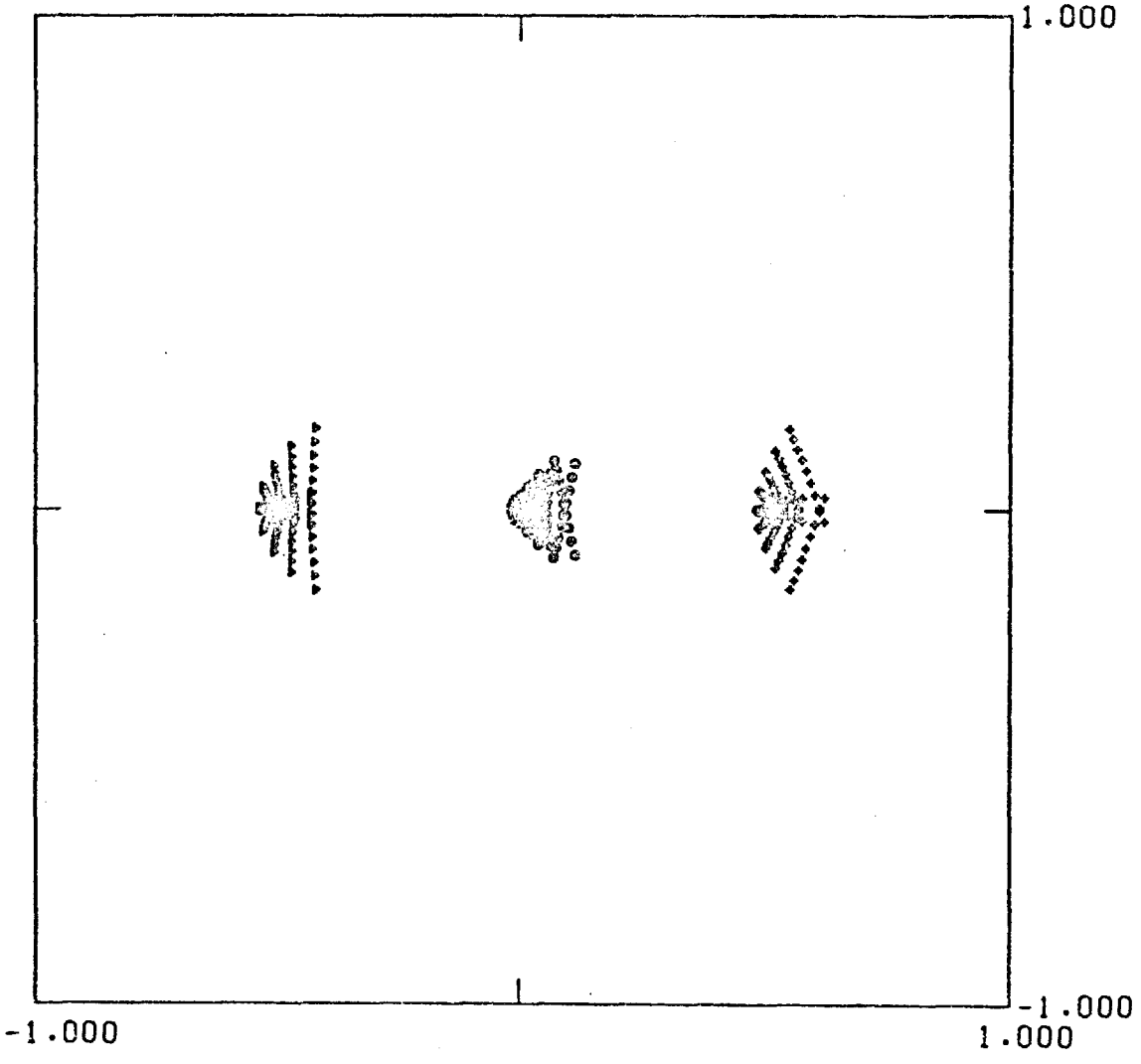

FIG. 46

TRANSVERSE ABERRATIONS
OF TYPE A TOROIDAL GRATING

R = 2000.0 RO = 5.7

ALPHA = 2.0 ORDER = 1.0

WAVELENGTHS

44.50 40.00 49.00 0.00 0.00

OBJECT DIST = 69.82 IMAGE DIST = 161.84

HALF-LENGTH = 20.00 HALF-WIDTH = 0.75

HEIGHTS

0.2 0.0 0.0 0.0 0.0

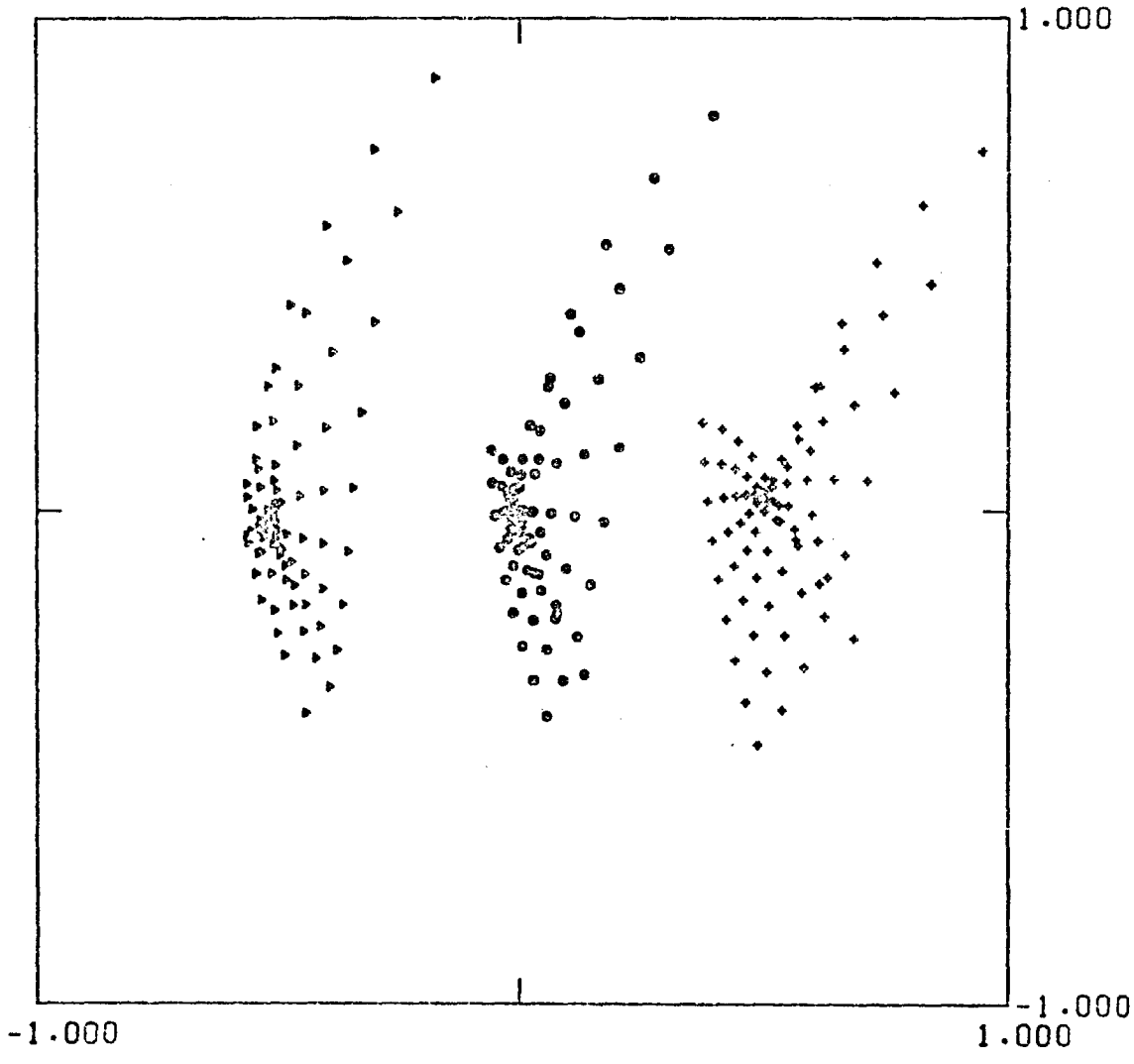

FIG. 47

TRANSVERSE ABERRATIONS

OF TYPE A TOROIDAL GRATING

R = 2000.0 RO = 5.7

ALPHA = 2.0 ORDER = 1.0

WAVELENGTHS

44.50 40.00 49.00 0.00 0.00

OBJECT DIST = 69.82 IMAGE DIST = 161.84

HALF-LENGTH = 5.00 HALF-WIDTH = 0.75

HEIGHTS

0.2 0.0 0.0 0.0 0.0

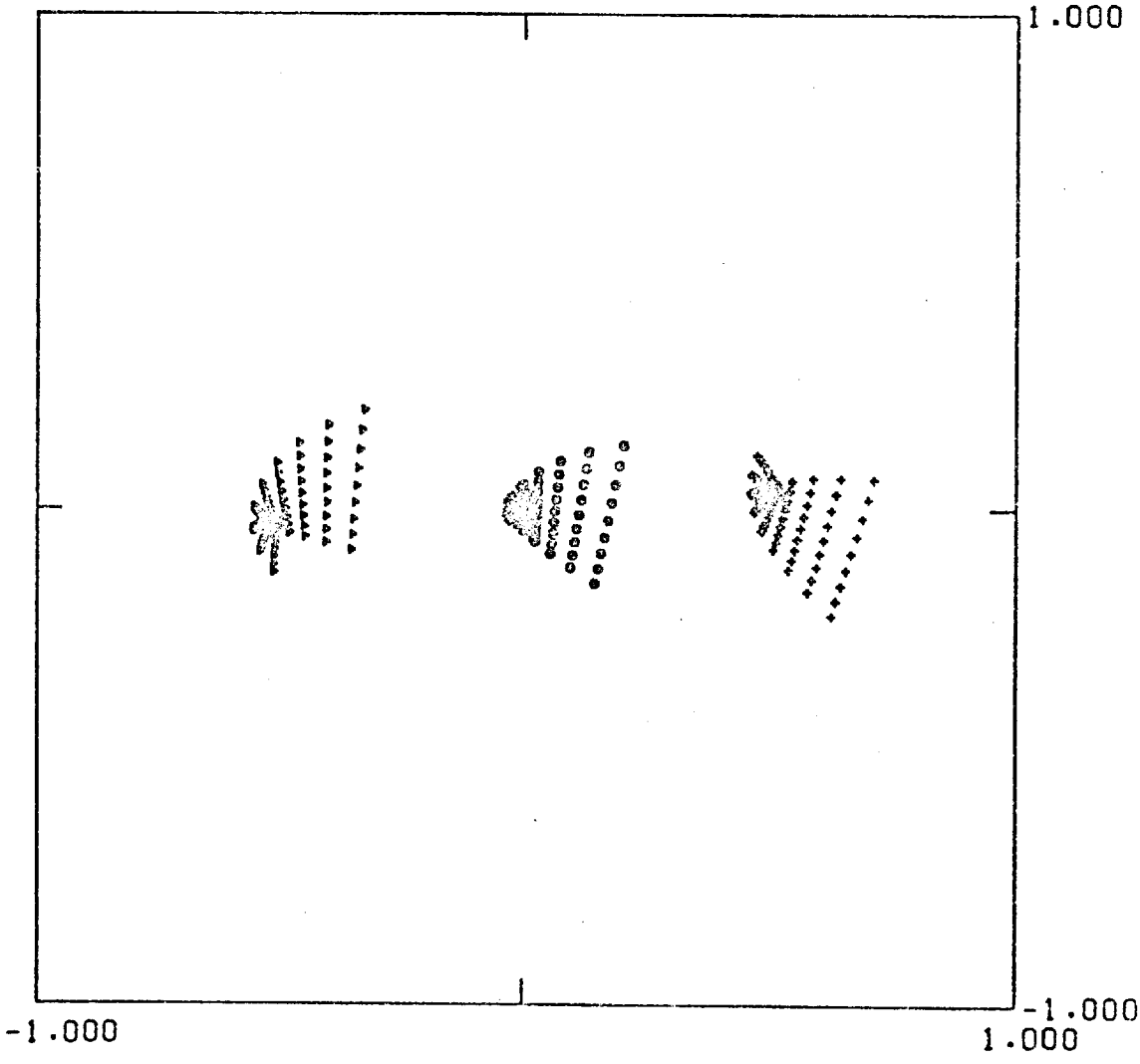

FIG. 48

TRANSVERSE ABERRATIONS
OF TYPE A TOROIDAL GRATING

R = 2000.0 RO = 5.7

ALPHA = 2.0 ORDER = 1.0

WAVELENGTHS

44.50 40.00 49.00 0.00 0.00

OBJECT DIST = 69.82 IMAGE DIST = 161.84

HALF-LENGTH = 5.00 HALF-WIDTH = 0.75

HEIGHTS

0.0 0.2 -0.2 0.0 0.0

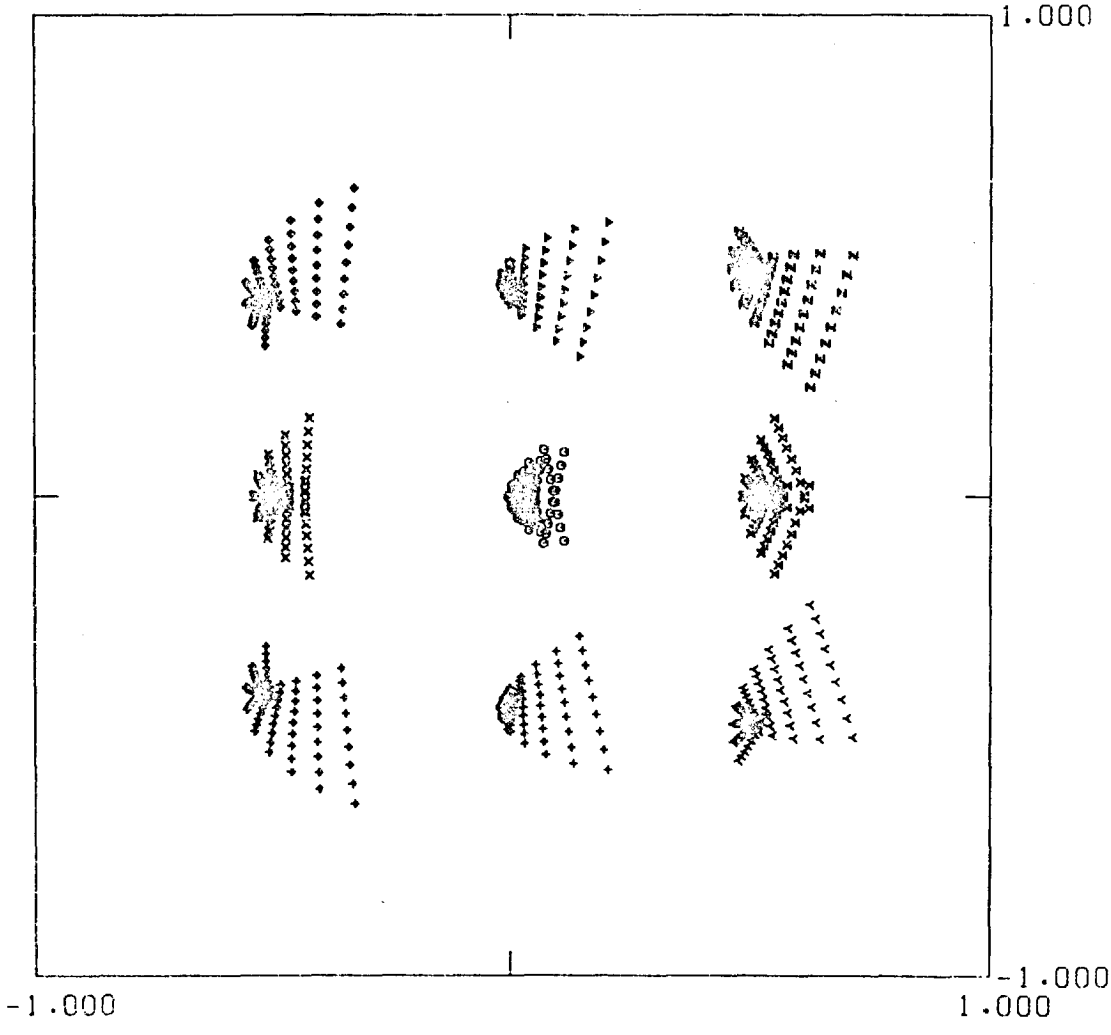

FIG. 49

restricted field angle it is possible to use a toroidal grating to provide both spatial and spectral resolution.

Although the aberrations of the fabricated toroidal grating are considerable, it is conceivable that they could be used for certain experiments to provide some simultaneous spatial and spectral information. The robust construction of grazing incidence systems compared to the delicate structure of zone-plates and transmission gratings means that it may be essential to use a grazing incidence system for some applications on mechanical grounds. It is possible to achieve a higher diffraction efficiency from grazing incidence gratings than from transmission zone-plates and transmission gratings in the soft x-ray region. The dispersion of grazing incidence systems can also be much higher than normal incidence systems. Therefore, it may be only possible to obtain the maximum useful data in some experiments by employing a correctly designed grazing incidence system.

In order to design a system which covers an adequate field, it will most probably be necessary to use a system with two or more elements. However, a second form of toric surface, which has been designated "Type B" to distinguish it from our first type of toroidal x-ray grating (now called "Type A") possesses superior zero-order imaging properties to the type of toroidal grating fabricated. As shown in Fig. 50 the "Type A" toric surface is formed by rotating a circle of radius ρ to describe an arc of radius R whereas the "Type B" torus is formed by rotating an arc of radius R about an axis through the ends of the arc. Thus, the type A torus has the shape of an internal section of a bicycle tyre and the type B toroid has the shape

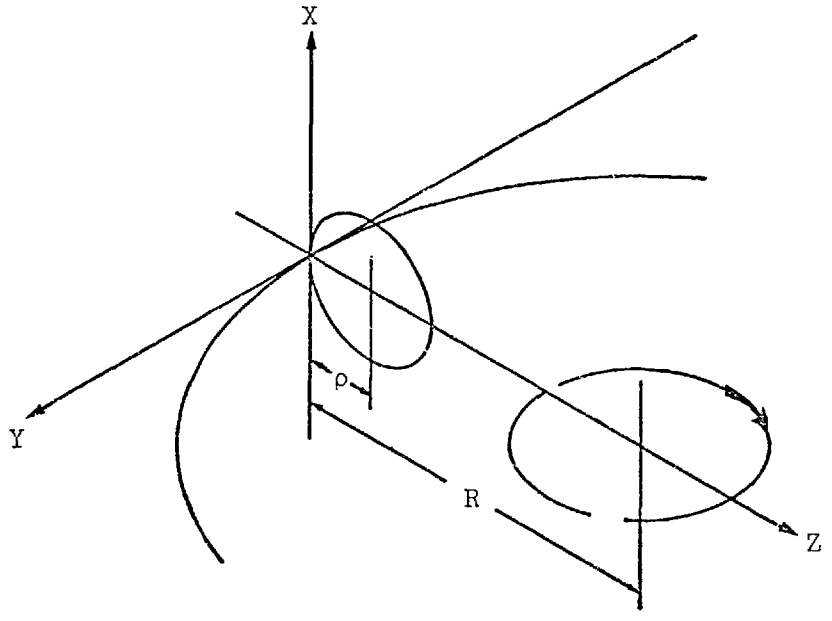

The "Type A" Toroid

This surface is generated by revolving a circle of radius ρ about a straight line, lying in the plane of the circle, at a distance R-ρ from its centre.

The "Type B" Toroid

This surface is generated by revolving a curve, f(y), in the y-z plane about an axis parallel to the y-axis. The profiles of the surface in planes parallel to the x-z plane are circles of radius ρ-f(y).

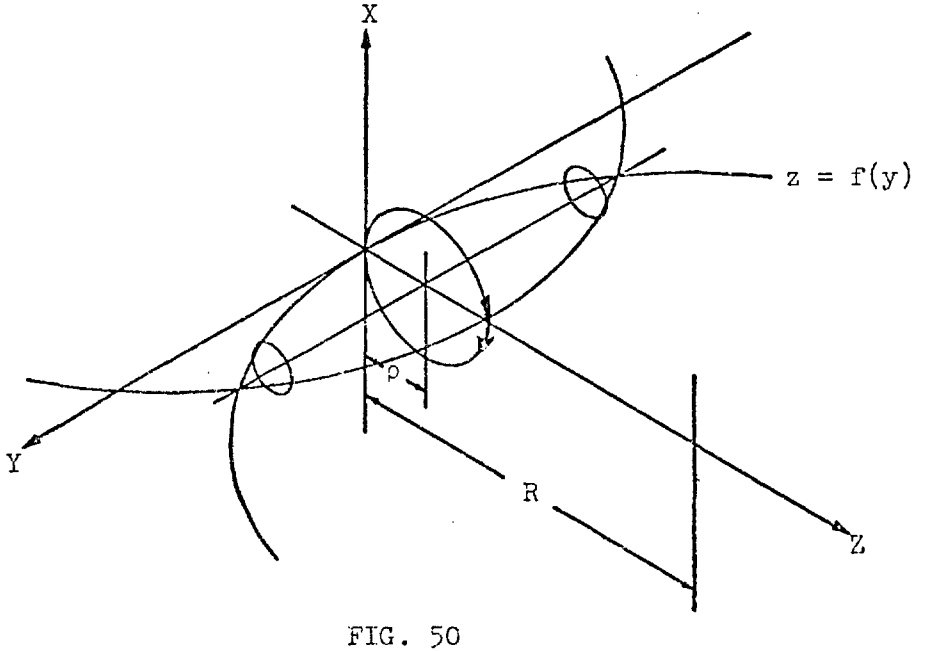

FIG. 50

of the inside of a tapering cigar or barrel.

The difference in the zero-order imaging of the two forms of toroid can be seen by comparing Fig. 51 and Fig. 52 which show spot diagrams produced with identical parameters. The additional curvature of the type B toroid has brought the extreme rays nearer the correct focus; however, since the grating width is much greater than the optimum, the image is broadened by spherical aberration.

Unlike the type A toroid the aberrations of the type B toroid are only slightly altered by increasing the grating aperture as can be seen from Fig. 53 which corresponds to Fig. 35 for the type A toroid. However, the off-axis imaging of the type B toroid is no better than the type A toroid, and by comparing Fig. 36 and Fig. 54 which show a series of spot diagrams for off-axis object points from 0.1 - 0.6mm for the type A and type B toroids respectively, it can be seen that there are only slight differences between them.

Since the zero-order imaging properties from the type B toroid were superior to those of the type A toroid, the next stage in the design was to calculate the images produced by a classical grating (i.e. one whose rulings are straight and equispaced in the tangent plane at the pole of the grating) formed on the type B substrate. Such a grating could be easily produced by utilising the interference field produced by two plane waves as used in the fabrication of the type A toroidal gratings. The transverse aberrations of a type B toroidal grating at wavelengths of 21 Å, 23 Å and 25 Å are shown in Fig. 55 which corresponds to Fig. 42 for the type A toroid. The aberrations of the type B toroidal grating are practically identical to those of the type A toroidal grating. Fig. 56 shows the composite

TRANSVERSE ABERRATIONS
OF TYPE A TOROIDAL GRATING

R = 2000.0 RO = 5.7

ALPHA = 3.0 ORDER = 0.0

WAVELENGTHS

0.00 0.00 0.00 0.00 0.00

OBJECT DIST = 106.30 IMAGE DIST = 106.30

HALF-LENGTH = 20.00 HALF-WIDTH = 3.95

HEIGHTS

0.0 0.0 0.0 0.0 0.0

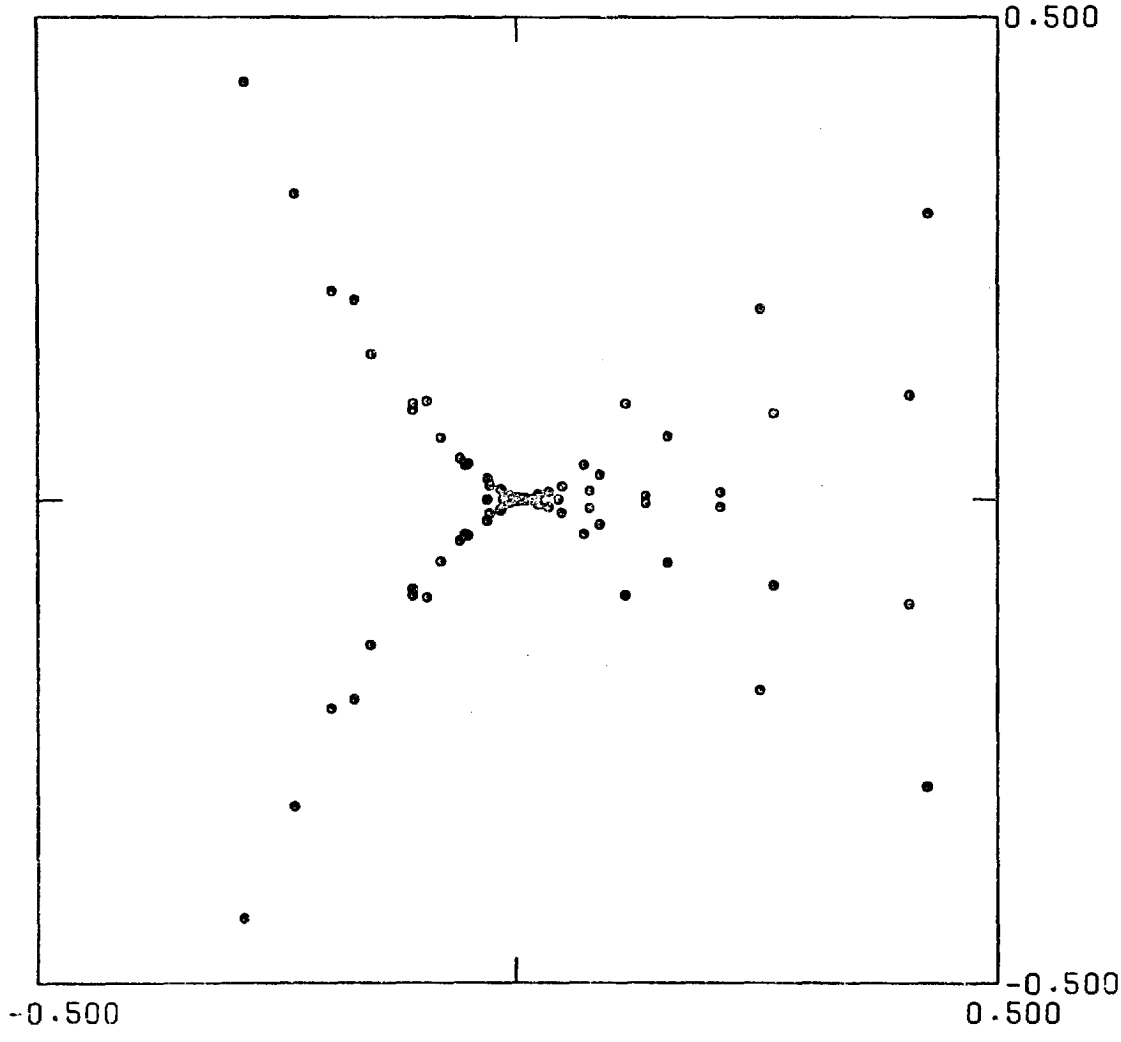

FIG. 51

TRANSVERSE ABERRATIONS

OF TYPE B TOROIDAL GRATING

R = 5.7 RO = 2000.0

ALPHA = 3.0 ORDER = 0.0

WAVELENGTHS

0.00 0.00 0.00 0.00 0.00

OBJECT DIST = 106.30 IMAGE DIST = 106.30

HALF-LENGTH = 20.00 HALF-WIDTH = 3.95

HEIGHTS

0.0 0.0 0.0 0.0 0.0

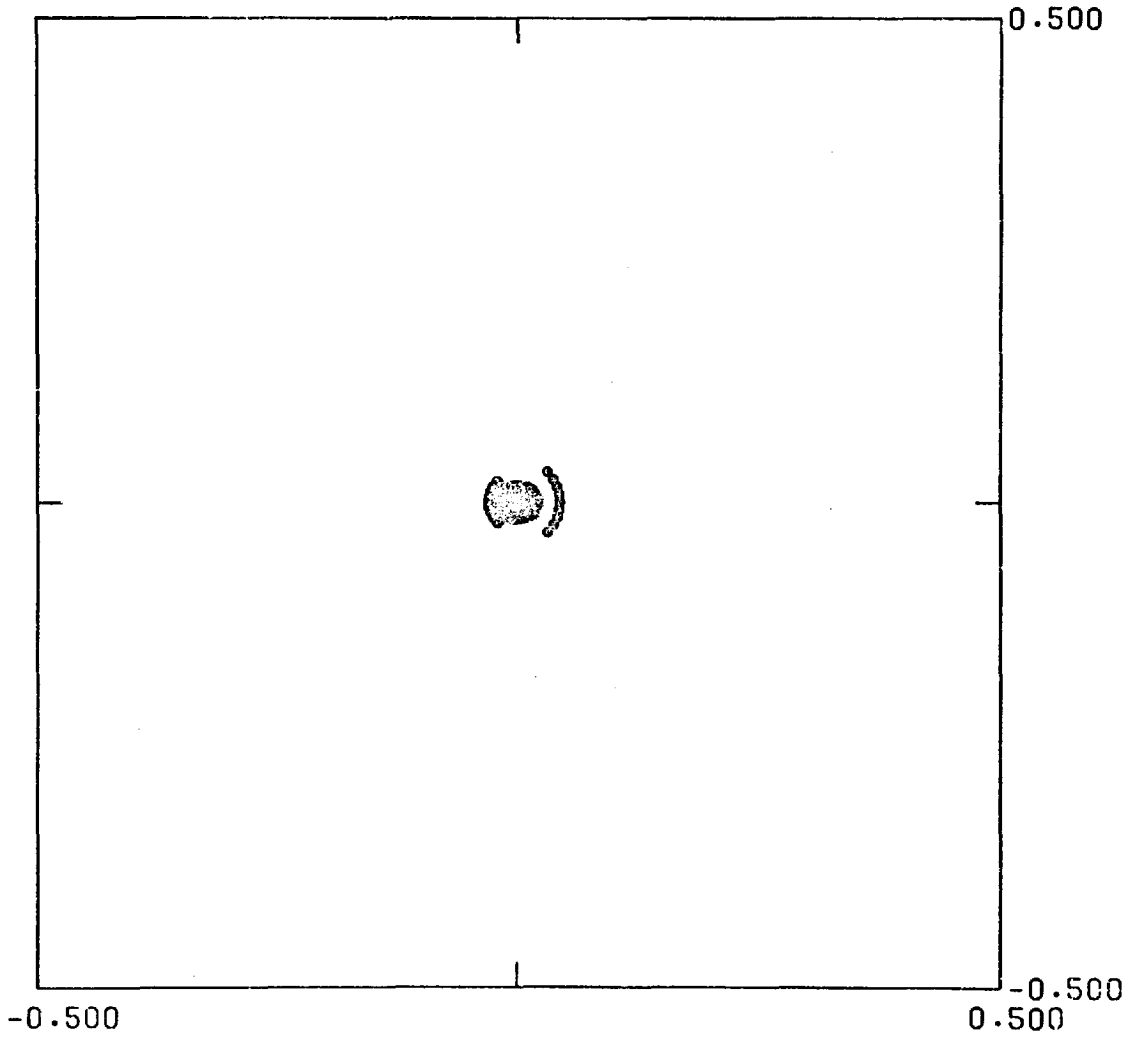

FIG. 52

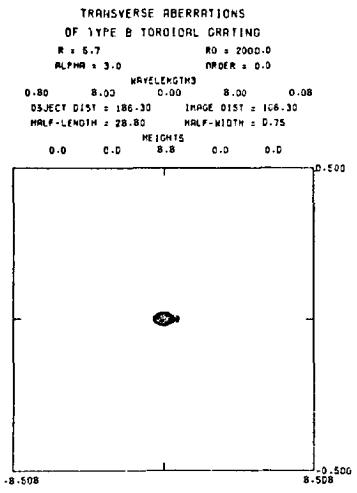
TRANSVERSE ABERRATIONS
OF TYPE B TOROIDAL GRATING
R = 5.7 RO = 2000.0
ALPHA = 3.0 ORDER = 0.0
WAVELENGTHS
0.80 0.00 0.00 0.00 0.00
OBJECT DIST = 186.30 IMAGE DIST = 106.30
HALF-LENGTH = 28.80 HALF-WIDTH = 0.75
WEIGHTS
0.0 0.0 0.0 0.0 0.0
0.500
-0.500
-0.500
0.500

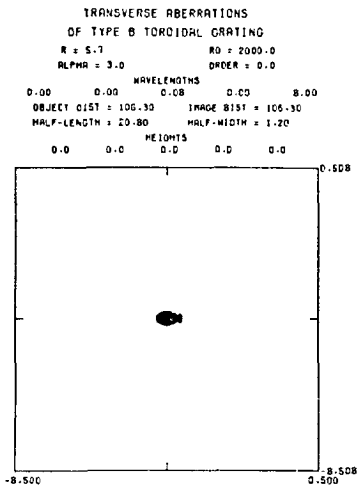
TRANSVERSE ABERRATIONS
OF TYPE B TOROIDAL GRATING
R = 5.7 RO = 2000.0
ALPHA = 3.0 ORDER = 0.0
WAVELENGTHS
0.00 0.00 0.00 0.00 0.00
OBJECT DIST = 106.30 IMAGE DIST = 106.30
HALF-LENGTH = 20.80 HALF-WIDTH = 1.20
WEIGHTS
0.0 0.0 0.0 0.0 0.0
0.500
-0.500
-0.500
0.500

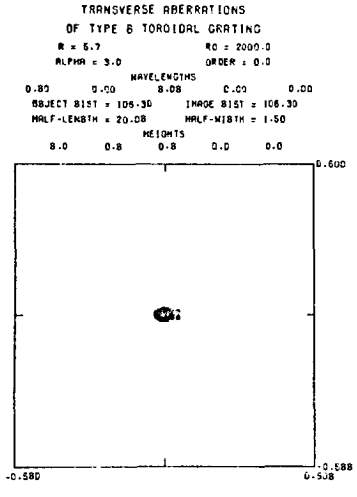
TRANSVERSE ABERRATIONS
OF TYPE B TOROIDAL GRATING
R = 5.7 RO = 2000.0
ALPHA = 3.0 ORDER = 0.0
WAVELENGTHS
0.80 0.00 0.00 0.00 0.00
OBJECT DIST = 186.30 IMAGE DIST = 106.30
HALF-LENGTH = 20.00 HALF-WIDTH = 1.50
WEIGHTS
0.0 0.0 0.0 0.0 0.0
0.500
-0.500
-0.500
0.500

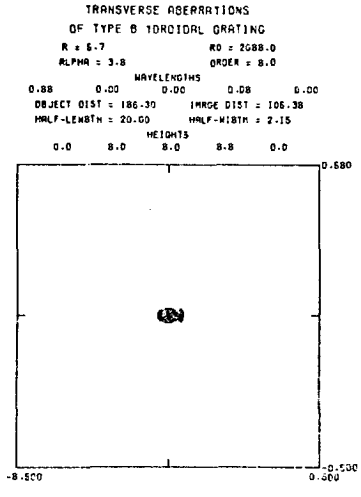
TRANSVERSE ABERRATIONS
OF TYPE B TOROIDAL GRATING
R = 5.7 RO = 2088.0
ALPHA = 3.8 ORDER = 0.0
WAVELENGTHS
0.88 0.00 0.00 0.00 0.00
OBJECT DIST = 186.30 IMAGE DIST = 106.38
HALF-LENGTH = 20.00 HALF-WIDTH = 2.15
WEIGHTS
0.0 0.0 0.0 0.0 0.0
0.500
-0.500
-0.500
0.500

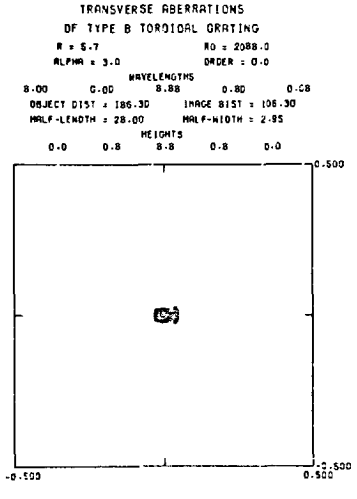
TRANSVERSE ABERRATIONS
OF TYPE B TOROIDAL GRATING
R = 5.7 RO = 2088.0
ALPHA = 3.0 ORDER = 0.0
WAVELENGTHS
0.00 0.00 0.00 0.00 0.00
OBJECT DIST = 186.30 IMAGE DIST = 106.30
HALF-LENGTH = 28.00 HALF-WIDTH = 2.85
WEIGHTS
0.0 0.0 0.0 0.0 0.0
0.500
-0.500
-0.500
0.500

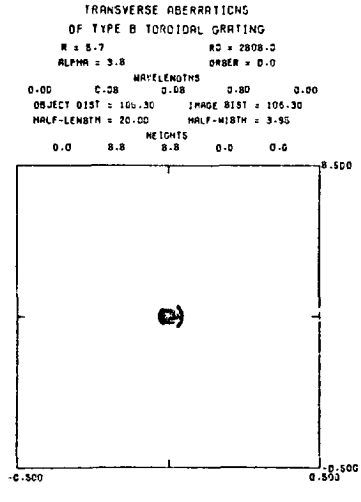
TRANSVERSE ABERRATIONS
OF TYPE B TOROIDAL GRATING
R = 5.7 RO = 2808.0
ALPHA = 3.8 ORDER = 0.0
WAVELENGTHS
0.00 0.00 0.00 0.00 0.00
OBJECT DIST = 106.30 IMAGE DIST = 106.30
HALF-LENGTH = 20.00 HALF-WIDTH = 3.95
WEIGHTS
0.0 0.0 0.0 0.0 0.0
0.500
-0.500
-0.500
0.500

FIG. 53

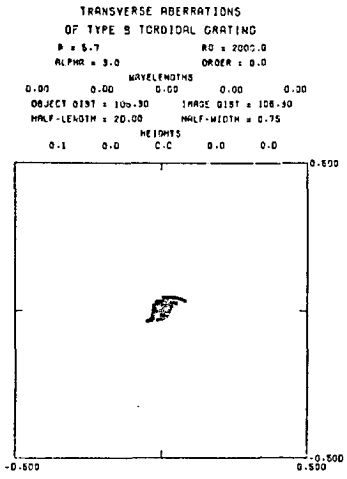
TRANSVERSE ABERRATIONS
OF TYPE B TORDIDAL GRATING
R = 5.7
RO = 2000.0
ALPHA = 3.0
ORDER = 0.0
WAVELENGTHS
0.00 0.00 0.00 0.00 0.00
OBJECT DIST = 105.30
IMAGE DIST = 106.30
HALF-LENGTH = 20.00
HALF-WIDTH = 0.75
WEIGHTS
0.1 0.0 0.0 0.0 0.0
0.500
-0.500
-0.500
0.500

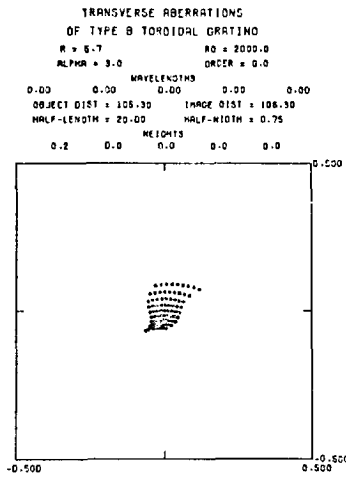
TRANSVERSE ABERRATIONS
OF TYPE B TORDIDAL GRATING
R = 5.7
RO = 2000.0
ALPHA = 3.0
ORDER = 0.0
WAVELENGTHS
0.00 0.00 0.00 0.00 0.00
OBJECT DIST = 105.30
IMAGE DIST = 106.30
HALF-LENGTH = 20.00
HALF-WIDTH = 0.75
WEIGHTS
0.2 0.0 0.0 0.0 0.0
0.500
-0.500
-0.500
0.500

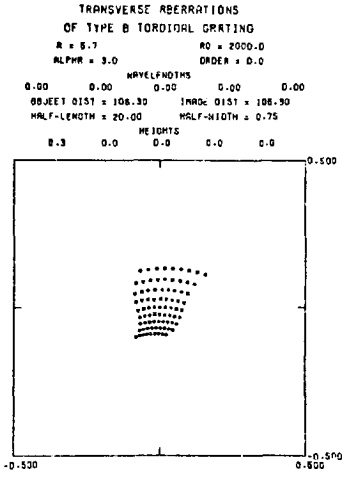
TRANSVERSE ABERRATIONS
OF TYPE B TORDIDAL GRATING
R = 5.7
RO = 2000.0
ALPHA = 3.0
ORDER = 0.0
WAVELENGTHS
0.00 0.00 0.00 0.00 0.00
OBJECT DIST = 106.30
IMAGE DIST = 106.30
HALF-LENGTH = 20.00
HALF-WIDTH = 0.75
WEIGHTS
0.3 0.0 0.0 0.0 0.0
0.500
-0.500
-0.500
0.500

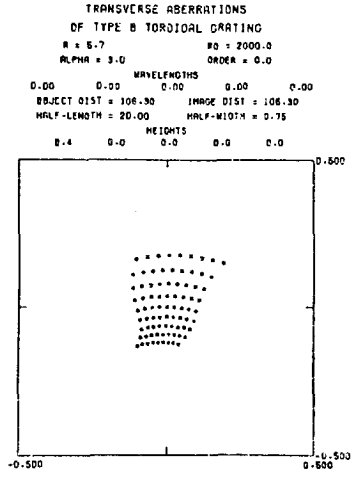
TRANSVERSE ABERRATIONS
OF TYPE B TORDIDAL GRATING
R = 5.7
RO = 2000.0
ALPHA = 3.0
ORDER = 0.0
WAVELENGTHS
0.00 0.00 0.00 0.00 0.00
OBJECT DIST = 106.30
IMAGE DIST = 106.30
HALF-LENGTH = 20.00
HALF-WIDTH = 0.75
WEIGHTS
0.4 0.0 0.0 0.0 0.0
0.500
-0.500
-0.500
0.500

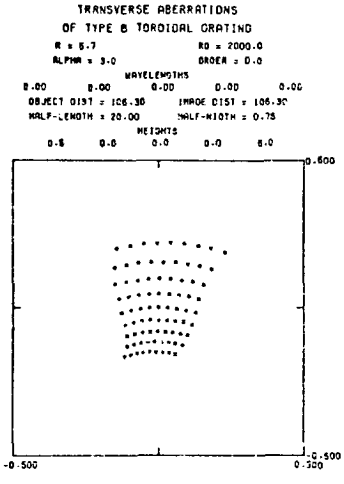
TRANSVERSE ABERRATIONS
OF TYPE B TORDIDAL GRATING
R = 5.7
RO = 2000.0
ALPHA = 3.0
ORDER = 0.0
WAVELENGTHS
0.00 0.00 0.00 0.00 0.00
OBJECT DIST = 106.30
IMAGE DIST = 106.30
HALF-LENGTH = 20.00
HALF-WIDTH = 0.75
WEIGHTS
0.5 0.0 0.0 0.0 0.0
0.500
-0.500
-0.500
0.500

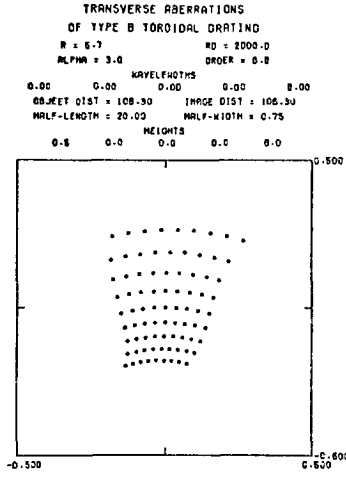
TRANSVERSE ABERRATIONS
OF TYPE B TORDIDAL GRATING
R = 5.7
RO = 2000.0
ALPHA = 3.0
ORDER = 0.0
WAVELENGTHS
0.00 0.00 0.00 0.00 0.00
OBJECT DIST = 106.30
IMAGE DIST = 106.30
HALF-LENGTH = 20.00
HALF-WIDTH = 0.75
WEIGHTS
0.5 0.0 0.0 0.0 0.0
0.500
-0.500
-0.500
0.500

FIG. 5⅓

TRANSVERSE ABERRATIONS
OF TYPE B TOROIDAL GRATING

R = 5.7 RO = 2000.0

ALPHA = 2.4 ORDER = 1.0

WAVELENGTHS

23.00 21.00 25.00 0.00 0.00

OBJECT DIST = 84.03 IMAGE DIST = 134.48

HALF-LENGTH = 20.00 HALF-WIDTH = 0.75

HEIGHTS

0.0 0.0 0.0 0.0 0.0

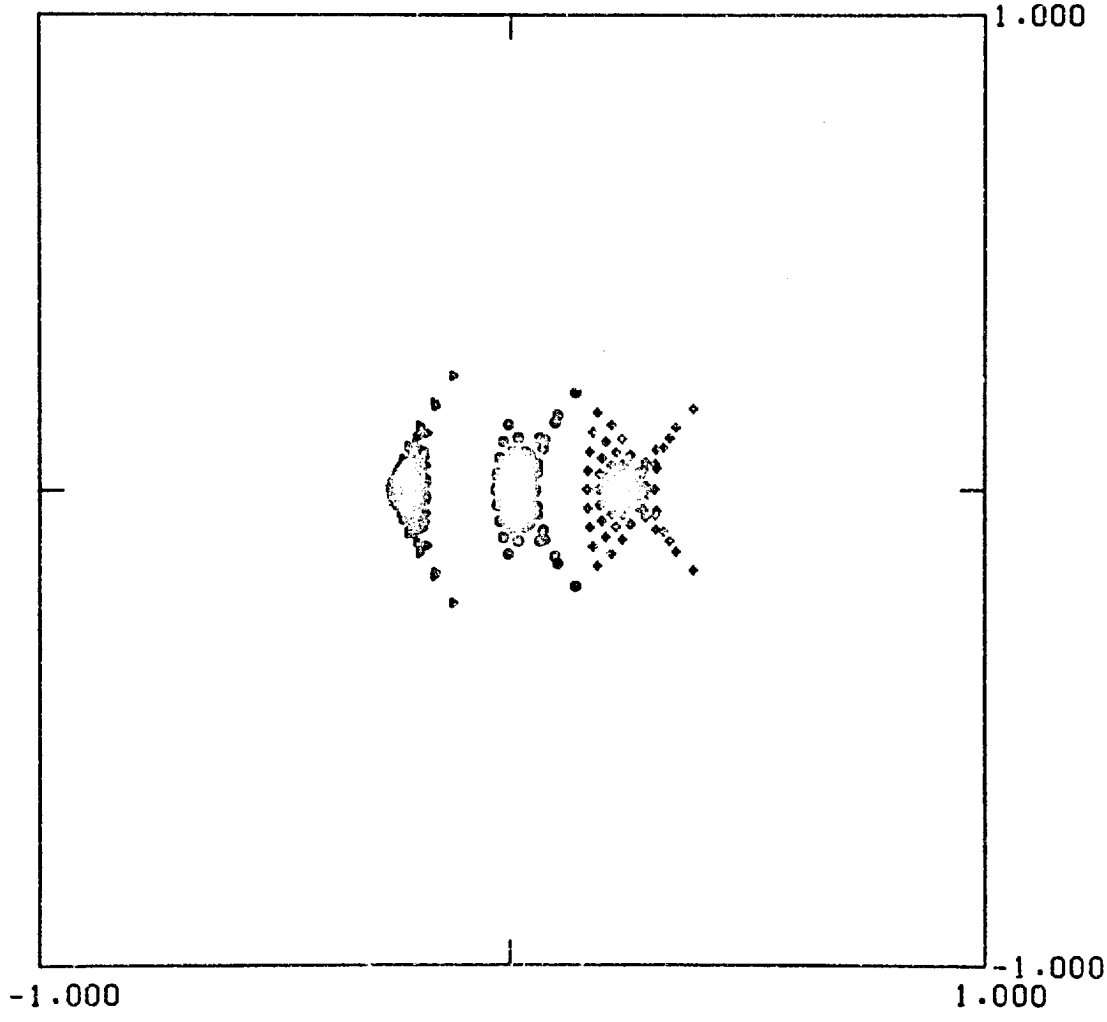

FIG. 55

spot diagrams for 21 Å, 23 Å and 25 Å, with on-axis and 0.2mm off-axis object points, and Fig. 57 shows similar spot diagrams for wavelengths of 40 Å, 44.5 Å and 49 Å. Since the differences in the aberrations produced by these two types of toroidal gratings are small, there is no advantage in using a type B toroid with a "classical" ruling pattern. Although the type B toroid has better inherent imaging properties than the type A toroid, the diffraction effects from the similar ruling patterns cause the dominant aberrations in both cases. Thus it is necessary to have both the correct shape of substrate and the correct grating frequency distribution on that substrate in order to provide optimum imaging.

We have already seen in Chapter 2 that it is possible to correct spherical aberration by systematically varying the grating frequency and that theoretically it should be possible to greatly increase the numerical aperture of monochromators for use in the soft x-ray region. If it were necessary to obtain the maximum intensity from a monochromator at only one fixed wavelength, it would be possible to make a grating with both astigmatism-correction by substrate curvature and spherical aberration correction with variable frequency. Such a grating could theoretically produce a geometrically perfect image for a monochromatic point source on axis. Wavelengths either side of the perfectly focussed wavelength would be aberrated but resolved from the focussed wavelength. This situation corresponds to Fig. 58 which shows the transverse aberrations for a variable frequency grating on a type B toroid at wavelengths of 21 Å, 23 Å and 25 Å. At 23 Å all the rays pass through the same point on the spot diagram - the halation around the central point has no significance and is simply due to

TRANSVERSE ABERRATIONS

OF TYPE B TOROIDAL GRATING

R = 5.7 RO = 2000.0

ALPHA = 2.4 ORDER = 1.0

WAVELENGTHS

23.00 21.00 25.00 0.00 0.00

OBJECT DIST = 84.03 IMAGE DIST = 134.48

HALF-LENGTH = 5.00 HALF-WIDTH = 0.75

HEIGHTS

0.0 0.2 -0.2 0.0 0.0

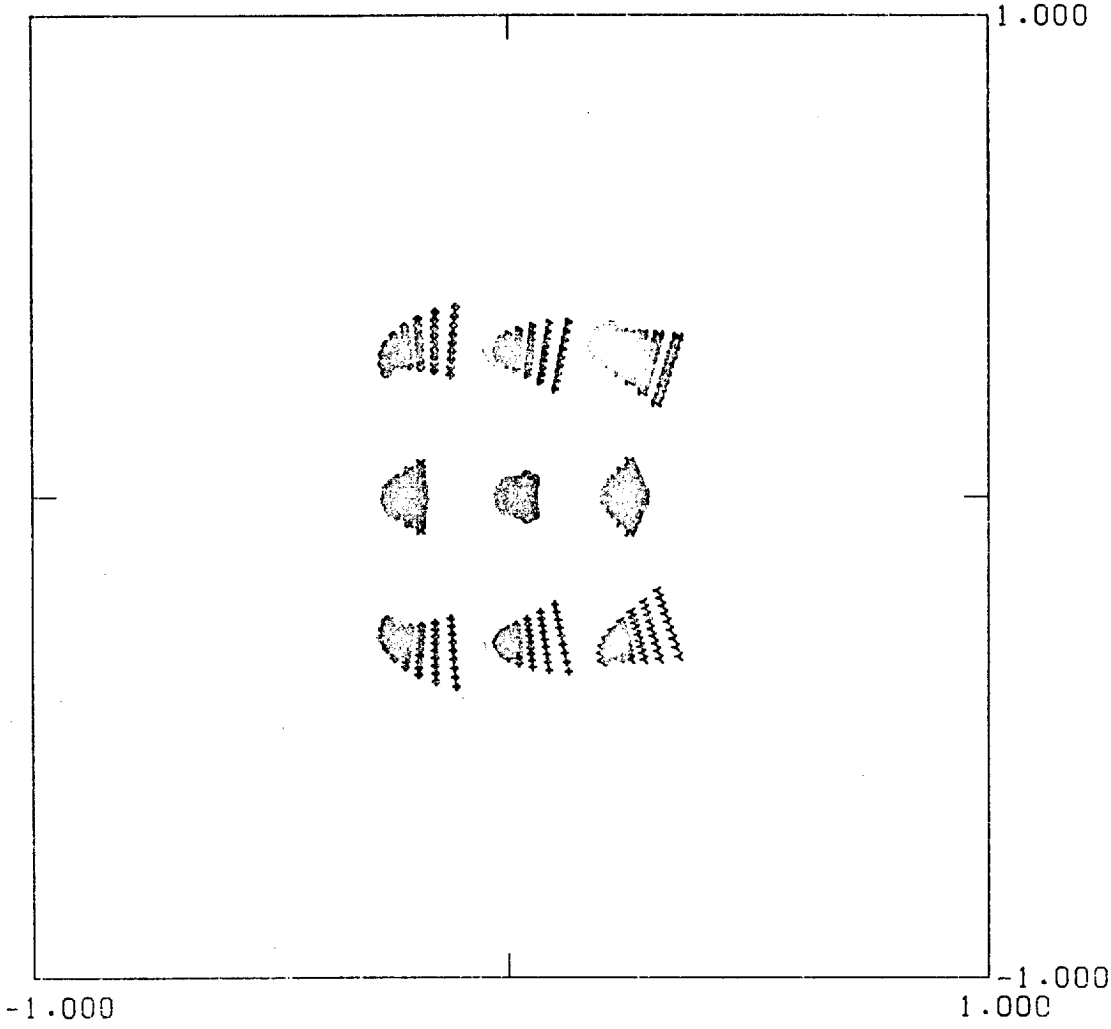

FIG. 56

TRANSVERSE ABERRATIONS

OF TYPE B TOROIDAL GRATING

R = 5.7 RO = 2000.0

ALPHA = 2.0 ORDER = 1.0

WAVELENGTHS

44.50 40.00 49.00 0.00 0.00

OBJECT DIST = 69.82 IMAGE DIST = 161.84

HALF-LENGTH = 5.00 HALF-WIDTH = 0.75

HEIGHTS

0.0 0.2 -0.2 0.0 0.0

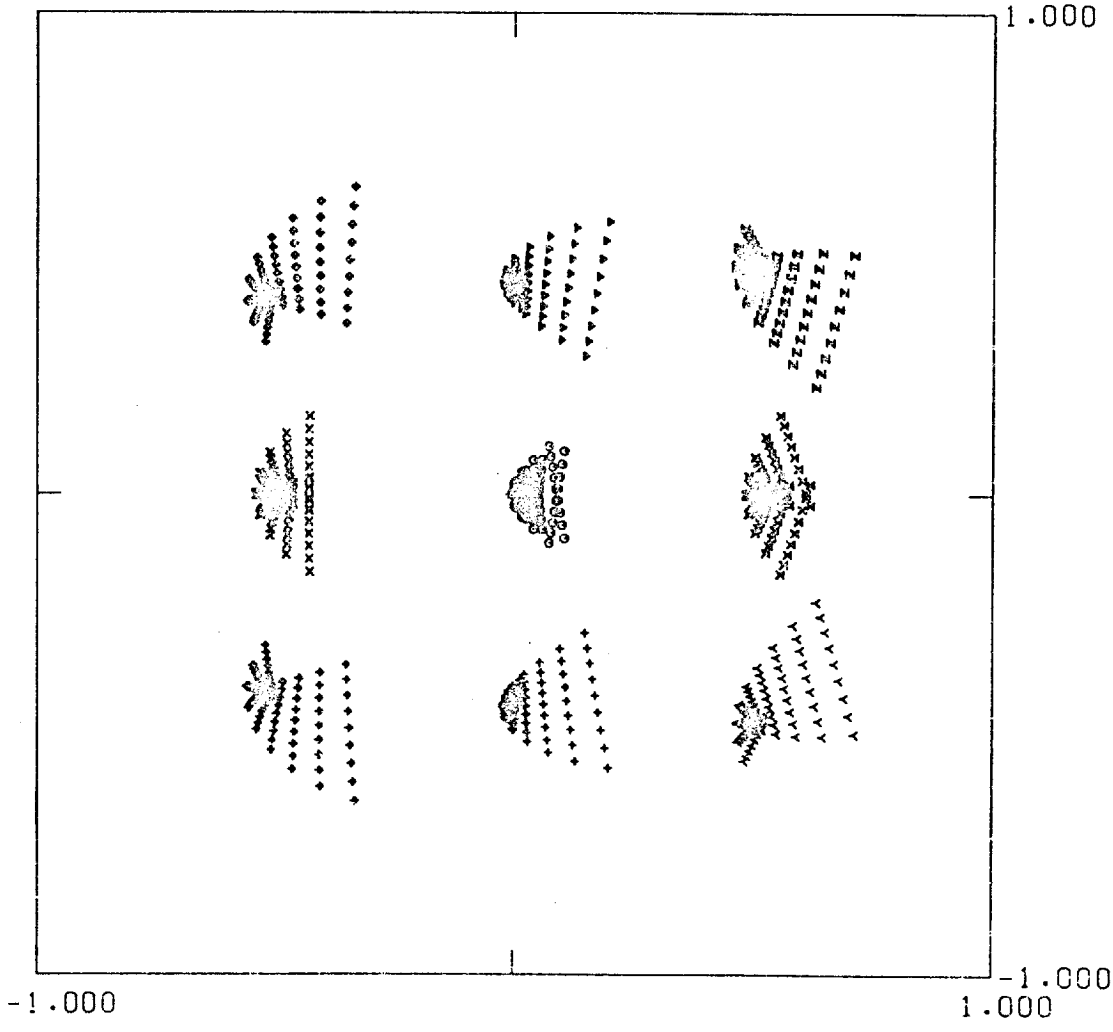

FIG. 57

TRANSVERSE ABERRATIONS OF VARIABLE FREQUENCY GRATING ON TYPE B TOROID

K-VALUE = 37929.9020

R = 9.5 RO = 2500.0

ALPHA = 2.5 ORDER = 1.0

WAVELENGTHS

23.00 21.00 25.00 0.00 0.00

OBJECT DIST = 218.10 IMAGE DIST = 218.10

HALF-LENGTH = 50.00 HALF-WIDTH = 1.00

HEIGHTS

0.0 0.0 0.0 0.0 0.0

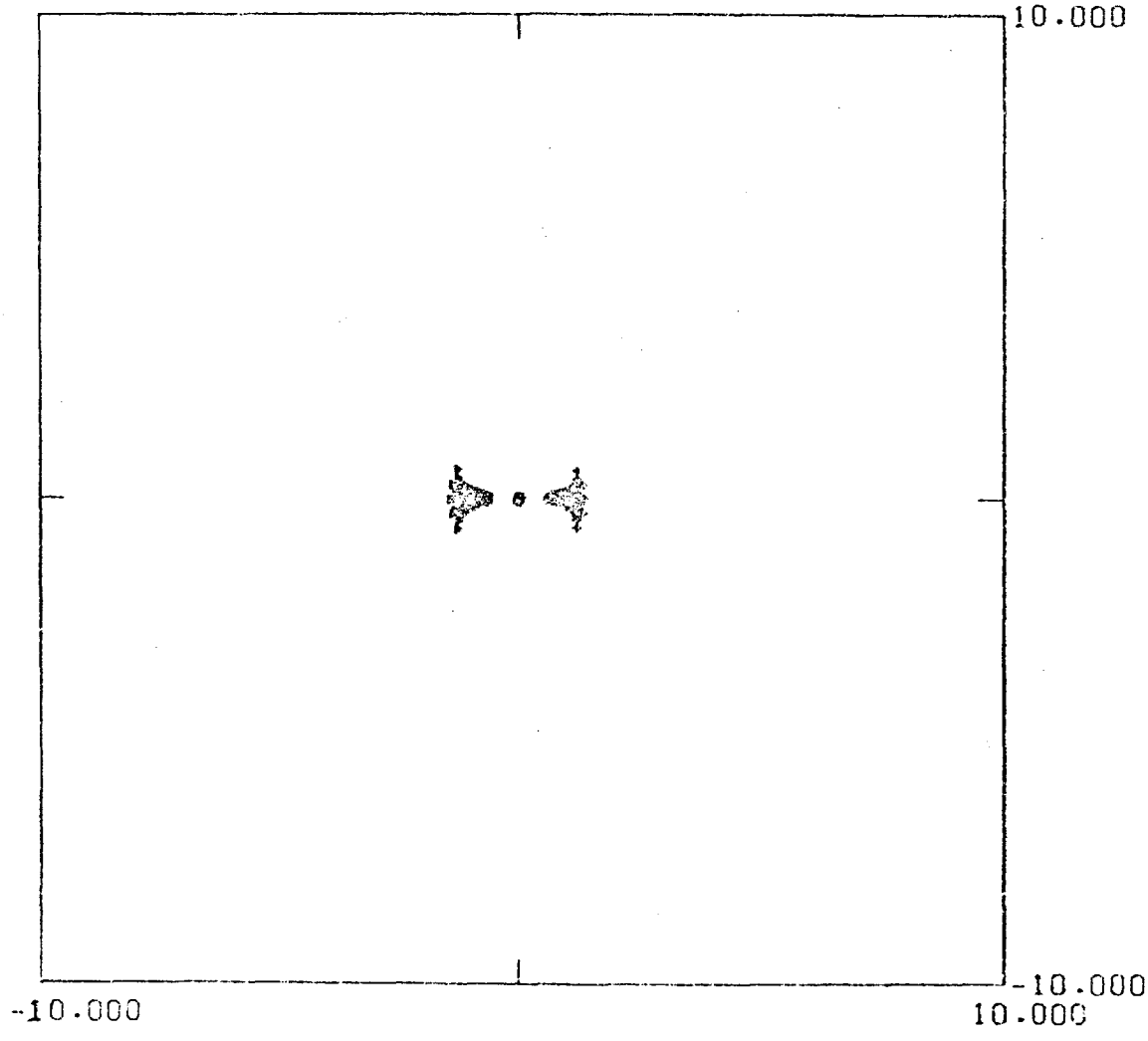

FIG. 58

overexposure of the microfilm. In this example the grating width is 100mm which is four times greater than the optimum width for a corresponding spherical grating. The wavelengths 21 Å and 25 Å are out of focus in the image plane for 23 Å but it can be shown by constructing a ray diagram that these wavelengths are focussed with degrees of spherical aberration near the line joining the ideal centre (i.e. the zero frequency point) of the grating to the perfect focus. Thus this grating has similar properties to a section of an off-axis zone plate.

Although this type of grating can theoretically achieve perfect imaging for an on-axis image point at one wavelength and usable imaging over a small range of wavelengths, it is to be expected that the off-axis imaging will be poor because the coma-type aberrations remain uncorrected. The off-axis images from the variable frequency type B toroid are shown in Fig. 59 and it can be seen that even small off-axis displacements cause significant aberrations which make this system impracticable. The combined effect of off-axis aberrations at the three wavelengths of 21 Å, 23 Å and 25 Å shown in Fig. 60 rules out the possible use of this grating at soft x-ray wavelengths.

It is clear that there are insufficient free parameters in a single element grazing incidence grating system to provide simultaneous spatial and spectral resolution over a large field angle. In order to design a usable system it is necessary either to increase the number of elements or tolerate the presence of certain aberrations. Since the efficiencies of diffraction and reflection are generally low in the soft x-ray region it is advantageous to minimise the number of elements in a system. A general ray tracing program capable of performing calculations on systems containing up to 27 surfaces, and

TRANSVERSE ABERRATIONS OF VARIABLE FREQUENCY GRATING ON TYPE B TOROID

K-VALUE = 37929.9020

R = 9.5 RO = 2500.0

ALPHA = 2.5 ORDER = 1.0

WAVELENGTHS

23.00 0.00 0.00 0.00 0.00

OBJECT DIST = 218.10 IMAGE DIST = 218.10

HALF-LENGTH = 50.00 HALF-WIDTH = 1.00

HEIGHTS

0.0 0.2 -0.2 0.0 0.0

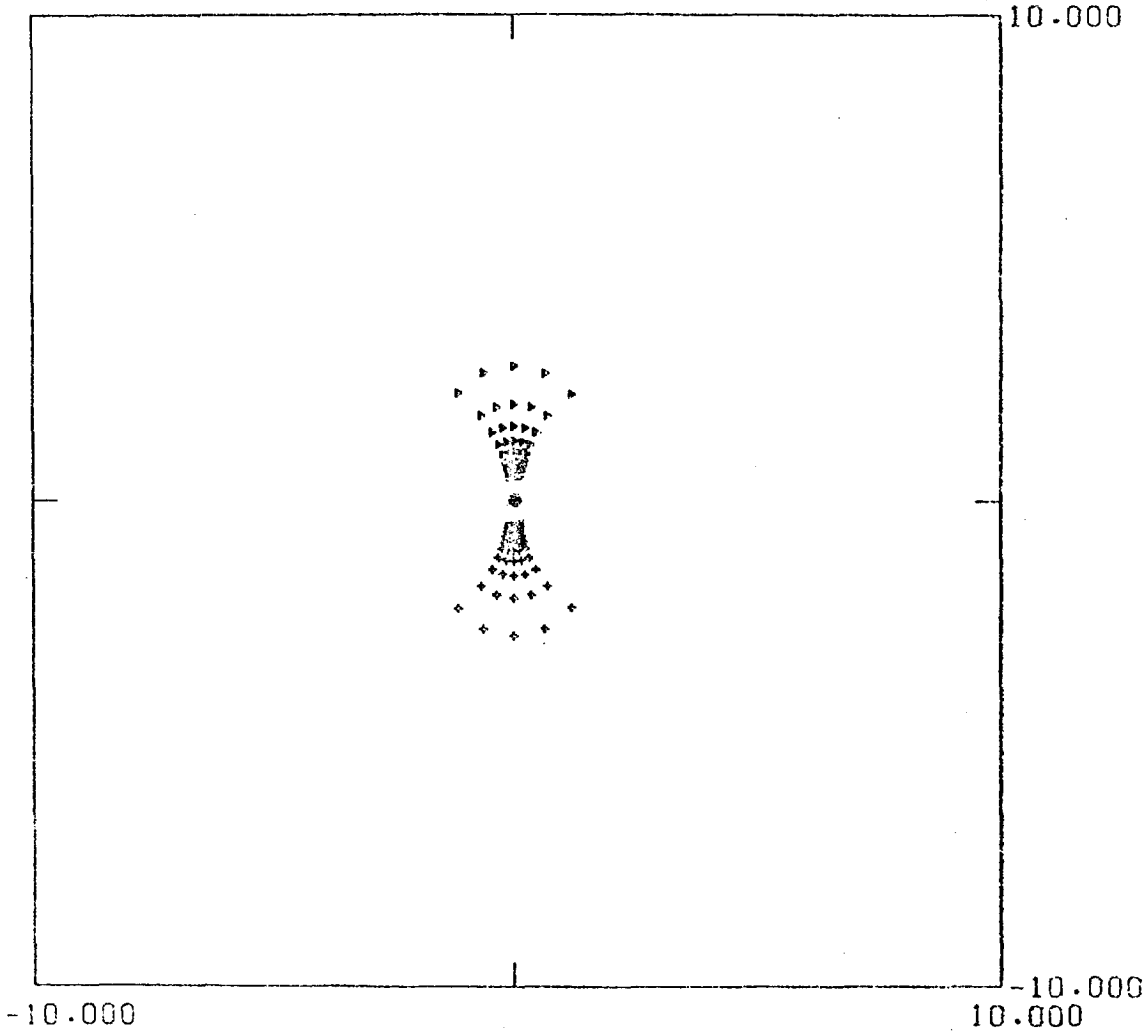

FIG. 59

TRANSVERSE ABERRATIONS OF VARIABLE FREQUENCY GRATING ON TYPE B TOROID

K-VALUE = 37929.9020

R = 9.5 RO = 2500.0

ALPHA = 2.5 ORDER = 1.0

WAVELENGTHS

23.00 21.00 25.00 0.00 0.00

OBJECT DIST = 218.10 IMAGE DIST = 218.10

HALF-LENGTH = 50.00 HALF-WIDTH = 1.00

HEIGHTS

0.0 0.2 -0.2 0.0 0.0

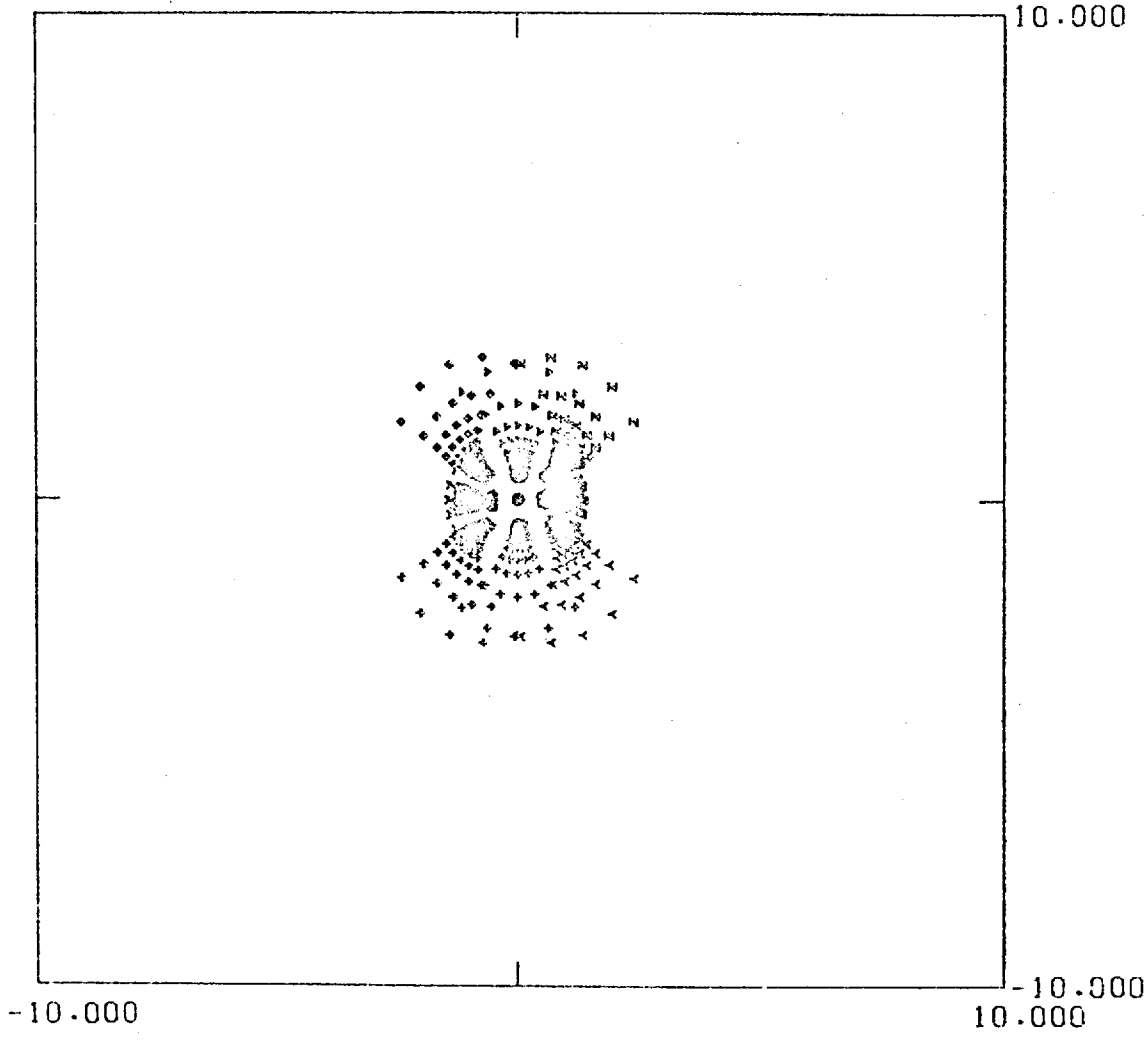

FIG. 60

10 diffraction gratings (including holographic types) has been used in this work and it would be a relatively easy matter to evaluate any proposed multi-element grazing incidence system with this program. However, such systems must be specialised solutions for particular problems and as such would be out of place in this thesis which is concerned more generally with holographic x-ray gratings.

Finally, in this chapter, the aberrations of a grating with straight equispaced rulings formed on a right elliptical cylinder will be analysed by ray tracing. For convenience these gratings will be called "elliptical" gratings in the following text. The author has made several holographic gratings of this type on thin optical flats which have been shaped so that they adopt an elliptical figure when deformed by bending. These gratings were initially designed for use as monochromator gratings in the grating test apparatus; however, as indicated in Chapter 2, similar gratings may be advantageously used for high resolution x-ray spectroscopy.

In order to design an elliptical grating for use in part of the soft x-ray region, it is necessary to calculate values for the semi-major axis, b, and semi-minor axis, c, using the formulae:

$$\sin\alpha \sin\beta = c^2/b^2 \qquad \text{and} \qquad R = b^2/c$$

where R is the Rowland circle diameter of the spectrograph in which the elliptical grating is to be used. Thus for a given instrument the elliptical grating must be designed for a fixed angle of grazing incidence and one wavelength but like the toroidal grating it is possible to achieve a range of useful wavelengths over which $\sin\alpha . \sin\beta$ is constant by allowing the angle of incidence to vary.

However, unlike the astigmatism correction provided by the toroidal grating, the spherical aberration correction provided by the elliptical grating is only small and is not strongly parameter dependent. Thus it is possible to use an elliptical grating over a wide wavelength range.

The design of elliptical grating featured in the ray tracing examples is based on the 5m spectrograph and an angle of grazing incidence of 3.0° at a wavelength of 45 Å and a grating frequency of 300 l/mm. These design conditions yield values for the semi-major and semi-minor axes of 310.5565mm and 19.2891mm respectively. The transverse aberrations for an elliptical grating with these parameters with a width of 50mm under these conditions are given in Fig. 61. Spot diagrams for the same grating illuminated with 100 Å and 25 Å are shown in Fig. 62 and Fig. 63 and it can be seen that although the aberrations have increased they are still smaller than those from a corresponding spherical grating.

It is most important to decide upon the necessary dimensional tolerances in order to be able to fabricate the elliptical grating blanks and this can be conveniently performed by ray tracing. Fig. 64 shows the effects of increasing the semi-major and semi-minor axes by 100μm. It can be seen from the relatively small increase in the aberrations that it is definitely a practical proposition to fabricate gratings on right-elliptical cylinders since the required tolerance can be achieved and measured using standard optical techniques and modern measuring methods.

The increase in grating width possible with the elliptical grating, however, involves a limitation on the range of angles of

TRANSVERSE ABERRATIONS
OF AN ELLIPTICAL GRATING

FREQUENCY = 300.0000

B = 310.6 C = 19.3

ALPHA = 3.0 ORDER = 1.0

WAVELENGTHS

45.00 0.00 0.00 0.00 0.00

OBJECT DIST = 261.68 IMAGE DIST = 368.56

HALF-LENGTH = 25.00 HALF-WIDTH = 5.00

HEIGHTS

0.0 0.0 0.0 0.0 0.0

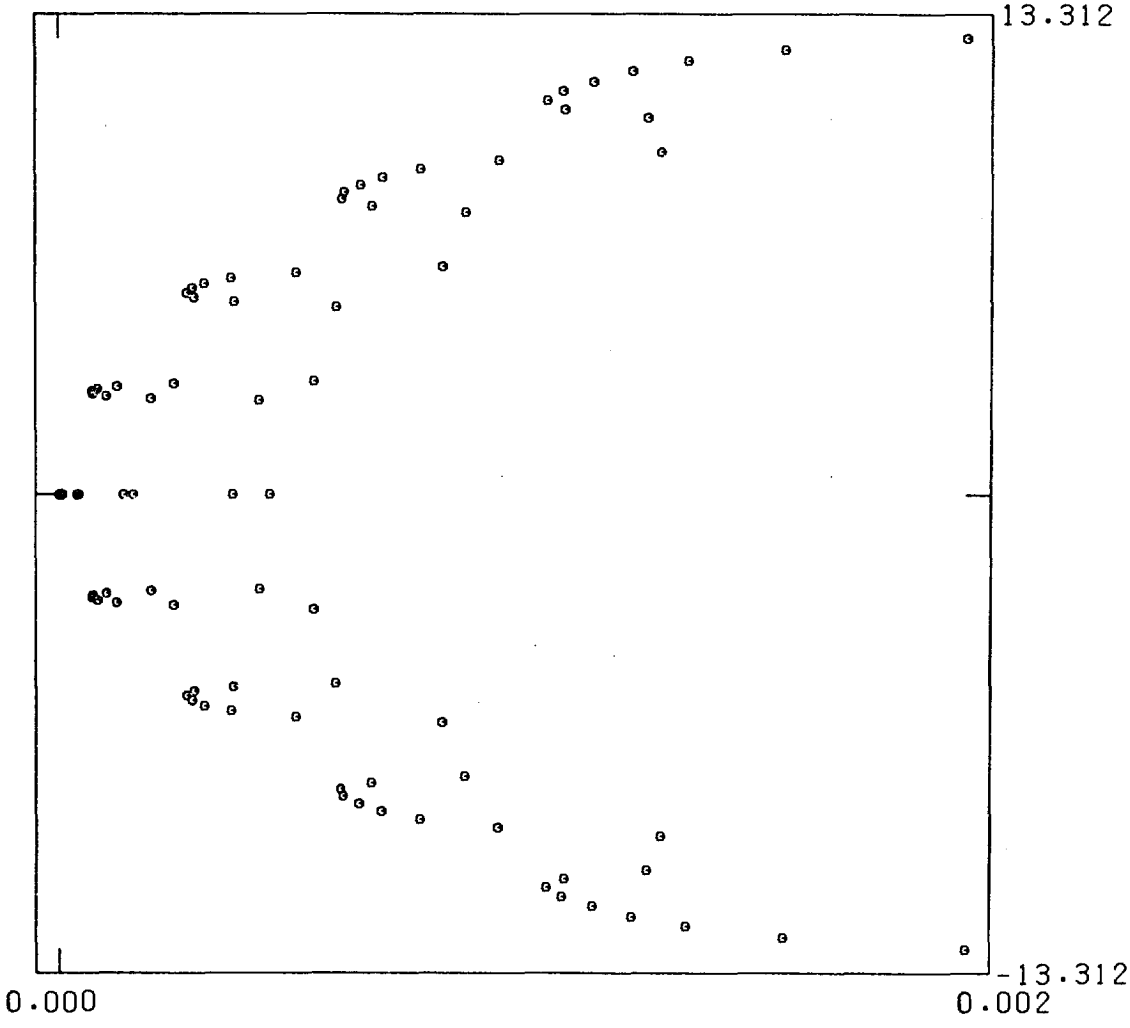

FIG. 61

TRANSVERSE ABERRATIONS
OF AN ELLIPTICAL GRATING

FREQUENCY = 300.0000

B = 310.6 C = 19.3

ALPHA = 3.0 ORDER = 1.0

WAVELENGTHS

100.00 0.00 0.00 0.00 0.00

OBJECT DIST = 261.68 IMAGE DIST = 466.95

HALF-LENGTH = 25.00 HALF-WIDTH = 5.00

HEIGHTS

0.0 0.0 0.0 0.0 0.0

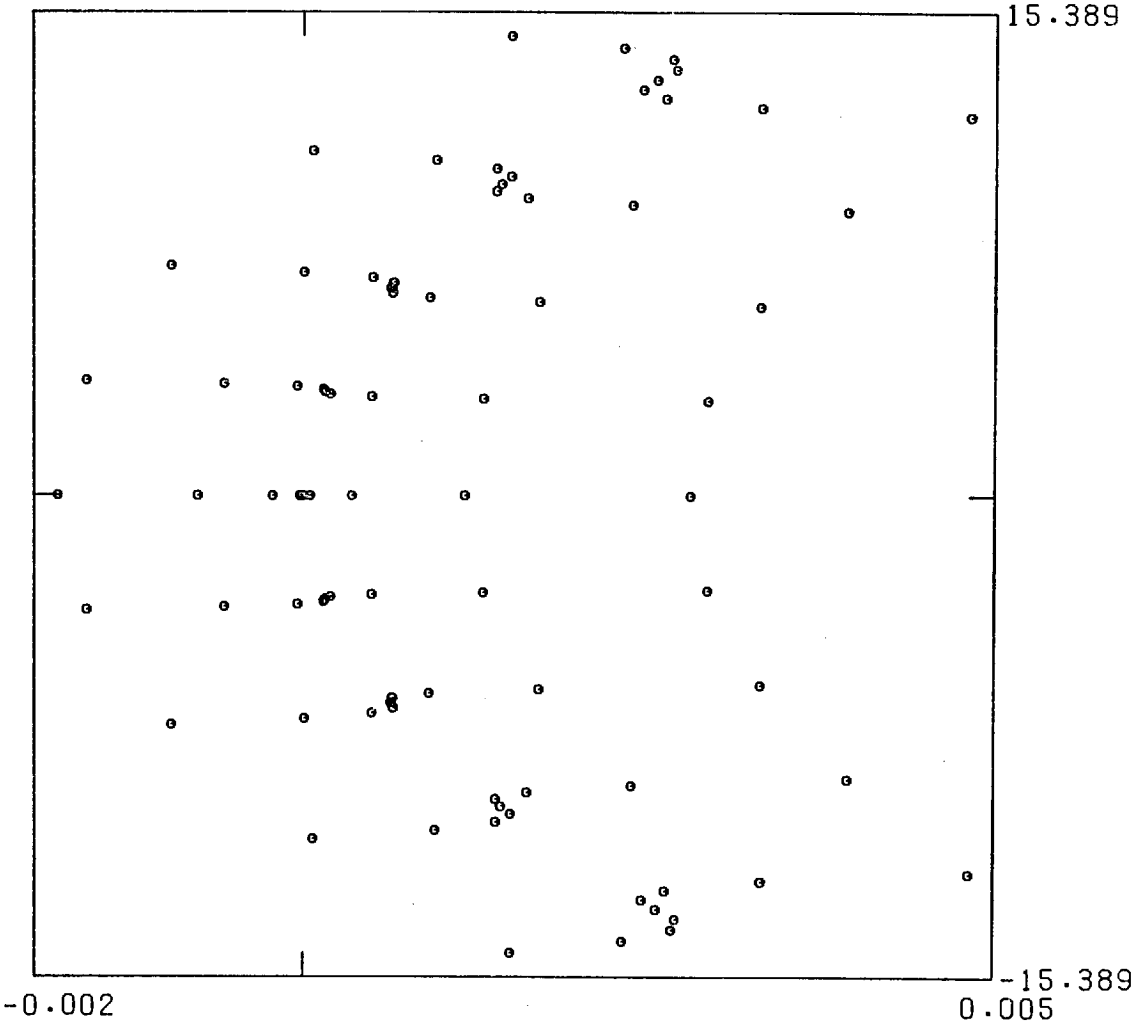

FIG. 62

TRANSVERSE ABERRATIONS
OF AN ELLIPTICAL GRATING

FREQUENCY = 300.0000

B = 310.6 C = 19.3

ALPHA = 3.0 ORDER = 1.0

WAVELENGTHS

25.00 0.00 0.00 0.00 0.00

OBJECT DIST = 261.68 IMAGE DIST = 325.44

HALF-LENGTH = 25.00 HALF-WIDTH = 5.00

HEIGHTS

0.0 0.0 0.0 0.0 0.0

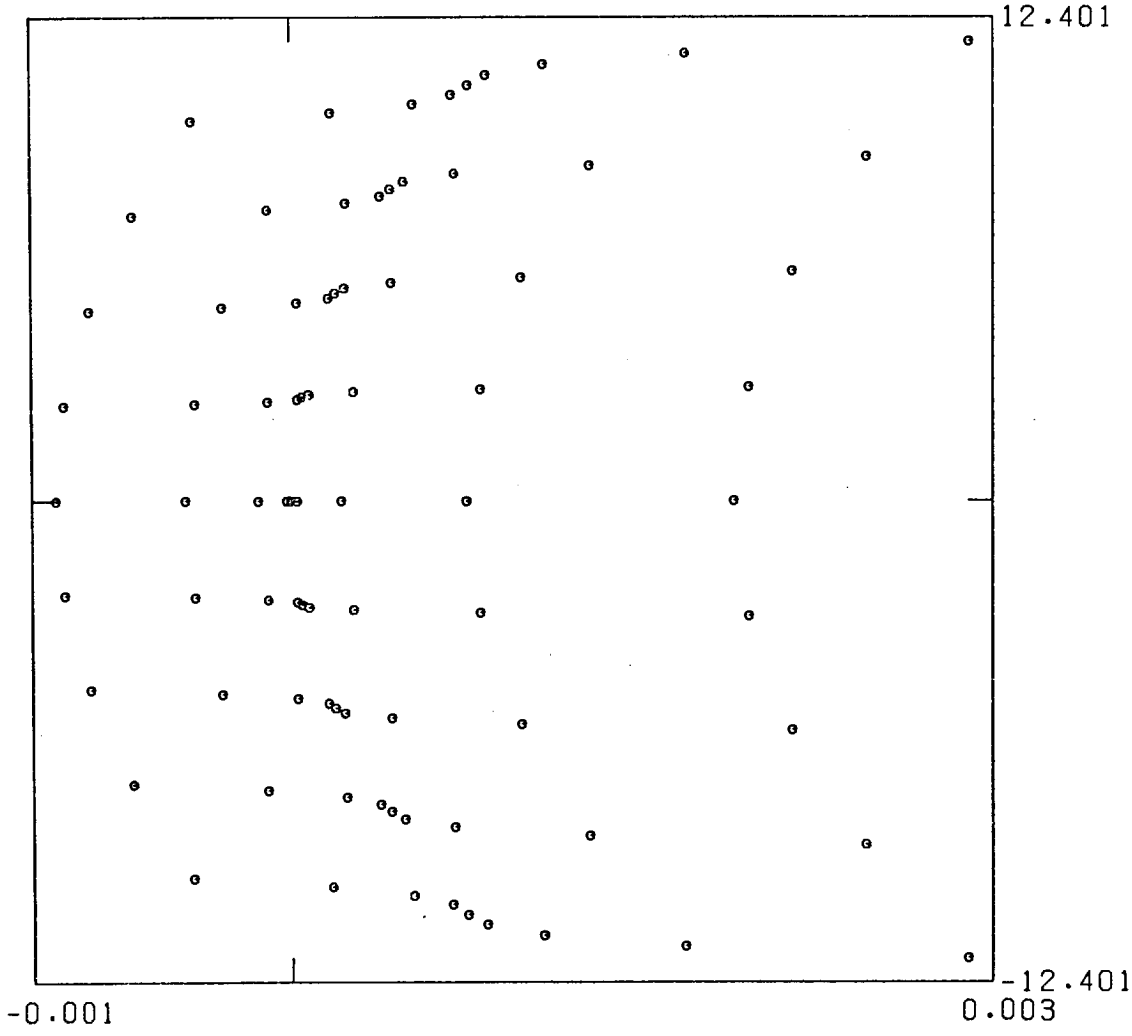

FIG. 63

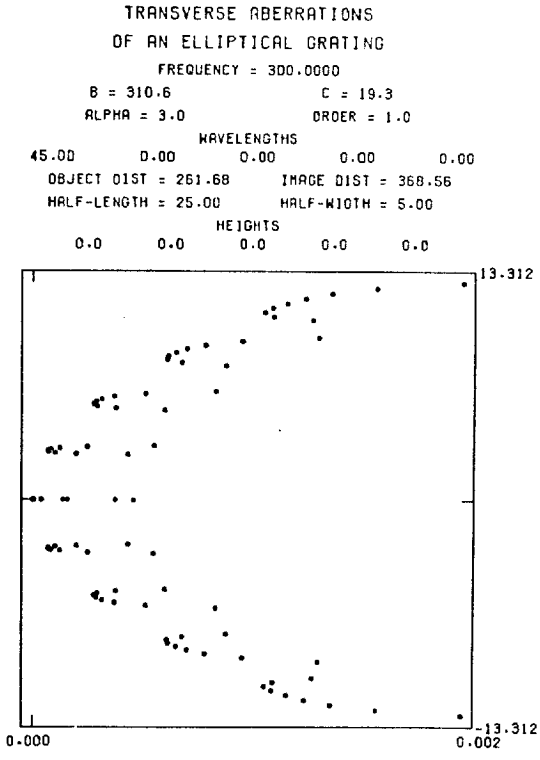
TRANSVERSE ABERRATIONS
OF AN ELLIPTICAL GRATING
FREQUENCY = 300.0000
B = 310.6
C = 19.3
ALPHA = 3.0
ORDER = 1.0
WAVELENGTHS
45.00 0.00 0.00 0.00 0.00
OBJECT DIST = 261.68
IMAGE DIST = 368.56
HALF-LENGTH = 25.00
HALF-WIDTH = 5.00
HEIGHTS
0.0 0.0 0.0 0.0 0.0
13.312
-13.312
0.000
0.002

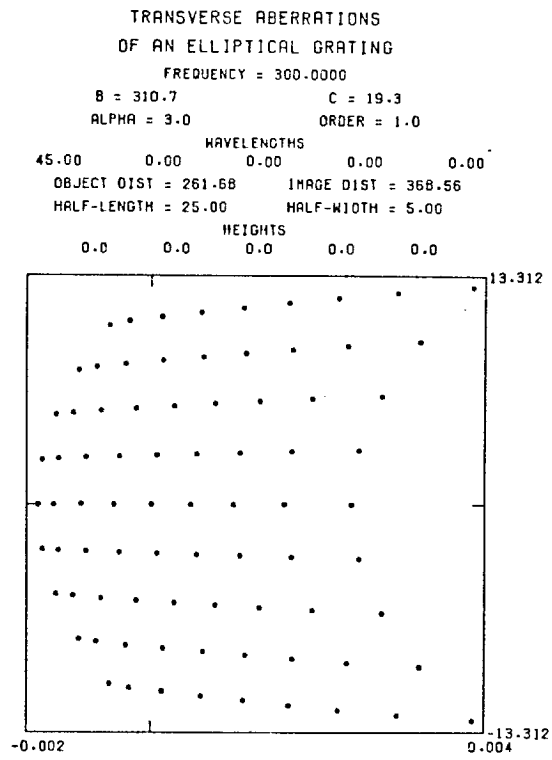
TRANSVERSE ABERRATIONS
OF AN ELLIPTICAL GRATING
FREQUENCY = 300.0000
B = 310.7
C = 19.3
ALPHA = 3.0
ORDER = 1.0
WAVELENGTHS
45.00 0.00 0.00 0.00 0.00
OBJECT DIST = 261.68
IMAGE DIST = 368.56
HALF-LENGTH = 25.00
HALF-WIDTH = 5.00
HEIGHTS
0.0 0.0 0.0 0.0 0.0
13.312
-13.312
-0.002
0.004

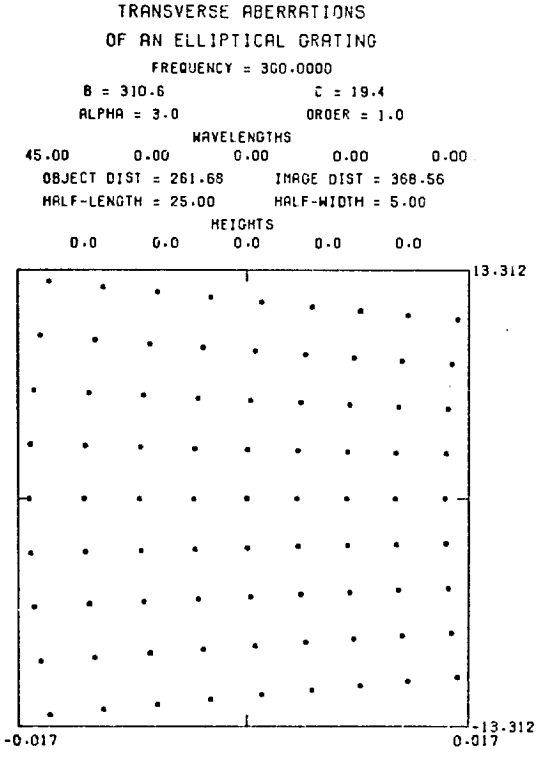
TRANSVERSE ABERRATIONS
OF AN ELLIPTICAL GRATING
FREQUENCY = 300.0000
B = 310.6
C = 19.4
ALPHA = 3.0
ORDER = 1.0
WAVELENGTHS
45.00 0.00 0.00 0.00 0.00
OBJECT DIST = 261.68
IMAGE DIST = 368.56
HALF-LENGTH = 25.00
HALF-WIDTH = 5.00
HEIGHTS
0.0 0.0 0.0 0.0 0.0
13.312
-13.312
-0.017
0.017

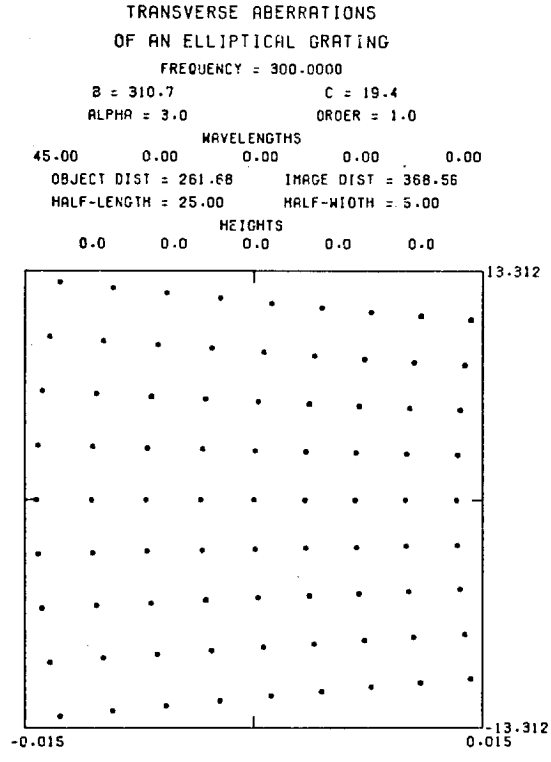
TRANSVERSE ABERRATIONS
OF AN ELLIPTICAL GRATING
FREQUENCY = 300.0000
B = 310.7
C = 19.4
ALPHA = 3.0
ORDER = 1.0
WAVELENGTHS
45.00 0.00 0.00 0.00 0.00
OBJECT DIST = 261.68
IMAGE DIST = 368.56
HALF-LENGTH = 25.00
HALF-WIDTH = 5.00
HEIGHTS
0.0 0.0 0.0 0.0 0.0
13.312
-13.312
-0.015
0.015

FIG. 64

incidence which may be used. The range of angles which may be used with the grating considered above is shown in Table 1 which also shows the "optimum" wavelength for each angle of incidence. Provided the width of the elliptical grating is not excessive, there is sufficient latitude in the angle of incidence to accommodate the usual experimental variations of the angle of incidence. Fig. 65 shows a spot diagram from the elliptical grating considered previously at 45 Å but with an angle of incidence of 3.1° and the object and image distances adjusted accordingly.

In conclusion gratings formed on elliptically figured cylinders may be usefully employed in existing grazing incidence spectrographs to provide an increase in both luminosity and resolution. For a given angle of incidence the maximum possible increase is obtained if the wavelength range is restricted, however, gains are possible over relatively wide wavelength ranges. When manufacturing an elliptical grating it is necessary to choose the lengths of the ellipse axes for the wavelength and angle of incidence to be used. Once the angle of incidence has been chosen it is only possible to use a range of angles of incidence in the vicinity of the design angle unlike the spherical grating which can be used over a wide range of angles. Thus the elliptical grating will primarily appeal to the user who requires the highest possible resolution and luminosity over a small wavelength range. Since gratings of this type are intended for specialist applications, they could only be produced individually. However, recent developments in optical working techniques stimulated by the work on x-ray telescopes should facilitate the production of high quality elliptically-figured blanks and high efficiency diffraction gratings

TABLE 1

Relation between Angle of Grazing Incidence and "Optimum" Wavelength for an Elliptical Grating with the following parameters:

Semi-major axis, b	=	310.556 mm
Semi-minor axis, c	=	19.2891 mm
Rowland circle diameter, R	=	5000 mm
Grating frequency	=	300 l/mm

Angle of Grazing Incidence (degrees)	Optimum Wavelength (Å)
2.0	183.97
2.1	162.86
2.2	144.18
2.3	127.52
2.4	112.51
2.5	98.898
2.6	86.443
2.7	74.965
2.8	64.313
2.9	54.359
3.0	45.000
3.1	36.146
3.2	27.723
3.3	19.668
3.4	11.925
3.5	4.4482
3.561	0.0

TRANSVERSE ABERRATIONS
OF AN ELLIPTICAL GRATING

FREQUENCY = 300.0000

B = 310.6 C = 19.3

ALPHA = 3.1 ORDER = 1.0

WAVELENGTHS

45.00 0.00 0.00 0.00 0.00

OBJECT DIST = 270.39 IMAGE DIST = 374.79

HALF-LENGTH = 25.00 HALF-WIDTH = 5.00

HEIGHTS

0.0 0.0 0.0 0.0 0.0

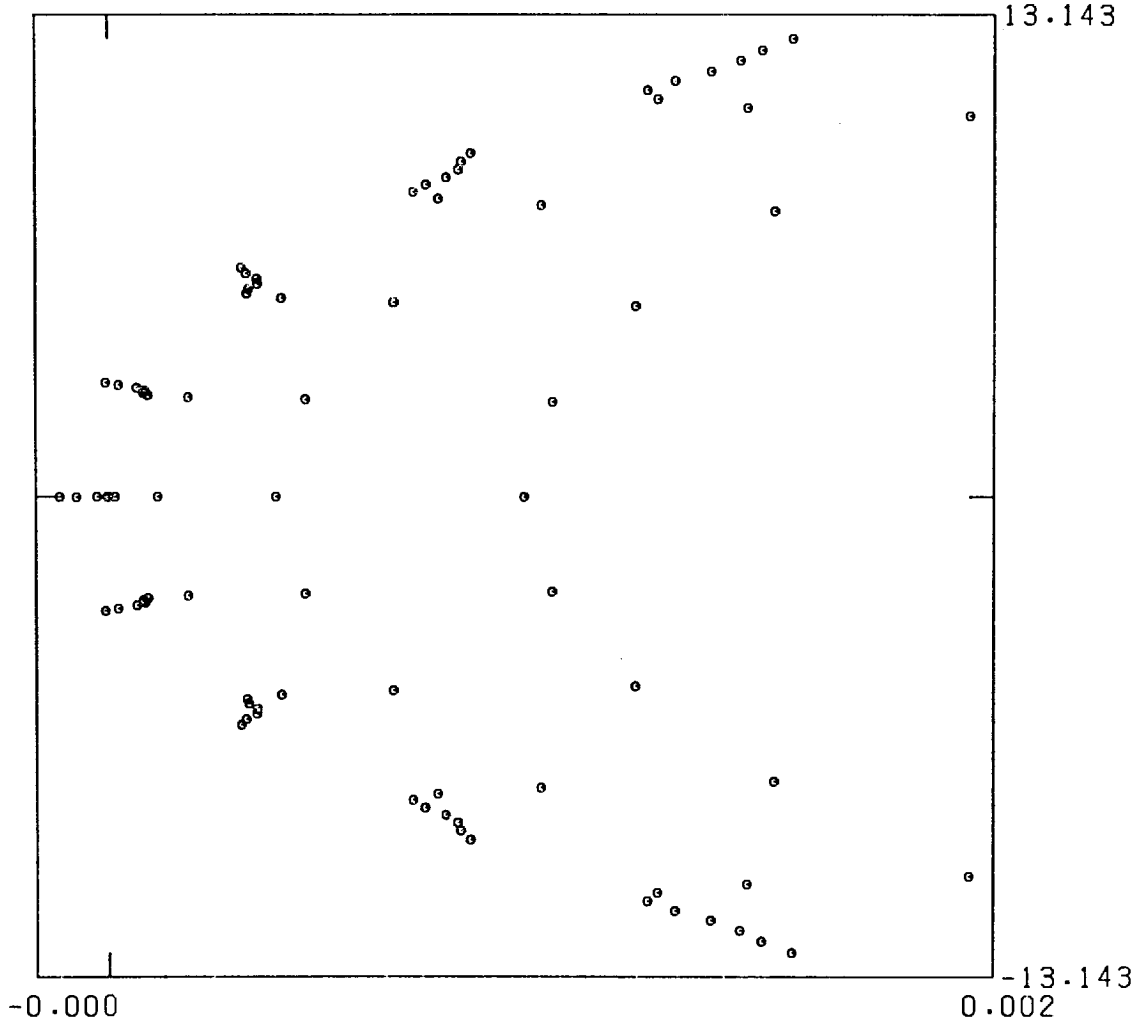

FIG. 65

can be readily formed on such blanks using the holographic process. Thus it is to be expected that the increase in resolution made possible by using an elliptical grating will be demonstrated experimentally in the near future.

CHAPTER 4

THE MANUFACTURE OF HOLOGRAPHIC X-RAY GRATINGS

The basic process for making holographic diffraction gratings is very simple. It is only necessary to accurately record the intensity distribution of the interference fringe system made by the superposition of two coherent monochromatic waves in order to make an optical element which has dispersive and also imaging properties. To produce high quality diffraction gratings is, however, not such an easy matter because of certain physical and technological constraints. The nature of some of these limitations will be described in this chapter together with a detailed account of the methods used by the author for the production of holographic soft x-ray gratings.

In 1964 Sayce and Franks (113) described several possible methods for producing efficient diffraction gratings for use in the x-ray region including the use of photoresist for photographically copying transmission gratings. They found a positive working photoresist; one rendered soluble in an aqueous alkaline solution after exposure to ultra-violet light, to be the most effective. However, only relatively coarse diffraction gratings with frequencies below 200 l/mm could be readily copied by this photographic method. The difficulties experienced when copying higher frequency gratings were attributed to limitations of the photoresist; however, it is more likely that the problems were due to other aspects of the copying process such as mask-substrate contact and collimation of the light rather than intrinsic limitations of the photoresist. It was also

mentioned that the quality of the resist surface was not easily controllable and depended upon the mode of application and "texture" of the resist. The resist gratings were therefore only used as masters from which x-ray gratings were prepared by subsequent processing. Two techniques were used for making the x-ray gratings; the first was to replicate the grating using epoxy resin and the second was to make chromium phase gratings from the masters by the stripping process. These techniques were applied to masters produced both by ruling in aluminium and by copying photographically.

The stripping process is well-known in the semiconductor industry and is used for high resolution applications when substrates present special processing problems. In this technique the photoresist is processed so as to leave exposed the areas of substrate which are to be coated with chromium. The resist and substrate are then coated with a uniform film of chromium of known thickness by vacuum evaporation. Since thin chromium films prepared in this way are porous, by treating the grating with organic solvents, it is possible to remove the undeveloped photoresist together with the overlying layer of unwanted chromium to leave strips of chromium adhering to the substrate. The steps of this process are shown in Fig. 66.

The development of the high-power continuous-wave Ar^+ laser enabled Rudolph and Schmahl in Germany to propose in 1967 the fabrication of diffraction gratings with photoresist and laser light. Although gratings had been produced earlier by photographing the interference fringes of two coherent light waves from a laser, these gratings were not suitable for spectroscopy because of their poor optical quality and low efficiency. Silver halide photographic

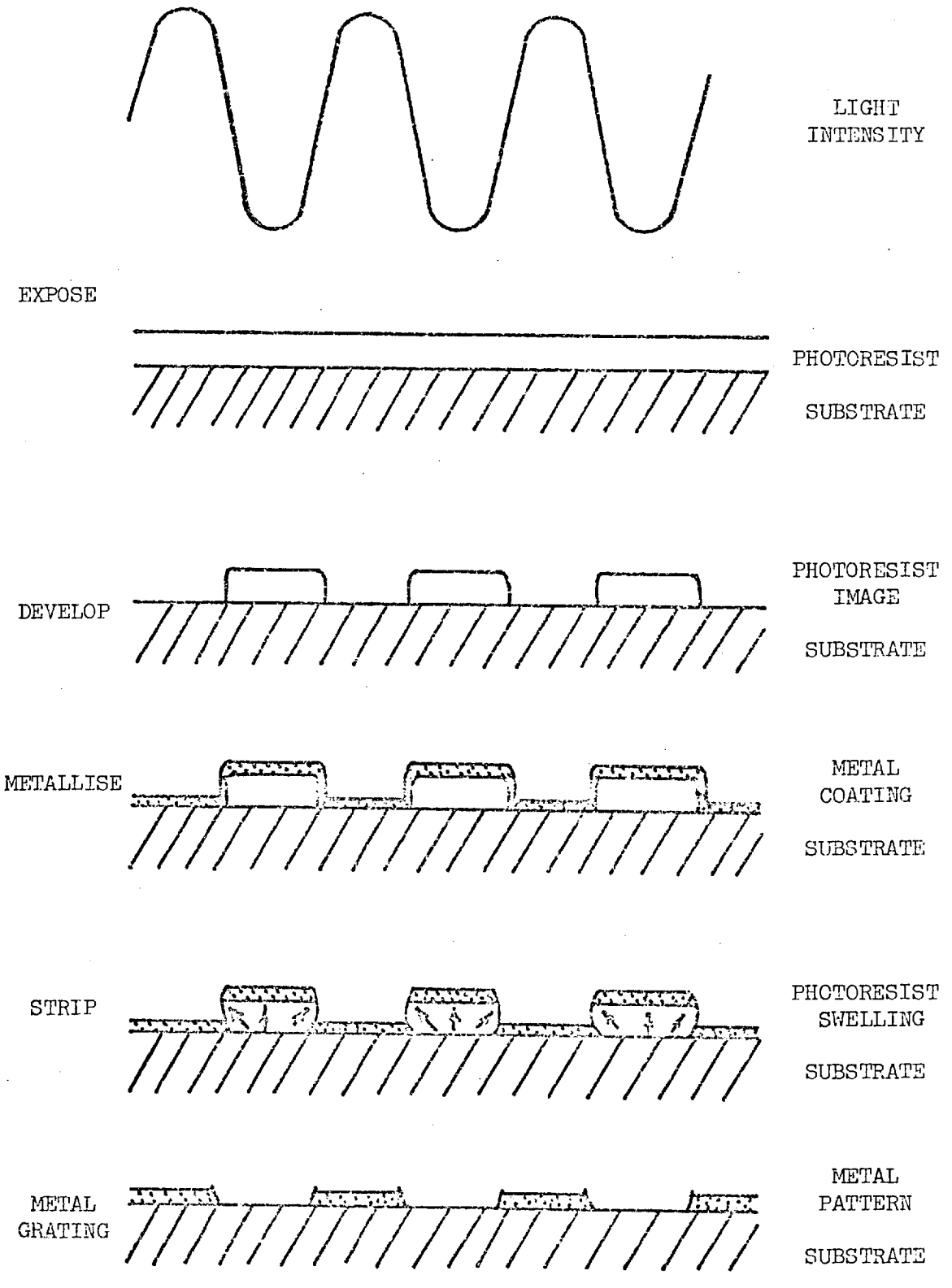

THE "STRIPPING TECHNIQUE" FOR PRODUCING HOLOGRAPHIC GRATINGS

FIG. 66

emulsions were not suitable for making high-quality diffraction gratings because of the granular nature of the process, and methods involving gelatin (either in photographic emulsions or gelatin-dichromate or similar materials) were also unsuitable because of the dimensional changes which occurred during processing. The necessary photosensitive medium was required to form a thin uniform layer of great dimensional stability and be capable of very high resolution. Fortunately, the photoresists used in the semiconductor industry possessed just these properties.

The first holographic gratings were produced by coating an optical flat with a thin uniform layer of photoresist and then exposing it in the interference field produced by two coherent plane waves from a laser. The exposed photoresist was subsequently developed to yield a grating with a periodically varying surface profile which was nearly sinusoidal. To complete the process the photoresist gratings were coated with aluminium in order to increase the reflectivity.

In 1967 Labeyrie and Flamand also produced gratings by this method at the firm of Jobin-Yvon in France. Although this firm has several ruling engines and is committed to the production of ruled gratings, they have become the major commercial suppliers of holographic gratings. The gratings supplied by Jobin-Yvon are mainly coated resist gratings with a nearly sinusoidal profile formed on plane or spherical blanks. They have designated three types of holographic gratings. Type 1 formed using the interference system of two plane waves and giving the same ruling pattern as a classical ruled grating; Type 2, using non-parallel beams to provide

aberration correction; and Type 3, stigmatic gratings formed using point sources.

In the visible and U.V. wavelength regions the properties of holographic and ruled gratings are largely complementary and the correct type of grating must be chosen for the particular application. Holographic gratings usually have lower stray light levels and are free from ghosts and can offer a higher signal to noise ratio than mechanically ruled gratings. It is also possible to make very large gratings which have uniform diffraction efficiency over the whole surface using the holographic method; such gratings could not be ruled mechanically because of diamond wear problems. However, the efficiencies of holographic gratings are usually less than those of ruled gratings because the optimum groove profile and blaze angle can be more readily attained in the mechanical method. Holographic gratings with sinusoidal profiles can have high efficiencies provided $0.8<\lambda/d<1.7$ which favours high grating frequencies. Thus the holographic method is best suited to making large high frequency gratings and gratings for applications where the scattered light levels are critical.

In the soft x-ray wavelength region the situation is completely different. It is not possible to use large concave gratings at grazing incidence because of the spherical aberration limitations and plane gratings are rarely used in the soft x-ray region because of the need for additional focussing optics which would reduce intensity. Experimental determinations of grating efficiency in the soft x-ray region show clearly that diffraction efficiency decreases rapidly with increasing grating frequency. It has also been found experi-

mentally that ruled gratings with a laminar profile have a higher efficiency than echelette type gratings. Thus it would appear that there would be no gain in using holographic gratings in the soft x-ray region. However, the holographic method does offer possibilities for aberration correction and the formation of gratings on surfaces which could not normally be ruled, but it was first essential to be able to make efficient holographic gratings for use in the soft x-ray region. With this aim in view a collaborative research programme was organised with Dr. Rudolph and Dr. Schmahl of the Universitäts-Sternwarte Göttingen. The results of this research programme have been most successful and by employing improvements to the holographic method developed by the author, it is now possible to make holographic diffraction gratings which have a very high efficiency in the soft x-ray region.

4.2 EXPERIMENTAL CONDITIONS NECESSARY FOR PRODUCING HOLOGRAPHIC GRATINGS

In order to produce a perfect plane holographic grating it is necessary to be able to produce interference fringes with exactly equal spacings, but such fringes can only be produced by perfectly plane wavefronts. However, in practice such wavefronts cannot exist because optical elements which introduce aberrations must be used to produce the wavefronts and also apertures in the system introduce divergence due to diffraction. Therefore, in practice holographic gratings will have variations in the spacing which give aberrations in the diffracted wavefronts and deviations from the ideal intensity distribution in a spectrum. However, provided the wavefront aberrations of low spatial frequency are $<\lambda/20$ and there are no high spatial frequency aberrations, a diffraction gratings is generally accepted to be of high quality. In order to achieve this quality in holographic gratings, it is necessary to use optics of similar quality when making the gratings for use in the first diffracted order and of higher quality when making gratings for use in higher orders. Therefore, high quality optical elements must be used for producing holographic gratings.

It has been shown by Schmahl and Rudolph (121) that it is possible to make high quality gratings from aberrated wavefronts provided the aberrations are identical in both beams. With normal optical elements this would be impossible but by using waves produced by holographic reconstruction from two holograms it is possible to produce identical waves. Superposition of the two waves produces an interference field of improved accuracy and the quality of the resultant grating becomes

nearly independant of the quality of the optical elements used. Provided the aberrations of the optics are less than a few wavelengths, it is possible, in this way, to increase the ruling accuracy by about two orders of magnitude. Thus it is possible to make holographic diffraction gratings whose quality is in practice only limited by the quality of the blank and photoresist layer.

Although laser lines can be very nearly monochromatic, it is necessary to consider the effect of the finite spectral bandwidth of laser lines in the production of holographic gratings. The contrast of the interference pattern depends on the width and profile of the laser line and the path difference between the interfering beams. In order that the contrast is uniform over the interference field, it is necessary that the path differences are small compared to the coherence length of the laser. Since the coherence length is given by $L \approx c/\Delta\nu$ and the path difference by $l = \frac{1}{2}W \sin\alpha$, it can be seen that the necessary line widths are narrower for large high frequency gratings and a typical value would be $\Delta\nu \approx 10^9 Hz$. In addition to a narrow line width it is essential that there is high frequency and wavelength stability otherwise the interference fringes will not remain stationary.

The frequency stability of a laser is dependant upon its design and the environmental conditions. For the Coherent Radiation Model 53 high power argon ion laser, used by the author in Göttingen, the individual argon lines are selected using a prism in the resonator and the design of the cavity and mirrors is such that the laser operates in TEM_{00}. However, due to Doppler broadening and Zeeman splitting, the argon lines are broadened and a number of axial modes

may be emitted separated by frequencies $\Delta\nu=c/2R_L$ where R_L is the length of the laser cavity. The cavity length for the Model 53 laser is 1.45m which gives a frequency interval between axial modes of 10^8Hz. By using an oven stabilized etalon it is possible to select one axial mode and a frequency stability of ±75MHz was measured experimentally over a period of 30 minutes for the 4579 Å line using a confocal scanning-interferometer. This stability is adequate for all applications and since the line width is only a small fraction of this value the coherence length is very large. For many applications it is not essential to use an etalon since the required stability can be achieved by optimising the operating conditions of the laser. However, for large high frequency gratings such frequency selection is essential.

Temperature, pressure and humidity changes in the atmosphere through which the laser beams pass will cause refractive index variations which alter the laser wavelength. Normally, atmospheric pressure changes and variations of humidity are only small during typical exposure times and have little effect on the interference field. However, thunderstorms can have a noticeable effect on the stability of the interference fringes. Temperature changes cause larger wavelength shifts and it is necessary to provide temperature stabilisation to better than 0.1K for the interference system and also to control the air temperature around the laser to ±1K. When changes are made to the optical system it is necessary to allow sufficient time for thermal transients to decay and for the system to stabilise mechanically.

It is of course most important to provide adequate vibration isolation for the optical system. In the Optical Laboratory of Göttingen Observatory a 700 kg optical bench 3.5m x 1m x 0.1m is supported by a combination of springs and damping elements on a massive concrete block which has its foundations set deep in the earth. The Optical Laboratory is separated from the other Observatory buildings and provides nearly ideal conditions. By optical methods it has been shown that the amplitudes of the residual vibrations in the interference system are less than 20nm.

The optical bench is located in a well insulated double-walled chamber with dimensions 5m x 1.8m x 2m which is inside a slightly larger room in the Optical Laboratory. Fig. 67 shows a view inside the interference chamber of an optical system set up on the optical bench. Temperature stabilisation is achieved by a most comprehensive system employing four heat exchangers in the interference chamber and one above the chamber and a temperature stability of $0.01<\Delta T<0.1$K is attained. The laser is set up in the main Optical Laboratory to avoid thermal and mechanical disturbances in the interference chamber and the whole outer laboratory is air-conditioned to provide temperature control to ± 1.5K. Thus, the facilities at the Optical Laboratory of Göttingen Observatory are such that holographic diffraction gratings of the highest quality may be produced.

FIG. 67 THE INTERFERENCE CHAMBER AT UNIVERSITÄTS-STERNWARTE GÖTTINGEN

4.3 THE PROPERTIES OF PHOTORESISTS

There are two basic types of photoresist: positive working photoresist which is rendered soluble by the action of light and negative working resist which becomes insoluble on exposure. Numerous photoresists of both types are available commercially and all have different characteristics which make them more suitable for certain applications. Photoresist systems have been used for many years in the photomechanical industry, however, the requirements of the semiconductor industry have led to the development of improved photoresist systems suitable for the fabrication of holographic diffraction gratings.

The action of light on negative photoresists causes photocrosslinking, or photopolymerisation, and the negative resist developer is an organic solvent which dissolves away the unexposed resist and tends to swell the exposed image. For positive materials the incident energy causes a photochemical reaction which converts the resist into a form which is soluble in an aqueous alkali developer. In this case the developer does not penetrate or swell the unexposed material which contributes to the excellent dimensional stability and sharp edge definition obtained with positive working resists. With positive working resist it is also easier to obtain an image which adheres well to the substrate because it is not necessary for the photoresist to photolyse through the whole thickness of the resist layer as in the case of negative working resists. Furthermore, the high purity positive photoresist systems are generally more convenient to work with than negative resist systems. However, by using a negative working resist sensitised in the blue

region (e.g. Kodak Ortho Resist), it is possible to use the strong line at 4880 Å from an Ar^+ laser and obtain a significant reduction in exposure time compared to positive working resists.

The photoresist used by the author to fabricate holographic gratings was Shipley AZ-1350 developed in concentrated AZ Developer which is highly alkaline (pH 12.7-12.8). AZ-1350 has a chemically combined photosensitiser of diazoanhydrides (quinone diazides) with a low molecular weight polymer of phenol-formaldehyde type. Exposure to UV light causes progressive photochemical conversion from the surface of the resist down to the substrate. The exact mechanism of the conversion is not completely understood, however, the combined action of the UV light and highly alkaline developer is to convert the quinone diazides into soluble carboxylic acids.

The polymer molecules in AZ-1350 have an uncoiled length of the order of 100 Å (the chain length of a typical negative working resist is about 5000 Å but tightly coiled structures can be formed). Since the changes which occur when the photoresist is exposed take place in the molecular structure, the resolution is extremely high. Usually the resolution is not limited by the photoresist but by some other experimental factors.

Photoresist films of optical quality with controlled thickness in the range 0.01 - 1μm can be readily formed on optical blanks by using the spinning technique. In this technique the blank is flooded with photoresist and is then rapidly spun at 2000 - 5000 rpm. Coating uniformity is achieved by an early high acceleration rate and the combined effects of centrifugal force and surface tension. The thickness of the resist layer depends on the viscosity and solids

content of the resist, the acceleration and final speed of the spinner, the substrate shape and preparation, the vapour pressure in the spinner, and the total spin time. In Göttingen a commercial spinner, as used in the semiconductor industry, is employed which enables the acceleration, maximum speed, spinning time and deceleration to be controlled and easily reproduced. By varying the dilution of the photoresist with photoresist thinners and by varying the spinning speed it is possible to obtain a wide range of resist thicknesses as shown in Fig. 68. Once the correct conditions have been determined to yield a uniform film of the required thickness, it is important that the conditions can be easily reproduced so that all the blanks coated for one session have identical properties. Blanks of unusual shapes can pose problems when spin coating, however, with ingenuity it is possible to achieve uniform coatings on very asymmetrical blanks. With spin coating there is always a small increase in resist thickness at the edge of the blank, however, this is usually of no consequence for holographic gratings.

The peak spectral sensitivity of most photoresists is in the region 3000 - 4500 Å due to the energy required to cause the photochemical reactions. In photoresists nearly all the energy for the chemical changes must come from the incident light since the resist developers act mainly as solvents whereas in normal photographic processes most of the chemical energy comes from the developer. Compared to normal photographic emulsions photoresists are extremely insensitive and require energy densities 10^3-10^4 times higher than slow, high resolution emulsions. Fortunately neither reciprocity-law failure nor photo-oxidation takes place with positive photo-

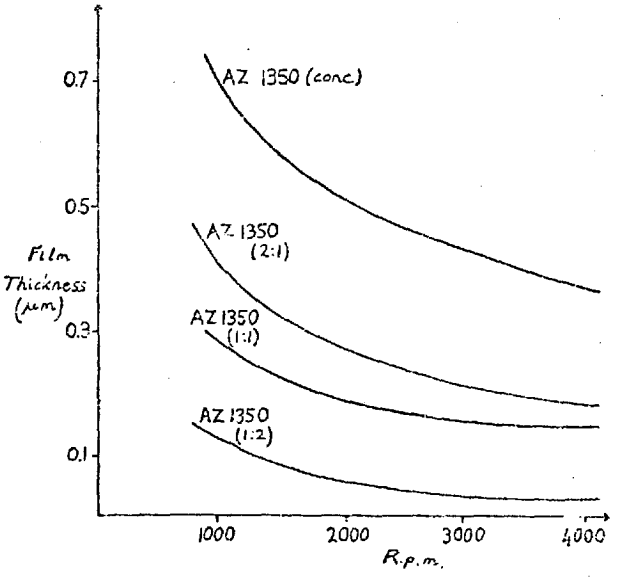

THE DEPENDENCE OF PHOTORESIST COATING THICKNESS ON SPINNING SPEED AND DILUTION

FIG. 68

resists which means that very long exposure times can be used. With AZ-1350 there is approximately an order of magnitude increase in sensitivity from a wavelength of 5000 Å to 4500 Å and a further order of magnitude increase from 4500 Å to 3500 Å. Thus it is advantageous to use light sources which have a high intensity in the UV region. However, there are very few high power coherent light sources in the UV region and a more favourable combination of laser power and resist sensitivity can be obtained by using slightly longer wavelength lines in which much higher powers can be attained.

The argon ion laser is particularly suitable for use in the manufacture of holographic gratings, and the lines at 3511, 3638, 4579, 4880 and 5145 Å may be used. Although higher powers are obtainable from the 4880 and 5145 Å lines with AZ 1350 it is advantageous to use the 4579 Å line because of the photoresist response. The lines of the Krypton-ion laser at 3507 Å and 3564 Å are suitable when a shorter laser wavelength must be used and the lines of the helium-cadmium laser at 3250 Å and 4416 Å can also be used. It has been found that from the point of stability, process control and ease of light intensity measurements, the Ar^+ line at 4579 Å is the most suitable for use with AZ-1350.

A characteristic curve can be drawn for positive photoresists showing the depth of resist removed against incident energy density. However, the characteristic will depend on the method of preparation of the film, its age and the drying technique used, the spatial frequency of the image and the development conditions. Therefore, it is necessary to perform individual evaluation of the process which

is normally achieved experimentally by making trial exposures. It is possible to obtain an increase in sensitivity by prolonging the development time or by using more concentrated developers, e.g. by using AZ-303 developer with AZ-1350 resist, a gain in sensitivity of about five can be achieved. However, when using thin photoresist layers control of the process and adhesion can be critical if too strong a developer is used. With concentrated AZ Developer unexposed resist is dissolved with reported rates up to 300 Å/sec whereas for developer diluted 1:1 the unexposed resist is dissolved at only ∿2Å/sec. Thus the development technique can greatly alter the characteristics and generally more diluted developer increases the exposure latitude but reduces sensitivity. Therefore, it is necessary to optimise the development technique for all the exposure conditions applicable.

An energy density of about $2.10^3 J.m^{-2}$ is required to obtain a modulation depth of 2000 Å in AZ-1350 resist with 15 seconds development time in concentrated AZ Developer for λ = 4579 Å. The output of the Coherent Radiation Model 53A laser in Göttingen has been measured as 450 mW at λ = 4579 Å with a plasma current of 35 A. Typical energy densities in the interference field would be up to about 5 $W.m^{-2}$ depending on the system used. Therefore, exposure times range from a few minutes for small gratings to 15 minutes for larger gratings. Thus the inherent low sensitivity and spectral response of present photoresist systems necessitate the use of high power, high stability, lasers which means that only a few discrete wavelengths can be used for the fabrication of holographic gratings.

4.4 METHODS FOR PRODUCING HOLOGRAPHIC X-RAY GRATINGS

It is well known that the superposition of two plane monochromatic beams of light produces interference fringes with a $\cos^2$ intensity distribution and the maximum fringe visibility is obtained when the two beams have equal intensity. The spacing between the fringes is given by:

$$d = \frac{\lambda_0}{\left(\sin(\theta+\phi)+\sin(\theta-\phi)\right)} = \frac{\lambda_0}{2\sin\theta\cos\phi}$$

where θ is the semi-angle between the two beams and ϕ is the angle the bisector of the beams makes with the normal to the surface. It can be seen that the highest grating frequencies are obtained when the beams are symmetrical about the normal to the surface ($\phi=0$) and that the maximum possible frequency is limited by the laser wavelength, λ_0. Some typical grating frequencies and beam intersection angles are shown in Table 2 for laser wavelengths 3507 Å and 4579 Å in a symmetrical geometry.

TABLE 2

Relation between grating frequency and intersection semi-angle between two parallel symmetrically incident laser beams.

Grating Frequency	Grating Spacing	Beam Intersection Semi-Angle (θ)	
(mm^{-1})	(μm)	λ = 3507 Å	λ = 4579 Å
100	10.0	1.00	1.31
300	3.33	3.02	3.94
600	1.67	6.04	7.90
1200	0.83	12.15	15.95
2400	0.42	24.89	33.33
3600	0.28	39.14	55.51

A standard optical system suitable for the production of holographic gratings of moderate size is shown diagrammatically in Fig. 69. The laser beam which has an initial diameter of about 1.5mm and a divergence of 0.6mR is expanded by means of a high quality microscope objective. The microscope objective and a 10μm spatial filter are on an adjustable stage which enables the focus of the microscope objective to be readily adjusted to the focus of the parabolic mirror. When this has been performed a parallel beam of light is produced by the parabolic mirror. The two high quality plane mirrors on either side of the microscope objective are adjusted to reflect two beams of equal intensity at the correct angle to produce the required grating frequency and they are positioned so that the path differences for both beams are nominally equal. The grating holder is placed at the intersection of the two beams and is set symmetrically. Final adjustment of the optical system can be most conveniently performed by putting a reference grating in the grating holder to produce a Moiré pattern. By rotating the grating through 180° it is easy to determine any residual aberrations in the system and make the necessary corrections. Using this method also enables the fringe stability and contrast to be readily examined. It has been found in Göttingen that it takes about three days for an optical system to become completely stable after it has been initially set up. For minor adjustments it is only necessary to allow one day for the system to stabilise before making any exposures.

The optical quality of a holographic grating is essentially determined by the quality of the substrate provided the optics used

A TYPICAL OPTICAL SYSTEM FOR PRODUCING HOLOGRAPHIC GRATINGS

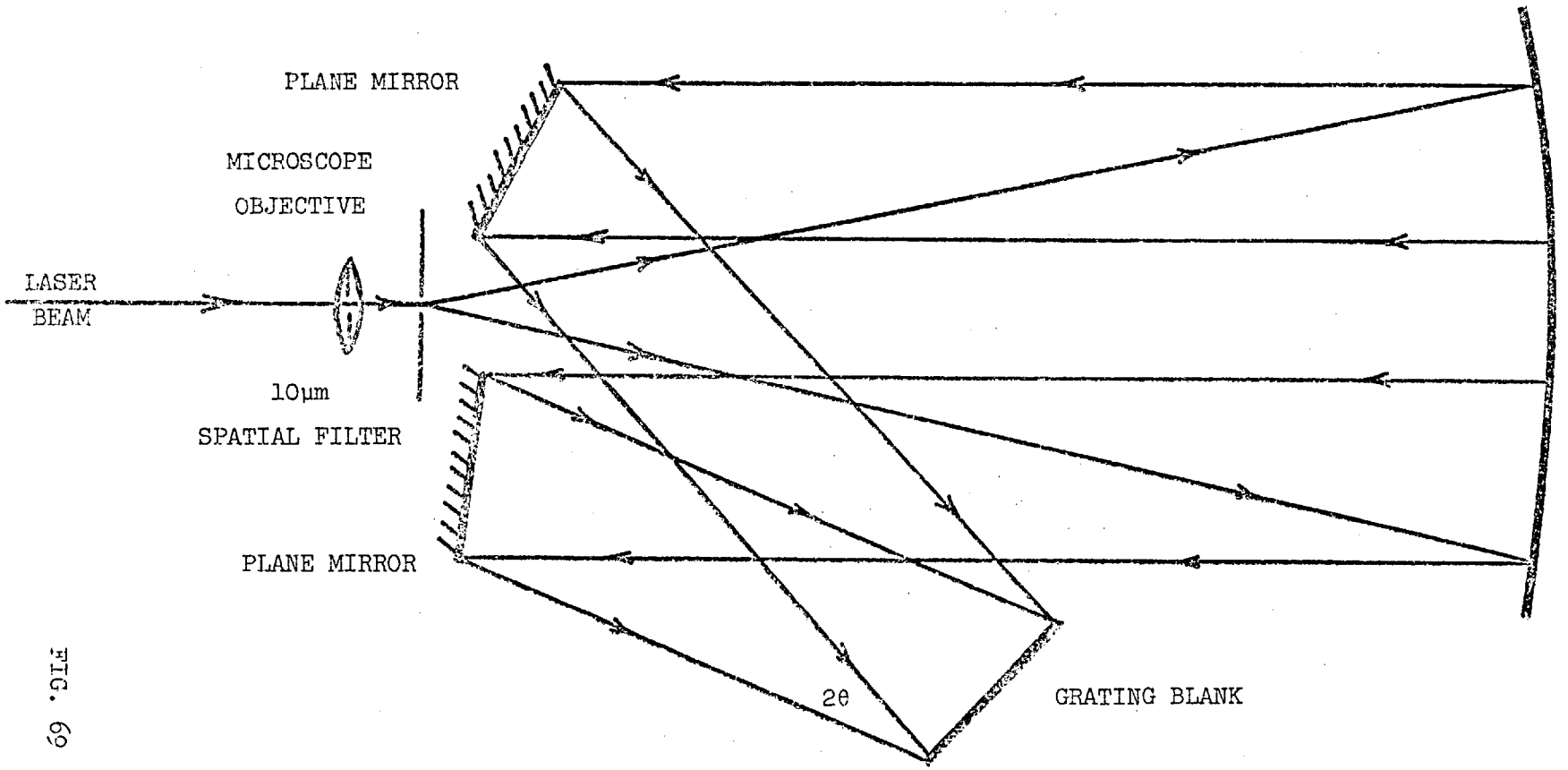

FIG. 69

for making the grating are of the highest quality and the optical system is correctly adjusted. The diffraction properties are largely determined by the profile of the individual grooves and this is determined by the technique used to produce the grating. The author has used two techniques to produce holographic gratings and has developed a third method by which gratings with a high diffraction efficiency in the soft x-ray region can be produced.

The basic method for making a holographic grating is to expose a photoresist-coated blank in an interference fringe system using light from a laser. By varying the thickness of the photoresist layer, the exposure, and development, it is possible to obtain various grating surface profiles. A symmetrical nearly sinusoidal profile is the one most readily obtainable as a result of the non-linear characteristic of the photoresist and also the possibly non-isotropic development of high spatial frequency structures. If resist layers are used which are thin compared to the grating spacing, it is possible to obtain a laminar profile. The resist which has been exposed is removed by development resulting in a grating consisting of strips of photoresist adhering to the substrate. In order to make a laminar phase grating for use in the soft x-ray region the groove depth must be ∿50 - 300 Å. It would be difficult to use photoresist films of this order of thickness; therefore, it is necessary to use some processing technique to convert the resist grating into the required form.

The first method used in Göttingen to produce holographic gratings suitable for the soft x-ray region was to vacuum coat a laminar resist grating with a layer of metal and then remove the underlying photoresist by the stripping technique to produce a grating consisting of

strips of metal on the substrate. Subsequent coating of this grating to enhance the reflectivity resulted in a grating with a usable diffraction efficiency in the soft x-ray region. In this technique the groove depth could be accurately controlled since it is determined by the thickness of the evaporated metal layer. The most suitable metal for making the gratings was chromium because it adhered well to glass, could be evaporated readily, and enabled the grating to be stripped easily. Titanium, which has similar properties, may also be used. The process of removing the unwanted metal and photoresist is achieved by immersing the grating in a suitable resist solvent (e.g. alcohol or acetone), the solvent passes through the thin porous chromium film and swells the photoresist enabling the unwanted chromium to be removed by gentle swabbing with cotton wool. It is essential to produce a clean break in the metal film where it leaves the substrate and begins to form the bridge over the photoresist. This can only be achieved if the photoresist has a sharp vertical profile and if the metal deposition is performed so that the atoms impinge at near normal incidence in order to obtain a thinner coating on the sides of the grooves than on the substrate and on top of the photoresist. An undercut resist profile like that obtained because of electron scattering in polymer film used in electron beam fabrication techniques would enable the desired laminar profile to be achieved more easily.

The stripping technique has several advantages over other possible methods. Firstly, this method is known to be able to produce high resolution and good edge acuity. Secondly, since metalising is only performed after the correct photoresist image is produced on the substrate the photoresist can be easily removed from unsuccessful trials

without significant degradation of the surface finish. Thirdly, since removal of the unwanted metal and photoresist is accomplished by organic solvents after processing the grooves of the grating still have the surface quality of the polished glass blank and the surface of the lands is determined by the quality of the metal coating. Therefore, by employing this technique it should be possible to produce robust holographic gratings free from organic material which have laminar profiles consisting of alternate optically smooth lands and grooves. In practice it is found that gratings produced by this technique have very high uniformity and excellent appearance when examined through optical or scanning electron microscopes. However, surface profile measurements using a Talystep have revealed that "bumps" ∿100 - 200 Å high are formed at the ends of the lands as shown in Fig. 70. For most applications bumps of this size would be negligible, however, these bumps cause a marked reduction in diffraction efficiency for diffraction gratings used at grazing incidence. Since a bump 100 Å high causes a shadow 2865 Å long for a grazing angle of 2°, it is clear that such bumps on either end of the lands of a grating will cause significant shadowing effects. Therefore, this technique is unsuitable for producing gratings for use in the soft x-ray region but may be used to produce gratings with great mechanical and thermal stability suitable for use with high power radiation and for metrological purposes. Metal gratings of this type may also be used as masks in the preparation of gratings etched in the substrate by ion bombardment. However, it was clear that an alternative method would have to be found to produce a laminar grating consisting of optically smooth lands and grooves.

GROOVE PROFILES OF HOLOGRAPHIC GRATINGS MADE BY THE "STRIPPING TECHNIQUE"

(MEASURED ON A "TALYSTEP" AT THE NPL)

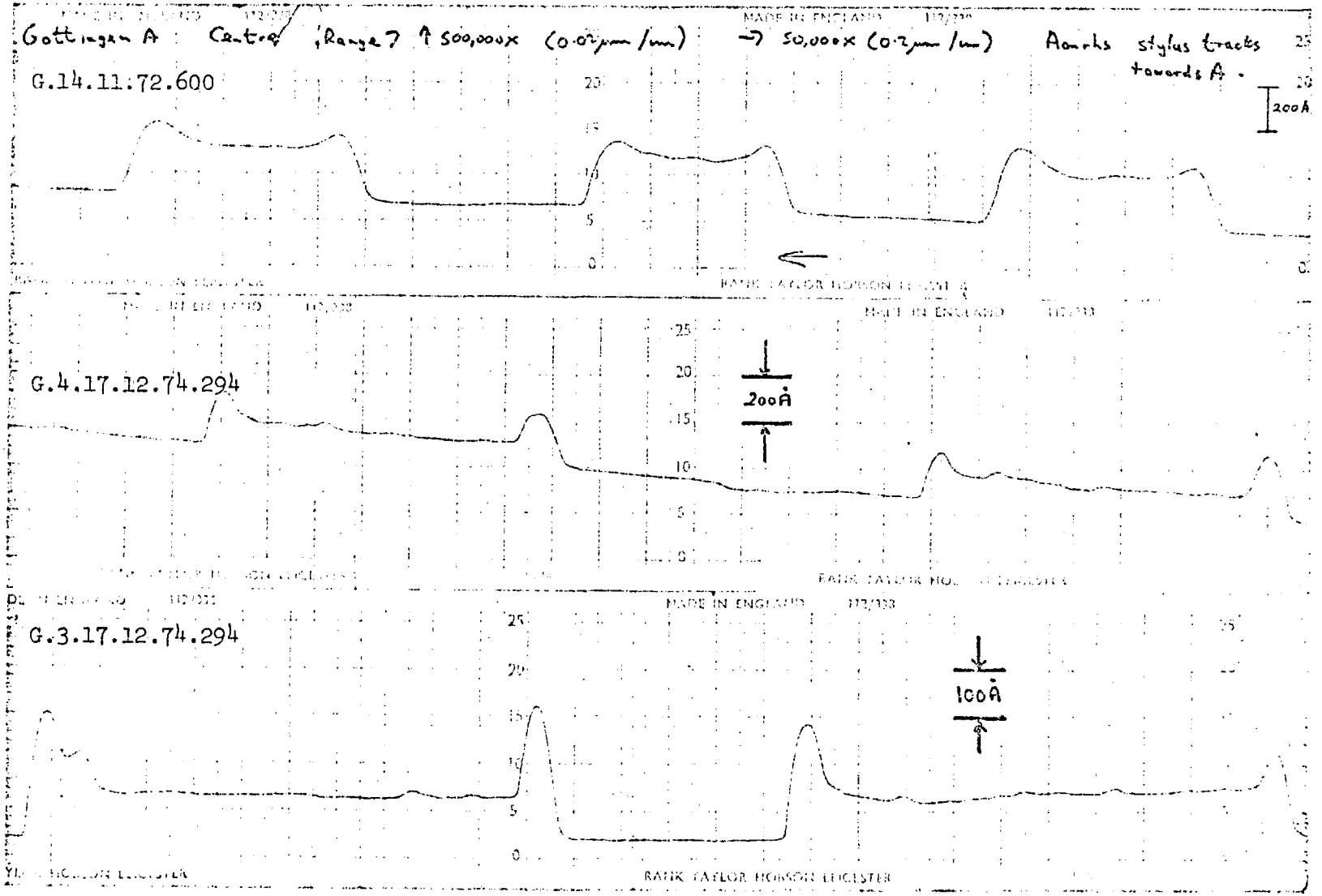

FIG. 70

The standard photofabrication technique of producing a photoresist image on a thin metallic film and then chemically etching the unprotected metal had apparently never been used for the production of diffraction gratings. By using this technique it was clear that no "bumps" could be formed on the lands but it was not known whether sufficient resolution could be achieved, or even if it was possible to controllably etch such fine structures. Since the groove depths required for soft x-ray gratings are only ∿100 Å the metal films would be much thinner than normally used in the semiconductor industry. It would be expected that this could increase the resolution, however, since there was no reported work in this field, the author performed in Göttingen a series of experiments to determine the feasibility of this method.

The first trials were performed by contact printing a 125 l/mm transmission grating onto microscope slides which had been coated with thin films of copper and photoresist. After the resist grating had been developed the exposed copper was etched in a dilute solution of ammonium persulphate. The results were most encouraging and it was found that uniform etching took place with no significant undercutting and the process could be readily controlled by varying the concentration of the etchant and the etching time. Thus, the etching technique enables a mask consisting of strips of photoresist to be readily converted into a laminar metallic structure suitable for diffraction in the soft x-ray region.

Diffraction gratings could obviously be formed in a large number of etchable materials (metals and non-metals) by using a holographic

mask. It is also evident that other methods besides chemical etching, such as electrolytic etching and ionic bombardment, could be used. However, it was essential to start somewhere and pursue the method in order to discover any limitations. Copper was chosen as the initial material in which to form the gratings for three reasons. Firstly, thin copper films which adhered well to glass could be readily produced by vacuum evaporation. Secondly, copper can be etched easily in a number of dilute etchants without evolution of gas. Thirdly, the photoresist was known to adhere well to copper. Silver, gold, platinum and magnesium fluoride were also considered to be suitable materials for etching.

The next stage in the research programme was the production of a series of 300 l/mm holographic gratings on plane optical blanks by the etching technique. These gratings were immediately sent to London for profile measurements to be performed using the "Talystep" at NPL Teddington and for subsequent soft x-ray efficiency measurements to be performed at Imperial College. The results of the Talystep measurements are shown in Fig. 71. It can be seen that the required profile has been achieved. The efficiency measurements confirmed the good profile because a maximum diffraction efficiency in excess of 10% was measured in the first order at 45 Å. By employing the etching technique to fabricate laminar holographic soft x-ray gratings, the efficiency was immediately increased by a factor of four. Thus, it became possible to readily make holographic gratings which had comparable efficiencies to the excellent NPL laminar x-ray gratings which were made by ion etching from a mask produced by mechanical ruling.

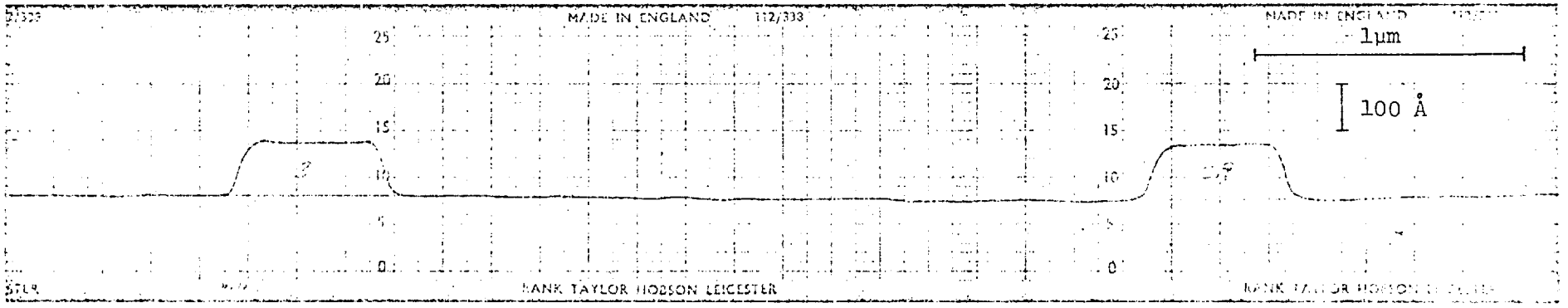

GRATING G.15.10.1.75.294

FIG. 71

GRATING G.9.10.1.75.294

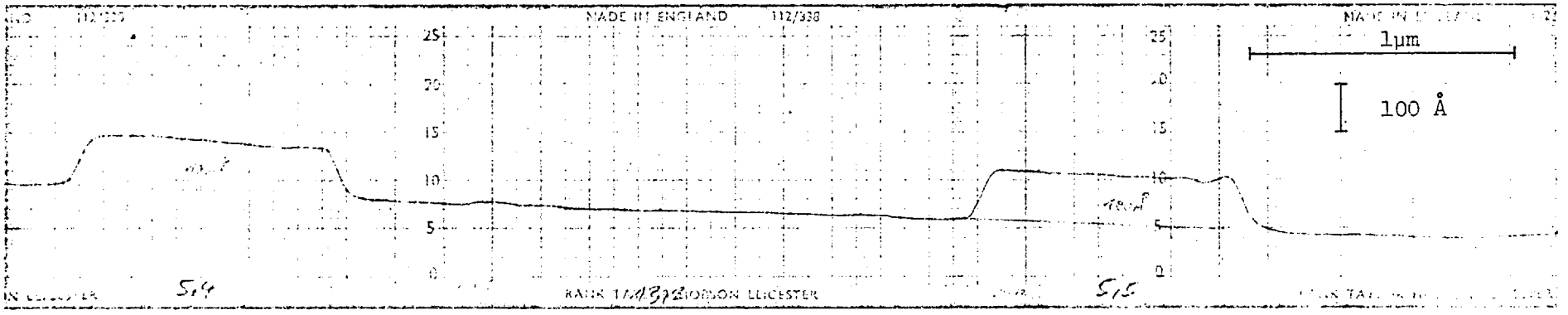

GROOVE PROFILES OF THE FIRST HOLOGRAPHIC LAMINAR SOFT X-RAY GRATINGS MADE BY THE AUTHOR USING THE "ETCHING TECHNIQUE"

In order to explore the process fully the author made a series of 300 l/mm gratings with various groove depths and land to groove ratios. Several 600 l/mm gratings were fabricated and a number of 1200 l/mm gratings were also made before the author had to return to London. In total the author produced nearly forty high quality diffraction gratings suitable for use in the soft x-ray region in a period of two months. The number of gratings produced was primarily limited by the availability of suitable optical blanks. Most of the prototype gratings were made on plane blanks, however, a number of gratings were made on 2m and 5m blanks and these gratings are already being used in spectrographs to produce new spectroscopic data.

The efficiencies of all the gratings have been measured at 45 Å and some of the gratings have also been examined at 8.3 Å. The results of these examinations will be fully discussed in Chapter 7, however, consistently high efficiencies have been measured for gratings produced by the etching technique. Typical maximum efficiency values at 45 Å range from 18% for a 300 l/mm grating to about 8% for a 1200 l/mm grating.

4.5 PREPARATION OF HOLOGRAPHIC GRATINGS BY THE "ETCHING TECHNIQUE"

The steps in the process used by the author to successfully produce soft x-ray diffraction gratings will be briefly described in this section.

The preparation of the grating blanks is the most important stage in the production of a holographic grating using this technique. It is essential that the substrate is free from molecular and particulate contamination and that the substrate is also free from surface defects. Freshly polished blanks require little cleaning apart from degreasing using alcohol. More grossly contaminated blanks are cleaned with hot detergents in an ultrasonic bath, and subsequently rinsed in several changes of distilled water before final rinses in alcohol. Contamination from dust particles is normally controlled by using a "Class 100 clean-room environment" or better, however, in Göttingen Observatory the natural conditions are so favourable that a "clean room" has been found unnecessary. The coating of the blanks with copper is performed using thermal evaporation in a standard vacuum coating plant with a source to substrate distance of about 20cm to ensure a uniform coating. The coating thickness and rate of deposition are monitored using a quartz crystal. The blanks are subjected to a glow discharge for five minutes to improve the adhesion of the copper film. After the blanks have been coated with the required thickness of copper they are allowed to cool before being spin coated with photoresist. Although microelectronic grade photoresists are filtered by the supplier the resist is filtered again by applying it to the blank using a syringe with a 0.5μm filter. After coating the blanks are placed in the interference room for 24 hours to thermally

stabilise and to allow the resist to dry completely. Generally photoresist films with thicknesses 2000 - 3000 Å have been found to be most suitable for this process.

The exposure would normally be controlled by using a light integrator to measure the intensity in the interference field and to terminate the exposure when the photoresist had received sufficient energy. Since the photocell had aged the author was not able to use this method and the correct exposure had to be determined by trial. The optimum exposure time was usually obtained after three or four trials and was generally about three minutes. No difficulty was experienced with standing wave effects due to reflection from the copper film but it was found that it was essential to keep the mirrors of the optical system completely dust free to avoid stray interference effects.

Development of the photoresist was performed in concentrated AZ Developer with a normal development time of about 30 seconds. The rate of development was visually monitored by looking at the diffraction from the grating and some latitude in the development was introduced in this way. The action of the developer was quenched by immersing the grating in flowing water. The trial exposures were usually blown dry with filtered air after washing and were inspected under a microscope to determine whether the exposure was correct. When the correct exposure had been determined after washing the grating was etched for 30 seconds in 1% ammonium persulphate solution to remove the exposed copper. The grating was then washed thoroughly and the photoresist was dissolved with acetone. The grating was finally washed with alcohol and dried with filtered

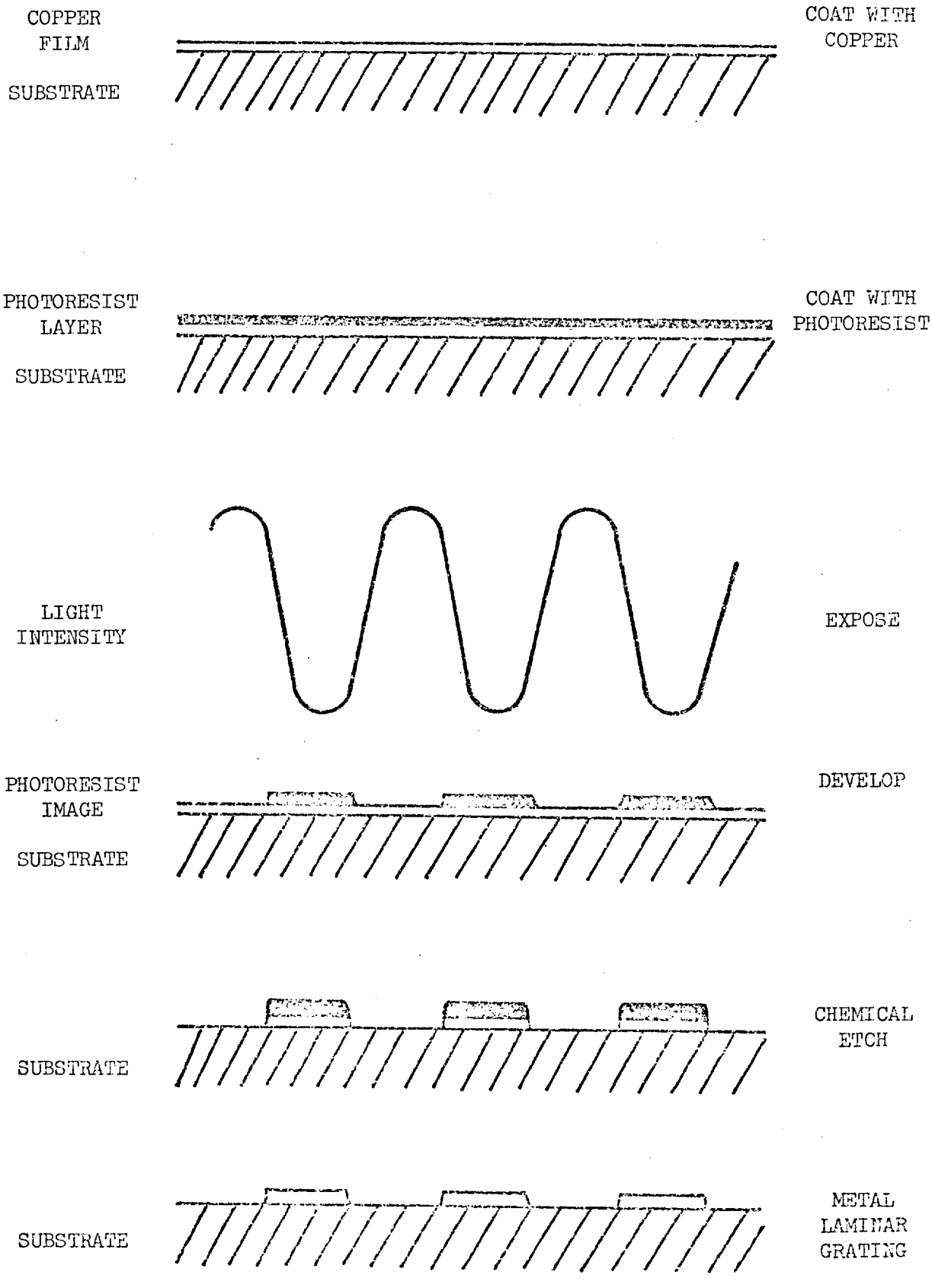

THE "ETCHING TECHNIQUE" FOR PRODUCING HOLOGRAPHIC GRATINGS

FIG. 72

air. The steps in the process are shown in Fig. 72.

Inspection of the grating was performed using light field and dark field illumination in an optical microscope. It is possible to measure the land to groove ratio of 300 l/mm and 600 l/mm gratings with a measuring eyepiece and it is also possible for 1200 l/mm gratings by using oil immersion. However, for gratings with frequencies higher than 2000 l/mm the optical microscope is of little use and the optimum exposure, development, and etch conditions cannot be so readily determined. It would be possible to determine when the correct profile had been achieved for high frequency gratings by measuring the diffraction properties of the grating or by using electron microscope examination. However, it is far more convenient to make gratings with frequencies less than 2000 l/mm since examination using an optical microscope is quick, simple and effective. If any significant defects are detected, or the land to groove ratio is unsuitable, the copper strips can be readily removed from the blank by immersing it in the dilute etchant and the blank can be used again. If there are no defects the grating consisting of strips of copper on glass is overcoated with a layer of gold to enhance the reflectivity and the production of the soft x-ray grating is completed.

4.6 FURTHER METHODS FOR THE PRODUCTION OF SOFT X-RAY GRATINGS

Theoretically it should be possible to obtain a higher diffraction efficiency from a grating with a sawtooth, or blazed, profile than from a laminar grating. However, in the soft x-ray region it is generally found experimentally that the diffraction efficiency is lower for shallow blazed ruled gratings than for laminar gratings. There are two main reasons for this: Firstly, the blaze angles required in the soft x-ray region are generally small and must be highly accurately controlled. Secondly, when a grating is ruled the metal is not removed but is simply pushed outwards and forms uneven ridges on either side of the groove. When a ruled blazed grating is used at grazing incidence only the tips of the profile are illuminated and it is this area over which there is least control during the ruling process. For replica gratings where the profile is inverted the situation is somewhat better, however, the technical difficulty of obtaining small blaze angles and the random errors which interferometric control cannot remove limit the diffraction efficiency of ruled blazed gratings in the soft x-ray region.

The limitations of the conventional ruling process have been overcome in the NPL method for making laminar x-ray gratings as described by Franks et al (122). In this method a grating is lightly ruled on an aluminium coated blank, the grating is processed to form an aluminium mask, and substrate is ion etched through the mask to produce a grating with a rectangular profile in the vitreous silica substrate. The lands and grooves of the NPL laminar gratings have exceptionally high smoothness because of the "super-polishing" effect of the ion etching process. These NPL gratings have been found to

have excellent diffractive properties throughout the soft x-ray region and even at wavelengths as short as 0.56 Å (Ag_K). Since the gratings are formed in the silica blanks they are very robust and can be cleaned and recoated without significantly altering their properties.

Laminar gratings have been made at NPL by using a grating formed in photoresist as the starting point in a process similar to that used for making an x-ray grating from a ruled master. The gratings produced from the holographic masters have been found to be virtually indistinguishable from the best NPL ruled x-ray gratings. The grooves were found to be well-defined and rectangular and the smoothness of the surfaces and the edge straightness and acuity were excellent (123, 124). Since it is generally quicker and more convenient to produce holographic gratings than mechanically ruled gratings, it is to be expected that most gratings for use in the soft x-ray region will be made by processes involving coherent photofabrication techniques. The holographic method will enable gratings to be produced which have a more consistently high performance and lower stray light levels than current ruled laminar gratings and it will also be possible to make new types of diffraction gratings.

There are several methods for producing holographic gratings with sawtooth profiles. The simplest method is that described by Sheridon (11) in which the photoresist coated blank is placed at an angle in the interference fringe system (see Fig. 73). The blaze wavelength, λ_b, is determined by the distance between the

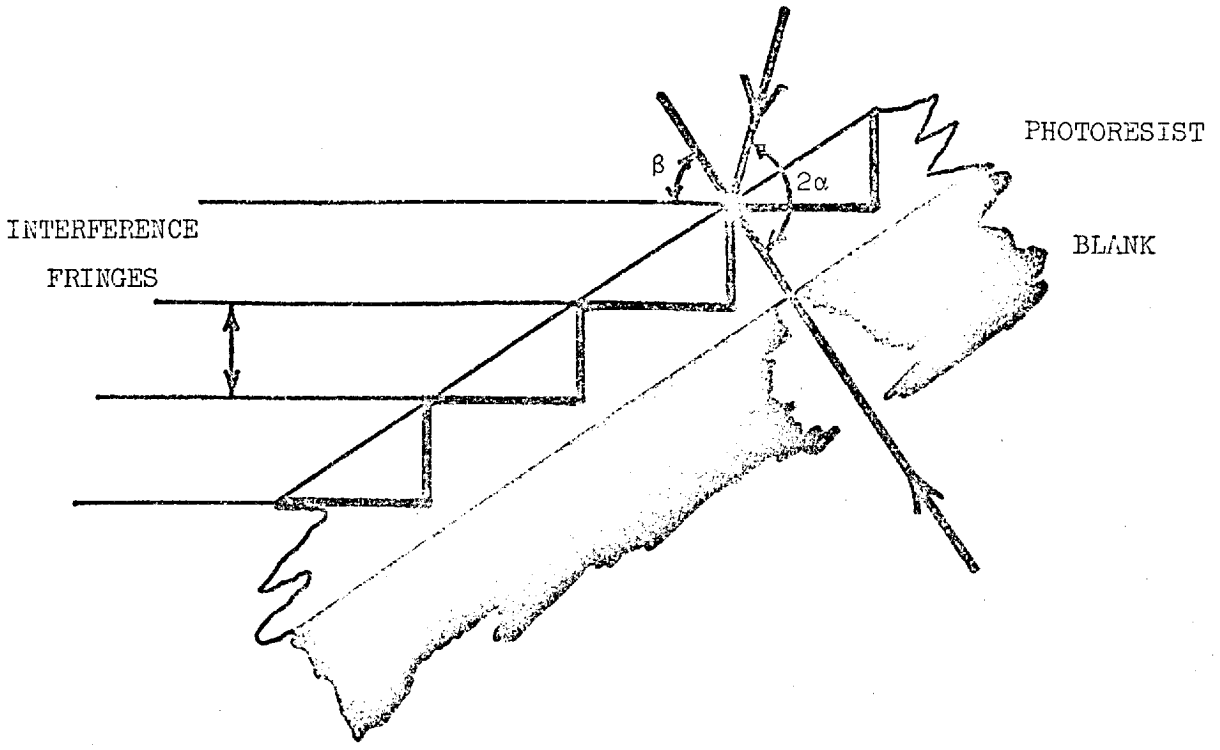

THE FORMATION OF A HOLOGRAPHIC GRATING WITH A SAWTOOTH PROFILE

FIG. 73

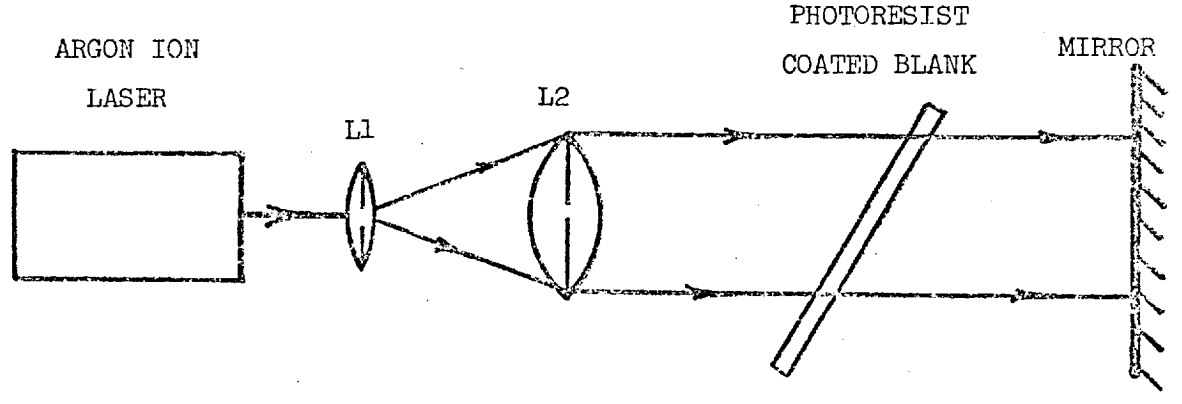

AN OPTICAL ARRANGEMENT FOR MAKING HOLOGRAPHIC GRATINGS WITH A SAWTOOTH PROFILE

FIG. 74

interference fringes

$$\lambda_b = \frac{\lambda_0'}{\sin\alpha'} = \frac{\lambda_0}{n \sin\alpha'}$$

where n is the refractive index of the photoresist. Nagata and Kishi (125) have successfully made blazed diffraction gratings with the optical system shown in Fig. 74. For this simple system the grating spacing is given by

$$d = \lambda_0/2\sin\psi$$

where ψ is the inclination of the blank to the mirror, the first order blaze wavelength is given by

$$\lambda_b = \lambda_0/n$$

and the groove depth is given by

$$h = \sqrt{1-(\lambda_b/2d)^2} \cdot \lambda_b/2$$

They found that a good blazed profile was retained up to 2000 l/mm and that it was possible to control the blaze wavelength and groove depth to a certain extent by development. Hutley (19) at NPL has also used similar methods for preparing blazed gratings for use in the UV region.

It is clear that holographic gratings prepared in this way are unsuitable for use in the soft x-ray region because the blaze angles and groove depths are too large as a result of the laser wavelengths which must be used. However, it has been discovered at NPL that it is possible to transfer the sawtooth profile from a photoresist

grating into a glass, or fused silica, substrate by using ion etching and at the same time reduce the blaze angle by a factor of up to 25. Therefore, it is now possible to make blazed gratings for use in the soft x-ray region which have the necessary small blaze angles and which have smooth well formed blaze facets. Efficiency measurements performed on one plane 600 l/mm and one plane 1200 l/mm grating of this type at NPL (123) show that below 10 Å they have comparable efficiencies to laminar gratings but at longer wavelengths somewhat higher efficiencies are obtainable. The author has also measured the efficiency of these two gratings at 45 Å and the results are shown in Fig. 75 and Fig. 76. A high blaze efficiency in the first positive order is obtained for both of these gratings. The 1200 l/mm grating was tested in both possible orientations and it can be seen that as expected the blaze shifts from the first positive to the first negative order and the peak efficiencies remain the same. Since most of the energy is diffracted in one order the other orders are weak making these gratings particularly suitable for spectroscopic purposes.

The method described above for making blazed holographic gratings has two disadvantages. Firstly, one of the interfering beams must pass through the blank which means that the blank must be optically homogeneous and optically worked on both sides. Secondly, gratings formed on concave blanks by this method will have blaze angle and frequency variations over the surface which may have to be compensated. An alternative method for making blazed holographic gratings is to use a Fourier synthesis technique as described by Rudolph and Schmahl (126, 127). By superposition of two interference fringe

GRATING IOENTIFICATION NPL IBG2 600 L/MM

I.C. REFERENCE 94 5 JUNE 1975
WAVELENGTH 45 A

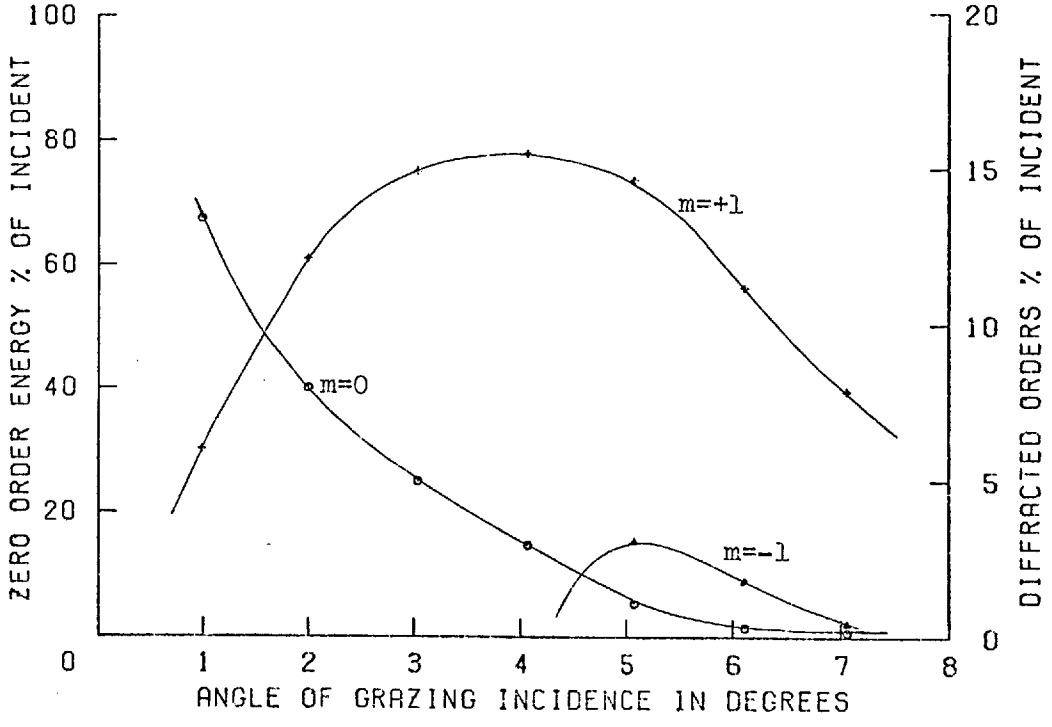

FIG. 75

GRATING IDENTIFICATION NPL 177 1200 L/MM

I.C. REFERENCE 99 18 JUNE 1975
WAVELENGTH 45 A

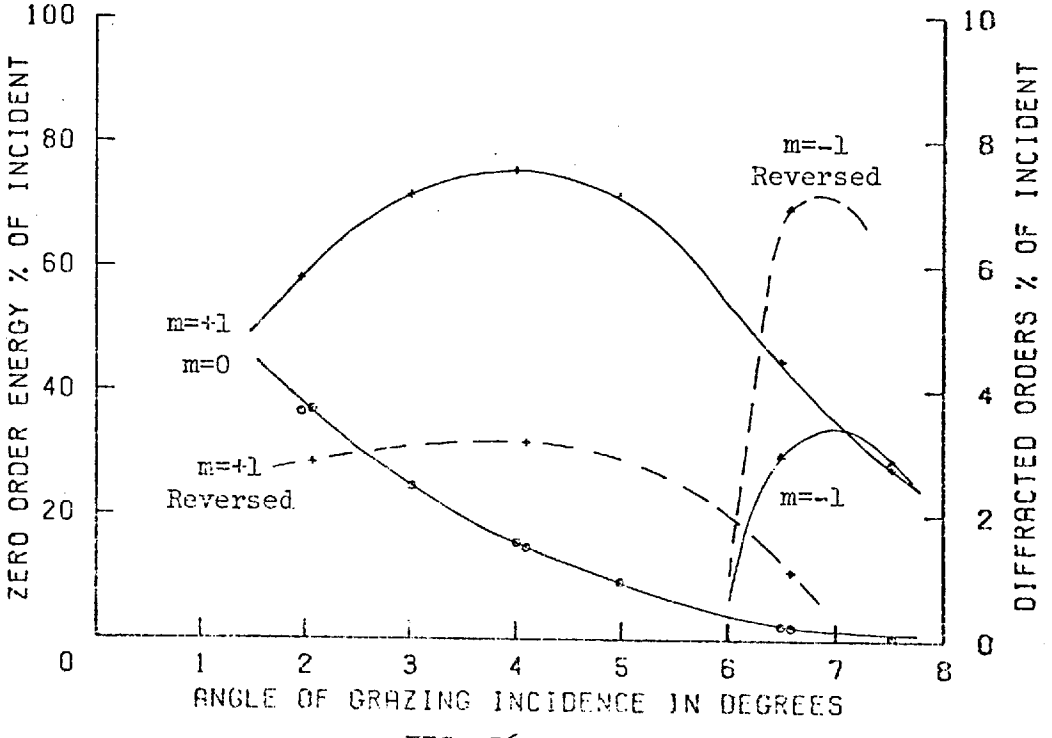

FIG. 76

systems it is possible to obtain to a good approximation a sawtooth profile. This method enables concave holographic gratings to be produced with sawtooth profiles and uniform blaze over the whole grating area. By subsequent processing of holographic gratings produced in this way it is hoped to be able to produce high quality gratings for soft x-ray spectroscopy with higher grating frequencies and efficiencies than previously obtainable.

CHAPTER 5

INSTRUMENTATION

5.1 GENERAL DESCRIPTION OF THE GRATING TEST APPARATUS

The grating test facility was originally designed by C. Green and W. Waller in 1966 to 1969. In 1967 J. M. Bennett started working on this project and in 1969 the original mechanical system was completed at A.W.R.E., Aldermaston, sponsored by UKAEA, Culham.

The original instrument as described by Bennett (30, pp 115-144) was rather elaborate and incorporated many novel features. However, it was found in practice that many of these features were definite disadvantages. The electronic displacement transducers, limit switches and remote controls have been removed because they caused electrical noise problems. It was found that the mechanical stability of the original system was insufficient for high precision measurements. Hence, the optical axis of the apparatus was lowered and a modular system was designed and constructed which allowed greatly increased precision to be achieved.

In order to obtain accurate results from high frequency gratings which usually have low efficiencies, it became evident that the sensitivity of the apparatus would have to be increased. Although it was possible to obtain measurements from the original apparatus which were of great importance to grating users in deciding whether or not a grating was suitable for a particular purpose, the original apparatus did not allow the maximum amount of useful information to be obtained. The sensitivity of the system was increased by increasing the output of the x-ray source, optimising the operating conditions of the detector and

improving the signal to noise ratio.

Initially, data reduction was performed by hand, albeit with an electronic calculator, and since for high accuracy high count rates and long integration times had to be used, the production of a complete grating calibration even at only one wavelength was a time-consuming and laborious exercise. Therefore, it was evident that in order to improve both accuracy and productivity a versatile computer data processing system was essential. The Interdata 70 computer in the Physics Department has been subsequently used for data reduction. Hence, the grating test facility is now greatly improved and we are able to perform efficiency measurements faster and with more accuracy than before.

The large vacuum chamber, which houses the tandem monochromator/spectrometer, was constructed from welded aluminium alloy sections and is 3.07 m long, 1.35m wide and 0.41 m high, with a volume of 1.7 m^3. Since the top and bottom of the chamber have areas of 4.14m^2 atmospheric pressure exerts some 40 tons when the chamber is evacuated which necessitates a highly braced structure. Although the method of construction is sufficiently rigid, the large number of welds in the chamber has caused serious vacuum problems. Since the chamber is frequently evacuated, the walls of the chamber flex causing microflaws, or porosity, in the welds to be opened, producing small leaks. With perseverance and the use of a leak-detector we managed to overcome the problems, and now we have a Micromass 2 mass-spectrometer on the system which enables us to detect and trace any leaks very quickly. The vacuum system is shown in Fig. 77

A typical mass spectrum of the residual gases in the vacuum chamber is shown in Fig. 78. The highest partial pressure is that of water vapour, then nitrogen, oxygen, CO_2, and residuals from the rotary pump

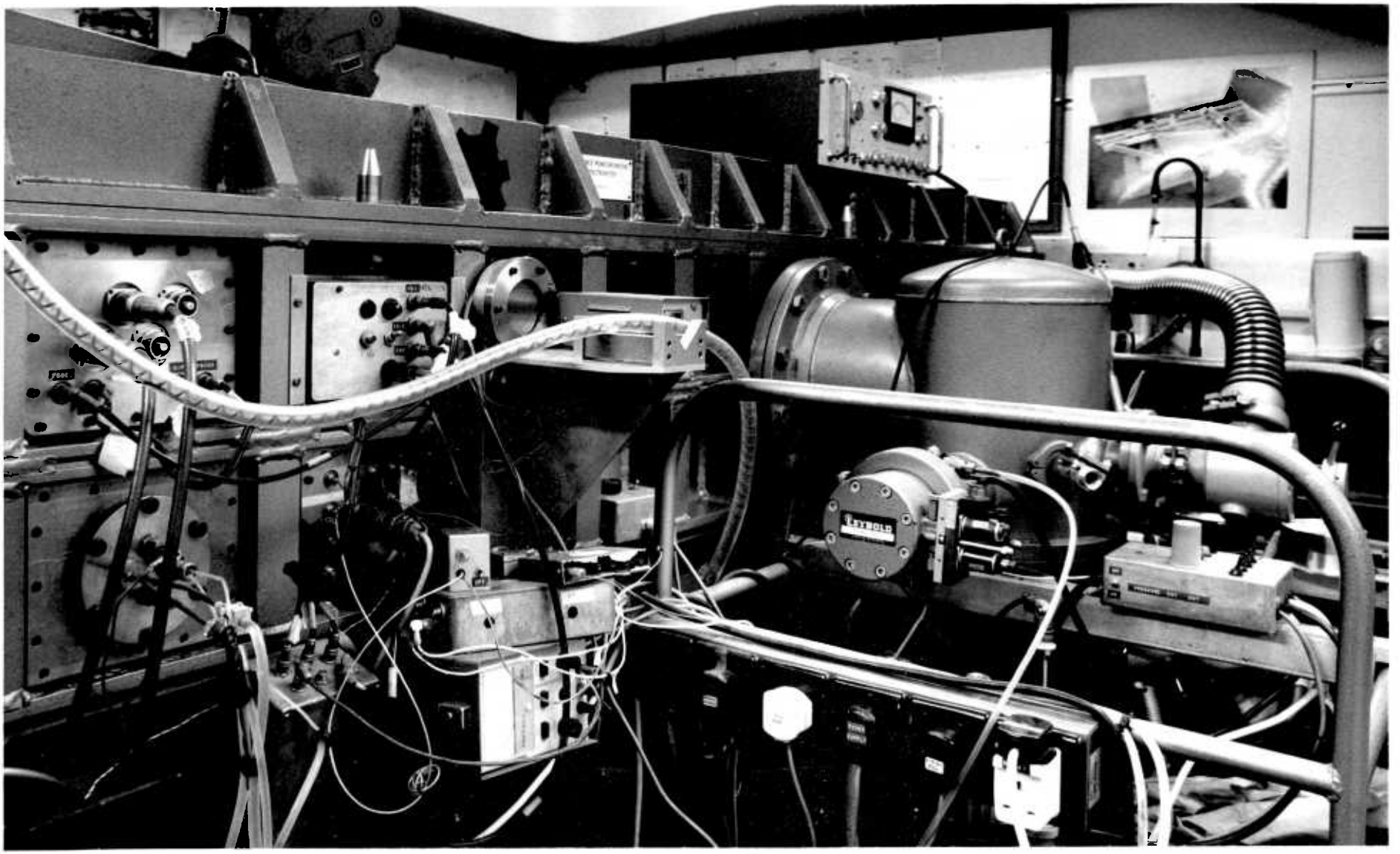

FIG. 77 THE GRATING TEST APPARATUS: VACUUM SYSTEM

A TYPICAL MASS SPECTRUM OF THE RESIDUAL GASES IN THE GRATING TEST APPARATUS VACUUM CHAMBER

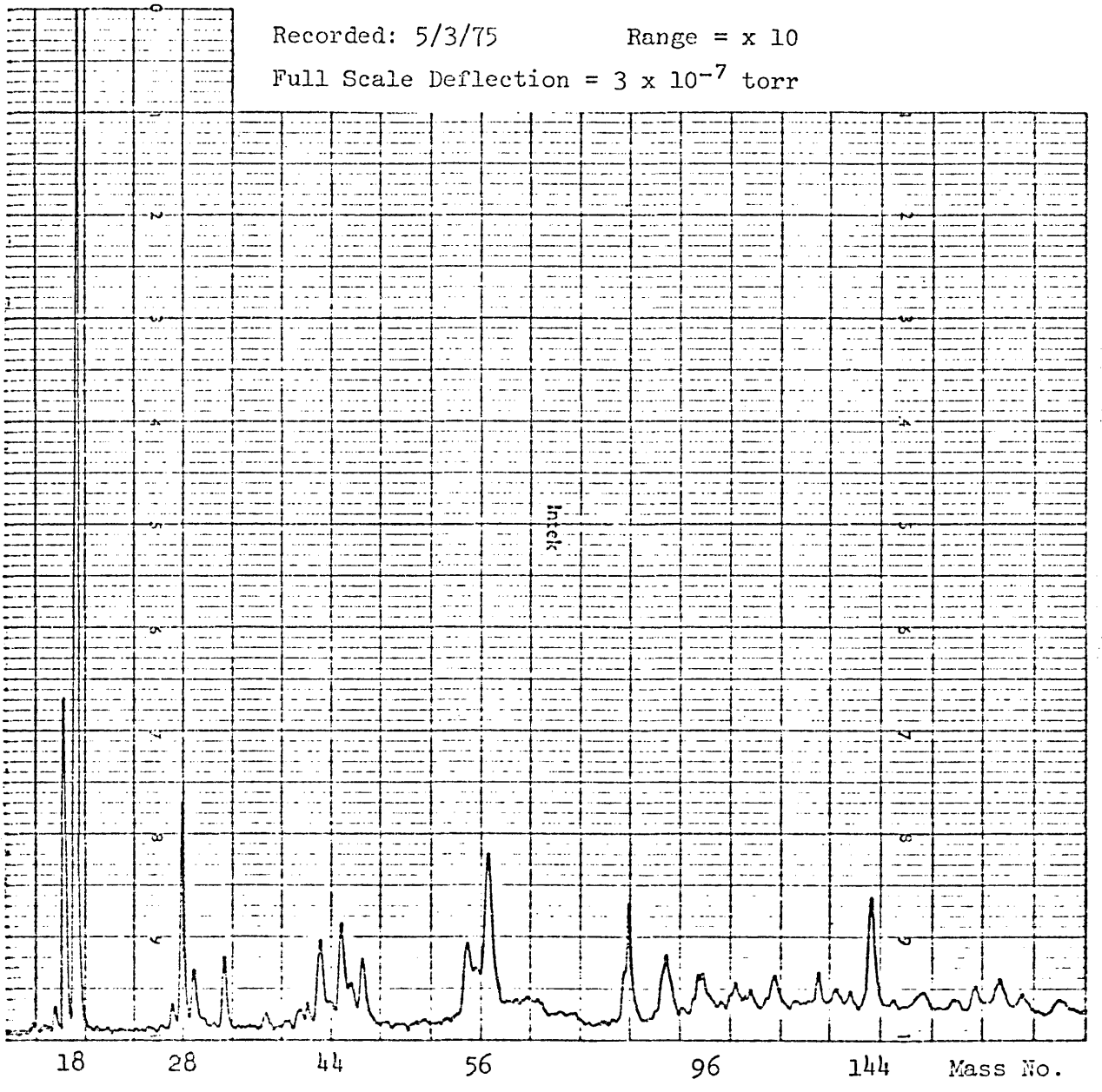

FIG. 78

oil and diffusion pump silicone oil. The most significant of these gases from the point of view of contamination in an x-ray source are water vapour and rotary pump oil. Fortunately these are pumped extremely well by liquid nitrogen cold-fingers. Hence, two cold-fingers are used in the chamber; one of which is closeable and is used to remove water vapour during the initial pump-down; the second is larger and is used to reduce the ultimate pressure when operating the system to approximately 10^{-6} torr.

The geometry of the grating test apparatus is shown in Fig. 79. The system consists basically of a long optical bench made from two ground stainless steel rods along which moves a second shorter optical bench orientated perpendicular to the first. These two optical benches define the X and Y directions along which the detector carriage is moved by two associated precision lead-screws. The displacement of the carriage is measured using counters to measure the rotation of the lead-screws. There are two further lead-screws running down the centre of the main optical bench which are normally used to move the grating carriage in the X-direction and vary the angle of the grating respectively but can also be used to move the source in the X-direction. On this framework any desired system can rapidly be built up from a number of components.

The central component is the carriage for the grating under test. This consists of a slide which rotates about a precision pivot, located centrally in a long L-shaped carriage which can be moved along the main optical bench by a lead-screw. The slide is operated by an electric motor driving a cam and enables the grating under test to be retracted from the incident x-ray beam and returned to its original position.

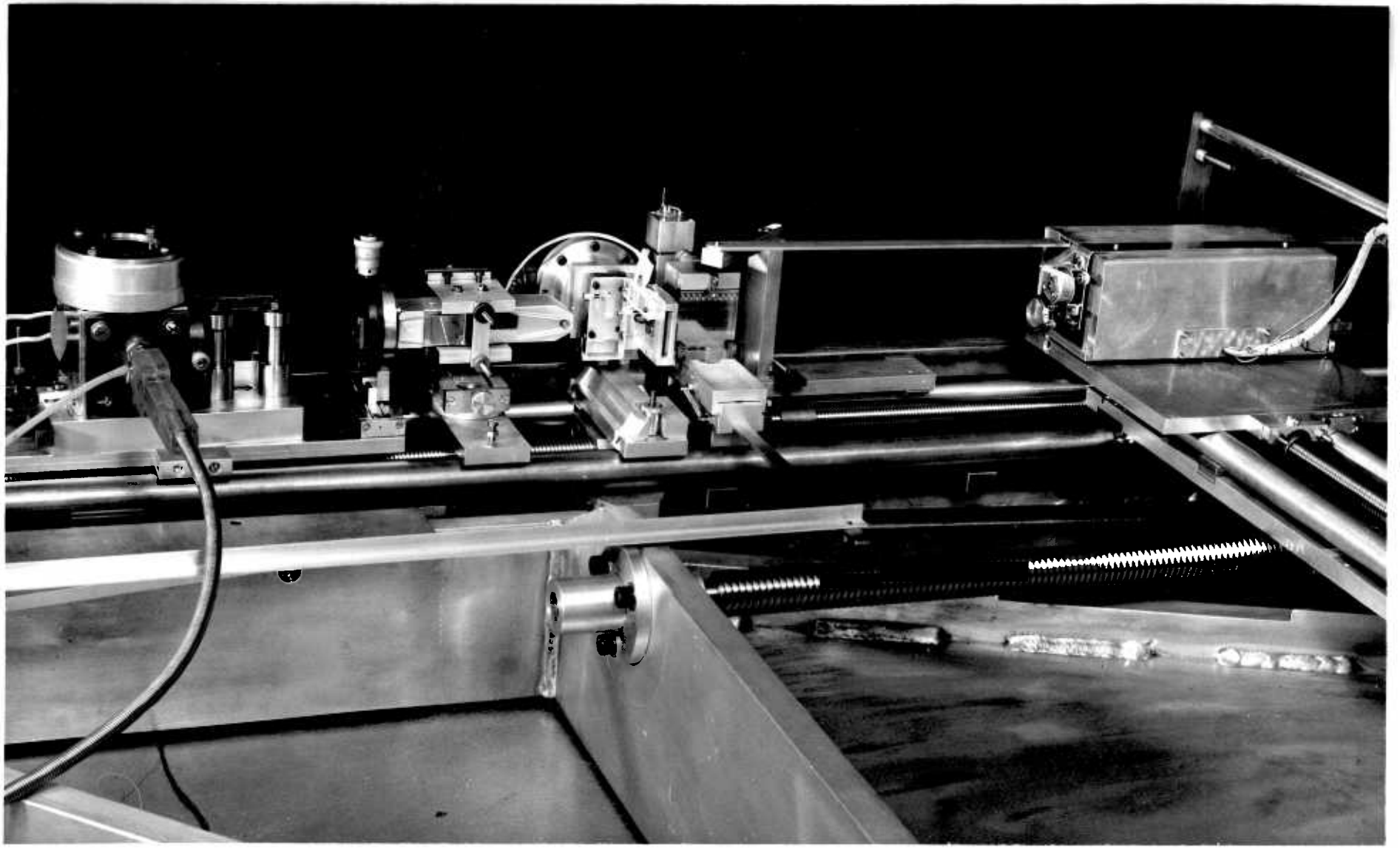

FIG. 79 THE GRATING TEST APPARATUS: OPTICAL SYSTEM

The test grating is held in a readily interchangeable holder using three point kinematic location. When concave gratings are tested shims are placed under the locating pads so that the pole of the grating is brought into the plane of the front of the grating holder. When the grating is brought into the x-ray beam the front of the grating holder contacts the centre of the pivot thus ensuring that the pole of the grating lies over the pivot point. The slide and grating holder are caused to rotate about the pivot via a mechanical linkage connected to a small carriage driven by the lead-screw at the end of the optical bench. This system enables angles to be set reproduceably to better than 0.1° over a range of 20° and also enables the source to grating distance to be varied without changing the angle of incidence and without moving the x-ray source. Should higher precision angle settings be required, it is an easy matter to increase the length of the lever arms. Similarly, should it be desired to move the source in the X-direction, the lead-screw can be coupled to the source carriage and angle variation can be achieved by moving the grating carriage in the X-direction.

The detector carriage is coupled to the grating carriage by a rod pivoted above the pole of the grating so that the detector always points towards the grating. The detector is housed in a rectangular box which is pivoted at one end and runs on ball races which allow it to rotate freely on the carriage which is driven in the Y-direction by a lead-screw. The entrance slit to the detector is located over the pivot point and behind the slit the windowless Bendix M-310 MEM photomultiplier is mounted on a pivot so that the angle of incidence of the x-rays

onto the cathode can be optimised. Also mounted in the detector housing is a preamplifier for the Bendix photomultiplier.

In order to limit the radiation falling on the grating to only the ruled area of the grating or even a smaller area of interest, a remotely-controlled motorised slit assembly is placed on a carriage close to the grating. If a concave grating is being tested the next components will be a slit and filter assembly the appropriate distance from the pole of the grating and then the x-ray source. For testing plane gratings an elliptical mirror is normally used and the mirror, slit, and source are all mounted in the correct positions on a separate carriage. When high performance gratings are being tested, the x-ray source is replaced by a monochromator section coupled to the x-ray tube.

The modular system outlined above permits great versatility coupled with high precision. For example, in order to observe the imaging properties of toroidal gratings the detector assembly was removed and a plate holder and shutter assembly were put in its place. The Y lead-screw was used in this case to move the plate across behind the shutter so that several exposures could be made on one plate. Hence, it is envisaged that the versatility of this instrument will enable it to cope with all possible developments in the field of x-ray gratings.

5.2 THE X-RAY SOURCES

Much of the early work I performed in the laboratory was directed towards producing an ideal x-ray source for use in the grating test apparatus. Unfortunately such an ideal source does not exist and a compromise solution has been found.

The $C_{K\alpha}$ 45 A source

This source is shown in Fig. 80 and is a modified version of the one which was originally employed in the grating test apparatus when it was first commissioned in 1970.

The first modification was required because it was found that the porosity of the PTFE tubing used to carry water to the anode of the x-ray source was allowing water to seep into the vacuum chamber considerably increasing the water partial pressure in the chamber. This problem was solved by encasing the PTFE in a stainless steel tube and using an insulator cast from epoxy resin to seal the tube at the anode end.

The second modification was to reduce the contamination of the target with barium emitted from the barium coated cathode. This was achieved by allowing the graphite target to reach an elevated temperature by reducing conduction heat loss. In this way the anode remains clean for long periods of time and an ample supply of photons are produced with an anode current of typically 5 mA and a voltage of 1.5 KV.

By using the monochromator section and monitoring the intensity in the 45 A monochromatised beam with a channeltron and employing the x-ray tube power supply servo system, we have an exceptionally stable

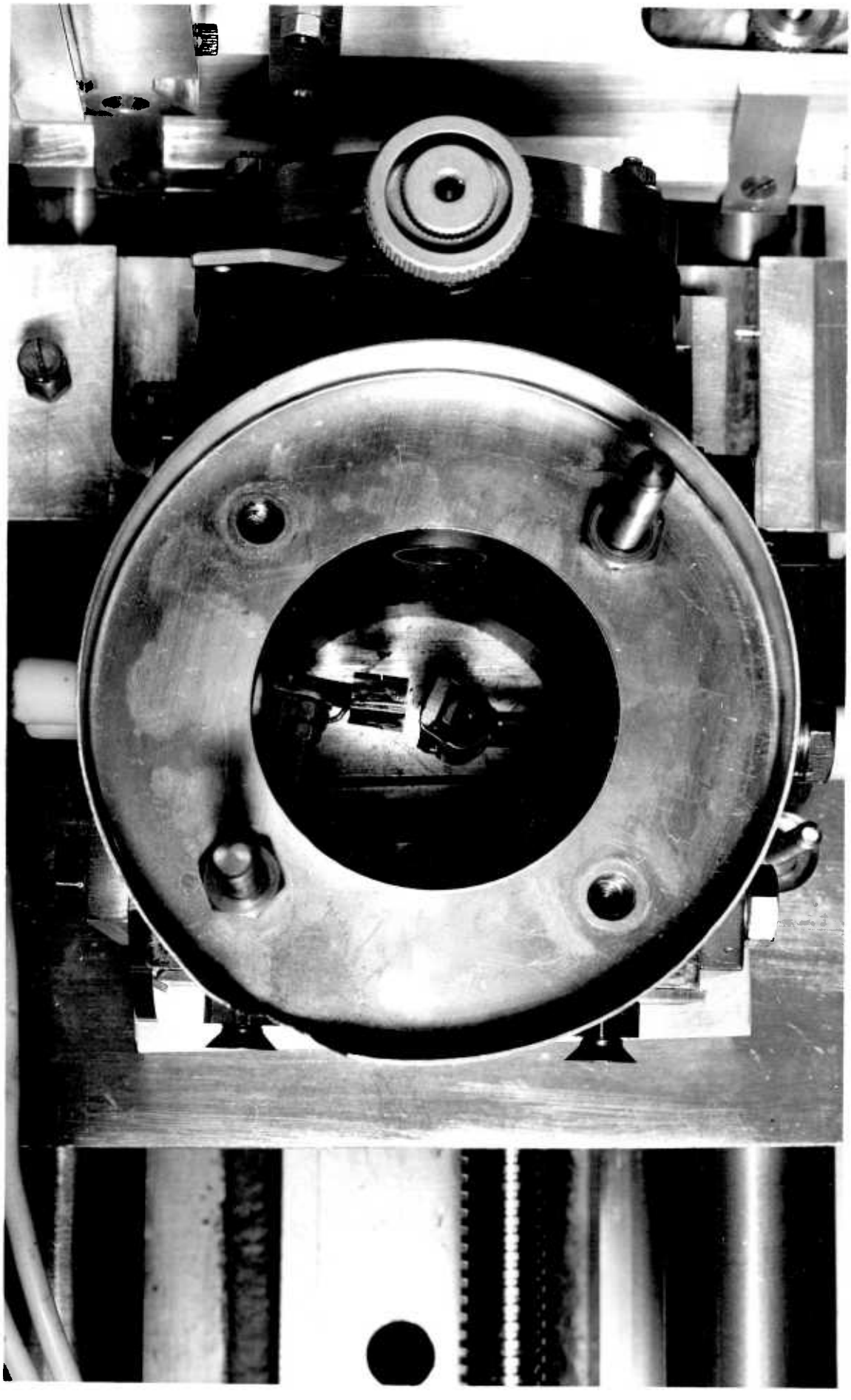

FIG. 80 THE 45 Å X-RAY SOURCE

monochromatic x-ray source which gives a constant intensity output over long periods of time, i.e. several hours. This system would seem to be ideal for a number of interesting experiments besides the current investigation of the properties of diffraction gratings.

The Henke Type Source (used mainly for 8.3 A $Al_{K\alpha}$)

This x-ray source is considerably more complex than that used for C_K radiation and can be seen from Fig. 81.

The design is based on that due to Henke and its most important features are the use of a tungsten filament in a configuration which hides it from the emitting areas of the target so that they are not contaminated with tungsten and the use of an ion pump and gate value which enables the x-ray source to be pumped to a lower pressure than that in the rest of the chamber. These features enable a high x-ray output with little contamination. The near ultra-high vacuum in this x-ray source means that anode materials which would normally become rapidly contaminated can be employed. Although this source can be used with any anode material, we have found it most useful at 8.3 A $Al_{K\alpha}$ where oxide contamination of the anode can be a serious problem.

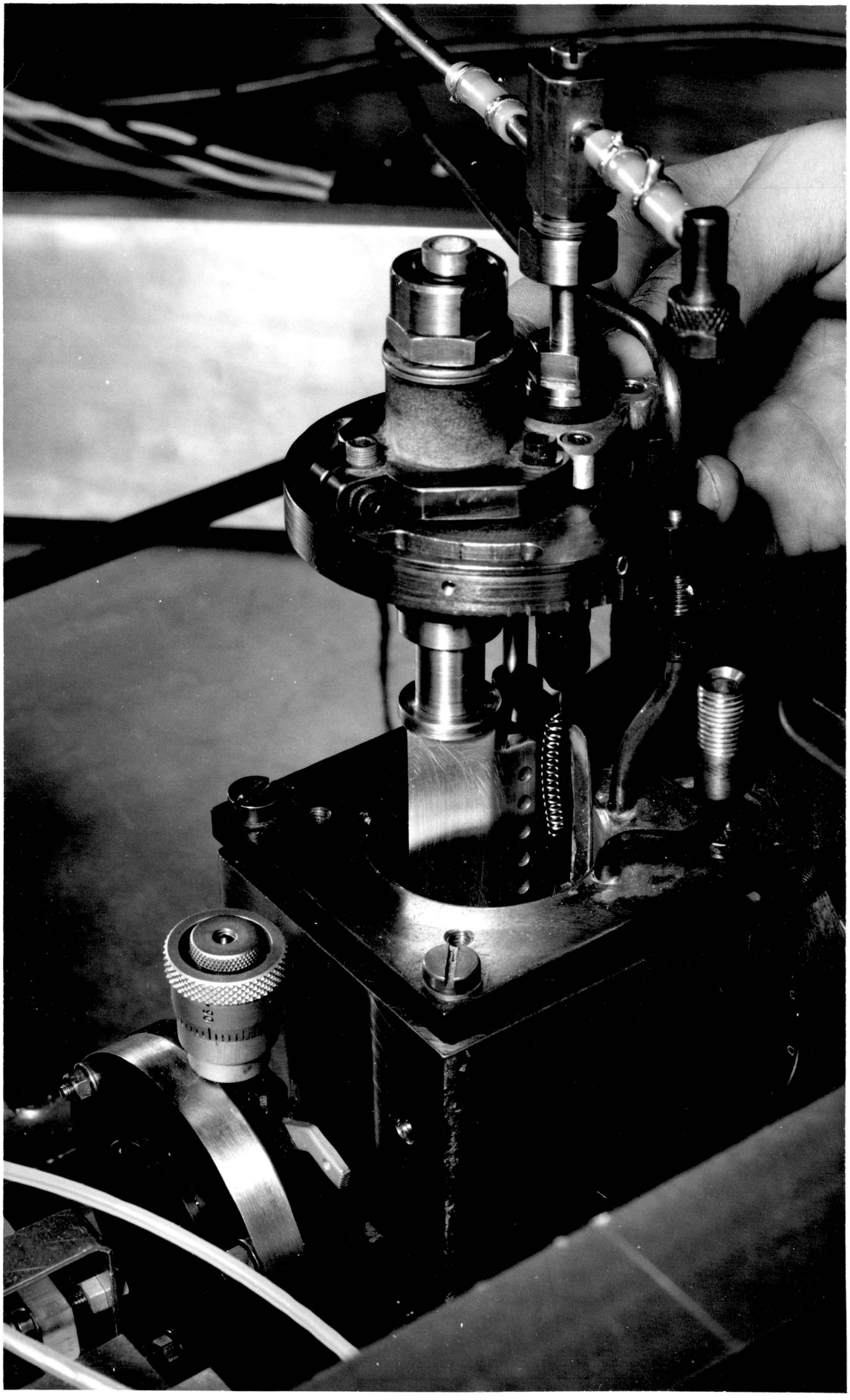

FIG. 81 THE "HENKE-TYPE" X-RAY SOURCE

5.3 EXPERIMENTAL METHOD

Alignment

The optical axis is defined by a He-Ne laser beam which is set to be in the middle of the two rails which form the main optical bench. By positioning the laser at either end of the bench alternately and moving a reversible alignment aperture along the rails the laser can be set accurately along the centre line of the bench. The pivot point for the grating holder is next set on the optical axis by adjusting the supporting pads.

With the laser in the source position the beam is sent onto a plane blank in the grating holder and is reflected off the blank to pass through the correctly positioned detector slit and onto the detector photocathode. The blank is rotated and the detector simultaneously scanned and the position of the laser spot on the photocathode is checked to be approximately half way along its length.

The laser is next placed at the detector end of the optical bench and the entrance slit is positioned the correct distance away from the pole of the grating. The slit is set on the optical axis and vertical using a plumb-line and microscope objective to project an image of the slit. The moveable slits are placed as near to the grating under test as possible and are also checked to be vertical by projecting their image using a microscope objective. The source is positioned behind the entrance slit so that the laser beam hits the centre of the anode.

This simple alignment method has been found to be completely adequate for all purposes and relies on the accurate kinematic location of the grating and metrology rather than the multiple adjustments which were provided on the original apparatus.

Plane Gratings

There are two possible modes of operation:

1. The source is placed a large distance (typically 50 cm) from the grating under test to illuminate the grating with a slightly divergent beam. A slit with a width of 400μm is placed very close to the anode in the x-ray source. When using a graphite anode a 2.2μm polypropylene filter is also mounted on the source to partially monochromate the radiation and prevent ions escaping into the chamber. When using an aluminium anode a 5μm aluminium filter is used on the source.

In this way a very uniform intensity distribution is obtainable as observed in the direct beam. The radiation distributions in the zero order and diffracted orders show the variations of reflectivity and diffraction efficiency over the surface of the grating.

This method is particularly suitable for gratings showing high diffraction efficiencies at angles of a few degrees. At small angles of incidence the small but finite divergence of the beam cannot be neglected and the variation in efficiency with angle of incidence must be considered when interpreting the intensity distribution from the grating as a map of its surface properties.

2. A convergent beam of radiation is produced by means of an elliptical collimator mirror. Originally a cylindrical mirror was used in the system to obtain separated focussed orders when testing plane gratings. The mirror system has two main advantages: Firstly, the count rates are increased and the peaks are narrower, and secondly, partial monochromatisation of reflected beam is obtained by utilising the short

wavelength cut-off of the mirror which is determined by the coating on the mirror and the angle of incidence. At 45 A there is very little difference between the reflectivity of a gold-coated or glass mirror. However, at 8.3 A there is a large difference, e.g. the reflectivity of the glass surface has become ≈1% at 2^{o} whereas that of the gold-coated surface is ≈45%. Hence, at 45 A a glass elliptical mirror should be used to enhance the short wavelength cut-off. At 8.3 A and 114 A the significantly higher reflectivity of gold-coated surfaces means that a gold-coated elliptical mirror should be used.

The elliptical mirror is set up with the source slit at one of the foci 4.6 cm from the end of the elliptical mirror; the radiation then converges to the second focus near the detector plane. The grating is positioned in the convergent beam close to the elliptical mirror, (see Fig. 82).

Spherical Gratings

When examining spherical gratings the source slit and detector slit are positioned nominally according to the Rowland circle geometry. The detector could be scanned along the Rowland circle by simultaneously incrementing the detector X and Y coordinates. Since it is the absolute efficiency of the grating which is measured it is unnecessary for the detector to be scanned along the Rowland circle. Instead the detector is simply traversed in the Y-direction to record the data which is subsequently numerically corrected for the vertical divergence of the x-ray beam.

Because very few gratings are ruled over their entire surface, when performing grating efficiency measurements it is essential to mask

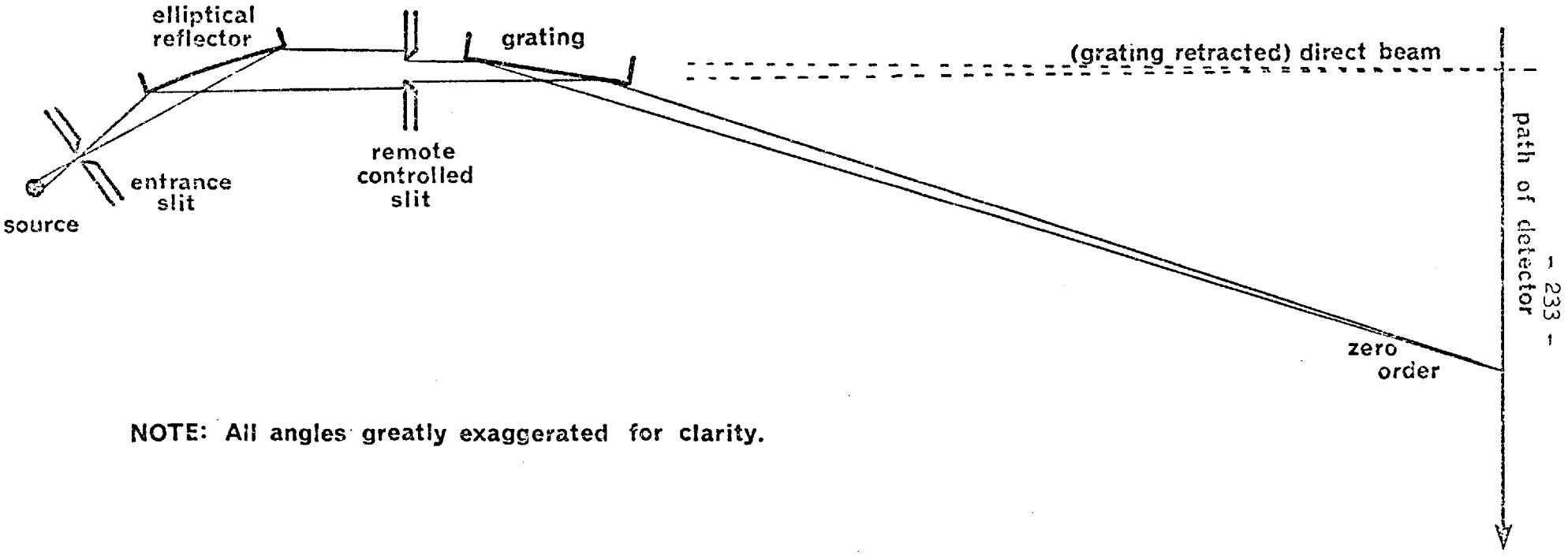

NOTE: All angles greatly exaggerated for clarity.

FIG. 82 DIAGRAM OF APPARATUS FOR TESTING PLANE GRATINGS

the unruled area of the grating otherwise the zero order efficiency would be enhanced and the diffraction efficiency reduced. In the grating test apparatus the masking is performed by the remotely-controlled motorised slit assembly adjacent to the test grating. For spherical gratings the setting of the slits is achieved by monitoring a strong focussed diffracted order and closing the slits until the count rate is reduced by 5% by each slit jaw. This method ensures that the grating is adequately masked and enables accurate data to be obtained from gratings which have uniform diffraction properties. If the gratings are not homogeneous, or have low diffraction efficiencies, it can be difficult to set the movable slits accurately, however, in such cases the highest accuracy is not required.

After the grating has been masked it has been found that it is generally advantageous to record the data under slightly defocussed conditions. This has the combined effect of reducing the peak count rates and broadening the peaks so that detector and statistical errors are reduced and it is possible to obtain information about efficiency variations over the surface of the grating.

Data Acquisition

Initial adjustments to the geometry of the system are made by manually rotating the lead-screws associated with the components of the system. All the adjustments can be performed with the chamber evacuated since the lead-screws are fitted with Wilson seals. After the mechanical adjustments have been completed and the operating conditions of the x-ray source have been optimised, data acquisition becomes a fully automated operation. A block diagram of the data

DATA ACQUISITION

SYSTEM

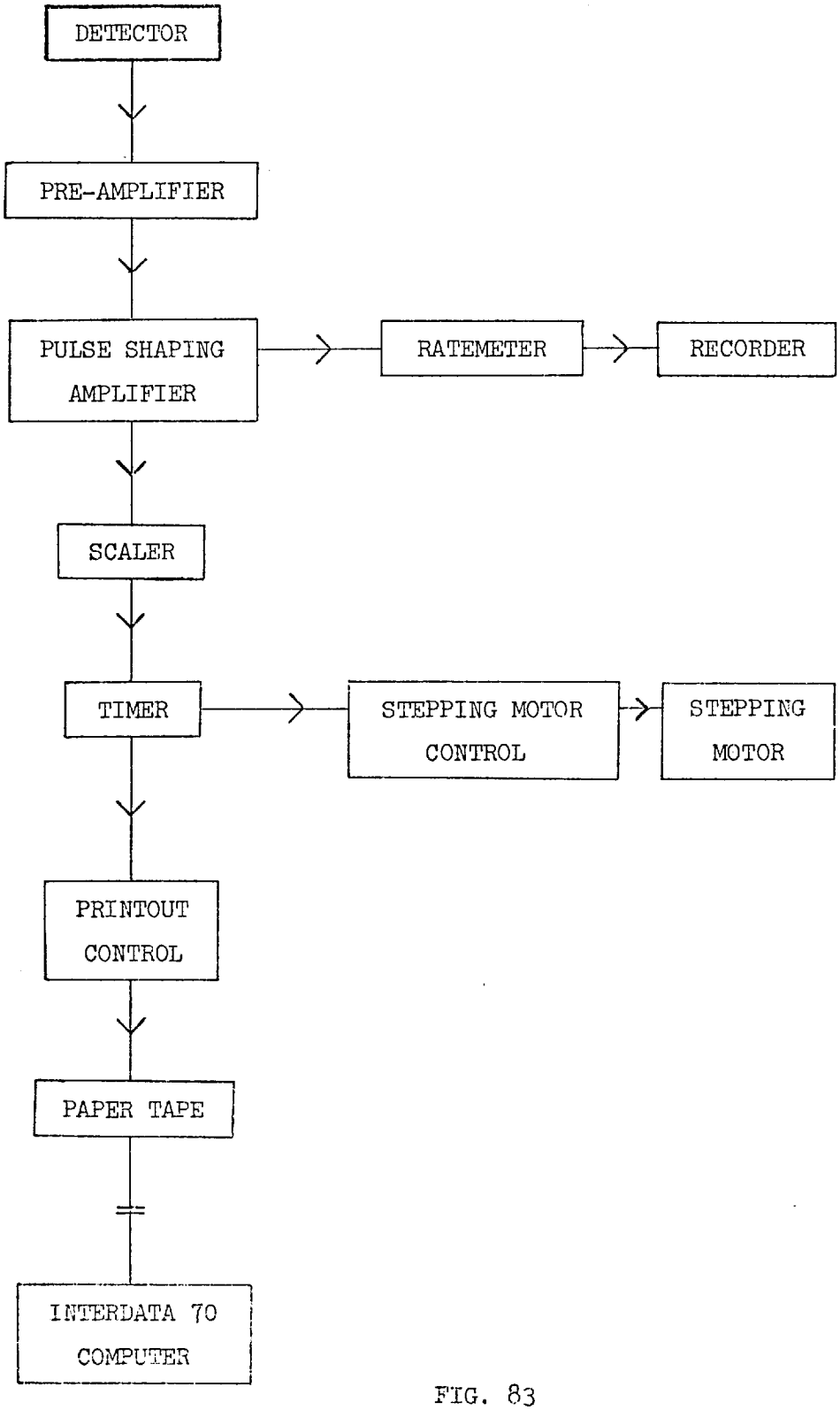

FIG. 83

acquisition system is shown in Fig. 83.

The operation of the system is controlled by a timer which determines the timer interval the detector remains in one position. The time interval may be preset over a wide range 1×10^{-2} - 9.9×10^{1}sec but it has been found that a time interval of 1.5 sec usually provides a suitable compromise between accuracy and the time taken to record a complete scan. During this time interval the number of pulses produced by the detector are counted with a 5-decade scaler. At the end of the timer interval the total number of pulses and the channel number are encoded and transferred to paper tape. The stepping motor is then incremented by the number of steps preset on the stepping motor control unit and the process is repeated to record data in the next channel. A single step on the stepping motor corresponds to a movement of the detector of 4.6μm and increments in the range 1 - 99 steps may be preset on the control unit. For a detector slit width of 120μm usually 14 steps/ increment are preset.

In order to provide a visual display of the recorded data the pulses from the detector amplifier are fed into a ratemeter which drives a linear chart recorder. The ratemeter reads from $3\text{-}3\times10^{4}$cps and also produces an audible signal which is most useful when making adjustments.

There is a second data recording system not shown on the block diagram which consists of an electronic counter connected to a printer. This system is used to totalise and print out the total number of counts in a peak and also totalise the background count rate on either side of the peak. By employing two data recording

systems reliability and versatility are considerably increased. The counter and printer are satisfactory for rapdily obtaining numerical data, however, the paper tape system allows more information to be recorded in a form suitable for subsequent data processing.

Fig. 84 shows a general view of the control console of the soft x-ray grating test facility. On the left are the pressure gauges for the vacuum system. In the centre, in front of the author, are the main control systems with the universal counter below and above are the printer and ratemeter. The paper tape punch is located on the top right-hand side of the console and on the extreme right of the picture the 100mA 10kV power supply for the x-ray source can be seen.

The most significant improvement in the grating test facility apart from the technical advances has been the development of a comprehensive computer data processing system. A block diagram of the system is shown in Fig. 85. The Interdata 70 computer in the Physics Department is used for routine data evaluation and enables the absolute efficiency results for a complete grating examination at one wavelength to be calculated in a few minutes. The large computers in Imperial College Computer Centre are used to write the data on magnetic tape, evaluate the data, and produce hardcopies on microfilm of the spectra and plot the absolute efficiency curves from the evaluated data. The data processing system has made the routine examination of x-ray gratings much easier and has also facilitated the storage and retrieval of the experimental data.

FIG. 84 THE GRATING TEST APPARATUS: CONTROL CONSOLE

COMPUTER PROCESSING

OF DATA

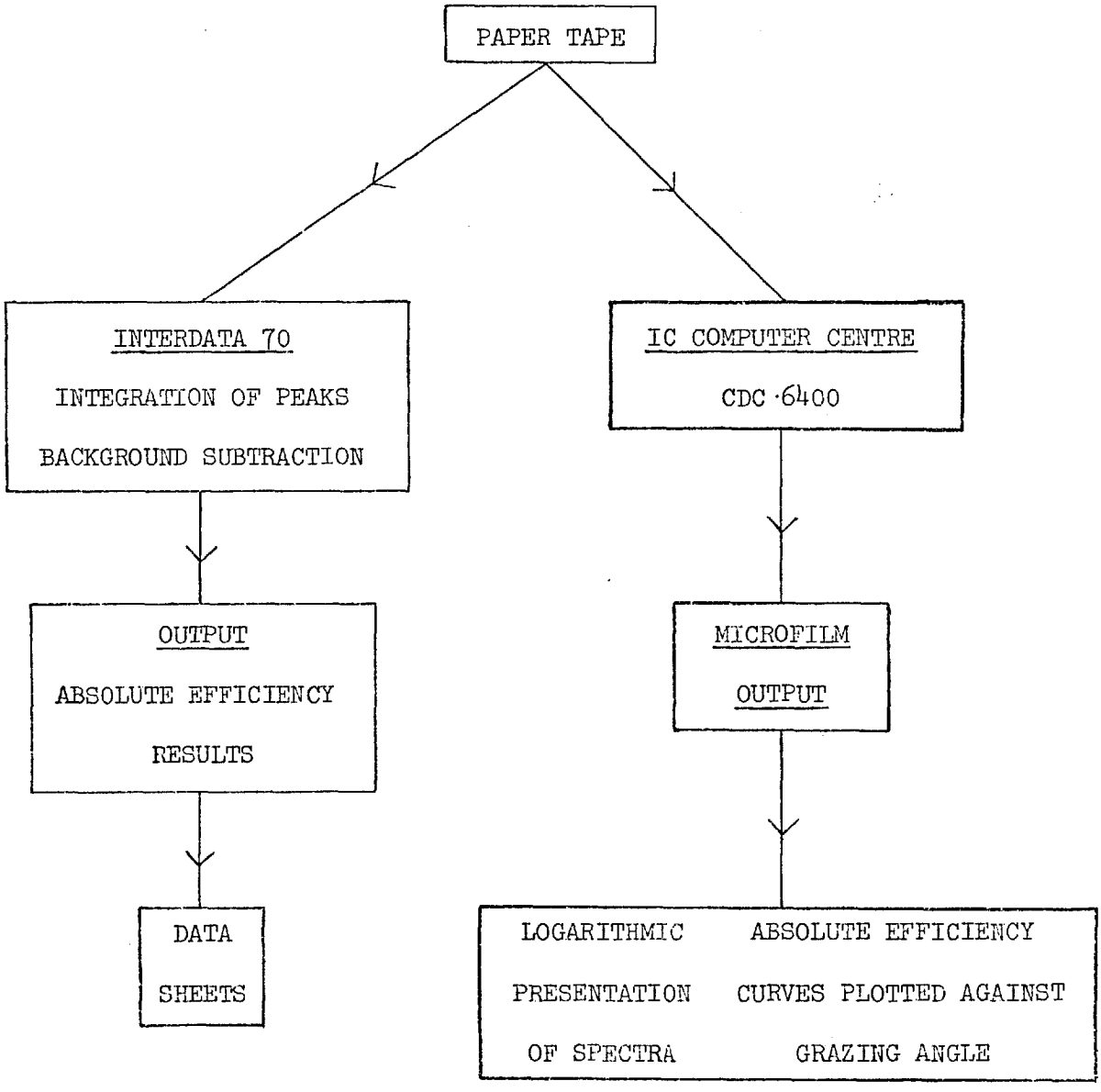

FIG. 85

Considerable effort has been expended in developing the soft x-ray grating test facility at Imperial College. The size of the vacuum chamber means that most gratings for use in the soft x-ray region can be readily accommodated and the design of the apparatus is such that high measuring accuracy can be attained. Since the optical system is of modular design it is possible to rapidly set up any required system and the apparatus can be easily used to perform other experiments in the soft x-ray region. The improvements to the apparatus and the data processing system have made it possible to perform a complete soft x-ray grating examination at one wavelength in one day. The data obtained from grating efficiency measurements in the soft x-ray region has been largely responsible for the rapid increase in the performance of soft x-ray gratings. It is to be hoped that this trend continues in the future and that grating users in the soft x-ray region will employ calibrated gratings in order to gain the best advantages from the improved diffractive properties of the new generation of x-ray diffraction gratings.

CHAPTER 6

THE REFLECTION OF SOFT X-RAYS

6.1 PREVIOUS WORK AND GENERAL CONSIDERATIONS

Since the refractive index of all materials is slightly less than unity in most of the x-ray region, x-rays incident upon a surface at small angles of grazing incidence will be totally externally reflected. Hence, it is possible to produce x-ray images by using catoptric systems. Although a knowledge of the optical constants and reflectivity of various materials is fundamental to the design of optical systems for use in the soft x-ray region, there is still a lack of accurate experimental data in this wavelength region.

The reflectivity of quartz at 45 Å was reported by Dershem and Schein (22), and Schon (23) also obtained data on a few substances at wavelengths from 3 to 13 Å. A complete list of these early works was given by Compton and Allison (24), and more recently by Henke and Dumond (25). Most of these experimenters, and also more recently Groth (26), who measured the reflectivity of glass, gold and silver films at about 9 Å, used photographic recording and obtained the intensities by photometry. A considerable gain in accuracy can be achieved by employing photon-counting techniques as used by Hendrick (27). Experimental data was obtained by Hendrick for glass, magnesium, aluminium, copper, silver and gold surfaces using aluminium-K radiation monochromatised with a 15μm aluminium foil. The samples were medium quality army-surplus optical windows from which the antireflection coatings had been dissolved and were therefore not particularly smooth. However, the samples were coated "in situ" in the reflectivity measuring apparatus which avoided exposure of the samples to air. The

apparatus used by Hendrick did not allow the sample to be withdrawn so that the direct beam could not be measured accurately in order to normalise the reflectance curves. Instead it was assumed that the reflectance approached unity at zero angle of grazing incidence. Despite these criticisms, Hendrick's data remains the most comprehensive at 8.3 Å. Wuerker (28) used Hendrick's apparatus to measure the reflectance of polished quartz, glass, gold and aluminium films at 45 Å. Measurements were performed at Stanford by Johnson (28) with beryllium -K (114 Å) x-rays on aluminium, gold and quartz reflectors using a larger system which enabled the reflector to be retracted to let the direct beam pass. In the above works filters were used to partially monochromate the incident radiation.

In Britain Stewardson and Underwood (29) measured the reflectivity of polished pyrex glass and stainless steel at a number of wavelengths in the region 5 - 16 Å, using a mica crystal monochromator. They came to the important conclusion that it is not possible to predict accurately the efficiency of x-ray reflection of a material at a given angle of incidence because real surfaces have a variable degree of roughness which is dependant upon the method of preparation and the extent of contamination. There is also an electron density gradient at the surface which affects the reflectivity and can only be determined, at present, by experiments on x-ray reflection. Thus, they concluded, we must rely on experimental and semi-empirical reflection data when designing systems using x-ray mirrors.

Bennett (30) has measured the reflectivity of a "spectrosil" blank coated with approximately 300 Å of gold at 45 Å ($C_{K\alpha}$) and 8.3 Å ($Al_{K\alpha}$). Summaries of all the results are shown in Fig. 86 and 87.

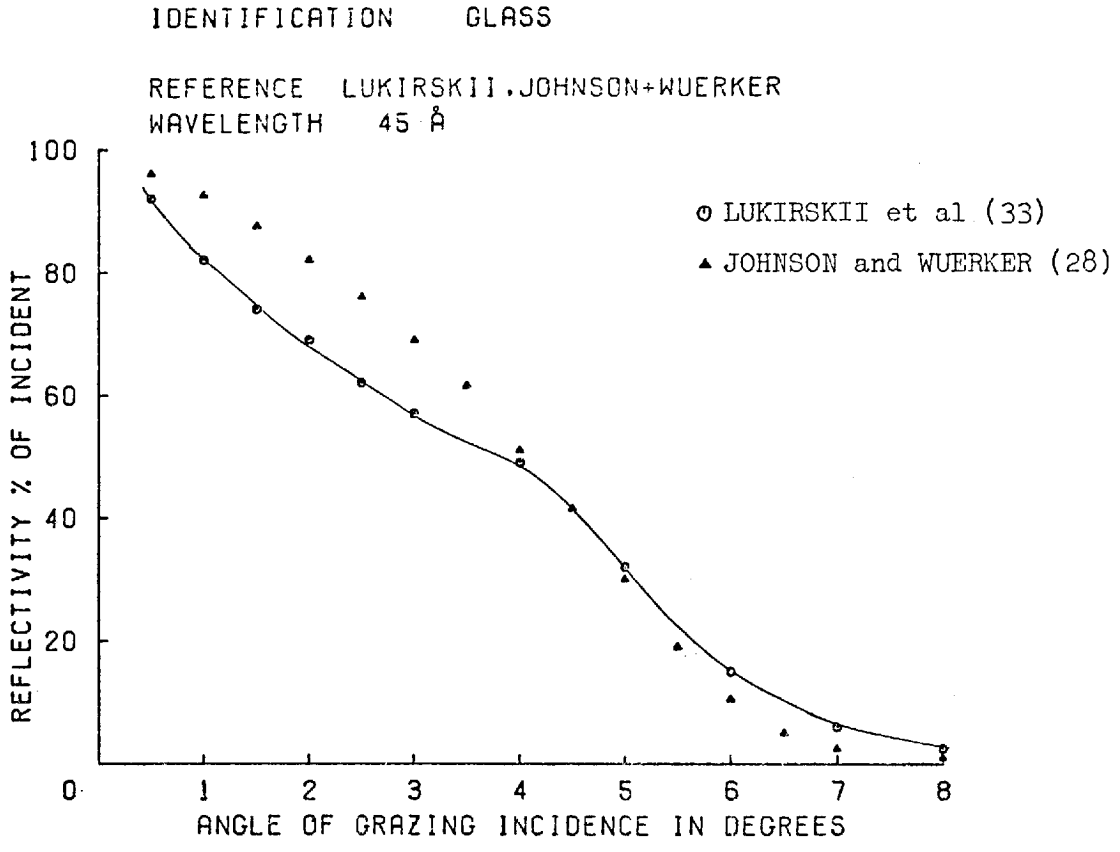
IDENTIFICATION GLASS
REFERENCE LUKIRSKII.JOHNSON+WUERKER
WAVELENGTH 45 Å
REFLECTIVITY % OF INCIDENT
ANGLE OF GRAZING INCIDENCE IN DEGREES
LUKIRSKII et al (33)
JOHNSON and WUERKER (28)

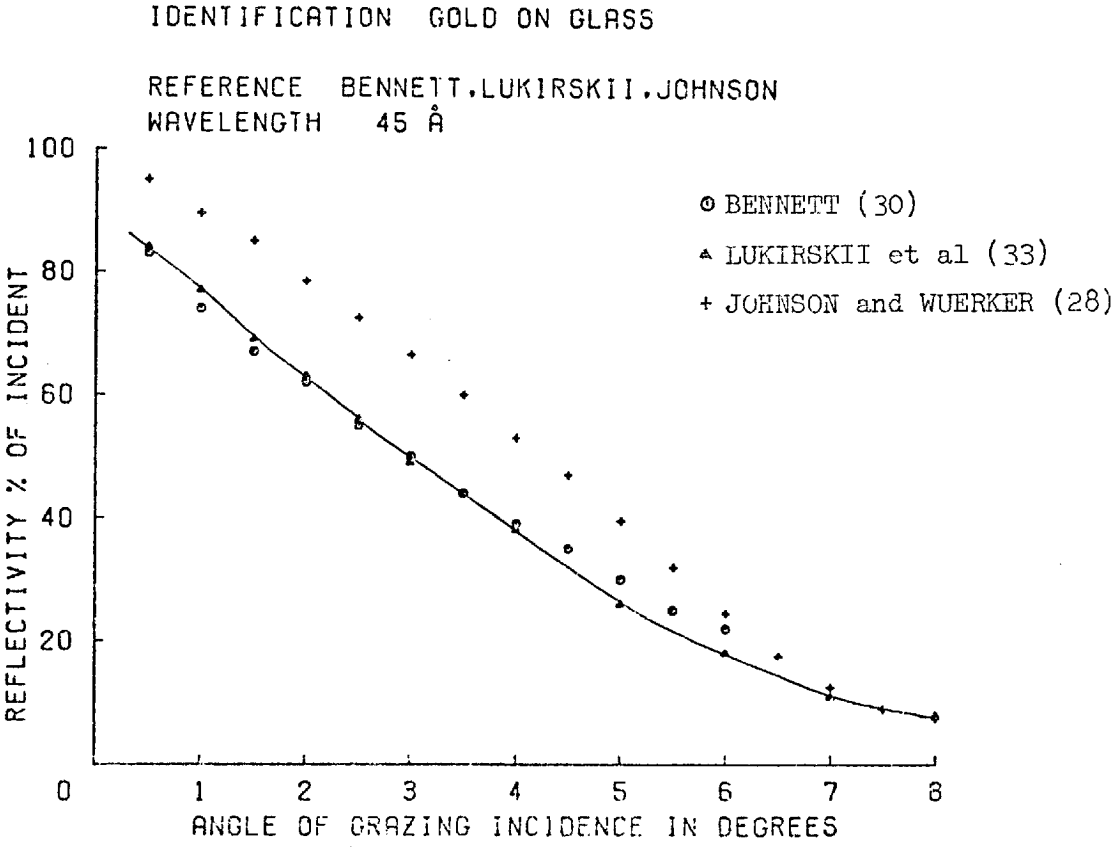
IDENTIFICATION GOLD ON GLASS
REFERENCE BENNETT.LUKIRSKII.JOHNSON
WAVELENGTH 45 Å
REFLECTIVITY % OF INCIDENT
ANGLE OF GRAZING INCIDENCE IN DEGREES
BENNETT (30)
LUKIRSKII et al (33)
JOHNSON and WUERKER (28)

FIG. 86

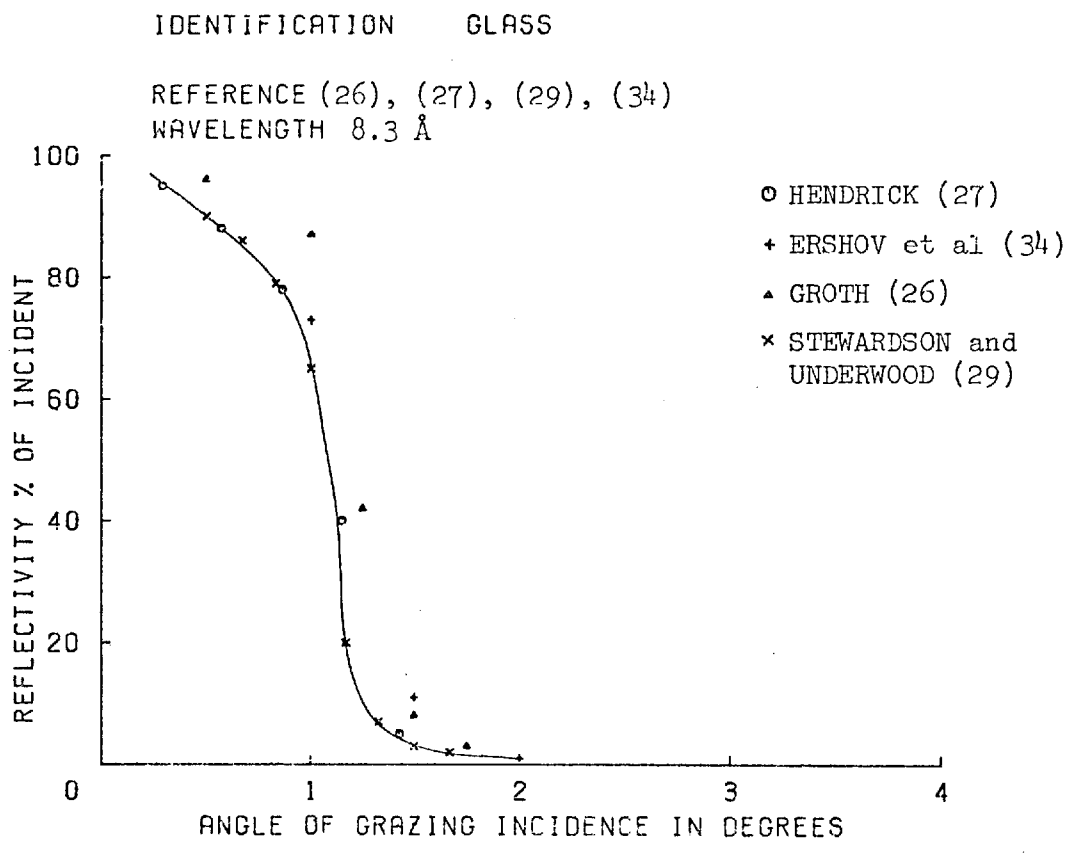
IDENTIFICATION GLASS
REFERENCE (26), (27), (29), (34)
WAVELENGTH 8.3 Å
REFLECTIVITY % OF INCIDENT
100
80
60
40
20
0
1
2
3
4
ANGLE OF GRAZING INCIDENCE IN DEGREES
HENDRICK (27)
ERSHOV et al (34)
GROTH (26)
STEWARDSON and UNDERWOOD (29)

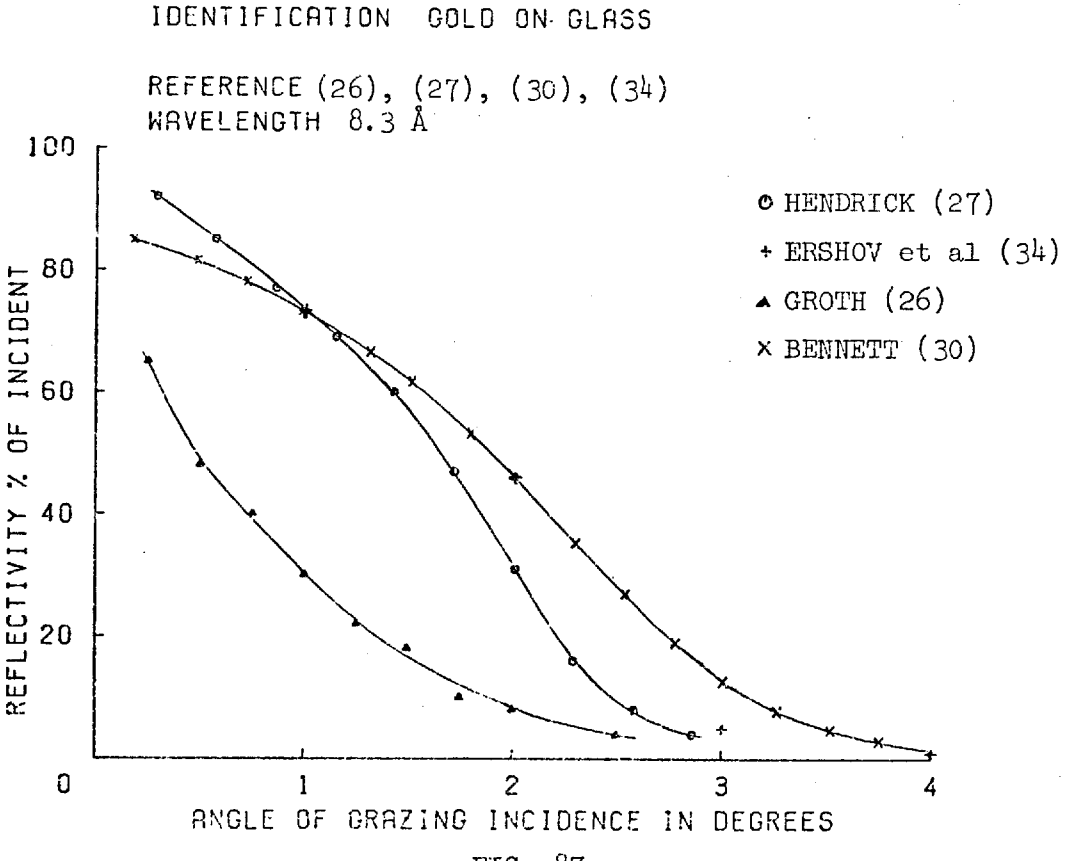
IDENTIFICATION GOLD ON GLASS
REFERENCE (26), (27), (30), (34)
WAVELENGTH 8.3 Å
REFLECTIVITY % OF INCIDENT
100
80
60
40
20
0
1
2
3
4
ANGLE OF GRAZING INCIDENCE IN DEGREES
HENDRICK (27)
ERSHOV et al (34)
GROTH (26)
BENNETT (30)

FIG. 87

The most comprehensive determination of reflection coefficients in the wavelength region 7 Å to 190 Å has been carried out by Lukirskii et al (31, 32, 33, 34). They measured the angular dependence of the reflection coefficient of Be, C, Al, Ti, V, Cr, Ni, Ag, Au, LiF, MgF_2, KCl, SrF_2, Ge, F-1 glass and polystyrene, using a grating monochromator to isolate many characteristic wavelengths. All the metal samples were prepared in the form of films nominally 1000 Å thick by vacuum deposition on glass substrates. The non-metallic films were deposited onto a conducting film of Al or Au on glass by vacuum evaporation and the polythene film was deposited from solution onto glass. Since the films were prepared in a separate coating plant and then transferred to the test apparatus, it seems likely that the samples may have been oxidised or have other surface contamination. Hence the measured reflection curves may not be truly characteristic of the elements but they can be taken to be characteristic of vacuum-deposited films. Since diffraction gratings are normally exposed to air before use and are coated with vacuum-deposited metallic films, a comparison of the results given by Lukirskii et al would be useful to decide which materials are suitable for coating diffraction gratings in order to enhance the reflectivity. When deciding upon the most suitable coating material for a diffraction grating, the wavelength region in which the grating is to be used must be born in mind since the presence of an absorption edge may cause a substantial reduction in the reflectivity of the coating material. It is also essential that the material forms a completely stable coating so that the properties of the grating do not change with time.

Examination of Table 3 shows that at 113 Å all the metallic coatings except Al have usefully high reflectivities. At 67 Å the reflectivity of Au has decreased significantly compared to the other coatings and continues to decrease at 45 Å and 31 Å. The reflectivity of Al recovers to be equal to the reflectivity of Ti and Cr at 31 Å and the reflectivity of Au again reaches a useful value at 23.6 Å. This table shows clearly that from the point of reflectivity in the wavelength region 30 - 100 Å, gold is not necessarily the optimum coating material.

Gold-coated diffraction gratings are normally used in the soft x-ray region because gold is extremely stable and has a high atomic number which means that the critical angle of grazing incidence is large.

Since from the elementary theory of metals

$$\sin \theta_c = \lambda \left(\frac{e^2}{mc^2} \frac{N}{\pi} \right)^{1/2}$$

where N = atomic number and the other symbols have their usual meaning.

Although gold coatings are easy to produce by vacuum evaporation, it is well known that thin gold films made in this way on glass substrate tend to form an island structure and not a continuous homogeneous film. The conglomerate structure will absorb the incident radiation more than a homogeneous film and will also scatter the radiation incoherently. The effects of absorption and incoherent scattering are to reduce the maximum reflectivity and the slope of the reflectivity curve against angle. This effect can be seen in the measured reflectivity curves.

TABLE 3

COMPARISON OF THE REFLECTIVITIES % OF SOME METALLIC COATINGS

(data from Lukirskii et al)

	α	1^0	2^0	3^0	4^0	6^0
23.6 Å	Al	88	73	51	7	
	Ti	74	44	20	5	
	Cr	81	56	18	1	
	Ag	70	38	21	10	
	Au	70	55	40	25	
31.4 Å	Al	90	78	62	42	
	Ti	89	77	58	21	
	Cr	89	77	66	50	
	Ag	65	36	17	6	
	Au	73	58	43	30	
45 Å	Al	91	78	68	53	25
	Ti	95	87	78	68	27
	Cr	93	82	72	62	40
	Ag	93	80	69	57	30
	Au	77	63	49	38	18

	α	2^0	4^0	6^0	8^0
67 Å	Al	78	68	38	22
	Ti	92	86	68	48
	Cr	91	83	62	45
	Ag	89	84	68	53
	Au	83	74	49	30
113 Å	Al	72	61	36	25
	Ti	92	88	75	67
	Cr	91	86	71	62
	Ag	96	93	83	77
	Au	90	86	75	69

Platinum is also used as a coating material for gratings since it has a high atomic number and forms stable films. It is not known whether any electron microscope studies of the structure of vacuum-deposited platinum films have been carried out. However, it is to be imagined that platinum films will not form such pronounced island structures as gold. Hence, platinum is most probably a more suitable coating material than gold in many cases. However, it is known that platinum films have high internal stresses the effects of which will only be known when a complete study has been carried out. Since the preparation of high-quality platinum films requires a high power electron beam evaporator, we have not yet been able to obtain any platinum-coated samples for examination. However, at both wavelengths the reflectivity of platinum films may be significantly higher than that of corresponding gold films.

It has been reported that chromium forms homogeneous smooth films when deposited on glass by vacuum evaporation, even for films only 20 Å thick. Since chromium also forms stable films and has a high reflectivity for typical angles of incidence used in the soft x-ray region at wavelengths above 25 Å, it would seem that chromium could be used advantageously as a coating material in place of gold. In order to verify this conclusion, a grating was made with one half of the grating coated with 300 Å gold and the other half coated with 100 Å chromium. Only in this way could it be guaranteed that the differences observed arise only from differences in the properties of the coating materials and not variations in the groove profile

which could easily occur if two separate but similar gratings were coated with different materials in an attempt to make a comparison.

Fig. 88 shows the efficiency curves obtained at 45 Å from grating G5.12.1.75.294 in its original form coated with 300 Å gold and Fig. 89 shows the results obtained after the gold coated grating had been half coated with 100 Å chromium. It can be seen that the efficiency of the chromium coated grating is significantly higher than that of the gold coated grating and the peak efficiency measured in the first positive order has increased from 6.8% to 8.9%.

From this one example it is not possible to state categorically that when a grating is coated with chromium it is more efficient at 45 Å than when it is coated with gold. It is conceivable that in this case the improvement in efficiency is partially due to the improved reflectivity of the chromium grating and partially due to some change in the profile of the grating. However, this result is indicative of the gains which can be achieved by optimising the grating coating material. It is evident that further work in this field would be of value.

It should be noted that in the vicinity of the K-edge of oxygen the reflectivity of chromium films drops rapidly due to the oxide film which forms on the chromium. Between 17 - 21 Å there are also the Cr L_I, L_{II}, and L_{III} absorption edges which cause changes in the reflectivity. However, in the wavelength region 25 - 60 Å the reflectivity of chromium films is significantly higher than that of gold and the films are much more durable. It can be imagined that for some experiments the short wavelength cut-off of a chromium

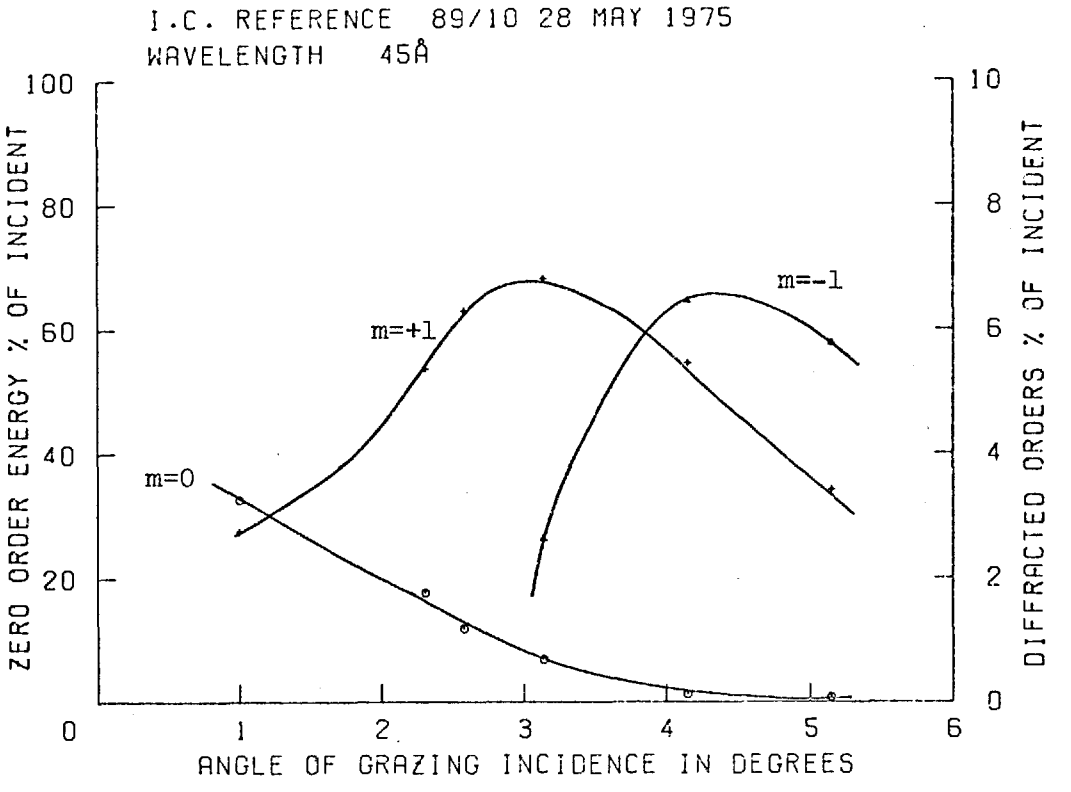
GRATING IDENTIFICATION G5.12.1.75.294 AU
I.C. REFERENCE 89/10 28 MAY 1975
WAVELENGTH 45Å
ZERO ORDER ENERGY % OF INCIDENT
DIFFRACTED ORDERS % OF INCIDENT
m=+1
m=-1
m=0
ANGLE OF GRAZING INCIDENCE IN DEGREES

FIG. 88

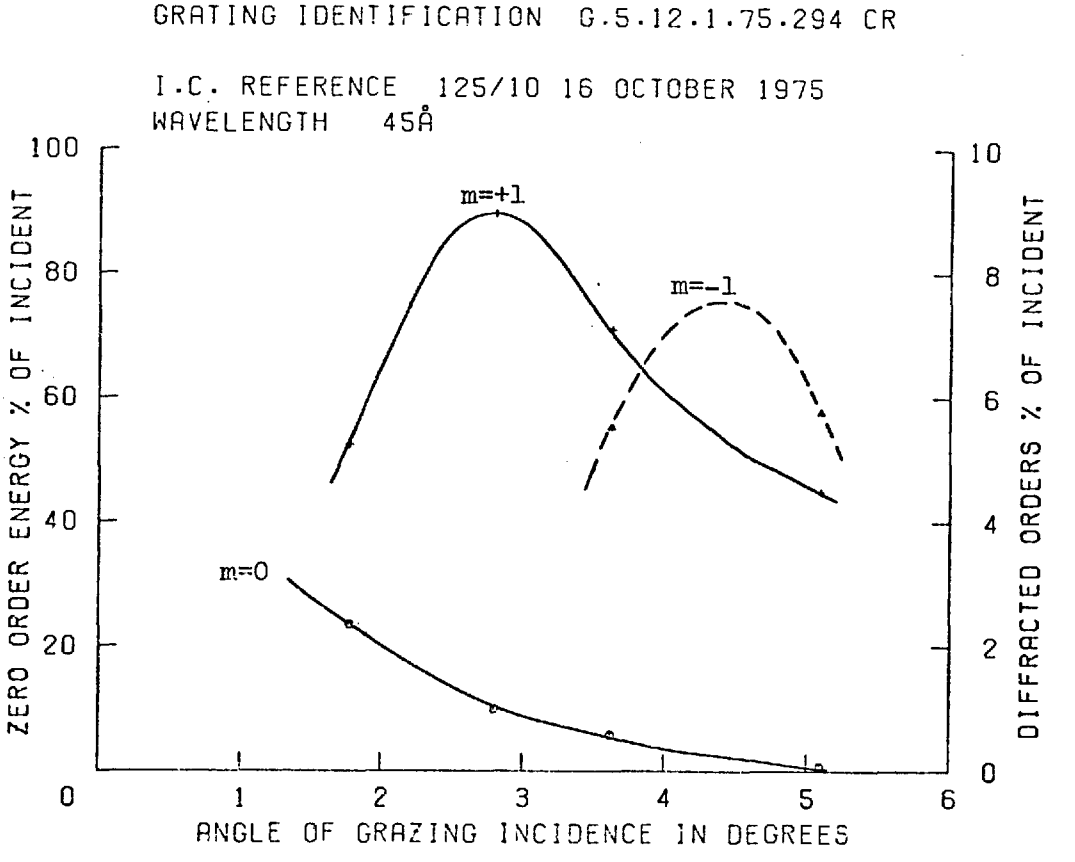
GRATING IDENTIFICATION G.5.12.1.75.294 CR
I.C. REFERENCE 125/10 16 OCTOBER 1975
WAVELENGTH 45Å
ZERO ORDER ENERGY % OF INCIDENT
DIFFRACTED ORDERS % OF INCIDENT
m=+1
m=-1
m=0
ANGLE OF GRAZING INCIDENCE IN DEGREES

FIG. 89

mirror may be exploited to attenuate unwanted shorter wavelengths or to remove overlapping orders in the case of diffraction gratings.

Normally, it is required that a diffraction grating should have a uniform efficiency over as wide a wavelength range as possible. In a spectrograph the minimum wavelength to be recorded determines the maximum angle of grazing incidence which may be used. Hence, if it is desired to record spectra over the range from 10 - 100 Å, it would be necessary to use a gold or platinum coated grating at an angle of 2^{o}. If the wavelength range to be recorded was reduced, it would be possible to considerably improve the efficiency of the system by employing a grating specifically designed for the application. The grating would have an optimised profile and coating material for the wavelength region of use and the results could be guaranteed by calibrating the efficiency of the grating.

6.2 THEORY

It has been shown that an approximate solution of the boundary value problem for the reflection of plane waves at an absorbing medium is adequate to obtain good fits between experimental x-ray reflection curves and theoretical curves obtained from the Fresnel equations and refractive indices derived from the quantum-mechanical dispersion theory in the wavelength region below 10 Å. In the wavelength region above 50 Å, the approximate solutions can introduce significant errors and a more exact approach is required.

The methods used to derive Fresnel's equations are well known and can be found in the standard textbooks on electromagnetic theory and the theory of optics (38, 78).

Most subsequent authors have followed the method described by Dershem and Schein (22) which enables the exact Fresnel equations to be simplified by treating the unit decrements to the complex refractive index, δ and β, as small quantities so that their squares and products can be neglected, and since the grazing angle is also small, $\sin\theta$ may be set equal to θ. The resulting Fresnel equations have two forms depending on whether the electric vector lies in the plane of incidence or perpendicular to it. However, for small glancing angles there is negligible difference between the intensities of the two polarisations. Hence, it is usual to take the ratio of the intensity of the incident beam polarised with the electric vector perpendicular to the plane of incidence to that of the reflected beam as being the reflectivity, R, of the surface.

Following Compton and Allison (24):

$$R = \frac{I}{I_0} = \frac{(\theta - a_0)^2 + b_0^2}{(\theta + a_0)^2 + b_0^2} \tag{1}$$

where

$$\begin{aligned} a_0^2 &= \frac{1}{2}\left[\theta^2 - 2\delta + \sqrt{(\theta^2 - 2\delta)^2 + 4\beta^2}\right] \\ b_0^2 &= \frac{1}{2}\left[2\delta - \theta^2 + \sqrt{(\theta^2 - 2\delta)^2 + 4\beta^2}\right] = \left(\frac{\beta}{a_0}\right)^2 \end{aligned} \tag{2}$$

$$n = 1 - \delta - i\beta \tag{3}$$

The unit decrements of the complex refractive index are related to the linear absorption coefficient by:

$$\mu_1 = \frac{4\pi\beta}{\lambda} \tag{4}$$

where λ is the wavelength of the incident radiation.

β is also known as the absorption index and the ratio $Y = \beta/\delta$ as the absorption ratio.

The critical angle of grazing incidence is given by:

$$\cos \theta_c = n = 1 - \delta \tag{5}$$

which for small values of θ may be written:

$$\theta_c = (2\delta)^{\frac{1}{2}} \tag{6}$$

The Fresnel equation given above may be rewritten in terms of the normalised angle of grazing incidence, $X = \theta/\theta_c$, and the absorption ratio Y by substituting for a_0 and b_0 in equation (1), multiplying the numerator and denominator by $2/\theta_c$ and using relation (6). The resulting equation was used to produce figure 90 which shows reflectivity, R, against normalised angle, X, plotted on logarithmic scales for several values of the absorption ratio, Y. As pointed out by Hendrick (27), this form of graphical representation enables experimental reflectivity data to be fitted easily to the theoretical curves.

The following equation was used to produce figure 90

$$R = \frac{\left\{\sqrt{2}X-\left|\{(X^2-1)^2+Y^2\}^{\frac{1}{2}}+(X^2-1)\right|^{\frac{1}{2}}\right\}^2+\{(X^2-1)^2+Y^2\}^{\frac{1}{2}}-(X^2-1)}{\left\{\sqrt{2}X+\left|\{(X^2-1)^2+Y^2\}^{\frac{1}{2}}+(X^2-1)\right|^{\frac{1}{2}}\right\}^2+\{(Y^2-1)^2+Y^2\}^{\frac{1}{2}}-(X^2-1)}$$

and is the same as the equations given in references (27) and (29).

It has been shown by Henke (36) that the approximate theory can be used safely for wavelengths below 10 Å. However, at longer wavelengths it can no longer be assumed that the reflectivity is the same for both states of polarisation. The angle of refraction is different for both polarisations and the linear x-ray absorption coefficient μ_1 is a function of the angle of grazing incidence. By using exact solutions to Fresnel's equations instead of the usual approximate solutions, Henke has shown that satisfactory fits to the experimental reflectivity data can be obtained in the longer wavelength region.

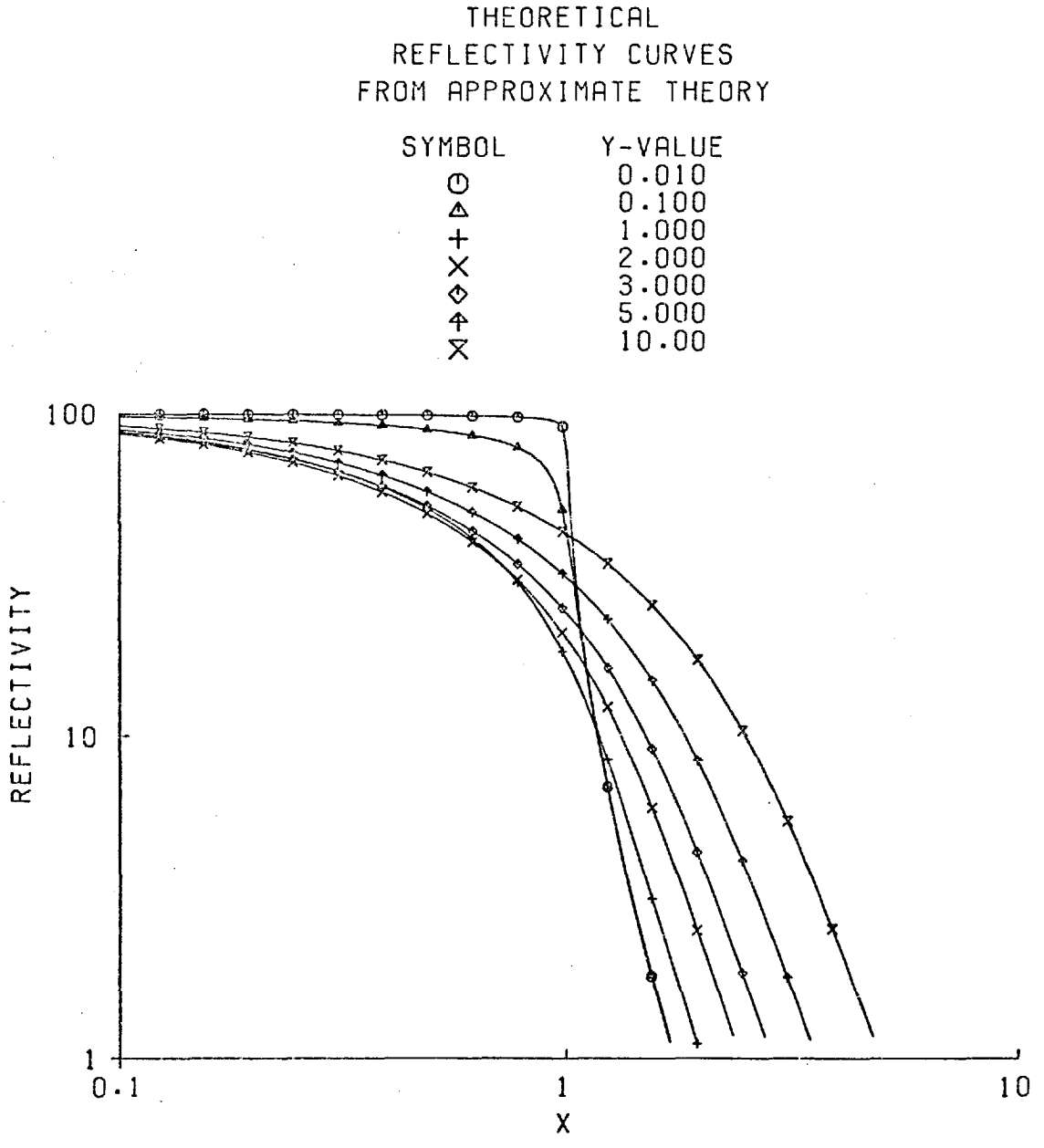
THEORETICAL
REFLECTIVITY CURVES
FROM APPROXIMATE THEORY
SYMBOL
Y-VALUE
0.010
0.100
1.000
2.000
3.000
5.000
10.00
100
10
1
REFLECTIVITY
0.1
1
10
X

FIG. 90

Henke (36) has given a most useful summary of results from the general solution of the boundary value problem of a plane electromagnetic wave at an absorbing interface. These results have been used in this work to calculate the optical constants of gold and chromium films from the experimental reflectivity curves. The results used are quoted here without proof since the original derivations are rather lengthy and can be found by the interested reader in references (37), (38).

Since we are concerned with the interaction of x-rays incident on a medium in vacuum, the material constants may be completely specified by the real and imaginary parts of a complex dielectric constant, K. The dielectric constant will incorporate permittivity ε, permeability, μ, conductivity, σ, of the material and also frequency, ν, of the incident radiation.

$$K = K' + iK'' \qquad \text{where } K' = \varepsilon\mu$$

$$\text{and } K'' = \frac{2\mu\sigma}{\nu}$$

Throughout the x-ray region K' is only slightly less than unity so that it is convenient to redefine the complex dielectric constant in terms of its unit decrements which, following Henke, we denote by α and γ.

Thus:

$$K = 1 - \alpha - i\gamma$$

The results are expressed as functions of the angle of grazing incidence θ, the material constants, α and γ, and a characteristic function, a. The function, a, measures the refraction angle and

approaches a_0 as defined in the approximate analysis for small θ, δ, and β. The function a is defined by:

$$a^2 = \frac{1}{2}\left[\sin^2\theta-\alpha+\sqrt{(\sin^2\theta-\alpha)^2+\gamma^2}\right]$$

The Fresnel coefficient or the ratio of the reflected to incident intensity I/I_0, for the electric vector perpendicular to the plane of incidence is given by:

$$R_1 = \frac{4a^2(\sin\phi-a)^2+\gamma^2}{4a^2(\sin\phi+a)^2+\gamma^2}$$

The ratio of the Fresnel coefficients for the two states of polarisation is:

$$\frac{R_2}{R_1} = \frac{4a^2(a-\cos\theta\cot\theta)^2+\gamma^2}{4a^2(a+\cos\theta\cot\theta)^2+\gamma^2}$$

The reflection coefficient for an unpolarised incident beam is therefore:

$$R = R_1\left[\frac{1+R_2/R_1}{2}\right]$$

The extinction coefficient, k, is given by:

$$k = \frac{\gamma}{2\sqrt{\cos^2\theta+a^2}}$$

and becomes equal to β given in the approximate analysis.

The linear x-ray absorption coefficient μ_1 can be defined as the limiting value as $\theta \to \pi/2$ of $4\pi k/\lambda$.

Hence:

$$\mu_1 = \frac{4\pi}{\lambda} \frac{\gamma}{\{2|(1-\alpha)+\sqrt{(1-\alpha)^2+\gamma^2}|\}^{\frac{1}{2}}}$$

When the incident beam is polarised with its electric vector normal to the plane of incidence, the depth at which the energy flow has dropped to 1/e is:

$$d_1 = \frac{\lambda a}{2\pi\gamma}$$

In the vicinity of the total reflection cut-off, i.e. $\sin\theta_c \simeq \sqrt{\alpha}$ the effective depth becomes:

$$d_{1c} = \frac{\lambda}{4\pi\sqrt{\gamma/2}}$$

The results of the approximate theory may be obtained from the exact theory by using the relations between the complex dielectric constant and the complex refractive index and taking the limits of small θ, δ, and β.

$$n = \sqrt{K}$$

$$1 - \alpha - i\gamma = (1-\delta-i\beta)^2$$

Therefore: $\alpha = 2\delta-\delta^2+\beta^2$

$$\gamma = 2(1-\delta)\beta$$

6.3 EXPERIMENTAL RESULTS

The angular dependence of the reflectivity of gold films of various thicknesses and chromium films on glass substrates have been measured at wavelengths of 45 Å and 8.3 Å.

The reflectivities of a series of gold films with thicknesses of 75, 100, 200, 300, 500 and 1000 Å deposited on float glass is shown in Fig. 91. These measurements were performed in 1973 when the apparatus was still being developed and the accuracy of the results is not as high as in recent measurements. However, it can be seen that the maximum reflectivity increases with increasing film thickness up to about 200 Å and then decreases again for thicker films. The explanation for this effect is that thin gold films deposited in vacuum have an island structure which grows as the film thickness increased to become a continuous film at between 100 and 200 Å, depending on the conditions of preparation. As the film thickness is increased above 200 Å the surface becomes progressively less smooth as conglomerates form. The results of an electron microscope study of the gold films are shown in Fig. 92. The island structure of the thin gold films is clearly visible and the high resistivity proves conclusively that the films are discontinuous. At 200 Å the resistivity has fallen and the electron micrographs no longer show the island structure, i.e. the film has become continuous, however, some granularity is apparent. As the film thickness increases to 1000 Å the size of the larger grains increases as does the granular background structure. Measurements on the angular dependence of reflectivity for gold films with thicknesses of 63, 131 and 590 Å using $Cu_{K\alpha}$ (1.54 Å) radiation by Lindsey (128) also indicate an optimum gold coating thickness of 150 - 400 Å.

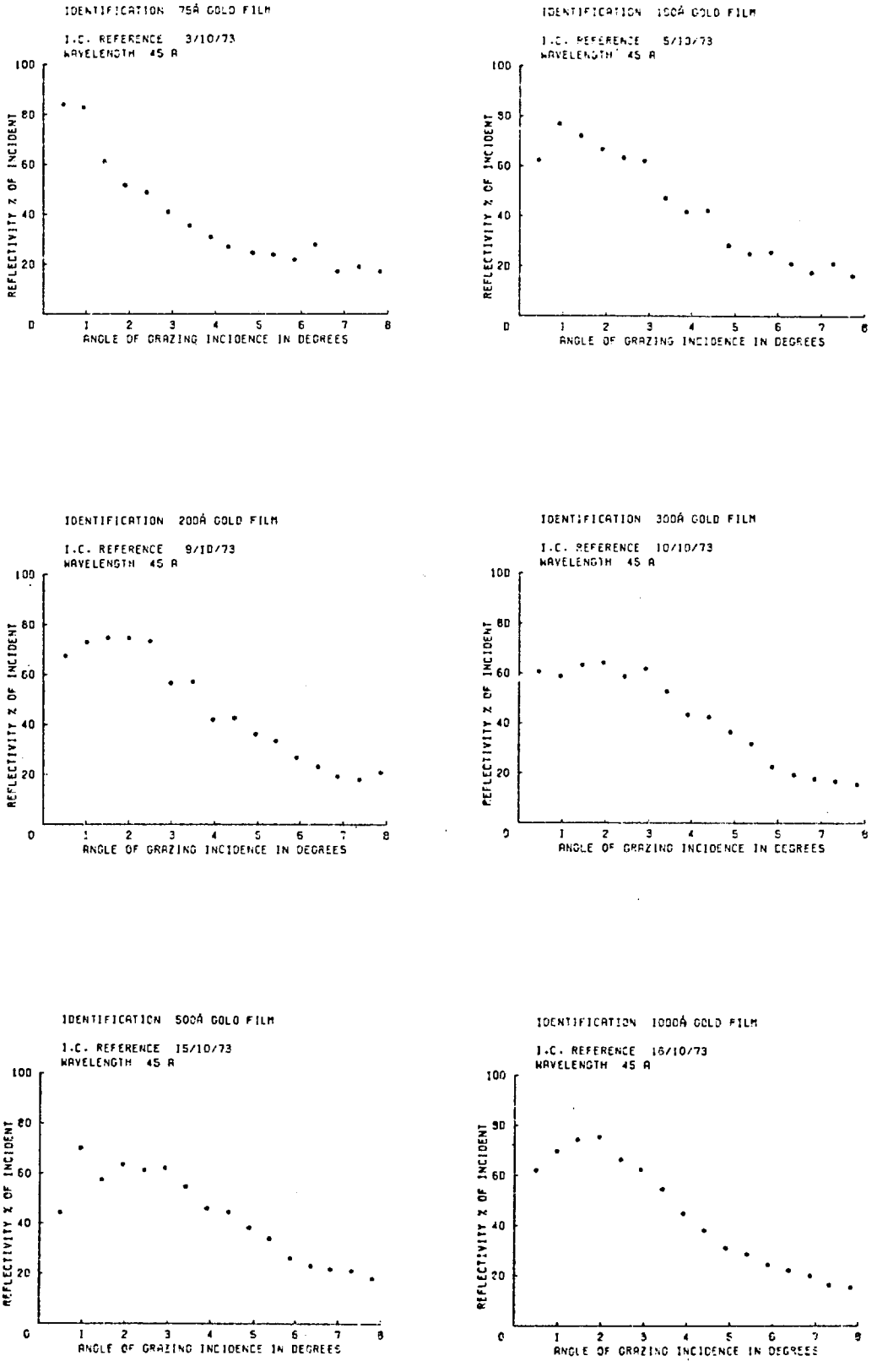
IDENTIFICATION 75Å GOLD FILM
I.C. REFERENCE 3/10/73
WAVELENGTH 45 A
REFLECTIVITY % OF INCIDENT
ANGLE OF GRAZING INCIDENCE IN DEGREES
IDENTIFICATION 100Å GOLD FILM
I.C. REFERENCE 5/10/73
WAVELENGTH 45 A
REFLECTIVITY % OF INCIDENT
ANGLE OF GRAZING INCIDENCE IN DEGREES
IDENTIFICATION 200Å GOLD FILM
I.C. REFERENCE 9/10/73
WAVELENGTH 45 A
REFLECTIVITY % OF INCIDENT
ANGLE OF GRAZING INCIDENCE IN DEGREES
IDENTIFICATION 300Å GOLD FILM
I.C. REFERENCE 10/10/73
WAVELENGTH 45 A
REFLECTIVITY % OF INCIDENT
ANGLE OF GRAZING INCIDENCE IN DEGREES
IDENTIFICATION 500Å GOLD FILM
I.C. REFERENCE 15/10/73
WAVELENGTH 45 A
REFLECTIVITY % OF INCIDENT
ANGLE OF GRAZING INCIDENCE IN DEGREES
IDENTIFICATION 1000Å GOLD FILM
I.C. REFERENCE 16/10/73
WAVELENGTH 45 A
REFLECTIVITY % OF INCIDENT
ANGLE OF GRAZING INCIDENCE IN DEGREES

FIG. 91

	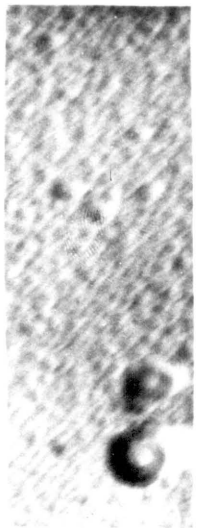	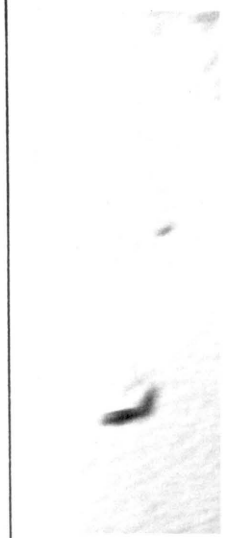	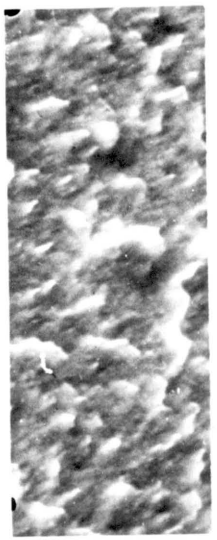	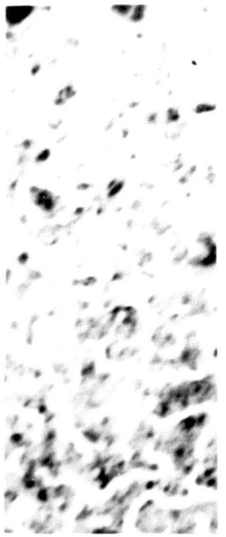			
PHOTO SCALE	100 nm	100 nm	100 nm	100 nm	100 nm	100 nm	100 nm
THICKNESS nm	100	50	20	10	5	2	1
SPECIMEN PREPARATION	C-Pt	C-Pt	Au	Au	Au	Au	Au
RESISTIVITY Ω m $\times 10^{-8}$	13	13	13	200	∞	∞	∞
AVERAGE CROSS-SECTIONS dimensions - nm	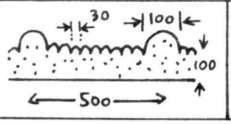		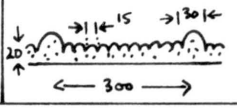	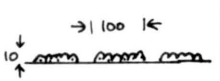	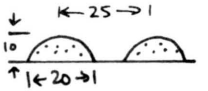	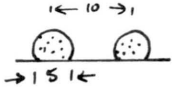	

FIG. 92

SUMMARY OF GOLD FILM DATA

The differences in the experimentally determined reflectivities of the mirrors coated with various thicknesses of gold can be more clearly seen in Fig. 93 in which all the curves are superimposed. Typical families of theoretical reflectivity curves as calculated from the exact Fresnel theory are shown in Fig. 94 for $\alpha = 0.02$ and $\alpha = 0.025$ for γ-values 0.002, 0.004, 0.006, 0.008 and 0.01. By fitting the theoretical curves to the experimental results it should be possible to accurately determine the material constants of the mirrors. However, from Fig. 93 and Fig. 94 it is immediately apparent that there are considerable discrepancies between the theoretical and experimental results. The most obvious difference between the curves is that instead of the experimental reflectivity becoming 100% as the grazing angle tends to zero a somewhat smaller value is attained. A similar effect for gold films has been observed by Groth (26) for measurements at 8.3 Å. Hendrick (27) found substantial agreement at 8.3 Å between theory and experiment for the critical angles if the films were assumed to have a density slightly less than the bulk metals but absorption ratios averaged 28% higher than predicted by the linear absorption ratios. Thus it is clear that a more sophisticated theoretical model is required to account for the reflectivity of gold films in the soft x-ray region.

Verhaeghe (129) has performed a theoretical study of the reflection of x-rays by thin gold films. The model suggested had two interfaces and the approximate electromagnetic field was calculated by a perturbation method using the ratio of the height of the defects to the wavelength as a parameter. The nature of substrates and gold surfaces were examined by interference microscopy and with an electron

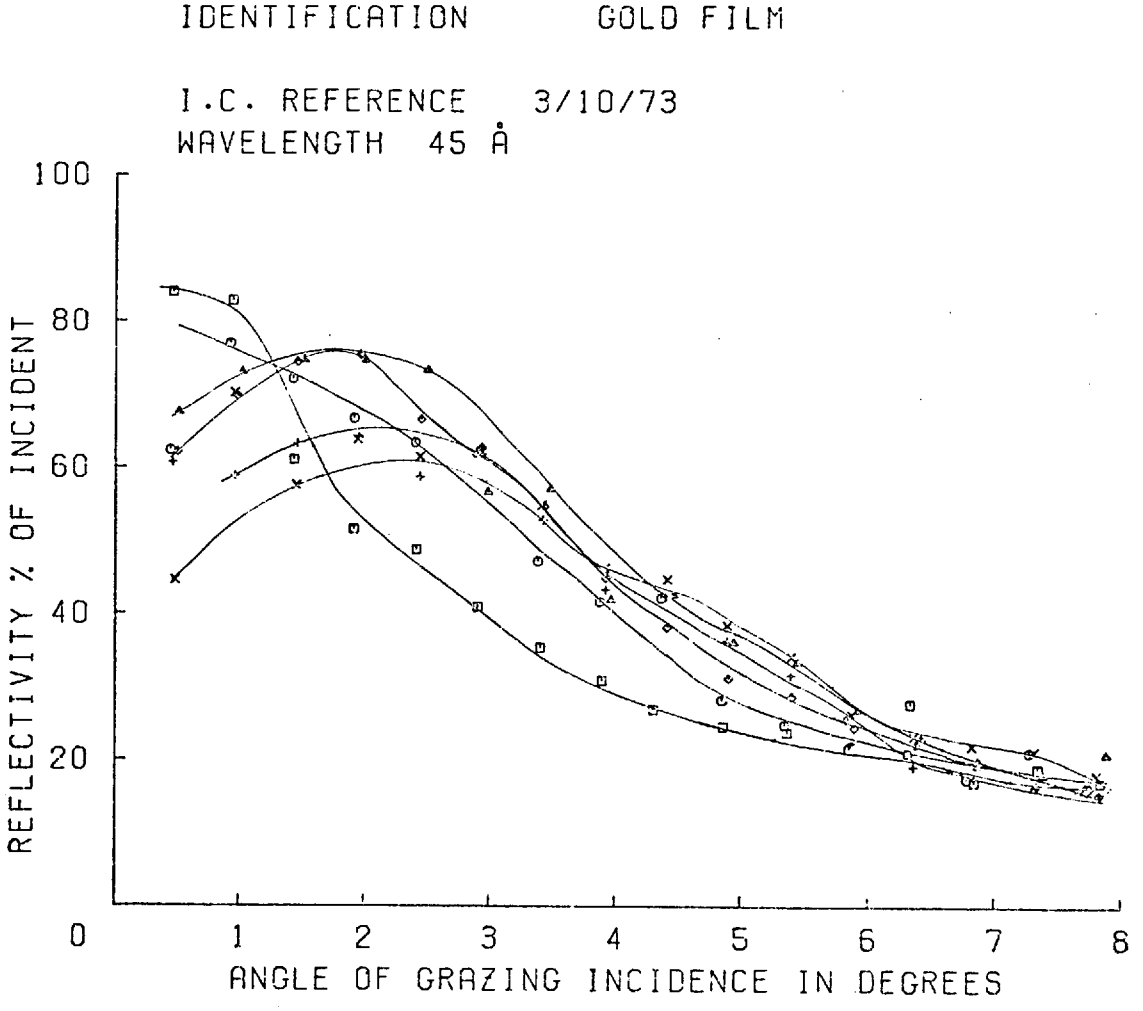

SYMBOL	THICKNESS
□	75 Å
○	100 Å
△	200 Å
+	300 Å
×	500 Å
◇	1000 Å

FIG. 93

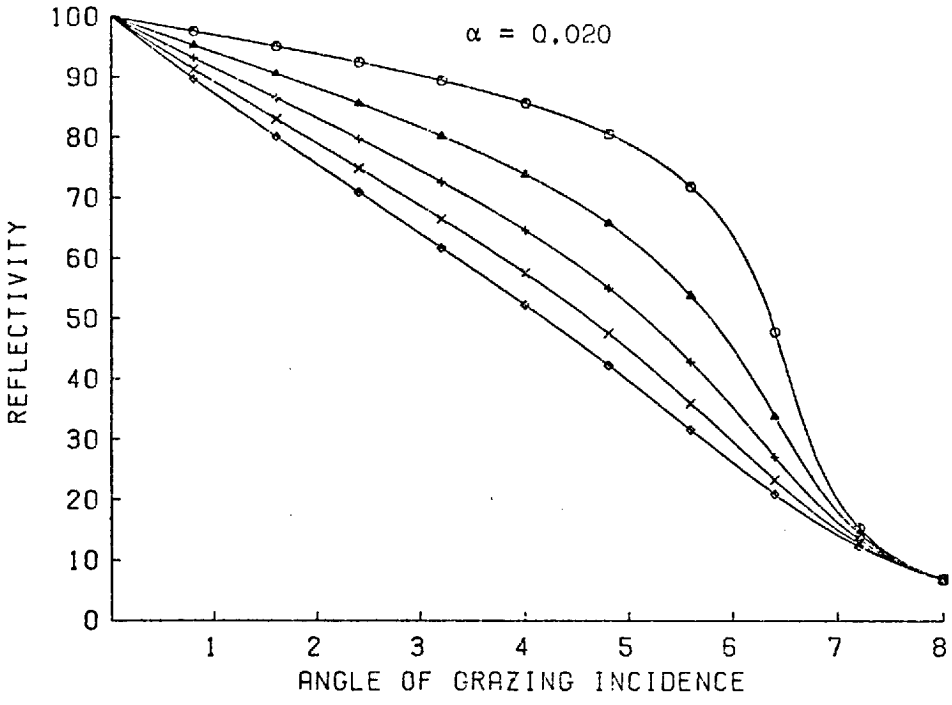

REFLECTIVITY CURVES CALCULATED FROM FRESNEL THEORY

α = 0.020 (above) α = 0.025 (below)

γ-values = 0.002, 0.004, 0.006, 0.008, 0.010

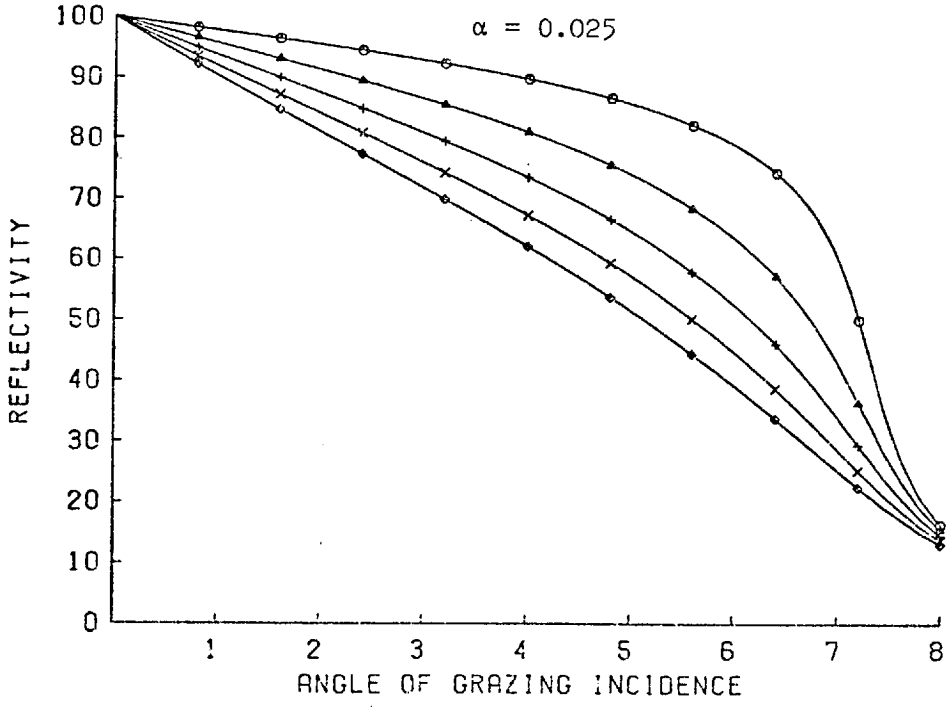

FIG. 94

microscope in order to provide numerical values for the theory. It was found that the gold surfaces have two types of defects; firstly, there are the polishing defects of the substrate which are mainly broad (10-20μm) with gentle slopes and rms heights 20-100 Å which are accurately contoured by thin films and secondly there are defects due to the crystallic structure of the films which have heights of one or two atomic dimensions (2.35 or 4.7 Å) and are spaced at ∿100-200 Å. By incorporating suitable values in the theory it was possible to obtain reasonable agreement with experimental results. Thus it is essential to be able to completely specify the parameters of a metal film and also measure the reflectivity accurately in order to develop a suitable theory applicable to the soft x-ray region. Since there are so many variable parameters it is questionable whether such a refined theory would have a wide applicability. However, the relationship between the techniques used for producing mirrors and the reflectivity of the mirrors in the soft x-ray region is of great practical importance.

A number of authors have investigated the relationship between the scattering of x-rays and polishing techniques. Most of these investigations have been performed with hard x-rays, usually $Cu_{K\alpha}$ (1.54 Å); the works of Ehrenberg (130), Elliott (131) and Schroeder and Klimasewski (132) are particularly interesting. The latter found that fused silica surfaces had consistently lower scattering than any of the other materials examined and that random polishing techniques produced least scattering. More recently Wriston and Froechtenigt (133) reported scattering measurements performed on twelve samples at 8.34 Å and 45 Å. The apparatus used was over 10.5m

long and had an angular resolution capability of the order of one arc second. The measurements on nine metal samples and three glass samples showed that more scattering occurred at 45 Å for both types of samples than at 8.3 Å when the glass samples produced the least scattering. The greatest scattering was found at small angles of incidence and the scattering increased again at angles larger than the critical angle. From these results it would seem that there may be an optimum angle of incidence at which scattering is minimised for a given wavelength. It is particularly important to perform repeated investigations under controlled conditions on numerous samples in order to obtain representative data because the properties of mirrors in the soft x-ray region are critically determined by the surface layers and surface structure at the atomic level. Thus the properties of mirrors produced under ostensibly the same conditions can be different even when the greatest care is taken in their production. Similarly variable results can be obtained from measurements in the soft x-ray region if the samples become contaminated.

From the preceding paragraphs it is clear that there is a need for accurate data on the reflectivity and relative scattering from surfaces in the soft x-ray region. Such data would have direct applicability in the design of soft x-ray optical systems and should enable optical manufacturing techniques to be improved. When related to surfaces of known structure such data would also enable a more complete theory of reflectivity in the soft x-ray region to be developed. Although the grating test apparatus in its original form was capable of measuring reflectivities in the soft x-ray region, the reflectivity measurements performed in 1973 indicated that the appa-

ratus had certain deficiencies. As described in Chapter 5 the apparatus has now been redesigned and considerably improved. Although these improvements have been made to facilitate grating efficiency determinations, they also enable more accurate reflectivity measurements to be made. The recent fabrication of a monochromator using one of the new high-performance holographic gratings is probably the most significant improvement to the test apparatus. It is now possible to select a known bandwidth of radiation and all the possible errors due to non-monochromatic radiation are eliminated. The monochromator enables the x-ray source to be operated at higher powers without contamination problems but, even so, the intensity of radiation from the monochromator is about an order of magnitude less than that from the usual x-ray source, depending on the bandwidth selected. The reduction in intensity means that longer integration times are required which necessitates high source stability. When the monochromator is used the required stability is achieved by continuously monitoring the output with a channeltron connected to an independent counting system which is used to control the current supplied to the x-ray source. Only preliminary trials of the monochromator have been performed at the time of writing, however, it is clear that the monochromator is most useful when examining high efficiency gratings when high count rates are obtainable. If the efficiencies of the gratings being tested are low (<1%) the integration times to obtain sufficient statistical accuracy become excessive. Since reflectivities of <1% are rarely of importance in the soft x-ray region, the monochromator system would appear to be ideal for performing reflectivity measurements. If a research programme was set up to systematically investi-

gate the properties of mirrors in the soft x-ray region, the grating test apparatus could be readily adapted to provide automated data acquisition. However, the apparatus in its present form is adequate for performing grating efficiency measurements and general reflectivity measurements.

Recently the reflectivities of gold and chromium films deposited on glass substrates have been measured at wavelengths of 45 Å and 8.3 Å. In these measurements partial monochromation was performed by using two 2.2μm polypropylene filters for C_K and a 5μm aluminium foil for Al_K. The measurements were principally performed in order to establish whether gratings could be advantageously coated with chromium instead of gold. As pointed out earlier in this chapter, gratings coated with chromium should be much more durable than gold-coated gratings enabling them to be cleaned without damage. However, such gratings should not be used at wavelengths near the absorption edges of oxygen or chromium. The reflectivities measured at 45 Å of two glass blanks coated with respectively 100 Å chromium and 100 Å gold are shown in Fig. 95. Since the coatings were prepared under similar conditions in the same vacuum evaporation apparatus a true comparison is possible and it can be seen that the reflectivity of the chromium film is significantly higher than that of the gold film for all the measured angles of grazing incidence (1°-8°). Fig. 96 shows the results of reflectivity measurements performed at 8.3 Å on the 100 Å chromium film and a 300 $Å_{\lambda}^{gold}$ film on a float glass substrate. For angles of grazing incidence less than 1.5° the reflectivity of the chromium film is again higher than that of the gold film but for larger angles the gold film has a higher reflectivity. Both these results indicate

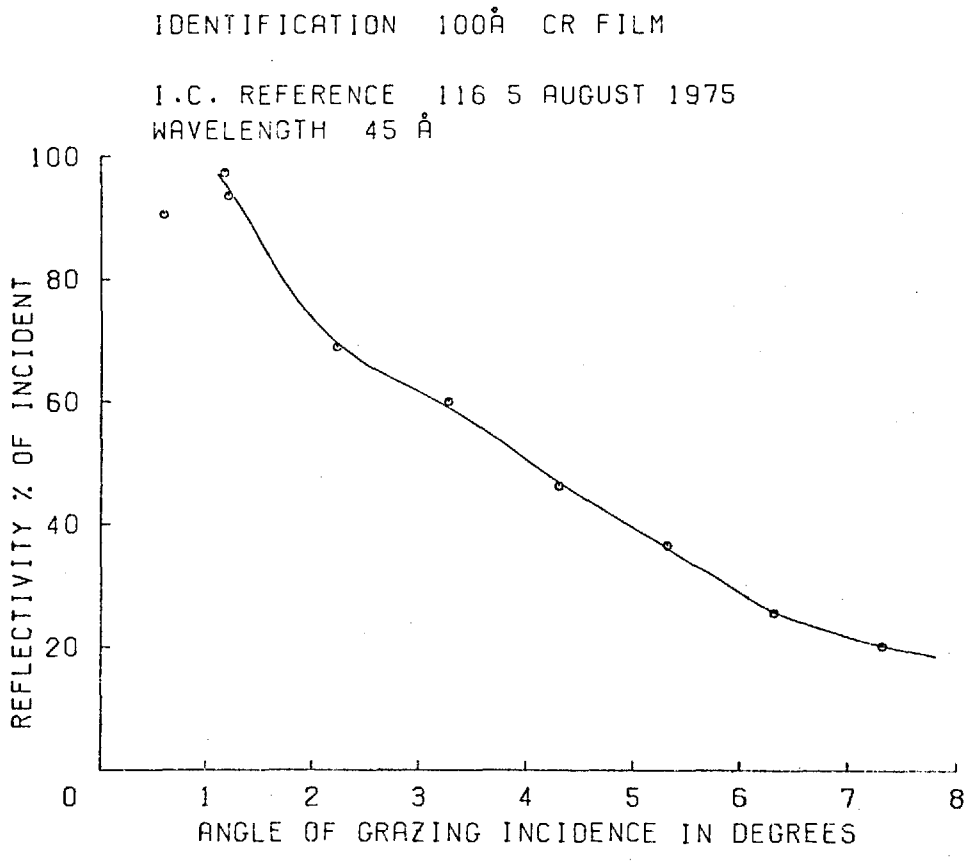
IDENTIFICATION 100Å CR FILM
I.C. REFERENCE 116 5 AUGUST 1975
WAVELENGTH 45 Å
REFLECTIVITY % OF INCIDENT
100
80
60
40
20
0
1
2
3
4
5
6
7
8
ANGLE OF GRAZING INCIDENCE IN DEGREES

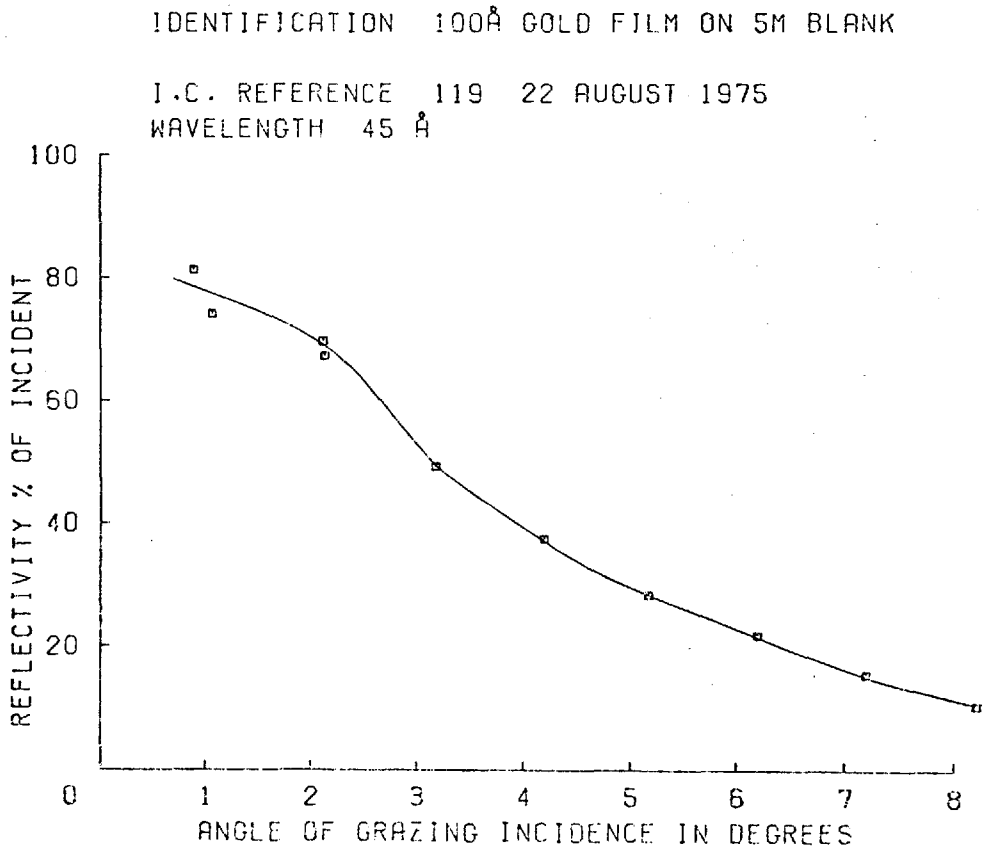
IDENTIFICATION 100Å GOLD FILM ON 5M BLANK
I.C. REFERENCE 119 22 AUGUST 1975
WAVELENGTH 45 Å
REFLECTIVITY % OF INCIDENT
100
80
60
40
20
0
1
2
3
4
5
6
7
8
ANGLE OF GRAZING INCIDENCE IN DEGREES

FIG. 95

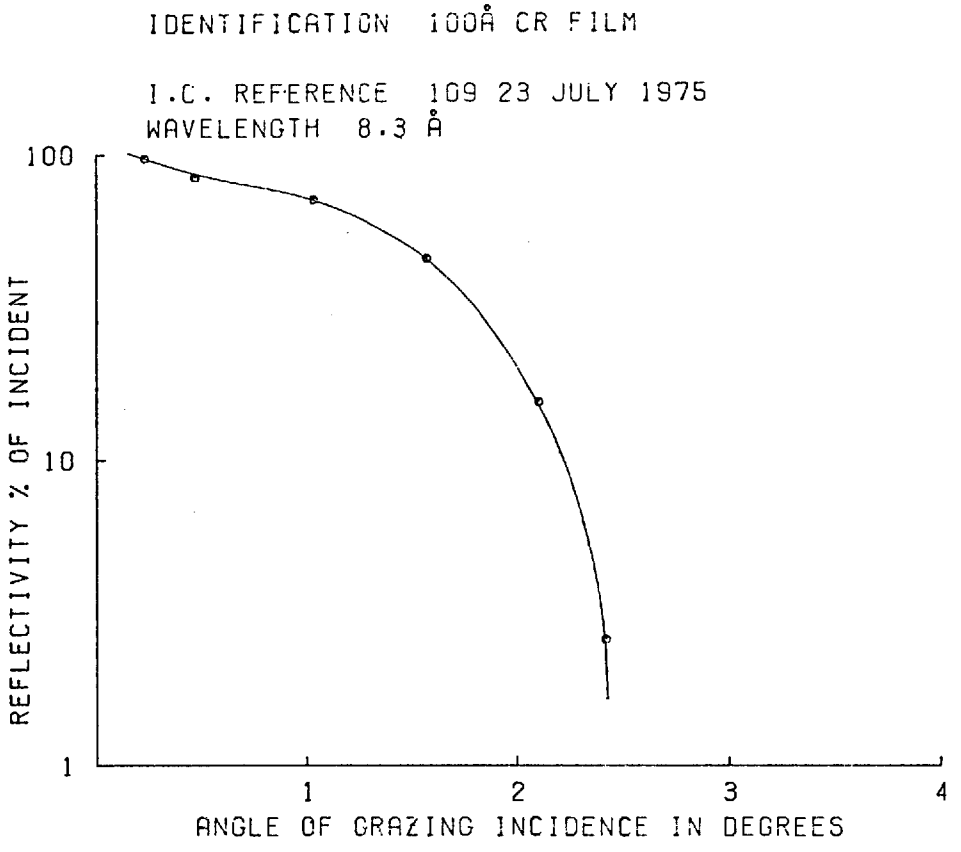
IDENTIFICATION 100Å CR FILM
I.C. REFERENCE 109 23 JULY 1975
WAVELENGTH 8.3 Å
100
10
1
REFLECTIVITY % OF INCIDENT
1
2
3
4
ANGLE OF GRAZING INCIDENCE IN DEGREES

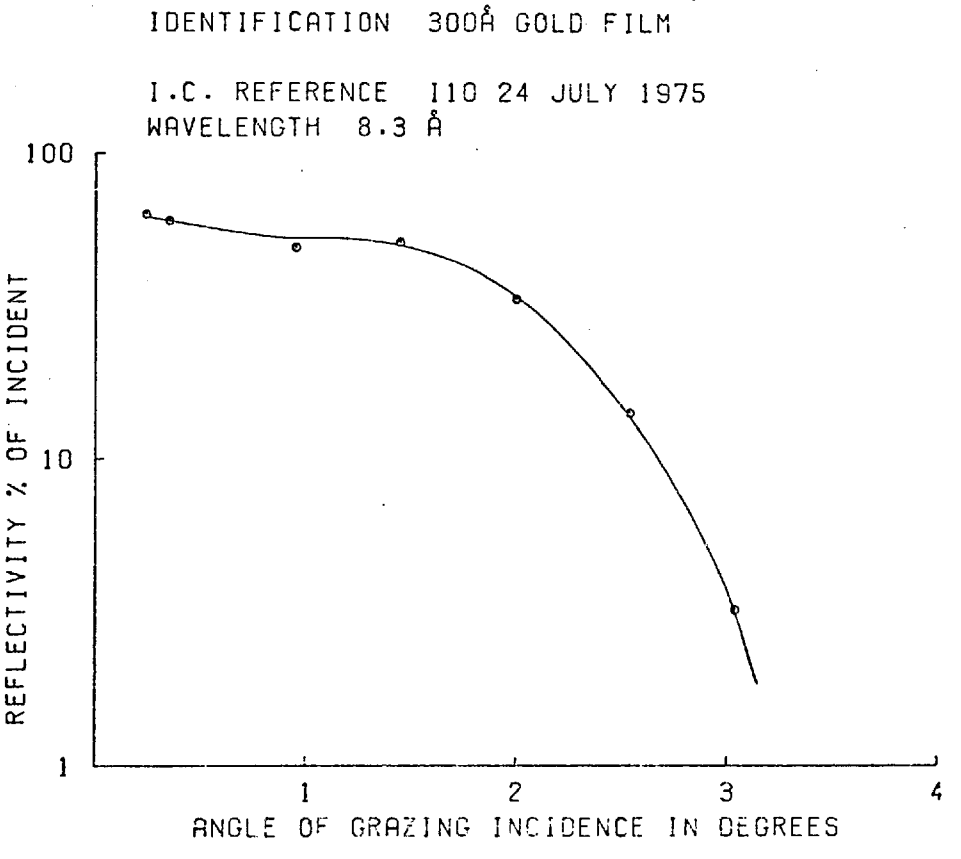
IDENTIFICATION 300Å GOLD FILM
I.C. REFERENCE 110 24 JULY 1975
WAVELENGTH 8.3 Å
100
10
1
REFLECTIVITY % OF INCIDENT
1
2
3
4
ANGLE OF GRAZING INCIDENCE IN DEGREES

FIG. 96

that the gold films have considerably higher absorption than the chromium films at both 45 Å and 8.3 Å.

Since only a few samples have been examined it is not possible to make any definite conclusions. The high absorption of the gold films may be in part due to the conglomerate structures of the films. The structure of the films will depend upon the preparation of the substrate, the conditions in the coating plant and the subsequent treatment and age of the film. Thus by careful preparation of the substrate and by optimising the coating conditions it is to be expected that the reflectivity of gold films could be improved. This idea is substantiated by Fig. 97 which shows the reflectivity of a high quality NPL laminar grating measured perpendicular to the rulings (i.e. the grating has been rotated by 90° from the orientation in which it would normally be used). The gold coating on this grating is 300 Å thick and even though the substrate is a grating, the reflectivity measured at 8.3 Å is higher than that of the 300 Å gold film on a float glass substrate. Normally it would be expected that the reflectivity of a grating measured in this orientation would be slightly less than that of a mirror, however, this result is indicative of the very high quality of the surfaces and gold coatings produced at NPL.

In this chapter theoretical and experimental aspects of the reflection of soft x-rays have been examined. It has been found that coating materials other than gold can be usefully employed on gratings designed for specific purposes in the soft x-ray region. Furthermore, by optimising the coating thickness and the conditions under which the coatings are formed, a significant increase in reflectivity is

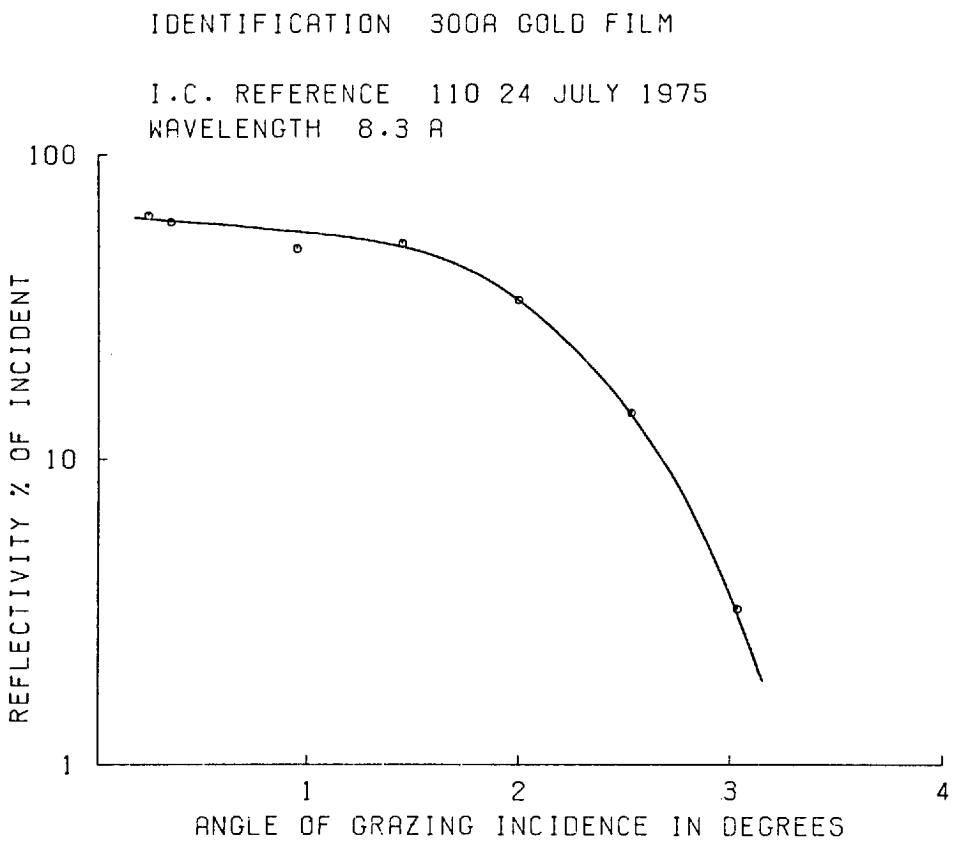
IDENTIFICATION 300A GOLD FILM
I.C. REFERENCE 110 24 JULY 1975
WAVELENGTH 8.3 A
100
10
1
REFLECTIVITY % OF INCIDENT
1
2
3
4
ANGLE OF GRAZING INCIDENCE IN DEGREES

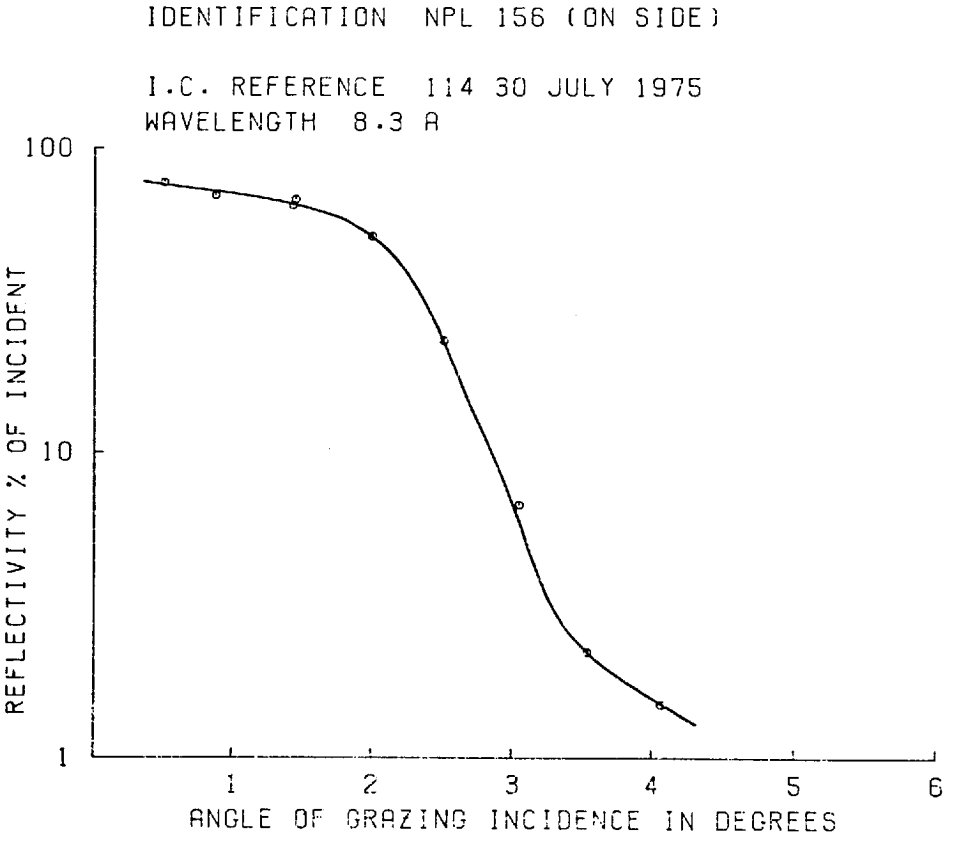
IDENTIFICATION NPL 156 (ON SIDE)
I.C. REFERENCE 114 30 JULY 1975
WAVELENGTH 8.3 A
100
10
1
REFLECTIVITY % OF INCIDENT
1
2
3
4
5
6
ANGLE OF GRAZING INCIDENCE IN DEGREES

FIG. 97

possible. The grating test apparatus in its present form can be readily adapted to making high precision reflectivity measurements which would be useful for optimising the coatings on diffraction gratings and would also provide fundamental data about thin films. In order to be able to obtain the maximum useful information, it is necessary to produce the coatings under controlled conditions on suitable substrates and to examine sufficient samples to obtain representative data. Since the test apparatus has now been equipped with a monochromator, it is possible for a comprehensive research programme to be undertaken on the properties of grating coatings suitable for use in the soft x-ray region.

CHAPTER 7

THE PERFORMANCE OF HOLOGRAPHIC X-RAY GRATINGS

7.1 THE EFFICIENCY OF DIFFRACTION GRATINGS IN THE SOFT X-RAY REGION

Prior to 1970 very few measurements of the performance of diffraction gratings had been performed in the soft x-ray region. The most comprehensive measurements published are those of Lukirskii et al (112) performed on gratings prepared in the State Optical Laboratory. Because of the rapidly increasing importance of the soft x-ray region, it became evident that a comprehensive soft x-ray grating calibration facility available to all manufacturers and grating users would be highly desirable. The x-ray grating laboratory at Imperial College was established in order to fulfil this need and the first grating measurements were performed there in July 1970. Since that time over eighty different gratings from five manufacturers have been examined at wavelengths in the soft x-ray region. The results of these examinations have enabled more efficient x-ray gratings to be developed and have made it possible to calibrate grazing incidence spectrographs for intensity measurements (135).

Many of the gratings have been tested at three wavelengths using the characteristic radiation from aluminium (8.3 Å), oxygen (23.6 Å) and carbon (44.8 Å). Some of the gratings have also been tested in two orientations. Thus a wealth of data on gratings of all types has been accumulated. Obviously, it is not possible to describe here the results of all the examinations; instead the data will be summarised and general trends indicated by some specific examples.

Since diffraction efficiency depends on the grating surface profile, it is convenient to categorise, according to profile, three types of soft x-ray grating. The first category is the shallow blazed, or echelette grating, which has a sawtooth profile. The second category is the laminar grating which has a rectangular profile, and the third type has a semi-sinusoidal profile. In addition to these three categories, depending on the technique used to produce the gratings, one can distinguish between mechanically-ruled and holographically-formed gratings.

All of the gratings examined before September 1972 were mechanically ruled. The majority of these gratings were shallow blazed replica gratings produced by Bausch and Lomb, USA. To date, twenty gratings of this type produced from ten masters with frequencies of 300, 600, 1200, 2400 and 3600 1/mm have been examined. The general trend in the results is a decrease in efficiency with increase in grating frequency, presumably due to a loss in control over the grating profile at higher frequencies. The highest efficiency measured from a shallow blazed grating at 45 Å was 7.4% obtained from a 600 1/mm grating. At 1200 1/mm the maximum recorded efficiency was 3.3% and at 2400 1/mm and 3600 1/mm the efficiencies were somewhat lower. Curves showing the typical dependence of diffraction efficiency on angle of incidence at 45 Å for two shallow blazed gratings with 600 1/mm and 1200 1/mm are given in Fig. 97 and Fig. 98. The results show considerable variability between different masters and, as can be seen from Fig. 99, there are differences between replicas off the same master although these are not so great. The results in

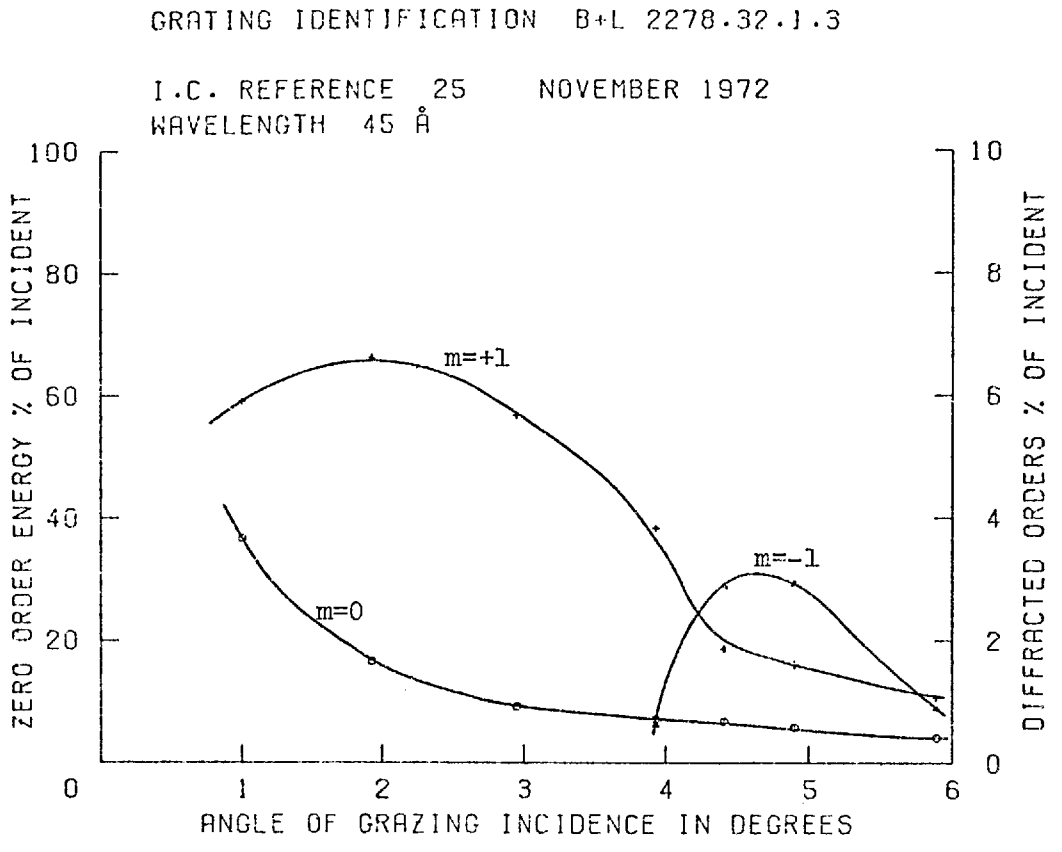
GRATING IDENTIFICATION B+L 2278.32.1.3
I.C. REFERENCE 25 NOVEMBER 1972
WAVELENGTH 45 Å
ZERO ORDER ENERGY % OF INCIDENT
DIFFRACTED ORDERS % OF INCIDENT
m=+1
m=0
m=-1
ANGLE OF GRAZING INCIDENCE IN DEGREES

FIG. 97

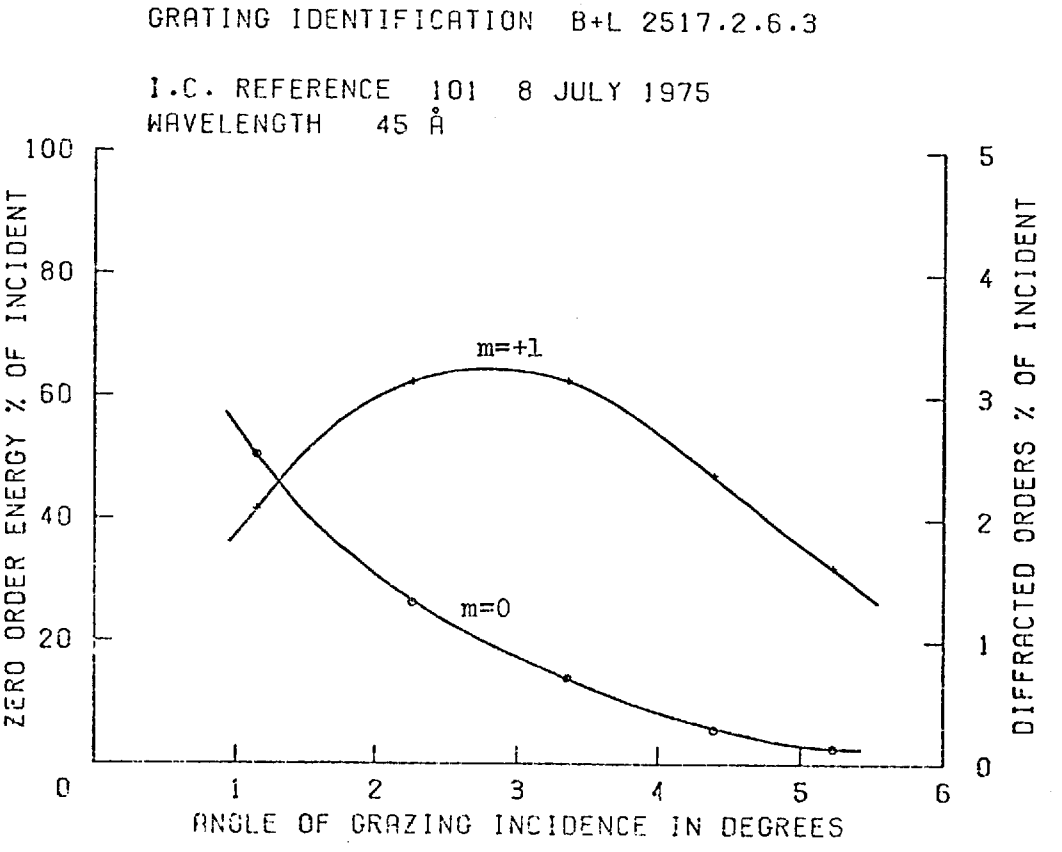
GRATING IDENTIFICATION B+L 2517.2.6.3
I.C. REFERENCE 101 8 JULY 1975
WAVELENGTH 45 Å
ZERO ORDER ENERGY % OF INCIDENT
DIFFRACTED ORDERS % OF INCIDENT
m=+1
m=0
ANGLE OF GRAZING INCIDENCE IN DEGREES

FIG. 98

COMPARISON OF EFFICIENCY vs GRAZING ANGLE FOR DIFFERENT REPLICAS
OFF THE SAME MASTER (B&L, 2517, 1200 l/mm) WITH Pt & Au COATINGS AT 44Å

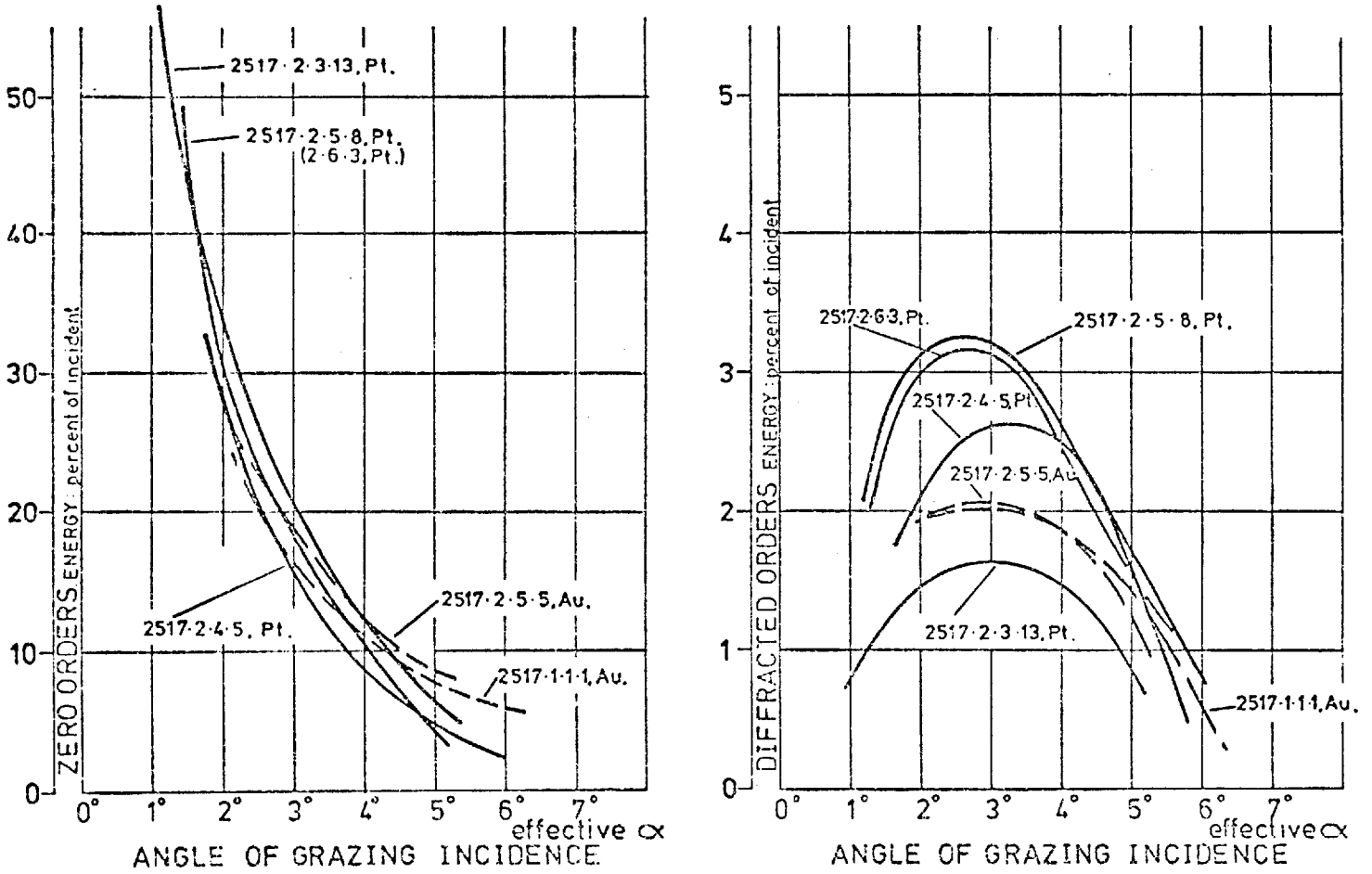

FIG. 99

Fig. 99 also indicate that platinum may be advantageously used as a grating coating material. At wavelengths below 10 Å the efficiency of shallow blazed gratings diminishes and the highest efficiency measured at 8.3 Å was 2.6% from a 600 l/mm grating and typical efficiency values for higher frequency gratings are ~1%. Since the blaze angles required in the short wavelength region are less than one degree, it is evident that standard mechanical ruling techniques will not permit the necessary accuracy to be attained and alternative methods must be used.

In order to overcome the limitations of the standard ruling technique methods have been developed at the NPL for producing gratings with laminar profiles, which are highly efficient at short wavelengths (122). A total of sixteen gratings of this type have been examined and the properties of five NPL laminar gratings have been fully described by Bennett (30). Recently, gratings have been produced from masks mechanically ruled at 316 l/mm and 632 l/mm. Efficiencies of 12% at 45 Å and 15% at 8.3 Å have been measured from gratings with 632 l/mm, and these gratings can have efficiencies of up to 5% at wavelengths as short as 1.5 Å. Typical curves showing the dependence of efficiency on angle of grazing incidence at 8.3 Å for two laminar x-ray gratings are shown in Fig. 100 and Fig. 101.

To obtain the maximum efficiency from a laminar grating, it is necessary to choose the correct groove depth for the wavelength region and conditions of use as one would choose the blaze angle of a blazed grating. The techniques for manufacturing laminar gratings enable the groove depths to be controlled to high accuracy so that it is possible to optimise gratings for use in specific wavelength

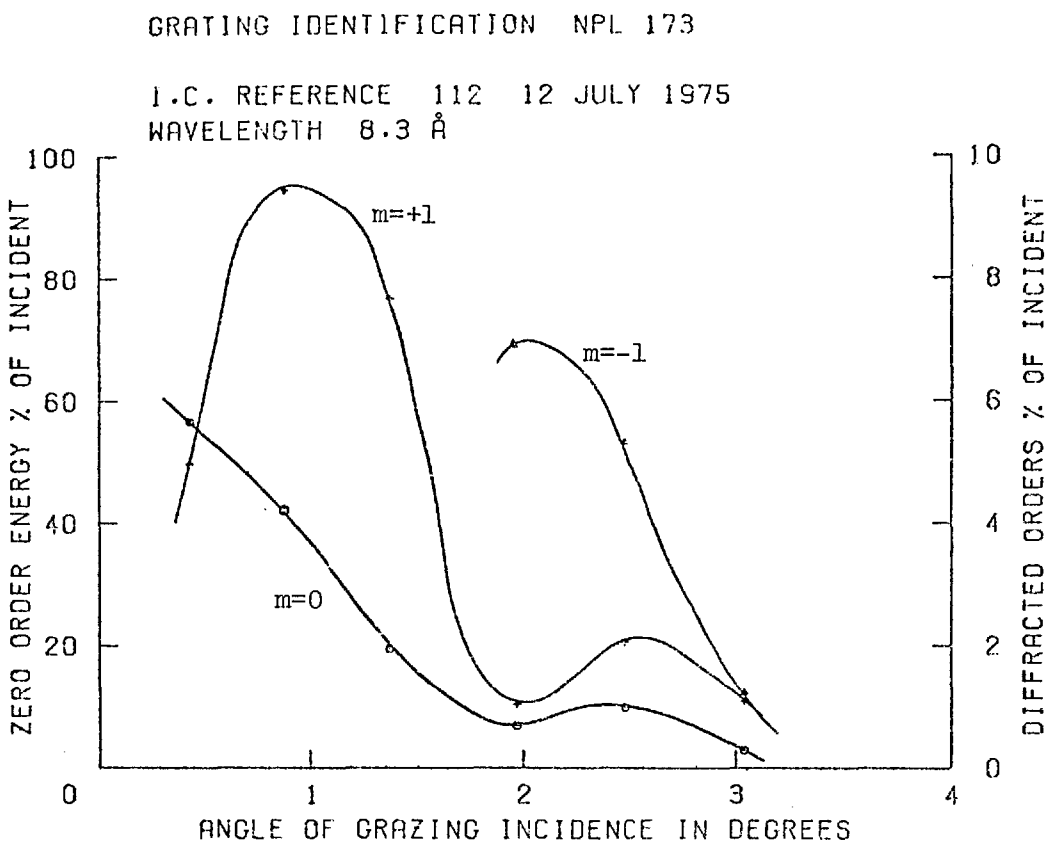

FIG. 100

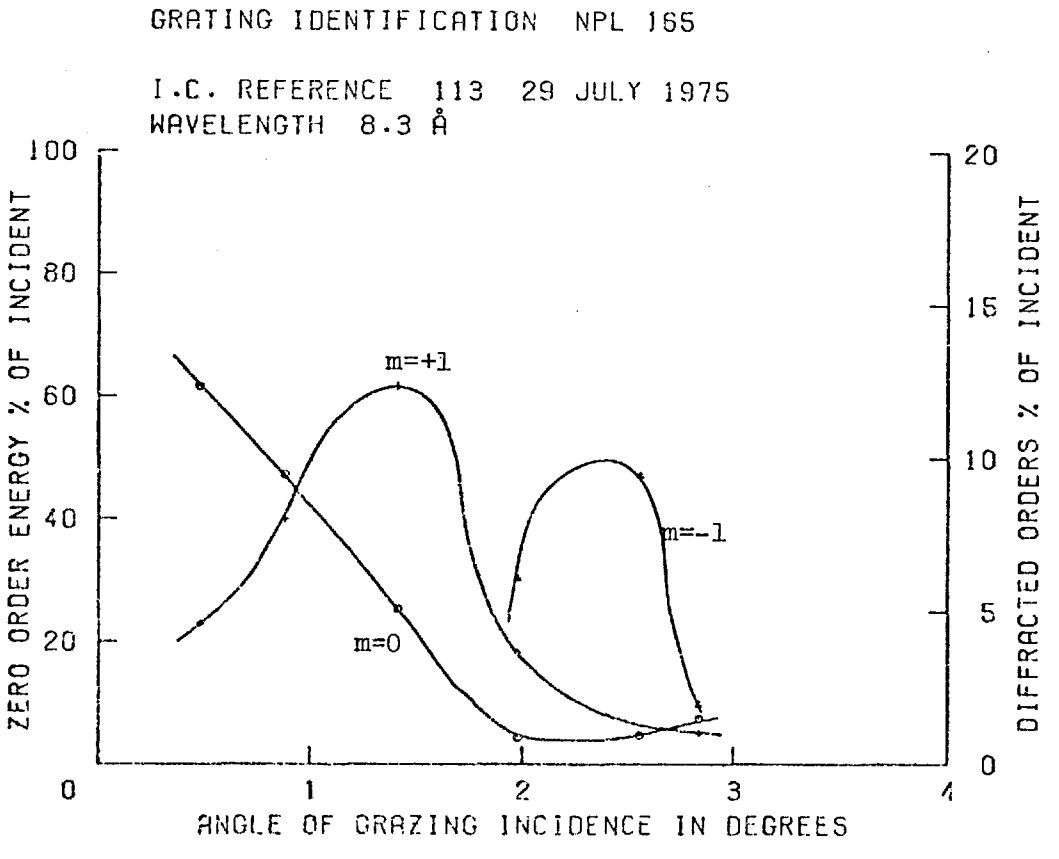

FIG. 101

regions. In the visible region it is generally accepted that blazed gratings are efficient over about an octave and a rule of thumb for coarse gratings is that the efficiency drops to half its maximum at two-thirds the blaze wavelength and again at three-halves the blaze wavelength. At soft x-ray wavelengths it is often necessary to simultaneously record a wide wavelength range but it is clear that this is incompatible with the requirements for maximum efficiency and resolution. For applications where the efficiency must be nearly constant over as large a wavelength range as possible, an amplitude grating is most suitable, however, the maximum theoretical diffraction efficiency is only ~10%. A higher efficiency is possible with a laminar grating and theoretically it would be expected that a laminar grating should be usable over a wider wavelength range than a blazed grating. Since x-ray gratings have until now only been tested at discrete, rather widely separated, characteristic wavelengths, it is not possible to directly compare the efficiencies of laminar and blazed gratings as a function of wavelength. However, from the shapes of the experimentally determined curves of diffraction efficiency against angle of incidence it appears that in practice laminar gratings and shallow blazed gratings have similar diffractive properties with respect to wavelength. In order to obtain the maximum useful wavelength range from a laminar grating, it is essential to utilise the "primary maximum of efficiency", i.e. to use the minimum groove depth consistent with phase cancellation. Within the primary maximum the efficiency only varies slowly with wavelength, however, at shorter wavelengths the theoretical efficiency curves of a laminar grating have an oscillatory form. This oscillatory behaviour could be misleading

when interpreting spectra and generally it is more favourable to use a laminar grating about the design wavelength and at longer wavelengths. One of the author's laminar holographic gratings has been tested using synchrotron radiation and spectra have been obtained which show smooth diffraction efficiency free from singularities in the wavelength range 40 - 200 Å. Although maximum efficiency is only obtained over a limited wavelength range, it is nevertheless possible to use laminar gratings to record a wide range of wavelengths.

Diffraction gratings with a semi-sinusoidal profile can be most easily made by recording interference fringes in photoresist. Only three gratings of this type have been examined at soft x-ray wavelengths and they had frequencies of 1200 l/mm and 1800 l/mm. The results of the examinations at 45 Å from two of the gratings are given in Fig. 1 and it can be seen that these gratings have a usable diffraction efficiency in the soft x-ray region. Similar results were obtained when the 1200 l/mm Jobin et Yvon grating was examined at 23.6 Å (O_K). It should be noted that these gratings were not specifically designed for soft x-ray use and it is remarkable that the first holographic gratings should exhibit such high diffraction efficiencies.

Because photoresist is an organic substance which is readily degradable by high energy radiation and has relatively large molecules, it would not appear to be the ideal material for making soft x-ray diffraction gratings. From the experience gained from ruled gratings it was clear that the laminar profile was most suitable for x-ray gratings. In Germany Rudolph and Schmahl had devised a method for pro-

ducing gratings in all-metallic laminar form by using photoresist and laser light. Since these gratings were free from photoresist and had a laminar profile, it would appear that they should be most suitable for use in the soft x-ray region. The efficiency at 45 Å of the first 600 l/mm grating made by this method is shown in Fig. 2. Although the maximum efficiency is only 2.6%, it is an encouraging result from a prototype grating and the zero order curve shows evidence of phase cancellation. In order to further explore the properties of gratings made by this process, gratings with 1200 l/mm and 2400 l/mm, and with different land to groove ratios at 600 l/mm were examined.

The higher frequency gratings had markedly lower efficiencies than the first 600 l/mm grating as can be seen from Fig. 102, and the gratings with land to groove ratios other than unity also had lower efficiencies. Examination of the grating profile with a "Talystep" indicated that the low efficiency was most probably caused by "ridges" at the edges of the lands produced by the "stripping process". Hence, it was necessary to devise a technique which produced completely smooth lands and grooves in a laminar profile from a holographically-formed photoresist grating. As described in Chapter 4, the author performed a series of experiments in order to discover whether it was possible to produce laminar gratings for use in the soft x-ray region by using a holographic photoresist grating as a mask in a chemical etching process. The author has successfully made forty-one diffraction gratings using this process and the properties of some of these gratings will be described and discussed in the following section.

FIG. 102

EFFICIENCY AT 44 ANGSTROMS vs GRAZING ANGLE

GÖTTINGEN HOLOGRAPHIC GRATINGS

600,1200,2400 l/mm, PLANE, DEPTH 150 - 200 Å, Au COATED.

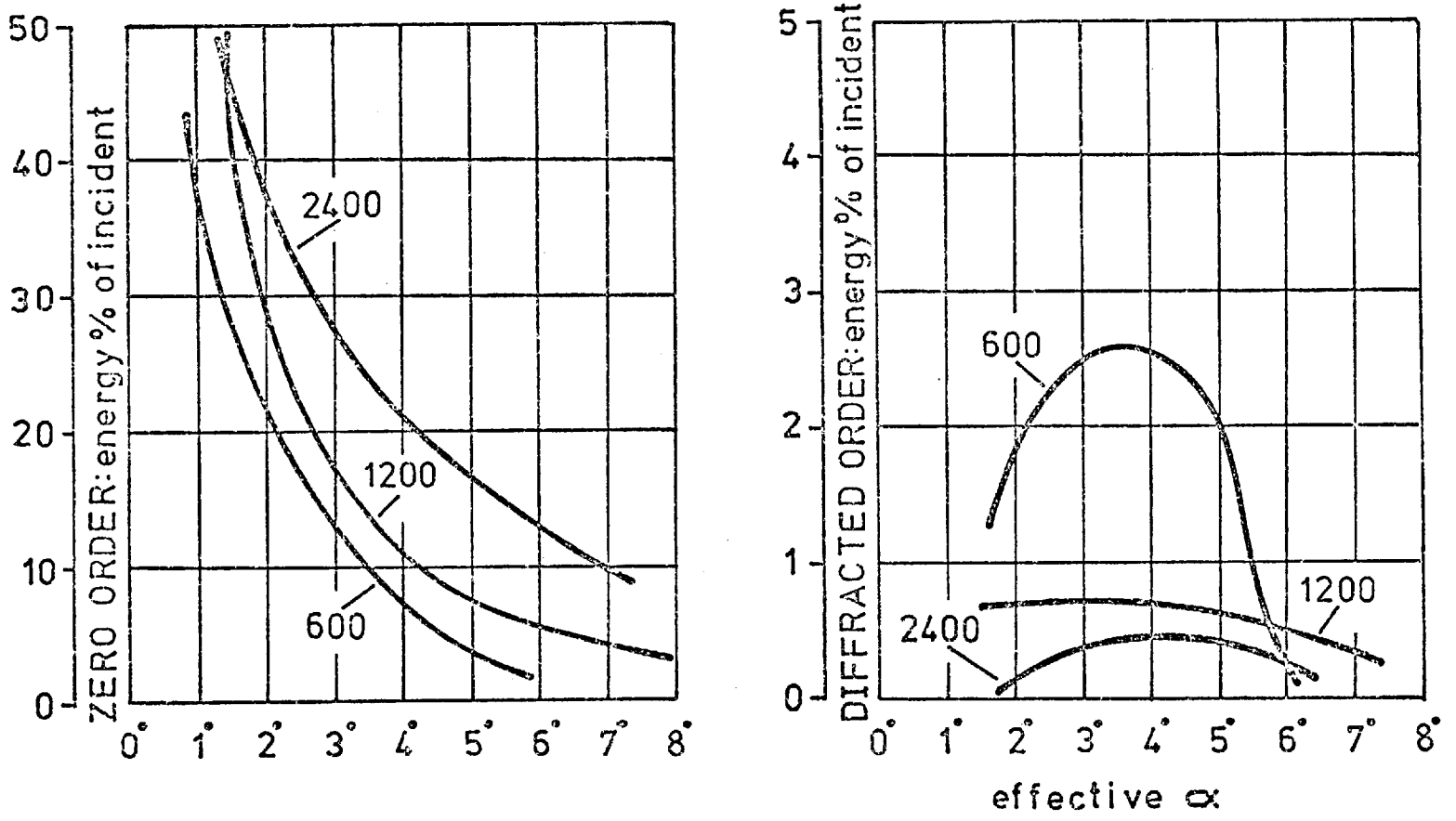

ANGLE OF GRAZING INCIDENCE

7.2 THE PROPERTIES OF HOLOGRAPHIC X-RAY GRATINGS MADE BY THE "ETCHING TECHNIQUE"

During the present research programme the author has made 27 gratings with a frequency of 294 l/mm, 8 gratings with 600 l/mm and 6 gratings with 1160 l/mm. The number of 294 l/mm gratings includes three uncoated trial gratings which were not tested at x-ray wavelengths. The gratings were fabricated with nominal groove depths of 100 Å, 150 Å and 200 Å and with various land to groove ratios. The efficiencies of all the gratings have been measured at 45 Å and the results of most of these examinations are given in Fig. 103 (a, b, c, d). A brief inspection of the results shows three important features. Firstly, the gratings have consistently high diffraction efficiencies. Secondly, the zero order efficiency curves have pronounced minima indicating phase cancellation. Thirdly, the shapes of the curves are similar with symmetrical positive and negative diffracted orders of the same magnitude. All these features show that the holographic gratings produced by the etching technique are behaving as phase gratings.

Before proceeding to a more detailed analysis of the results, it must be emphasised that these gratings were prototypes. The substrates on which the gratings were formed had, in many cases, been used in previous experiments and were therefore not of the highest quality. The metal coatings were produced in a standard commercial vacuum coating plant at pressures of $\sim 10^{-5}$ torr and better quality coatings could be made using more sophisticated equipment. Finally, the gratings were made with a wide range of parameters in order to discover experimentally the effects of varying groove depth

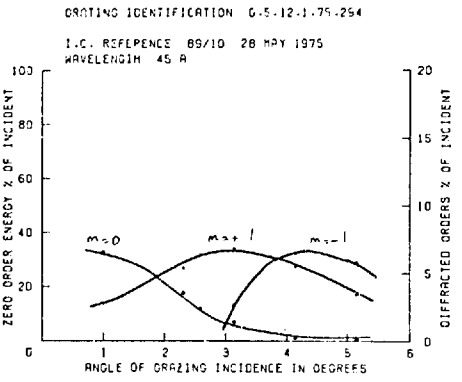
GRATING IDENTIFICATION G.5.12.1.75.294
I.C. REFERENCE 89/10 28 MAY 1975
WAVELENGTH 45 A
ZERO ORDER ENERGY % OF INCIDENT
DIFFRACTED ORDERS % OF INCIDENT
m=0
m=+1
m=-1
ANGLE OF GRAZING INCIDENCE IN DEGREES

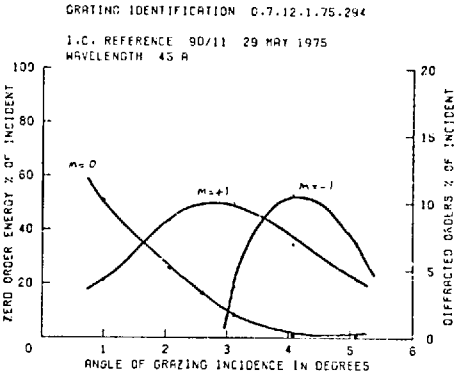
GRATING IDENTIFICATION G.7.12.1.75.294
I.C. REFERENCE 90/11 29 MAY 1975
WAVELENGTH 45 A
ZERO ORDER ENERGY % OF INCIDENT
DIFFRACTED ORDERS % OF INCIDENT
m=0
m=+1
m=-1
ANGLE OF GRAZING INCIDENCE IN DEGREES

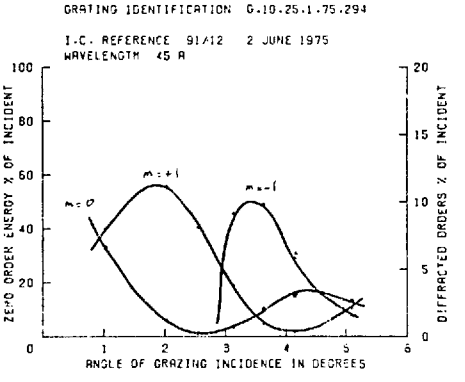
GRATING IDENTIFICATION G.10.25.1.75.294
I.C. REFERENCE 91/12 2 JUNE 1975
WAVELENGTH 45 A
ZERO ORDER ENERGY % OF INCIDENT
DIFFRACTED ORDERS % OF INCIDENT
m=0
m=+1
m=-1
ANGLE OF GRAZING INCIDENCE IN DEGREES

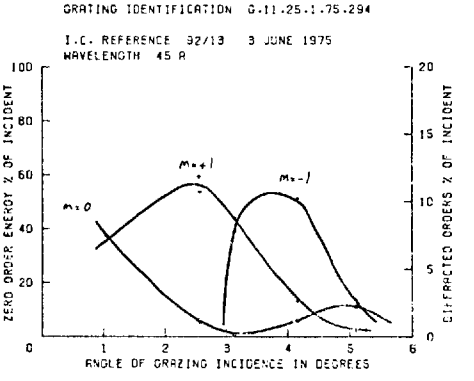
GRATING IDENTIFICATION G.11.25.1.75.294
I.C. REFERENCE 92/13 3 JUNE 1975
WAVELENGTH 45 A
ZERO ORDER ENERGY % OF INCIDENT
DIFFRACTED ORDERS % OF INCIDENT
m=0
m=+1
m=-1
ANGLE OF GRAZING INCIDENCE IN DEGREES

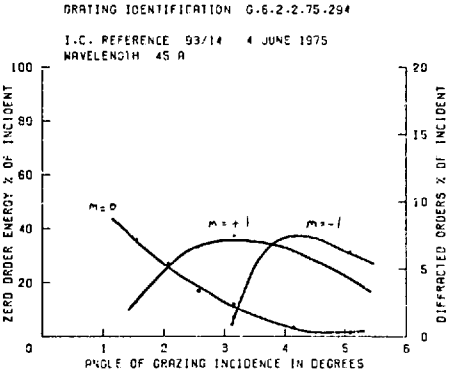
GRATING IDENTIFICATION G.6.2.2.75.294
I.C. REFERENCE 93/14 4 JUNE 1975
WAVELENGTH 45 A
ZERO ORDER ENERGY % OF INCIDENT
DIFFRACTED ORDERS % OF INCIDENT
m=0
m=+1
m=-1
ANGLE OF GRAZING INCIDENCE IN DEGREES

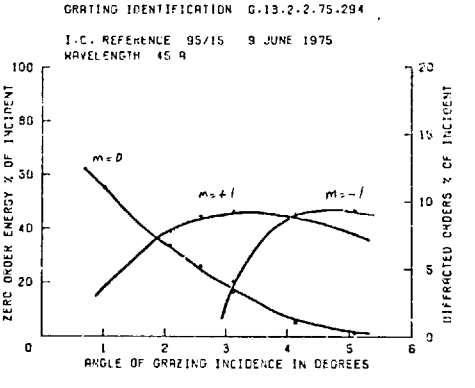
GRATING IDENTIFICATION G.13.2.2.75.294
I.C. REFERENCE 95/15 9 JUNE 1975
WAVELENGTH 45 A
ZERO ORDER ENERGY % OF INCIDENT
DIFFRACTED ORDERS % OF INCIDENT
m=0
m=+1
m=-1
ANGLE OF GRAZING INCIDENCE IN DEGREES

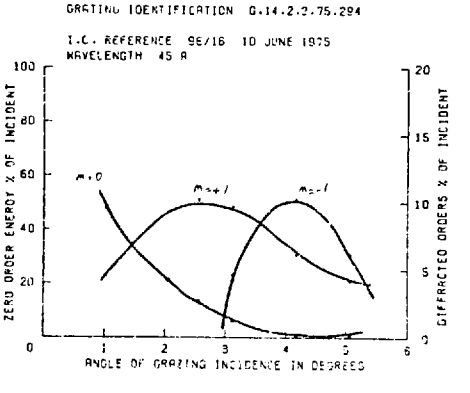
GRATING IDENTIFICATION G.14.2.2.75.294
I.C. REFERENCE 96/16 10 JUNE 1975
WAVELENGTH 45 A
ZERO ORDER ENERGY % OF INCIDENT
DIFFRACTED ORDERS % OF INCIDENT
m=0
m=+1
m=-1
ANGLE OF GRAZING INCIDENCE IN DEGREES

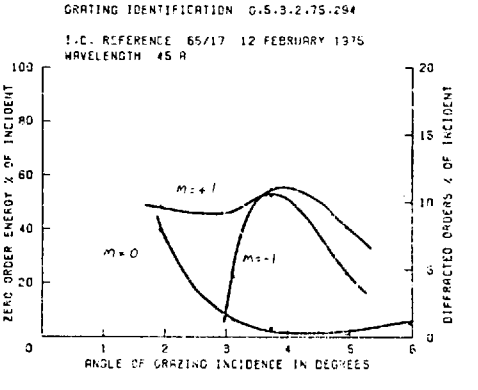
GRATING IDENTIFICATION G.5.3.2.75.294
I.C. REFERENCE 65/17 12 FEBRUARY 1975
WAVELENGTH 45 A
ZERO ORDER ENERGY % OF INCIDENT
DIFFRACTED ORDERS % OF INCIDENT
m=0
m=+1
m=-1
ANGLE OF GRAZING INCIDENCE IN DEGREES

FIG. 103 (a)

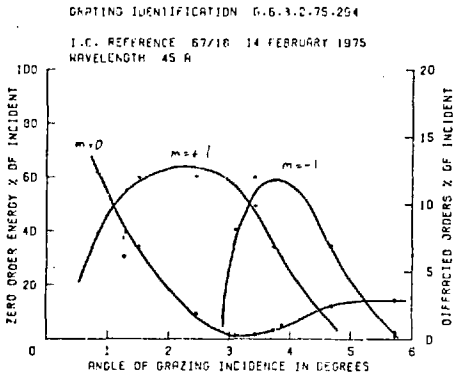
GRATING IDENTIFICATION G.6.3.2.75.294
I.C. REFERENCE 67/18 14 FEBRUARY 1975
WAVELENGTH 45 A
ZERO ORDER ENERGY % OF INCIDENT
DIFFRACTED ORDERS % OF INCIDENT
m=0
m=+1
m=-1
ANGLE OF GRAZING INCIDENCE IN DEGREES

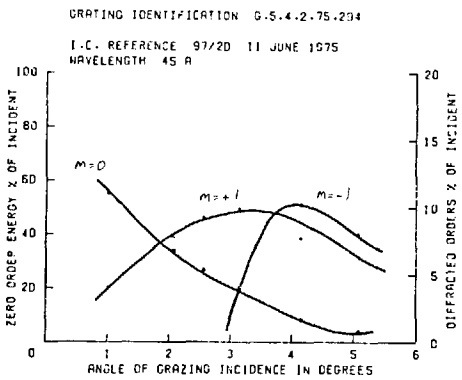
GRATING IDENTIFICATION G.5.4.2.75.294
I.C. REFERENCE 97/20 11 JUNE 1975
WAVELENGTH 45 A
ZERO ORDER ENERGY % OF INCIDENT
DIFFRACTED ORDERS % OF INCIDENT
m=0
m=+1
m=-1
ANGLE OF GRAZING INCIDENCE IN DEGREES

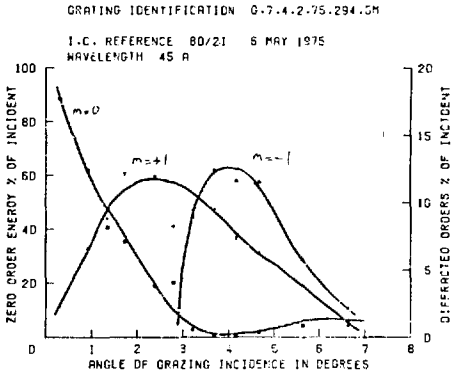
GRATING IDENTIFICATION G.7.4.2.75.294.5M
I.C. REFERENCE 80/21 6 MAY 1975
WAVELENGTH 45 A
ZERO ORDER ENERGY % OF INCIDENT
DIFFRACTED ORDERS % OF INCIDENT
m=0
m=+1
m=-1
ANGLE OF GRAZING INCIDENCE IN DEGREES

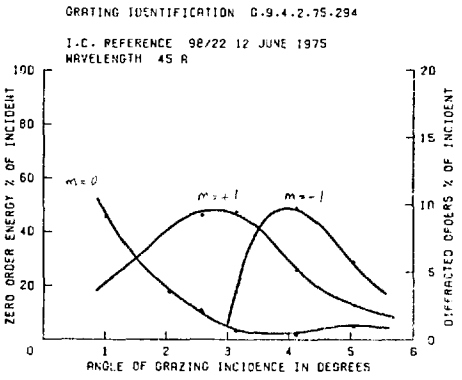
GRATING IDENTIFICATION G.9.4.2.75.294
I.C. REFERENCE 98/22 12 JUNE 1975
WAVELENGTH 45 A
ZERO ORDER ENERGY % OF INCIDENT
DIFFRACTED ORDERS % OF INCIDENT
m=0
m=+1
m=-1
ANGLE OF GRAZING INCIDENCE IN DEGREES

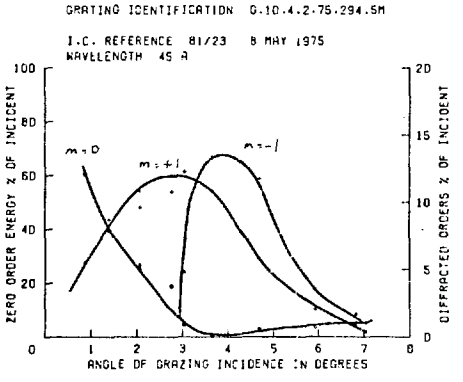
GRATING IDENTIFICATION G.10.4.2.75.294.5M
I.C. REFERENCE 81/23 8 MAY 1975
WAVELENGTH 45 A
ZERO ORDER ENERGY % OF INCIDENT
DIFFRACTED ORDERS % OF INCIDENT
m=0
m=+1
m=-1
ANGLE OF GRAZING INCIDENCE IN DEGREES

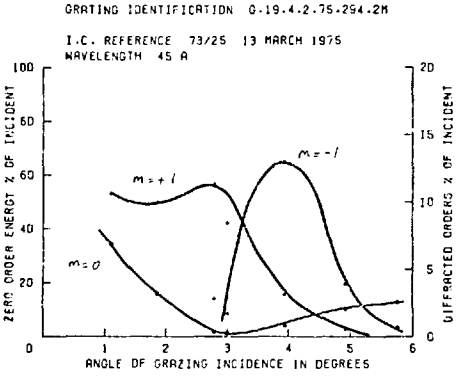
GRATING IDENTIFICATION G.19.4.2.75.294.2M
I.C. REFERENCE 73/25 13 MARCH 1975
WAVELENGTH 45 A
ZERO ORDER ENERGY % OF INCIDENT
DIFFRACTED ORDERS % OF INCIDENT
m=0
m=+1
m=-1
ANGLE OF GRAZING INCIDENCE IN DEGREES

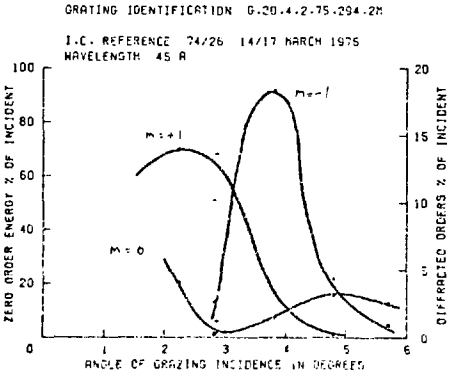
GRATING IDENTIFICATION G.20.4.2.75.294.2M
I.C. REFERENCE 74/26 14/17 MARCH 1975
WAVELENGTH 45 A
ZERO ORDER ENERGY % OF INCIDENT
DIFFRACTED ORDERS % OF INCIDENT
m=0
m=+1
m=-1
ANGLE OF GRAZING INCIDENCE IN DEGREES

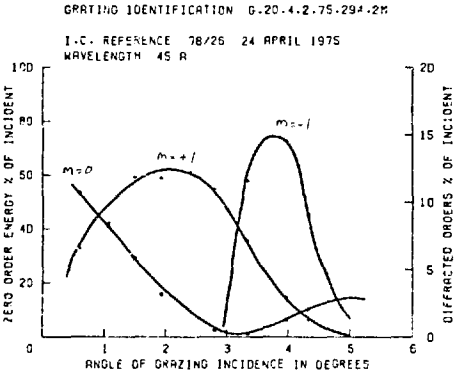
GRATING IDENTIFICATION G.20.4.2.75.294.2M
I.C. REFERENCE 78/26 24 APRIL 1975
WAVELENGTH 45 A
ZERO ORDER ENERGY % OF INCIDENT
DIFFRACTED ORDERS % OF INCIDENT
m=0
m=+1
m=-1
ANGLE OF GRAZING INCIDENCE IN DEGREES

FIG. 103 (b)

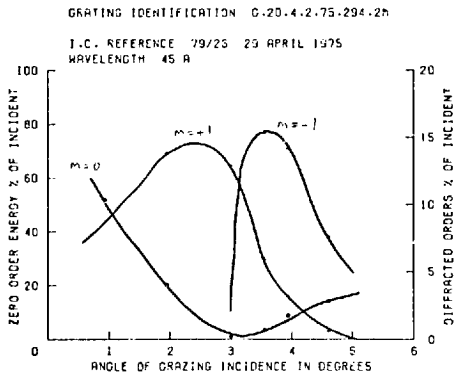
GRATING IDENTIFICATION G.20.4.2.75.294.2M
I.C. REFERENCE 79/23 29 APRIL 1975
WAVELENGTH 45 A
ZERO ORDER ENERGY % OF INCIDENT
DIFFRACTED ORDERS % OF INCIDENT
m=0
m=+1
m=-1
ANGLE OF GRAZING INCIDENCE IN DEGREES

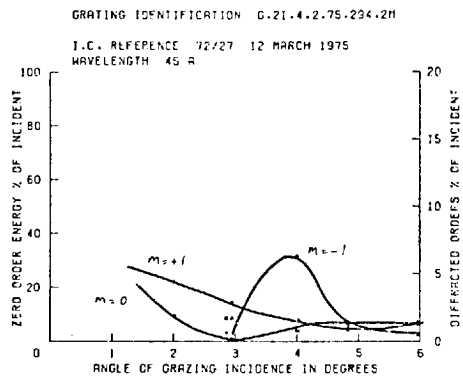
GRATING IDENTIFICATION G.21.4.2.75.294.2M
I.C. REFERENCE 72/27 12 MARCH 1975
WAVELENGTH 45 A
ZERO ORDER ENERGY % OF INCIDENT
DIFFRACTED ORDERS % OF INCIDENT
m=0
m=+1
m=-1
ANGLE OF GRAZING INCIDENCE IN DEGREES

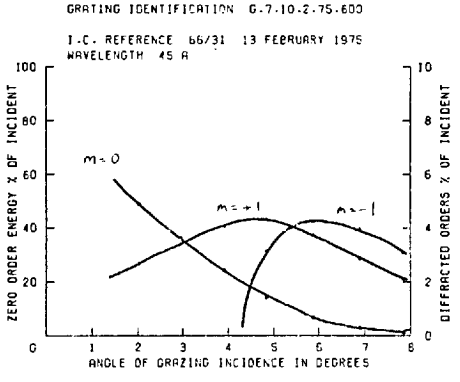
GRATING IDENTIFICATION G.7.10.2.75.600
I.C. REFERENCE 66/31 13 FEBRUARY 1975
WAVELENGTH 45 A
ZERO ORDER ENERGY % OF INCIDENT
DIFFRACTED ORDERS % OF INCIDENT
m=0
m=+1
m=-1
ANGLE OF GRAZING INCIDENCE IN DEGREES

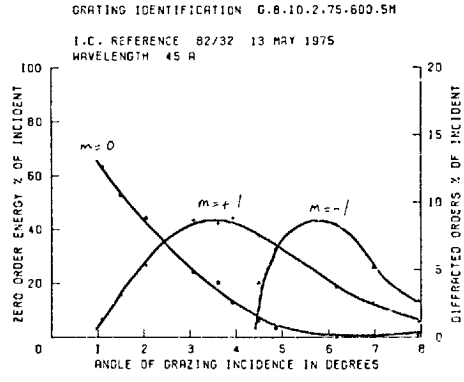
GRATING IDENTIFICATION G.8.10.2.75.600.5M
I.C. REFERENCE 82/32 13 MAY 1975
WAVELENGTH 45 A
ZERO ORDER ENERGY % OF INCIDENT
DIFFRACTED ORDERS % OF INCIDENT
m=0
m=+1
m=-1
ANGLE OF GRAZING INCIDENCE IN DEGREES

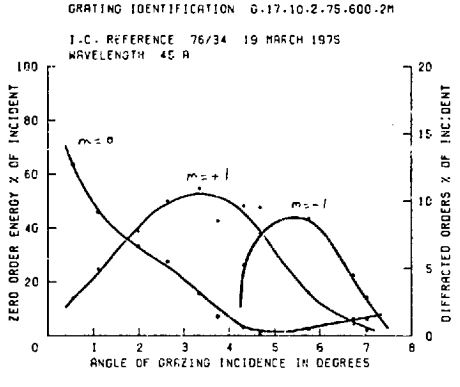
GRATING IDENTIFICATION G.17.10.2.75.600.2M
I.C. REFERENCE 76/34 19 MARCH 1975
WAVELENGTH 45 A
ZERO ORDER ENERGY % OF INCIDENT
DIFFRACTED ORDERS % OF INCIDENT
m=0
m=+1
m=-1
ANGLE OF GRAZING INCIDENCE IN DEGREES

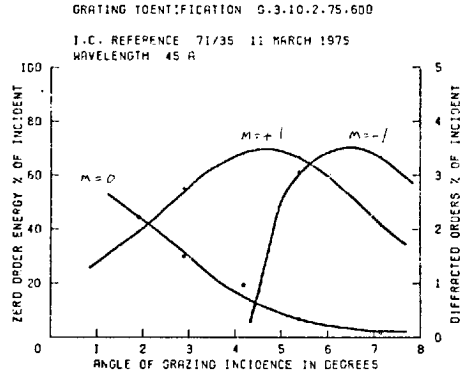
GRATING IDENTIFICATION G.3.10.2.75.600
I.C. REFERENCE 71/35 11 MARCH 1975
WAVELENGTH 45 A
ZERO ORDER ENERGY % OF INCIDENT
DIFFRACTED ORDERS % OF INCIDENT
m=0
m=+1
m=-1
ANGLE OF GRAZING INCIDENCE IN DEGREES

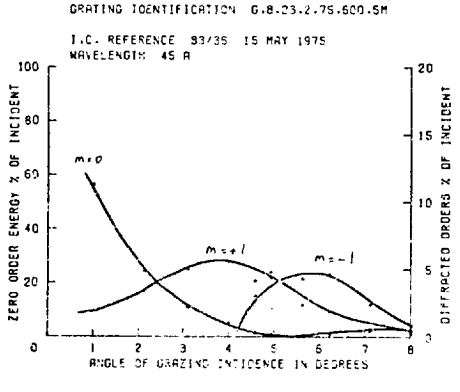
GRATING IDENTIFICATION G.8.23.2.75.600.5M
I.C. REFERENCE 83/35 15 MAY 1975
WAVELENGTH 45 A
ZERO ORDER ENERGY % OF INCIDENT
DIFFRACTED ORDERS % OF INCIDENT
m=0
m=+1
m=-1
ANGLE OF GRAZING INCIDENCE IN DEGREES

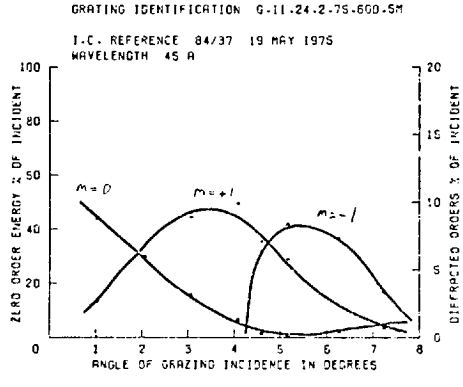
GRATING IDENTIFICATION G.11.24.2.75.600.5M
I.C. REFERENCE 84/37 19 MAY 1975
WAVELENGTH 45 A
ZERO ORDER ENERGY % OF INCIDENT
DIFFRACTED ORDERS % OF INCIDENT
m=0
m=+1
m=-1
ANGLE OF GRAZING INCIDENCE IN DEGREES

FIG. 103 (c)

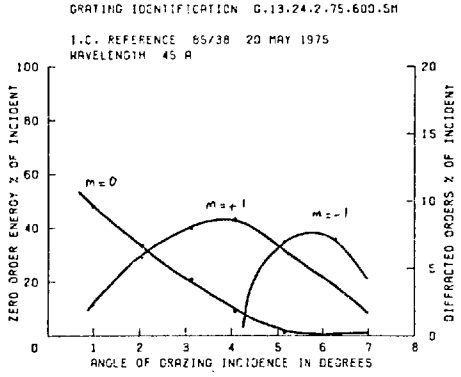
GRATING IDENTIFICATION G.13.24.2.75.600.SM
I.C. REFERENCE 86/38 20 MAY 1975
WAVELENGTH 45 A
ZERO ORDER ENERGY % OF INCIDENT
DIFFRACTED ORDERS % OF INCIDENT
m=0
m=+1
m=-1
ANGLE OF GRAZING INCIDENCE IN DEGREES

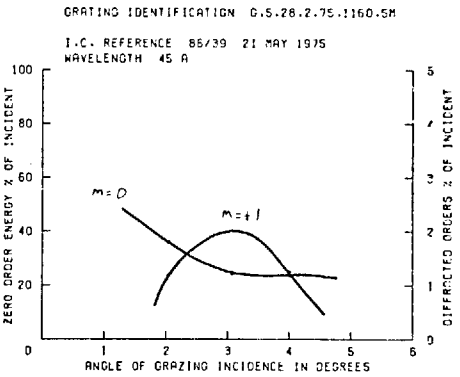
GRATING IDENTIFICATION G.5.28.2.75.1160.SM
I.C. REFERENCE 86/39 21 MAY 1975
WAVELENGTH 45 A
ZERO ORDER ENERGY % OF INCIDENT
DIFFRACTED ORDERS % OF INCIDENT
m=0
m=+1
ANGLE OF GRAZING INCIDENCE IN DEGREES

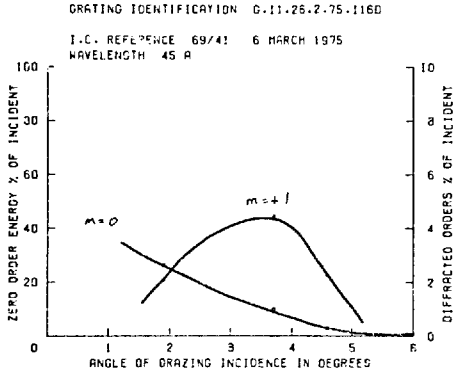
GRATING IDENTIFICATION G.11.26.2.75.1160
I.C. REFERENCE 69/41 6 MARCH 1975
WAVELENGTH 45 A
ZERO ORDER ENERGY % OF INCIDENT
DIFFRACTED ORDERS % OF INCIDENT
m=0
m=+1
ANGLE OF GRAZING INCIDENCE IN DEGREES

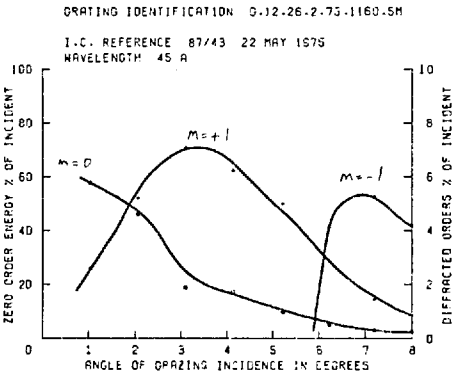
GRATING IDENTIFICATION G.12.26.2.75.1160.SM
I.C. REFERENCE 87/43 22 MAY 1975
WAVELENGTH 45 A
ZERO ORDER ENERGY % OF INCIDENT
DIFFRACTED ORDERS % OF INCIDENT
m=0
m=+1
m=-1
ANGLE OF GRAZING INCIDENCE IN DEGREES

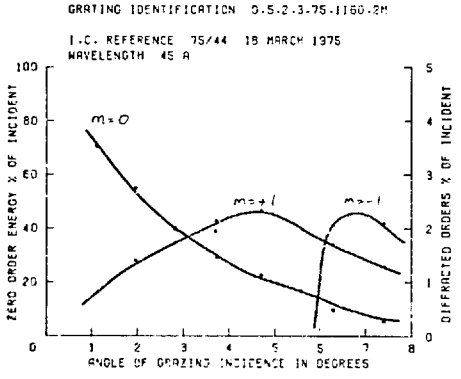
GRATING IDENTIFICATION G.5.2.3.75.1160.SM
I.C. REFERENCE 75/44 18 MARCH 1975
WAVELENGTH 45 A
ZERO ORDER ENERGY % OF INCIDENT
DIFFRACTED ORDERS % OF INCIDENT
m=0
m=+1
m=-1
ANGLE OF GRAZING INCIDENCE IN DEGREES

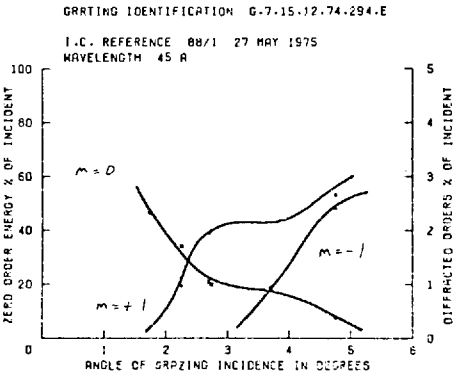
GRATING IDENTIFICATION G.7.15.12.74.294.E
I.C. REFERENCE 88/1 27 MAY 1975
WAVELENGTH 45 A
ZERO ORDER ENERGY % OF INCIDENT
DIFFRACTED ORDERS % OF INCIDENT
m=0
m=+1
m=-1
ANGLE OF GRAZING INCIDENCE IN DEGREES

FIG. 103 (d)

and land to groove ratio so that it could not be expected that all of the gratings would have high efficiencies. However, it was a pleasant surprise to find that most of the gratings had high diffraction efficiencies.

The 294 l/mm gratings form the most complete set and since shadowing effects are least at low frequencies, data from these gratings can be readily compared with results from the scalar theory of the laminar grating.

From the equation for optical path length and the grating equation relations for predicting the positions of efficiency maxima and minima may be readily derived, as follows:

$$\text{Optical path length} \quad h(\sin\alpha + \sin\beta) = \frac{n\lambda}{2}$$

$$\therefore \quad \sin\beta = \frac{n\lambda}{2h} - \sin\alpha$$

$$\text{From the grating equation} \quad \cos\beta = \cos\alpha \frac{-m\lambda}{d}$$

Squaring and adding yields:

$$\frac{n^2\lambda}{4h^2} - \frac{n}{h}\sin\alpha - \frac{2m.\cos\alpha}{d} + \frac{m^2\lambda}{d^2} = 0 \qquad (7.1)$$

Hence, maxima and minima in the efficiency curves occur when:

$$\lambda = \frac{2m\cos\alpha/d + n.\sin\alpha/h}{n^2/4h^2 + m^2/d^2}$$

Alternatively, Eq. 7.1 yields a quadratic in h.

$$(8md\cos\alpha - 4m^2\lambda)h^2 + 4nhd^2\sin\alpha - n^2\lambda d^2 = 0$$

$$\sin\alpha = \frac{n\lambda}{4h} - \frac{2mh.\cos\alpha}{nd} + \frac{m^2\lambda h}{nd^2}$$

Minima in the zero order efficiency curve occur for:

$$\sin\alpha_{0\ \min} = \frac{\lambda}{4h}, \frac{3\lambda}{4h} \cdots \tag{7.2}$$

In the first positive order the peak of the primary maximum occurs at:

$$\sin\alpha_{+1\ \max} = \frac{\lambda}{4h} - \frac{2h.\cos\alpha_{+1\ \max}}{d} + \frac{\lambda h}{d^2} \tag{7.3}$$

In the first negative order the peak of the primary maximum occurs at:

$$\sin\alpha_{-1\ \max} = \frac{\lambda}{4h} + \frac{2h.\cos\alpha_{-1\ \max}}{d} + \frac{\lambda h}{d^2} \tag{7.4}$$

The above equations may be used to calculate the effective groove depth of a laminar grating from the angular positions of the maxima and minima in the experimental efficiency curves. If distinct maxima are obtained in the first positive and negative orders, the following equations may be applied:

Adding equations 7.3 and 7.4 yields:

$$h = \lambda/2(\sin\alpha_{+1\ \max} + \sin\alpha_{-1\ \max}) \tag{7.5}$$

Subtracting equations 7.3 and 7.4 and assuming $\cos\alpha \simeq 1$ yields:

$$h = \frac{1}{4} d\ (\sin\alpha_{-1\ \max} - \sin\alpha_{+1\ \max}) \tag{7.6}$$

In order to check whether the experimental results are in basic agreement with the theory of the laminar grating, it is convenient to tabulate the maximum efficiencies and the angles of maximum efficiencies

in the diffracted orders and also the minimum zero order efficiency and the angle at which it occurs. The results for the 294 l/mm gratings are tabulated, according to the nominal groove depths, in Table 4. It can be seen that the angles at which the zero order minima occur are consistent between the groups of gratings with given nominal groove depths apart from one exception, grating no. 17 (this grating will be considered in greater detail later).

From equation 7.2 an angle $\alpha_{0\,min} = 5^{o}$ corresponds to a groove depth h = 128 Å, $\alpha_{0\,min} = 4^{o}$ corresponds to h = 160 Å, and $\alpha_{0\,min} = 3^{o}$ corresponds to 214 Å. Thus, there is broad general agreement between the nominal groove depths and those predicted by equation 7.2.

The positions of the maxima in the first positive and negative orders are not as consistently defined as the zero order minima, however, by taking averages it was hoped to obtain more significant data. Application of equations 7.5 and 7.6 to the average in Table 4 yielded good agreement for the gratings with a nominal 20nm groove depth but produced excessively large results for the other data. Equation 7.5 produced a groove depth of 21nm from the averaged 20nm data and equation 7.6 produced a groove depth of 22nm. Thus it appears that equation 7.2 has more general validity than equations 7.5 and 7.6.

From the sample of data given in Table 4 it is not possible to find any direct correlation between grating efficiency and land to groove ration although land to groove ratios of about unity seem to be most favourable. The variations in the positions and magnitude of the efficiency maxima indicate that there are some structural differences between the gratings. If grating no. 24, which was made

TABLE 4

SUMMARY OF RESULTS FROM THE 294 1/mm GRATINGS AT 45 Å

	Grating Number	Land/Groove Ratio	Efficiency maxima m=+1	Efficiency maxima m=-1	Efficiency minimum m=0	Angle of Grazing Incidence maxima α_{+1}	Angle of Grazing Incidence maxima α_{-1}	Angle of Grazing Incidence minimum α_0
h = 7nm	20	1.5	9.8	10.1	-	3.2	4.2	5+
h = 10nm	15	0.6	9.3	9.3	1	3.5	5.0	5+
	14	0.7	7.5	7.4	1	3.2	4.25	5
	10	0.8-0.9	6.8	6.4	0.5	3.25	4.2	5.2
	16	0.9	10.2	10.1	0.8	2.5	4.2	5
	11	1	10	10.5	0.5	3	4.2	5
						Av. 3.09	4.37	5.08
						σ 0.37	0.35	0.11
h = 15nm	23	0.9	11.0	12.7	0.5	2.75	3.75	3.8
	22	1	9.4	9.8	1.5	3.1	4.2	4
	21 (5M)	1.1	12.3	12.3	0.8	2	4	4
						Av. 2.62	3.98	3.93
						σ 0.56	0.23	0.12
h = 20nm	12	0.4-0.5	11	10	1	2	3.5	2.5
	13	0.5-0.6	11	10.5	1	2.5	4.0	3.2
	17	1	10.5	10.9	2	3.1	3.8	5
	18	1	12.3	12	1.1	2.1	3.4	3.1
	24 (2M,R)	<1	6	5.6	4.3	3.1	4.1	3.1
	25 (2M)	<1	11	12.8	2	2.3	4.2	3.2
	26 (2M)	<1	14	18	1	2.1	3.7	3.1
	27 (2M)	<1	4.4	6.4	0.7	2	3.8	3
						Av. 2.3	3.81	3.03
						σ 0.40	0.30	0.24

All the above gratings were coated with 30nm gold except no. 17 which had 10nm and no. 18 which had 50 nm.

on a low-quality replica blank, and grating no. 27 are excluded, the six gratings with a nominal 20nm groove depth have an average first order efficiency in excess of 11.6%. The three gratings with a nominal groove depth of 15nm have an average first order efficiency of 10.9% and the other gratings have an average first order efficiency of 8.9%. Thus gratings produced by the author's method exhibit consistently high diffraction efficiencies at 45 Å comparable to the best available gratings.

The consistent results indicate that the process has high stability especially considering that only an optical microscope was used to inspect the gratings when they were made. An optical microscope has only sufficient resolution to show the gross structure and defects in diffraction gratings and is incapable of showing the groove profile and fine structure which have a marked influence on diffraction efficiency. The nature of the "etching process" is such that the groove depth is determined by thickness of the deposited metal layer which can be controlled accurately. In order to verify that the correct groove profiles were formed, some of the grating profiles were measured using a modified "Talystep" as described by Verrill (136). Groove profiles measured from grating nos. 17, 18 and 19 are shown in Fig. 104. The three gratings were prepared sequentially under the same conditions and they appeared to be identical under the optical microscope. As noted earlier grating no. 17 had unusual diffractive properties and these are clearly due to the non-laminar profile. Since grating no. 17 also has a high diffraction efficiency

GROOVE PROFILES MEASURED FROM GRATINGS NOS. 17, 18 AND 19

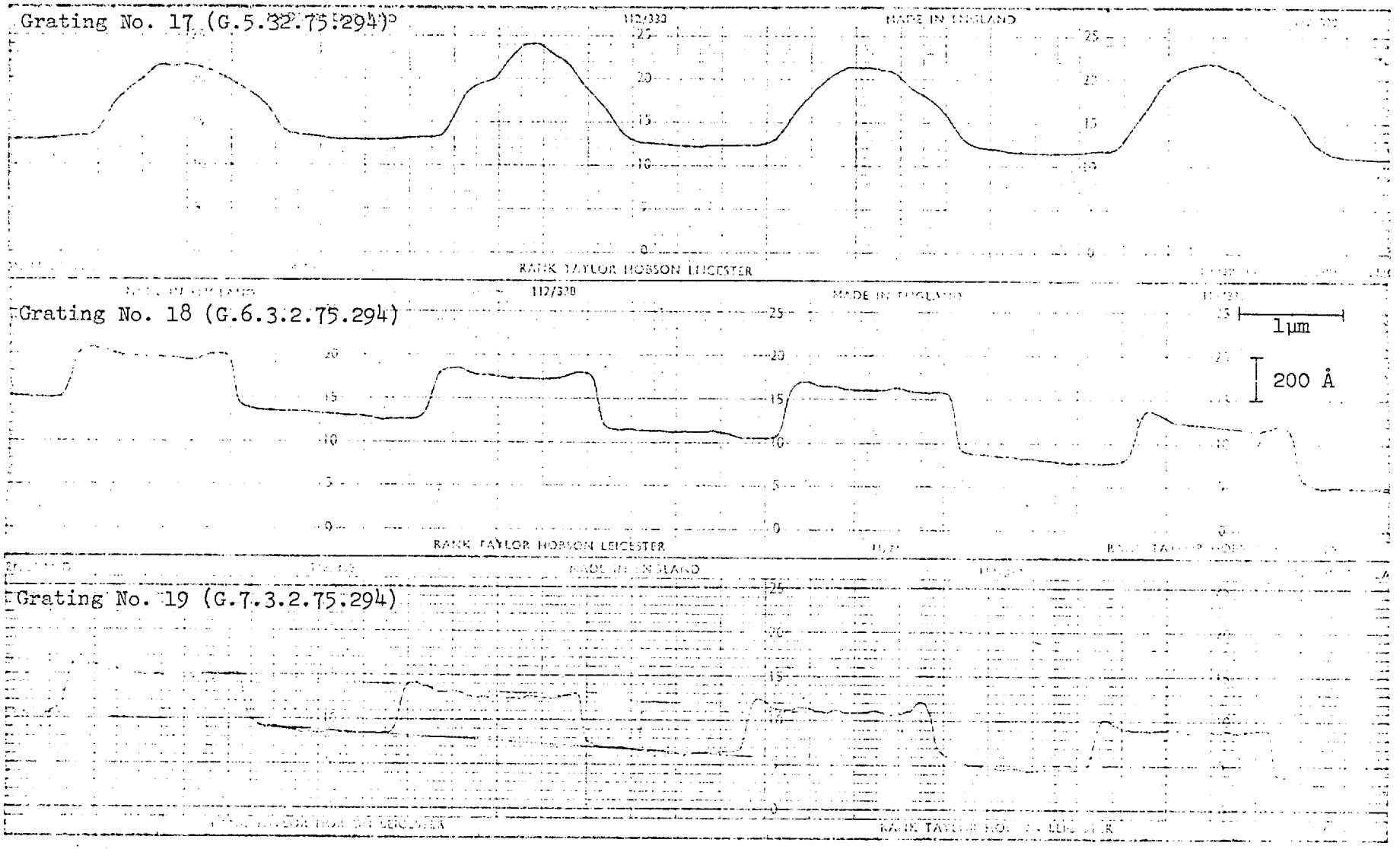

FIG. 10h

it indicates that gratings with other than laminar profiles can have high efficiencies in the soft x-ray region. It is conceivable that gratings with profiles intermediate between laminar and blazed gratings could provide high efficiencies over extended wavelength ranges.

The 294 l/mm gratings were produced over a period of one month, the 600 l/mm gratings in two weeks and the 1160 l/mm gratings during the last few days of my stay in Germany. The results from the 600 l/mm and 1160 l/mm gratings are summarised in Table 5 and Table 6. The maximum efficiency recorded from the 600 l/mm gratings was 11% and although the average efficiency is somewhat less than that of the 294 l/mm gratings, four of the gratings have efficiencies >8%. It is interesting to note that all the 600 l/mm gratings with high efficiencies were formed on high-quality blanks (gratings nos. 31 and 35 were formed on old plane blanks and grating no. 33 was formed on a replica blank). It is possible that surface roughness on the blanks causes anisotropic etching and a consequent reduction in diffraction efficiency.

The few gratings made with 1160 l/mm do not form a representative sample since they were produced quickly using the few remaining grating blanks. It was quite easy to control the processing of these higher frequency gratings by visual observation with an oil-immersion objective on the microscope. However, the efficiencies of these gratings are considerably less than those of the lower frequency gratings apart from one exception - grating no. 43. This grating had a maximum efficiency of 7.1% in the first positive order which indicates that high efficiencies may be obtained from high frequency gratings

TABLE 5

SUMMARY OF RESULTS FROM THE 600 l/mm GRATINGS AT 45 Å

	Grating Number	Land/Groove Ratio	Efficiency maxima m=+1	Efficiency maxima m=-1	Efficiency minimum m=0	Angle of Grazing Incidence maxima α_{+1}	Angle of Grazing Incidence maxima α_{-1}	Angle of Grazing Incidence minima α_0
h = 10nm	31	0.6	4.3	4.3	0.3	4.7	6.2	10
	32 (5M)	<1	8.8	8.3	0.3	3.75	6.1	7
	37 (5M)	1	9.8	8.7	1	3.6	5.4	5.2
	38 (5M)	1	8.25	7.6	0.5	3.8	5.7	6.5
	34 (2M)	>1	11	9.5	0.9	3.25	4.8	4.8
	35	1.5	3.4	3.3	1.8	5	7.2	7
	33 (2M,R)	>2	2	-	-	3	-	-
h = 14nm	36 (5M)		5.5	5	1	4	5.5	5.2

The gold coating on gratings nos. 31 and 32 was 30nm, on gratings nos. 33 and 34 it was 45nm and on gratings nos. 35, 36, 37 and 38 it was 60nm.

TABLE 6

SUMMARY OF RESULTS FROM THE 1160 l/mm GRATINGS AT 45 Å

	Grating Number	Land/Groove Ratio	Efficiency Maxima m=+1	m=-1	Angle of Grazing Incidence α_{+1}	α_{-1}
h = 10nm	39 (5m)	0.4	2	-	3	-
	42	>1	1.3	-	2.2	-
h = 11nm	41	>1	4.4	-	3.75	-
	43 (5m)	>1	7.1	5.2	3	7
h = 12nm	44 (2m)	>>1	2.3	2.2	4.5	7
h = 17nm	40	>1	2.78	-	3.8	-

All coated with 60nm gold.

made by the "etching technique".

In order to discover why some of the 1160 l/mm gratings had reduced efficiencies compared with the lower frequency gratings, it was decided to investigate the surface topography of the gratings. The use of the "Talystep" has already been mentioned and it is most useful for obtaining surface profiles. However, for obtaining general details about the surface structure, transmission electron micrographs produced from a replica of the surface are more suitable. Electron micrographs made from carbon-platinum shadowed replicas taken from gratings no. 40 and no. 18 are shown in Fig. 105.

The profile of grating no. 40 measured with a Talystep is reproduced in Fig. 106 and it is clear that there are discrepancies between this profile and that in the electron micrograph. The second profile shown in Fig. 106 is that of the 1200 l/mm Jobin et Yvon grating which should be sinusoidal. Hence it is clear that the Talystep has limited applicability to gratings with frequencies greater than 1000 l/mm and it is necessary to consider the shape and size of the stylus when interpreting Talystep results. The lands of grating no. 40 are only 0.3μm wide and it is remarkable that chemical etching of such fine structures can be readily achieved. The electron micrograph of grating no. 40 clearly shows that the substrate is scratched and has other imperfections and it appears that the surface imperfections lead to a reduction of edge acuity. Although grating no. 18 has a much higher efficiency than grating no. 40, the electron micrograph of grating no. 18 shows that the surface of the grating is also imperfect and it appears to be pitted.

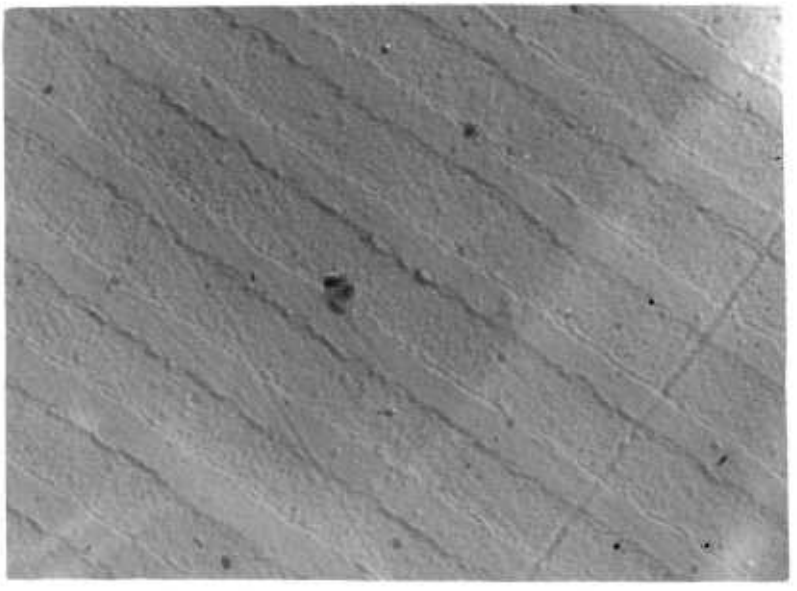

TRANSMISSION ELECTRON MICROGRAPHS FROM GRATINGS
NO. 40 (G.2.26.2.75.1160) AND NO. 18 (G.6.3.2.75.294)
C-Pt SHADOWED AT 45°

FIG. 105

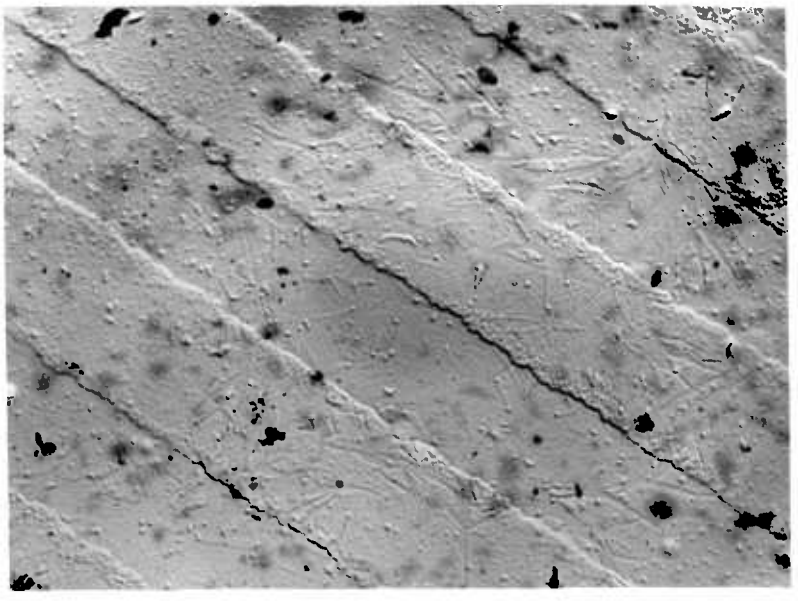

THE GROOVE PROFILE OF GRATING NO. 40 (G.2.26.2.75.1160)

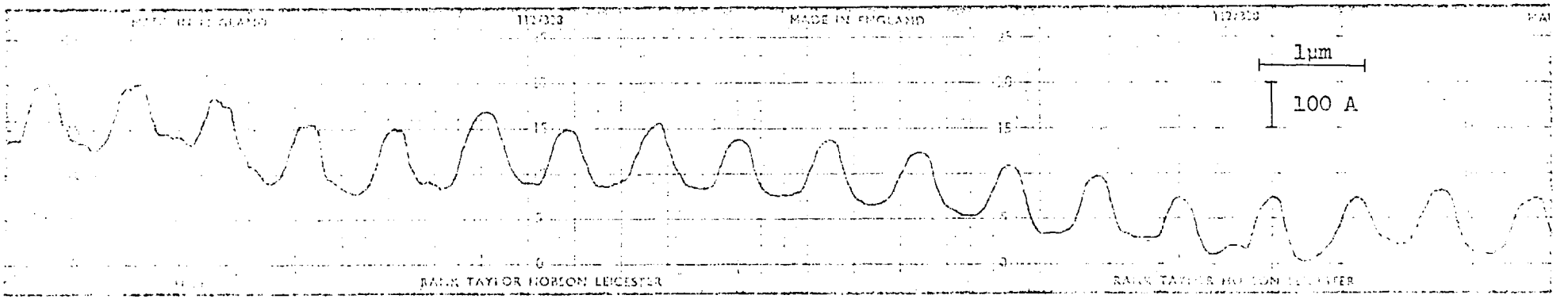

FIG. 106

THE GROOVE PROFILE OF A JOBIN-YVON 1200 l/mm HOLOGRAPHIC GRATING

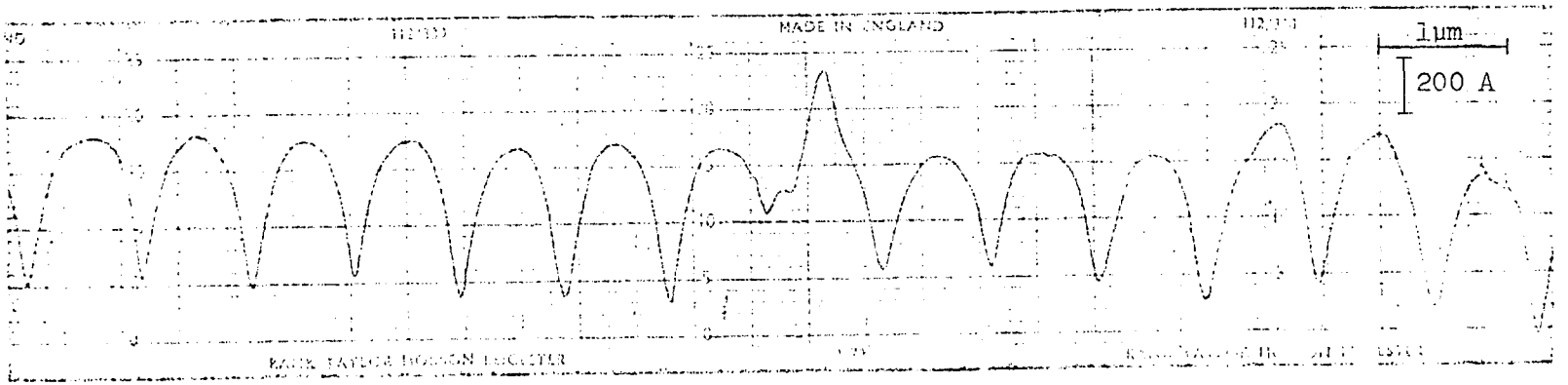

The electron micrographs prepared from the two gratings do not show the cause of the reduced efficiency of the higher frequency gratings but they do show that the surface finish of the substrates used for these prototype gratings is rather low. It is to be expected that the use of higher quality blanks will enable consistently better results to be obtained.

A selection of six of the gratings made by the etching technique have been tested at 8.3 Å. The peak efficiencies of these gratings are summarised in Table 7 and the dependence of grating efficiency on grazing angle for gratings nos. 11, 32, 37 and 43 are shown in Fig. 107 and Fig. 108. It can be seen that the gratings produced by the author also have high efficiencies at 8.3 Å. The maximum efficiencies are somewhat less than those achieved by the N.P.L. laminar gratings and this can be attributed to substrate imperfections of the author's gratings. It is clear that the N.P.L. techniques are more suitable for producing laminar gratings for use at very short wavelengths. However, the author's technique enables laminar holographic gratings, which are highly efficient in the soft x-ray region, to be readily fabricated without specialised equipment.

A summary of the best 22 results obtained at 45 Å arranged according to grating frequency is shown in Fig. 109 and the individual gratings may be identified by referring to Table 8. As a result of intensive research the efficiencies of gratings with 300 l/mm and 600 l/mm have now reached satisfactory levels. The aim of future research on soft x-ray gratings should be to increase the performance of gratings with 1200 l/mm and higher frequencies so that higher spectral resolution can be attained.

TABLE 7

SUMMARY OF GRATING EFFICIENCY MEASUREMENTS AT 8.3 Å

Grating Number	Frequency (mm^{-1})	Groove Depth (nm)	Efficiency Maxima m+1	m-1	Angle of Grazing Incidence α_{+1}	α_{-1}
11	294	10	4.2	7.5	1.6	2.1
21	294	15	5.5	-	1.0	-
32	600	10	7.9	6.6	1.7	2.2
37	600	10	5.8	4.5	1.1	2.1
38	600	10	6.5	5.3	1.1	2.2
43	1160	11	1.4	1.1	1.6	3.1

GRATING IDENTIFICATION G.7.12.1.75.294

I.C. REFERENCE 111/11 25 JULY 1975
WAVELENGTH 8.3 Å

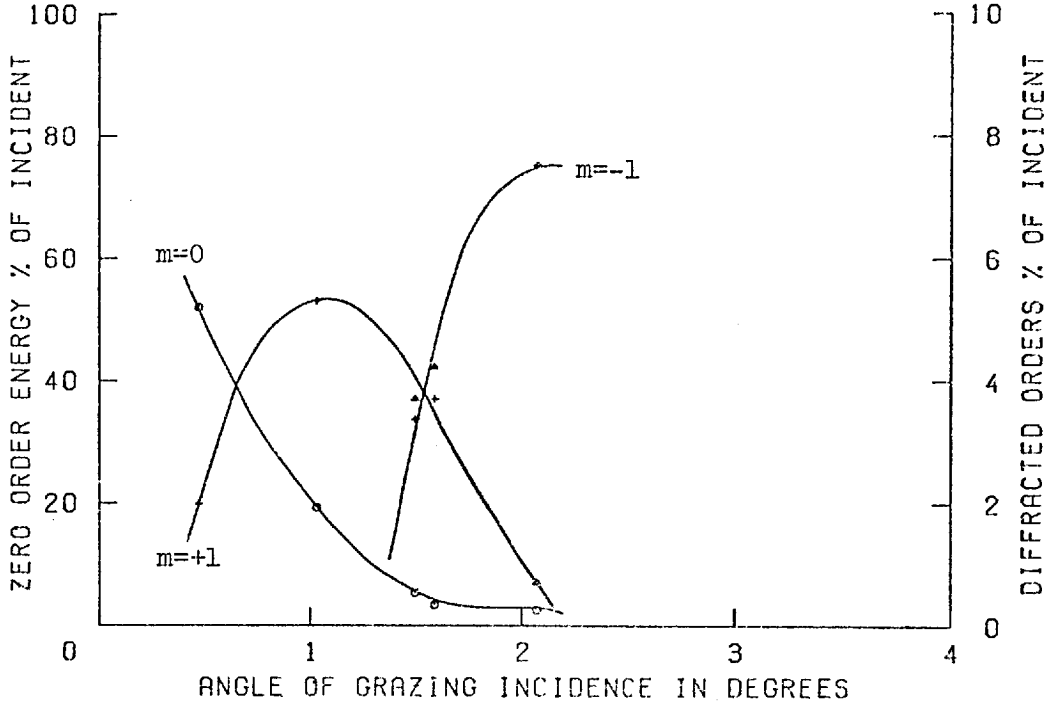

GRATING IDENTIFICATION G.8.10.2.75.600.5M

I.C. REFERENCE 104/32 15 JULY 1975
WAVELENGTH 8.3 Å

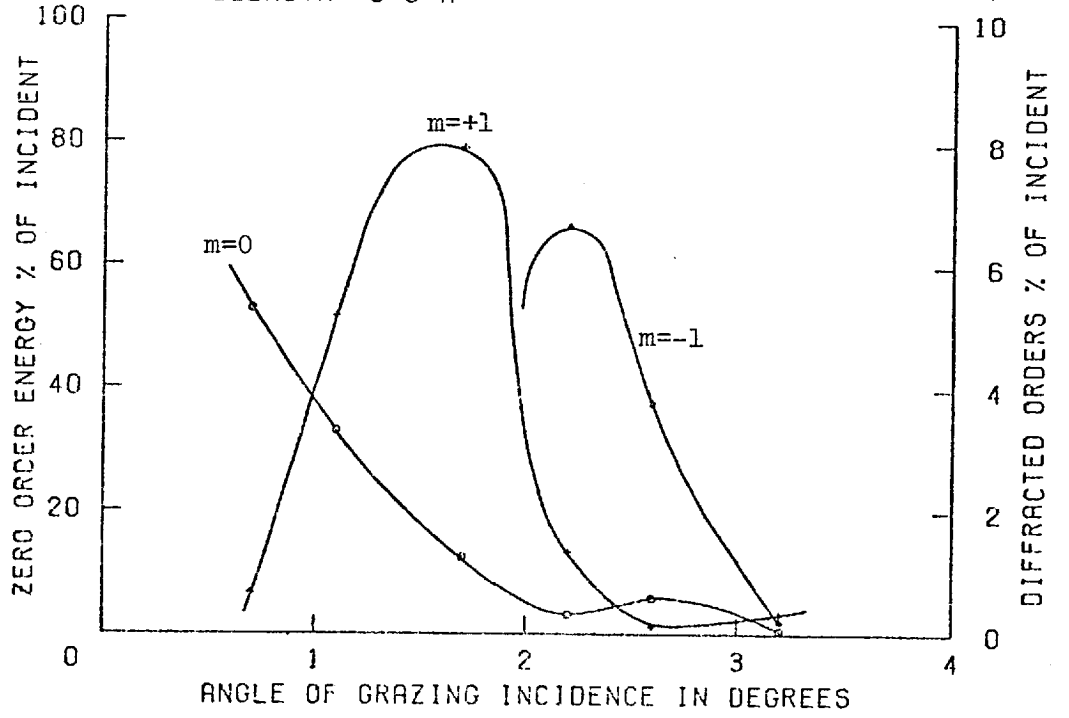

FIG. 107

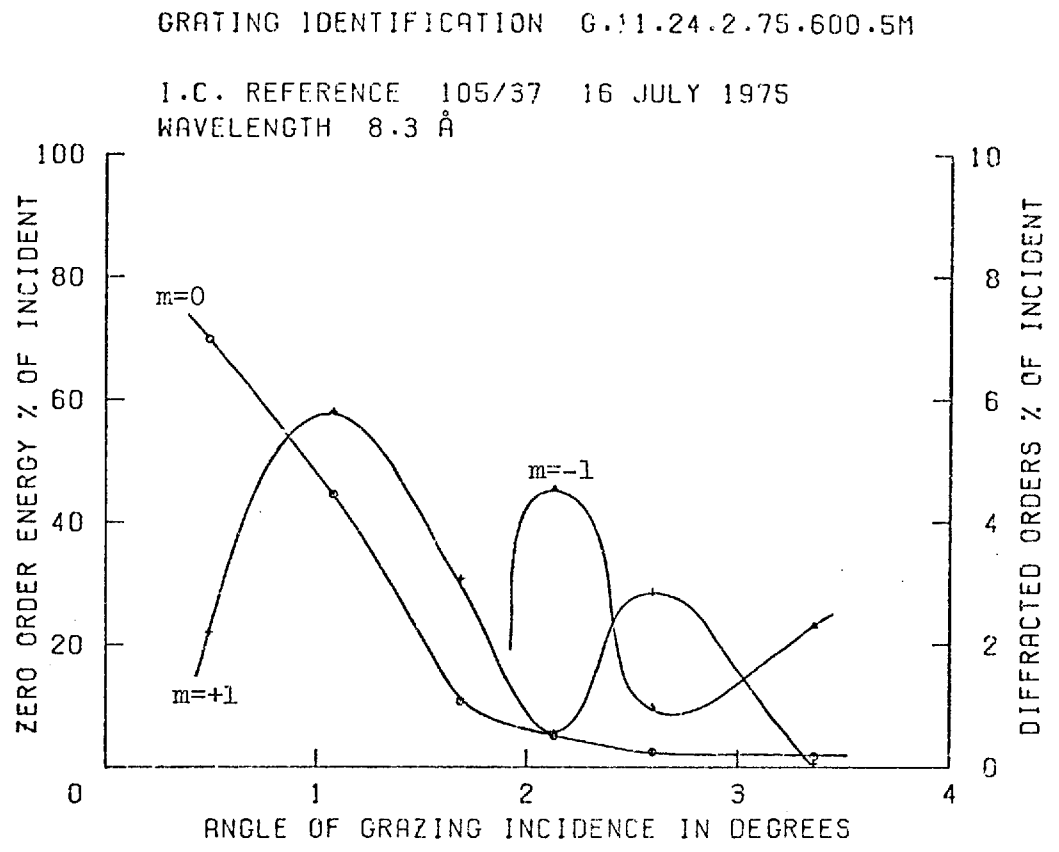
GRATING IDENTIFICATION G.11.24.2.75.600.5M
I.C. REFERENCE 105/37 16 JULY 1975
WAVELENGTH 8.3 Å
ZERO ORDER ENERGY % OF INCIDENT
DIFFRACTED ORDERS % OF INCIDENT
m=0
m=-1
m=+1
ANGLE OF GRAZING INCIDENCE IN DEGREES

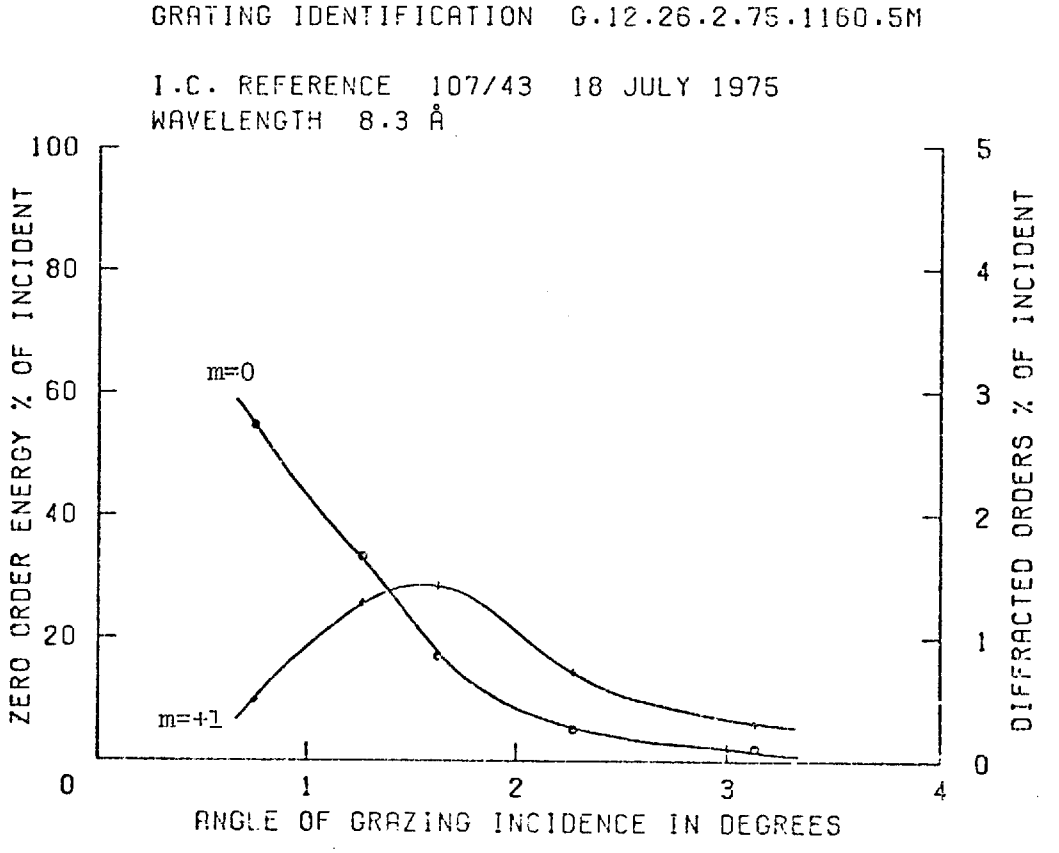
GRATING IDENTIFICATION G.12.26.2.75.1160.5M
I.C. REFERENCE 107/43 18 JULY 1975
WAVELENGTH 8.3 Å
ZERO ORDER ENERGY % OF INCIDENT
DIFFRACTED ORDERS % OF INCIDENT
m=0
m=+1
ANGLE OF GRAZING INCIDENCE IN DEGREES

FIG. 108

SUMMARY OF THE BEST 22 RESULTS AT 45 Å ARRANGED ACCORDING TO GRATING FREQUENCY

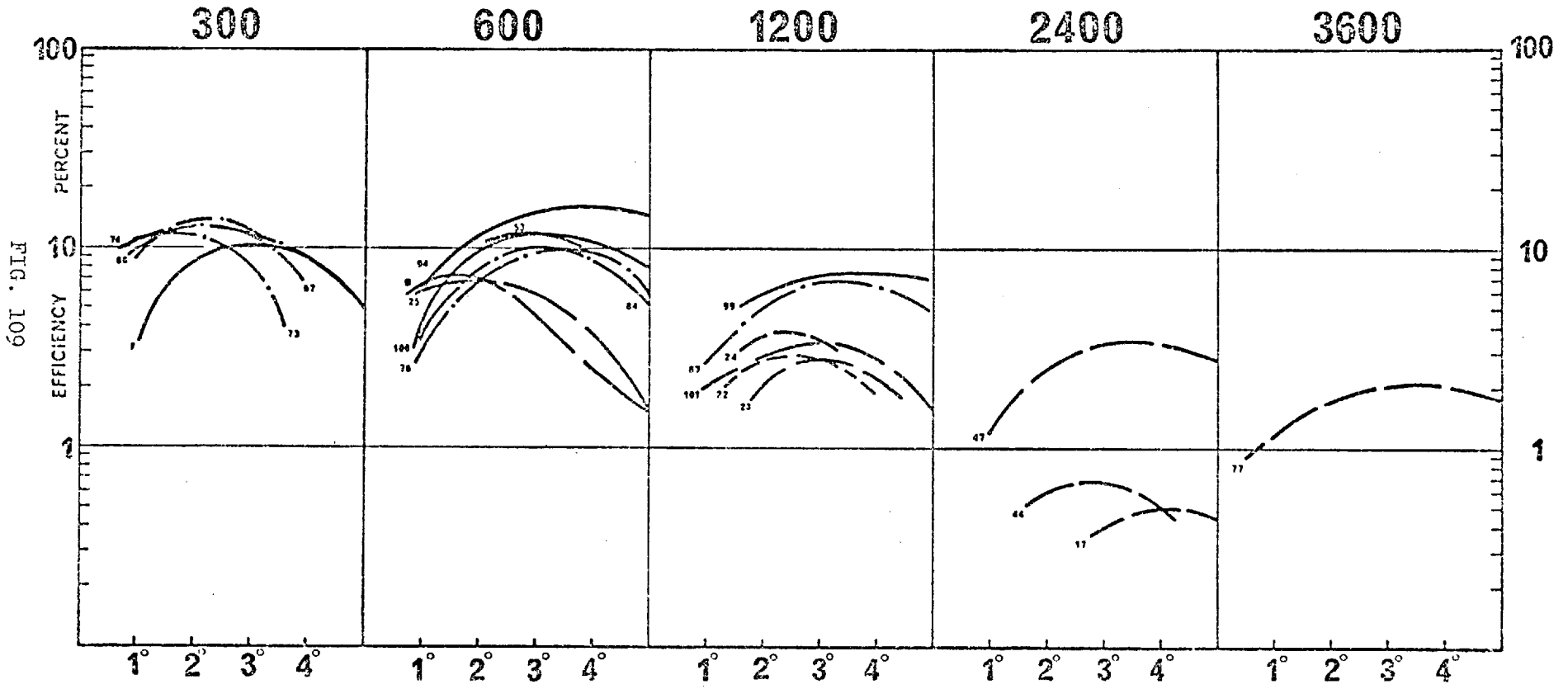

FIG. 109

TABLE 8

A LIST OF THE 22 GRATINGS WHICH PRODUCED THE BEST RESULTS AT 45 Å

Code	Radius	Origin	Catalogue No.	Serial No.	Type
17	2 M	B + L	35-52-37-800	2553-6-1-1	Shallow Blazed, Ruled
22	Plane	J.Y.	-	-	Holographic
23	2 M	B + L	35-52-40-700	2517-2-4-5	Shallow Blazed, Ruled, Pt.
24	2 M	B + L	35-52-40-700	2517-2-5-8	Shallow Blazed, Ruled, Pt.
25	2 M	B + L	35-52-40-400	2278-32-1-3	Shallow Blazed, Ruled, Pt.
44	2 M	B + L	35-62-41-800	1194-6-3	Shallow Blazed, Ruled, Pt.
47	2 M	B + L	35-52-41-800	1194-5-2	Shallow Blazed, Ruled, Au.
53	5 M	N.P.L.	-	156	Laminar, Ruled, Au.
67	Plane	Göttingen/IC	G.6.3.2.75.294	18	Laminar, Holographic, Au.
73	2 M	Göttingen/IC	G.19.4.2.75.294.2M	25	Laminar, Holographic, Au.
74	2 M	Göttingen/IC	G.20.4.2.75.294.2M	26	Laminar, Holographic, Au.
76	2 M	Göttingen/IC	G.17.10.2.75.600.2M	34	Laminar, Holographic, Au.
77	1 M	B + L	55-72-36-900	1068-1-1-1-4	Shallow Blazed, Ruled, Au.
80	5 M	Göttingen/IC	G.7.4.2.75.294.5M	21	Laminar, Holographic, Au.
84	5 M	Göttingen/IC	G.11.24.2.75.600.5M	37	Laminar, Holographic, Au.
87	5 M	Göttingen/IC	G.12.26.2.75.1160.5M	43	Laminar, Holographic, Au.
94	Plane	N.P.L.	-	194 (IBG 2)	Shallow Blaze, Holographic, Au.
99	Plane	N.P.L.	-	177	Shallow Blaze, Holographic, Au.
100	5 M	N.P.L.	-	173	Laminar, Ruled, Original, Au.
101	2 M	B + L	35-52-40-700	2517-2-6-3	Shallow Blazed, Ruled, Pt.
B	2 M	B + L	35-52-40-400	2278-30-2-6	Shallow Blazed, Ruled, Pt.
F	Plane	N.P.L.	-	83	Laminar, Ruled, Original, Au.

7.3 COMPARISON OF SCATTERED LIGHT DISTRIBUTIONS

In the visible and UV regions it has been observed that holographic gratings can have lower scattered light than mechanically ruled gratings (137). One can distinguish between two forms of scattered light from diffraction gratings; the first form is due to errors in the positioning of the rulings and the second form, diffused scattering, is due to surface imperfections. Since holographic gratings are produced by an essentially static process, ruling errors are eliminated resulting in reduced scattered light and an absence of "ghosts".

In the soft x-ray region it has been found that holographic gratings generally have lower scattered light levels than mechanically ruled gratings. The most direct method for assessing scattered light is to compare spectra recorded under identical conditions from different gratings. It is necessary to examine a large number of spectra recorded at different angles of incidence in order to be able to form general conclusions. Hence, to facilitate intercomparisons of spectra and enable quantitative measurements of scattered light to be made in the future, the geometry and conditions in the grating test apparatus have now been standardised. However, at present the differences between ruled and holographic gratings will be illustrated by direct comparisons of the experimentally observed energy distributions.

Typical experimental data recorded from a shallow blazed ruled grating at two angles of incidence is shown in Fig. 110. A logarithmic histogram presentation is used in which the ordinate is the logarithm of the number of counts recorded per channel and

GRATING IDENTIFICATION B+L 2517.2.6.3

I.C. REFERENCE 101 8 JULY 1975
WAVELENGTH 45 Å
ANGLE = 2.27

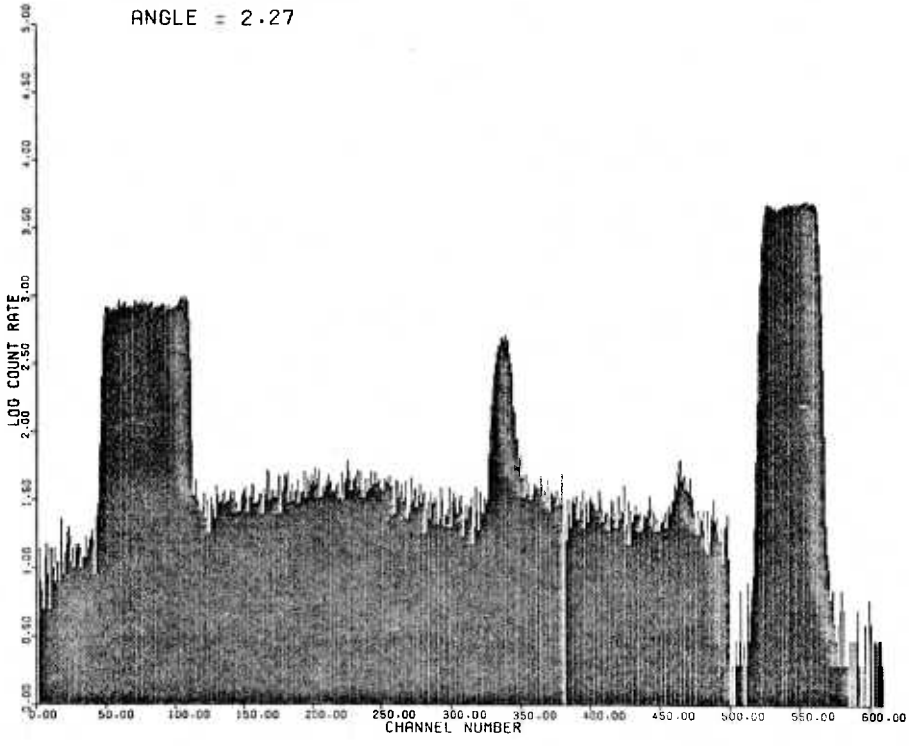

GRATING IDENTIFICATION B+L 2517.2.6.3

I.C. REFERENCE 101 8 JULY 1975
WAVELENGTH 45 Å
ANGLE = 3.36

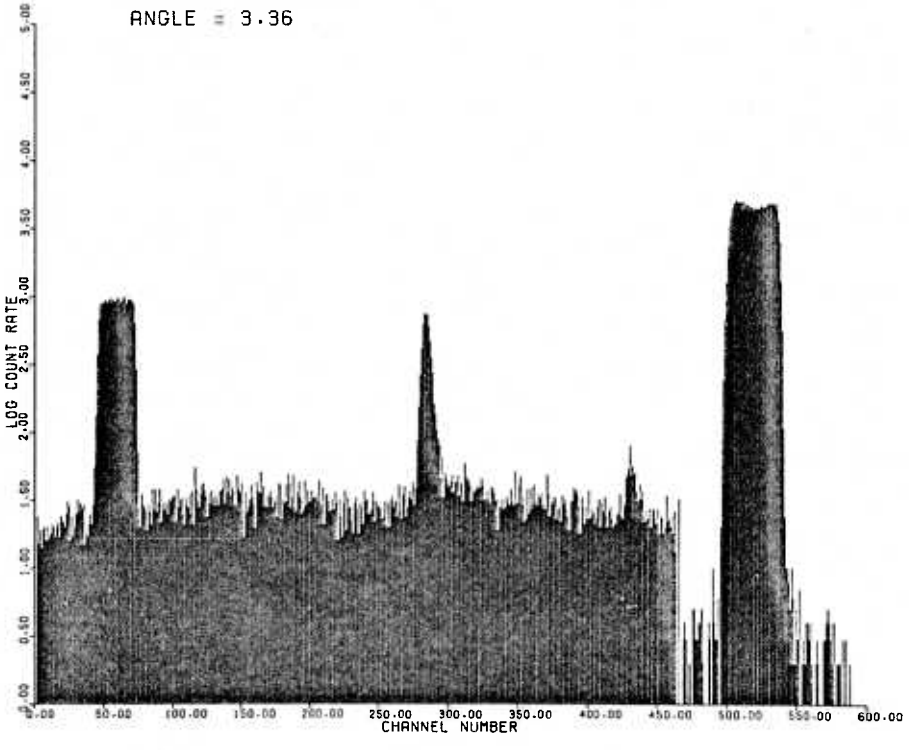

FIG. 110

the abscissa is the channel number, which corresponds to the detector position. The peaks in Fig. 110 represent the zero order, first positive order, second positive order and finally the direct beam which is recorded after the grating has been retracted. The instrument noise level can be seen in the portions of the spectra adjacent to the direct beam (it is ∿2cps). It is clear from these spectra that the ruled grating produces a significant level of scattered radiation.

In Fig. 111 are shown a series of spectra recorded from a shallow blazed grating with 3600 l/mm. The scattered radiation from this grating has a different form from that shown in Fig. 110 but it is clear that the grating is producing scattered light levels much greater than the background.

A typical spectrum produced by one of the author's laminar holographic gratings is shown in Fig. 112. It can be seen that the count rates between the peaks are much lower than for the ruled gratings and that they are closely approaching the background count rates. A series of spectra in Fig. 113 shows the dependence of the scattered light distributions on angle of grazing incidence for this holographic grating. It can be seen that the low scattered light levels from holographic x-ray gratings provides a marked increase in signal to noise ratio.

In the visible and UV regions it appears that the scattered light is reduced because of the increased ruling accuracy of holographic gratings. However, in the soft x-ray region the principal cause of stray light is surface imperfections. A spectrum produced from a laminar grating made by processing a ruled mask is shown in Fig. 114

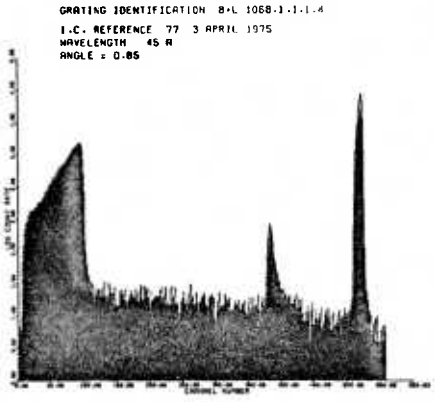
GRATING IDENTIFICATION B+L 1068.1.1.1.4
I.C. REFERENCE 77 3 APRIL 1975
WAVELENGTH 45 A
ANGLE = 0.85

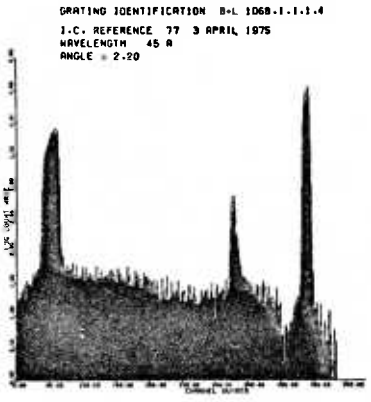
GRATING IDENTIFICATION B+L 1068.1.1.1.4
I.C. REFERENCE 77 3 APRIL 1975
WAVELENGTH 45 A
ANGLE = 2.20

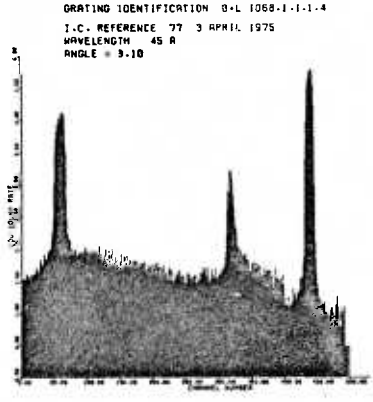
GRATING IDENTIFICATION B+L 1068.1.1.1.4
I.C. REFERENCE 77 3 APRIL 1975
WAVELENGTH 45 A
ANGLE = 3.10

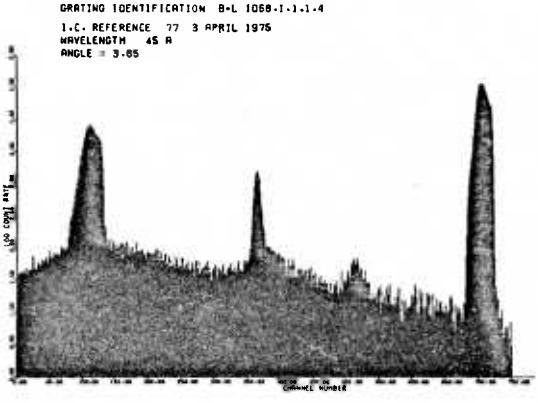
GRATING IDENTIFICATION B+L 1068.1.1.1.4
I.C. REFERENCE 77 3 APRIL 1975
WAVELENGTH 45 A
ANGLE = 3.85

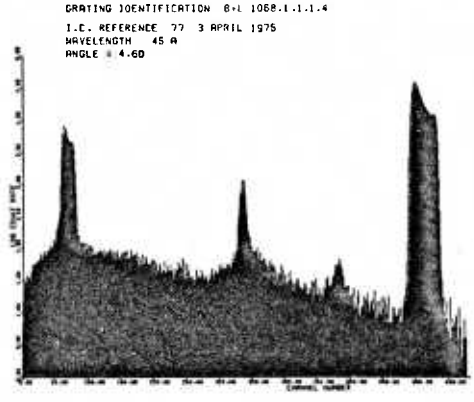
GRATING IDENTIFICATION B+L 1068.1.1.1.4
I.C. REFERENCE 77 3 APRIL 1975
WAVELENGTH 45 A
ANGLE = 4.60

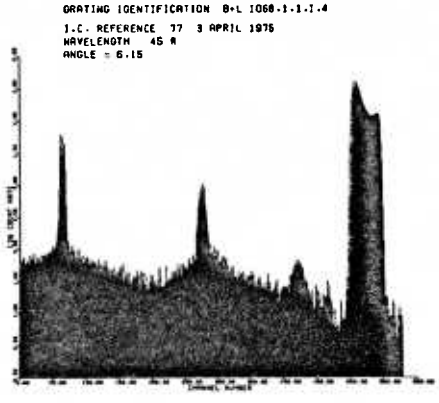
GRATING IDENTIFICATION B+L 1068.1.1.1.4
I.C. REFERENCE 77 3 APRIL 1975
WAVELENGTH 45 A
ANGLE = 6.15

FIG. 111

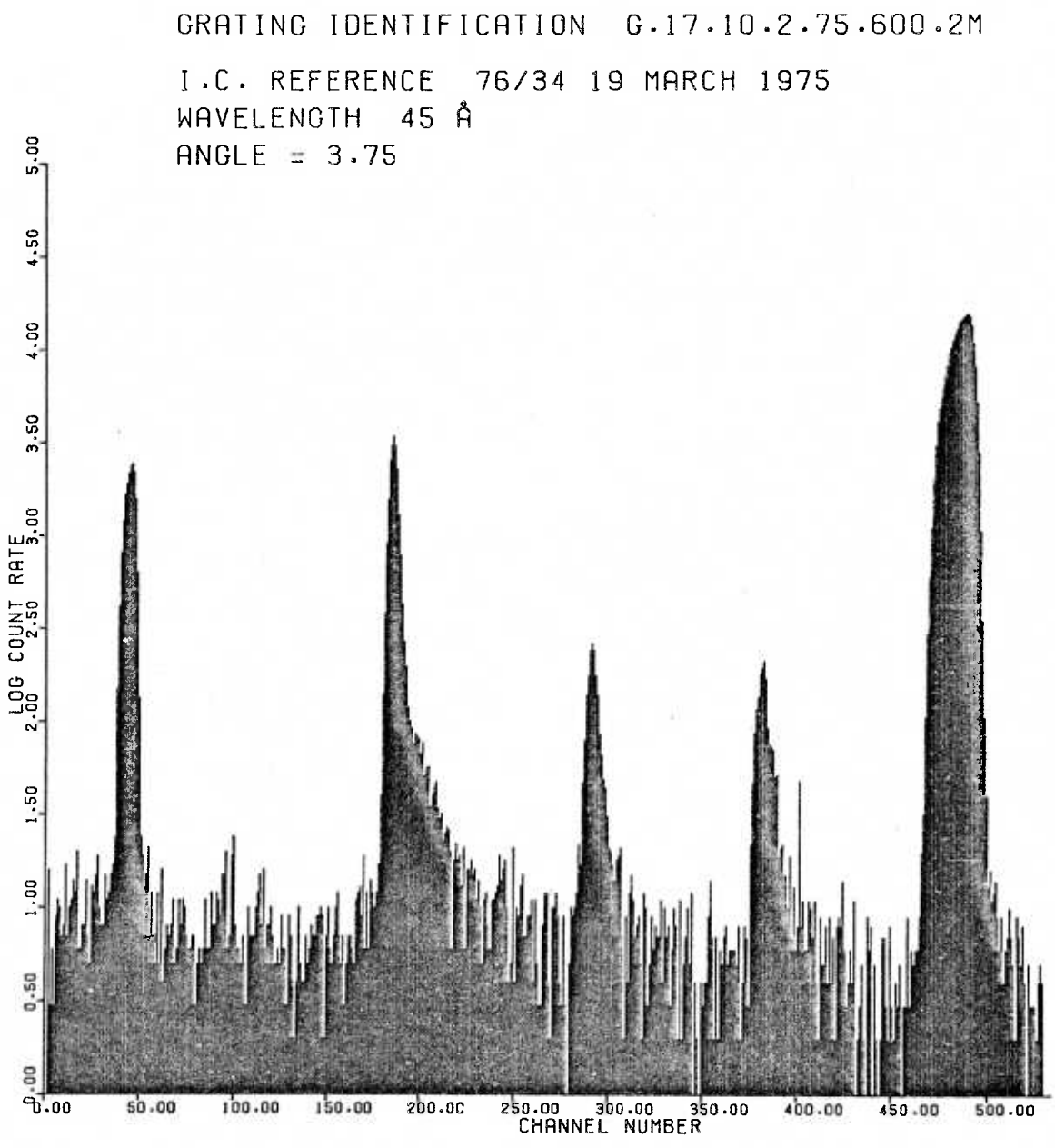
GRATING IDENTIFICATION G.17.10.2.75.600.2M
I.C. REFERENCE 76/34 19 MARCH 1975
WAVELENGTH 45 Å
ANGLE = 3.75
LOG COUNT RATE
0.00
0.50
1.00
1.50
2.00
2.50
3.00
3.50
4.00
4.50
5.00
0.00
50.00
100.00
150.00
200.00
250.00
300.00
350.00
400.00
450.00
500.00
CHANNEL NUMBER

FIG. 112

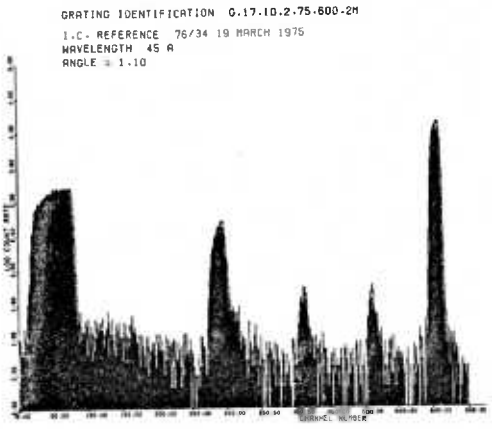
GRATING IDENTIFICATION G.17.10.2.75.600.2M
I.C. REFERENCE 76/34 19 MARCH 1975
WAVELENGTH 45 A
ANGLE = 1.10

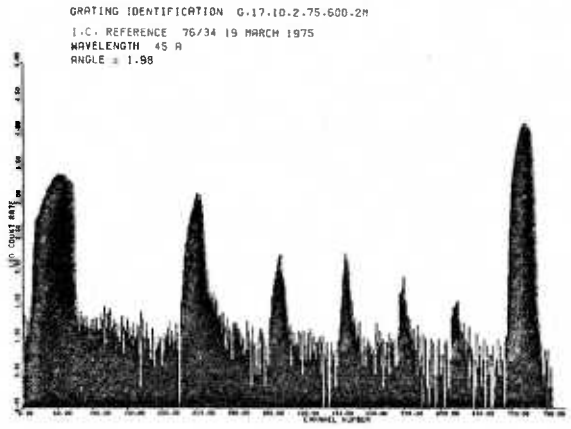
GRATING IDENTIFICATION G.17.10.2.75.600.2M
I.C. REFERENCE 76/34 19 MARCH 1975
WAVELENGTH 45 A
ANGLE = 1.98

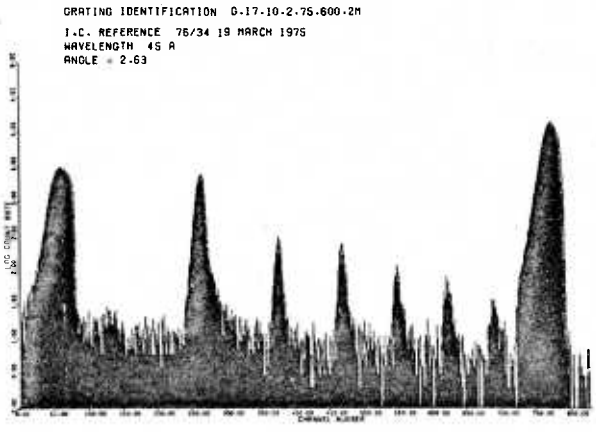
GRATING IDENTIFICATION G.17.10.2.75.600.2M
I.C. REFERENCE 76/34 19 MARCH 1975
WAVELENGTH 45 A
ANGLE = 2.63

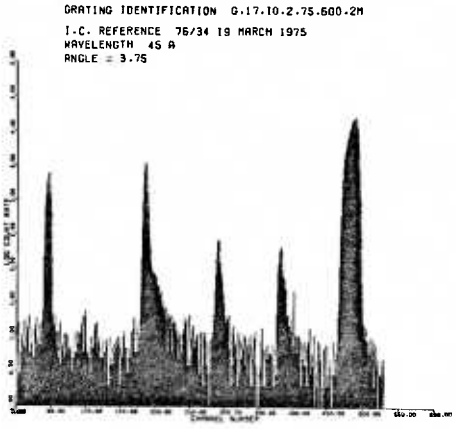
GRATING IDENTIFICATION G.17.10.2.75.600.2M
I.C. REFERENCE 76/34 19 MARCH 1975
WAVELENGTH 45 A
ANGLE = 3.75

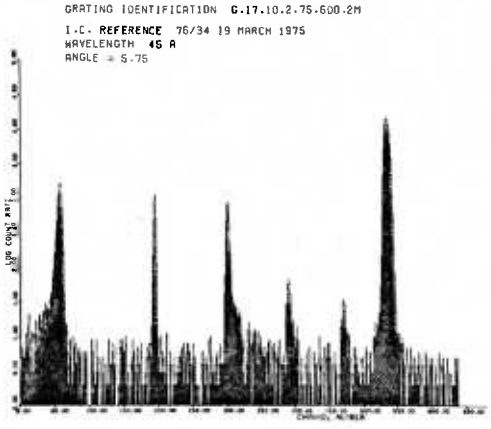
GRATING IDENTIFICATION G.17.10.2.75.600.2M
I.C. REFERENCE 76/34 19 MARCH 1975
WAVELENGTH 45 A
ANGLE = 5.75

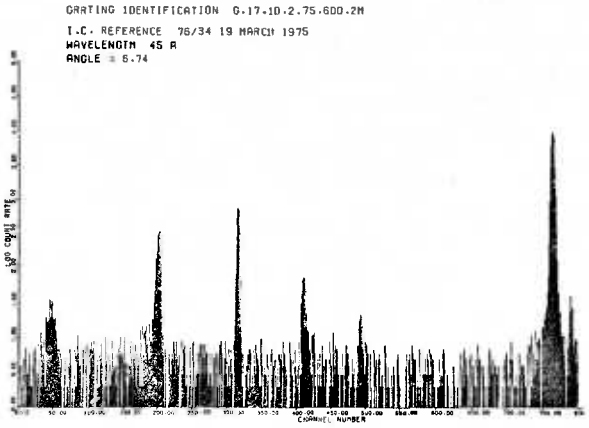
GRATING IDENTIFICATION G.17.10.2.75.600.2M
I.C. REFERENCE 76/34 19 MARCH 1975
WAVELENGTH 45 A
ANGLE = 6.74

FIG. 113

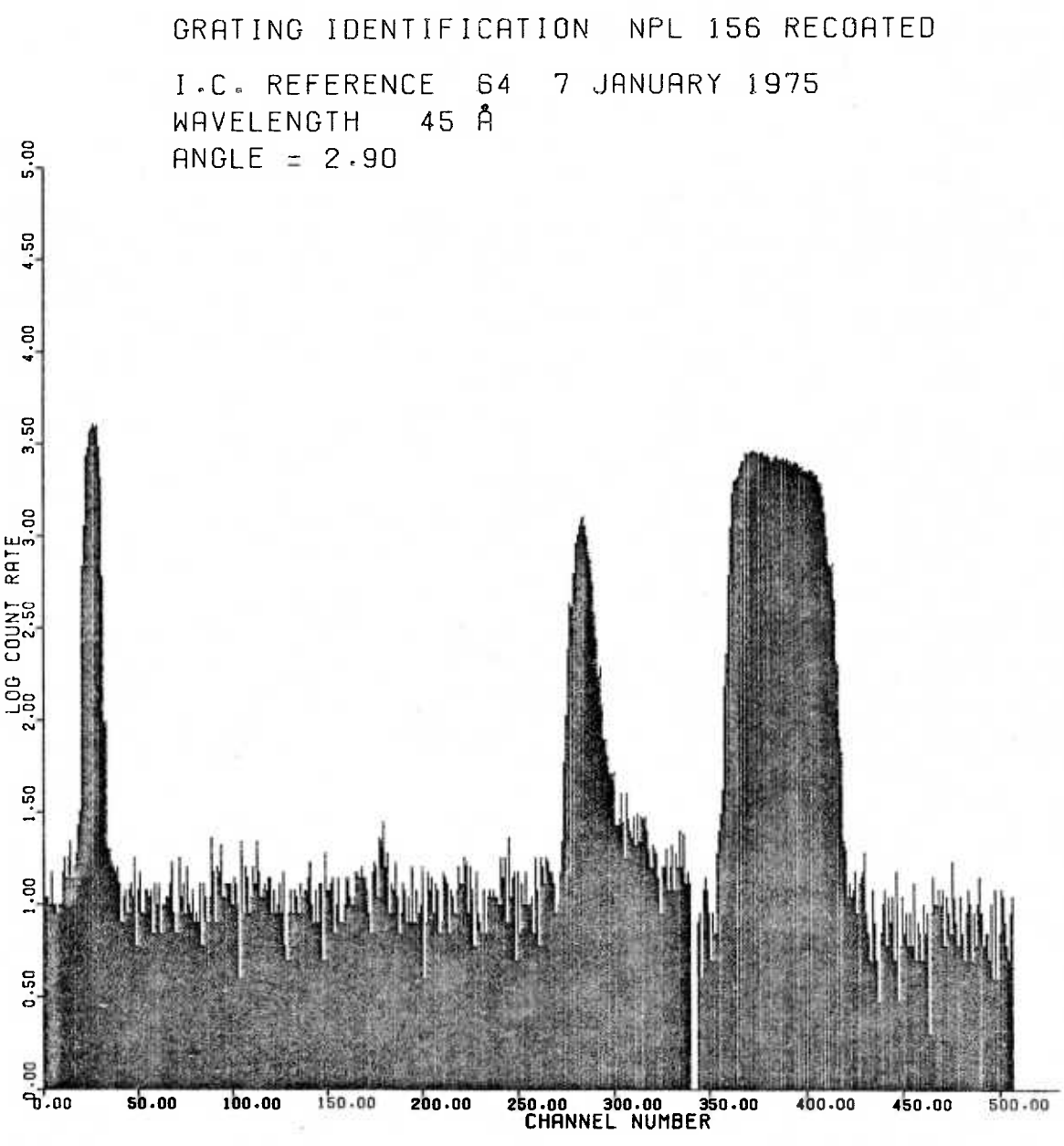
GRATING IDENTIFICATION NPL 156 RECOATED
I.C. REFERENCE 64 7 JANUARY 1975
WAVELENGTH 45 Å
ANGLE = 2.90
LOG COUNT RATE
0.00
0.50
1.00
1.50
2.00
2.50
3.00
3.50
4.00
4.50
5.00
0.00
50.00
100.00
150.00
200.00
250.00
300.00
350.00
400.00
450.00
500.00
CHANNEL NUMBER

FIG. 114

and the scattered light level is close to background. Thus, it appears that the technique for producing x-ray gratings is immaterial provided the grating surface produced is adequately smooth. However, by combining holographic techniques with the ion-etching process for producing super-smooth surfaces, extremely low scattering levels can be achieved as shown in Fig. 115 and Fig. 116. The gratings which produced these spectra are plane holographic blazed gratings with 600 l/mm and 1200 l/mm and blaze angles of 0.65° and 1.5° respectively. Spectra recorded at a number of angles of incidence from these gratings are shown in Fig. 117 and Fig. 118. These two blazed holographic gratings produced at the NPL are particularly interesting since they have exceptionally high efficiencies and are the first blazed gratings which are really suitable for use in the soft x-ray region. Since these gratings have been made on plane blanks, unfortunately they have little value for experimental spectroscopy.

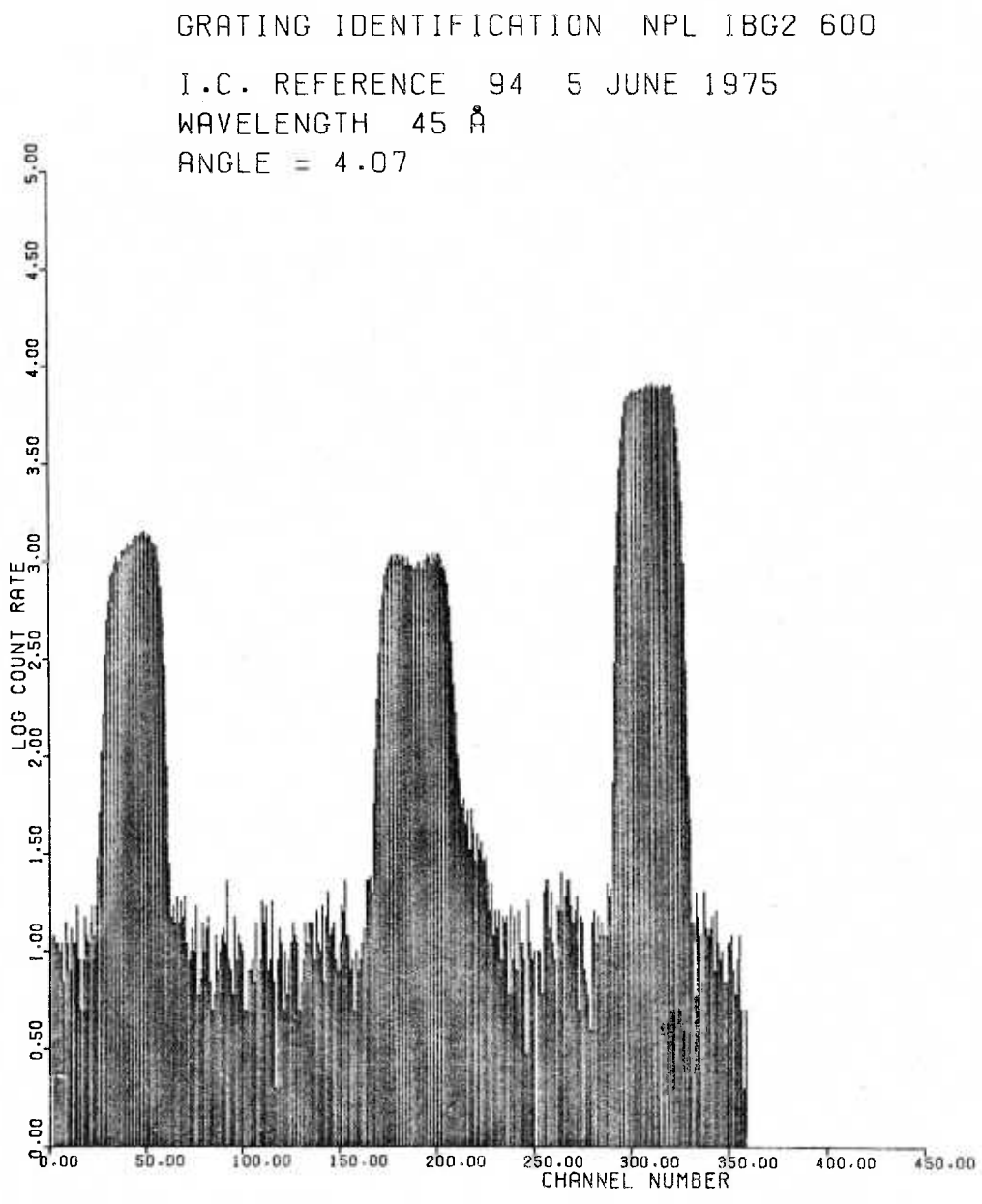
GRATING IDENTIFICATION NPL IBG2 600
I.C. REFERENCE 94 5 JUNE 1975
WAVELENGTH 45 Å
ANGLE = 4.07
LOG COUNT RATE
0.00
0.50
1.00
1.50
2.00
2.50
3.00
3.50
4.00
4.50
5.00
0.00
50.00
100.00
150.00
200.00
250.00
300.00
350.00
400.00
450.00
CHANNEL NUMBER

FIG. 115

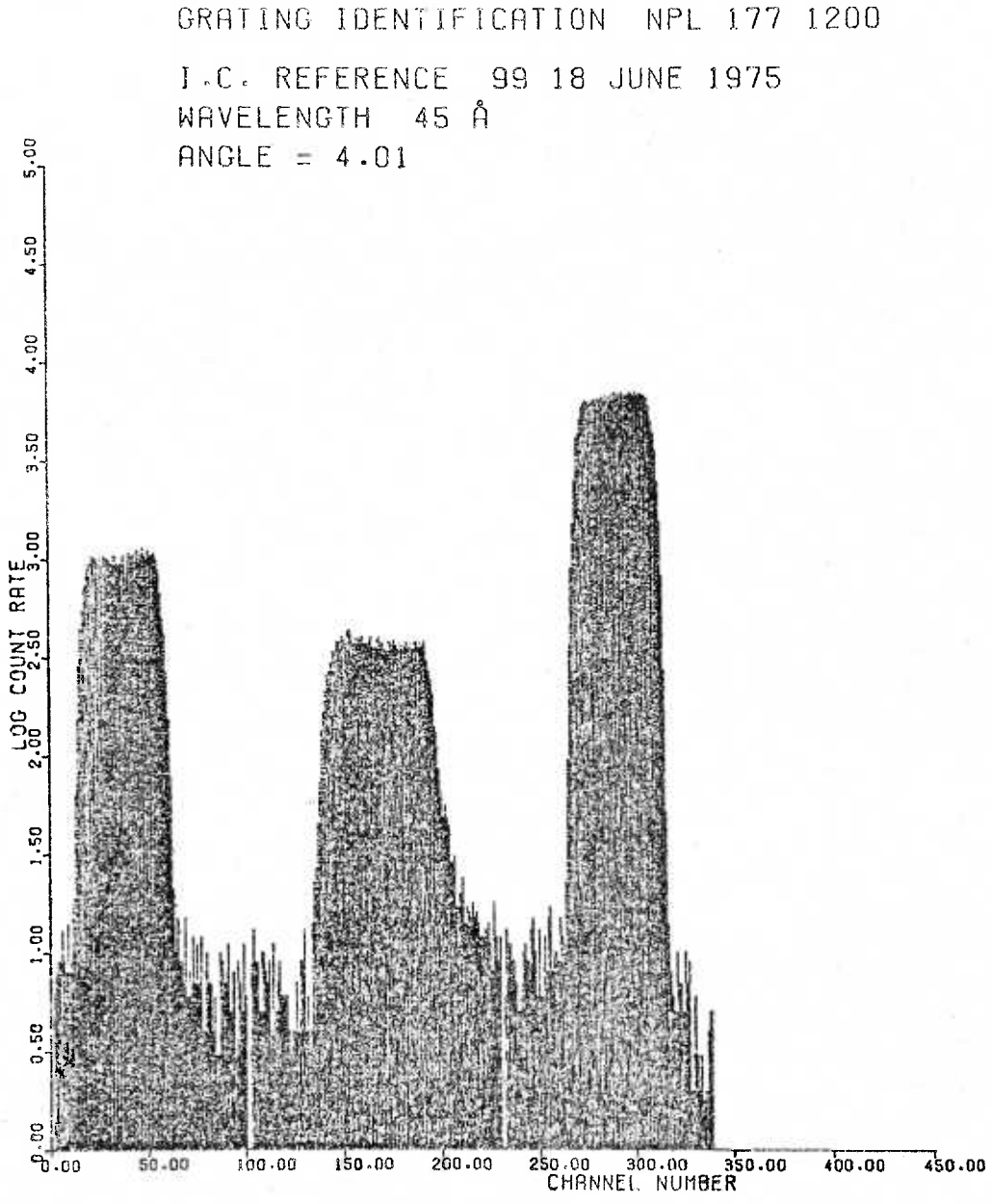
GRATING IDENTIFICATION NPL 177 1200
I.C. REFERENCE 99 18 JUNE 1975
WAVELENGTH 45 Å
ANGLE = 4.01
LOG COUNT RATE
0.00
0.50
1.00
1.50
2.00
2.50
3.00
3.50
4.00
4.50
5.00
0.00
50.00
100.00
150.00
200.00
250.00
300.00
350.00
400.00
450.00
CHANNEL NUMBER

FIG. 116

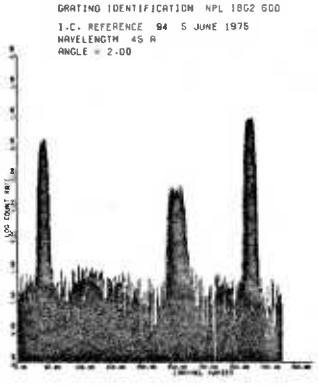
GRATING IDENTIFICATION NPL 1802 600
I.C. REFERENCE 94 5 JUNE 1975
WAVELENGTH 45 A
ANGLE = 2.00

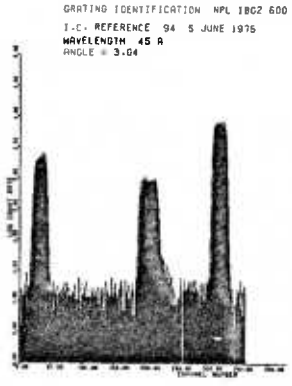
GRATING IDENTIFICATION NPL 1802 600
I.C. REFERENCE 94 5 JUNE 1975
WAVELENGTH 45 A
ANGLE = 3.04

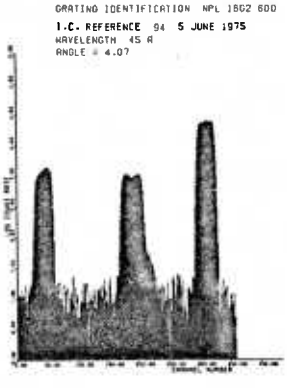
GRATING IDENTIFICATION NPL 1802 600
I.C. REFERENCE 94 5 JUNE 1975
WAVELENGTH 45 A
ANGLE = 4.07

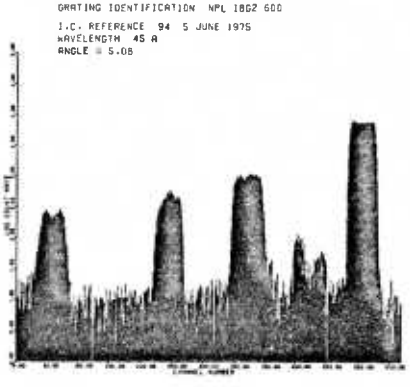
GRATING IDENTIFICATION NPL 1802 600
I.C. REFERENCE 94 5 JUNE 1975
WAVELENGTH 45 A
ANGLE = 5.08

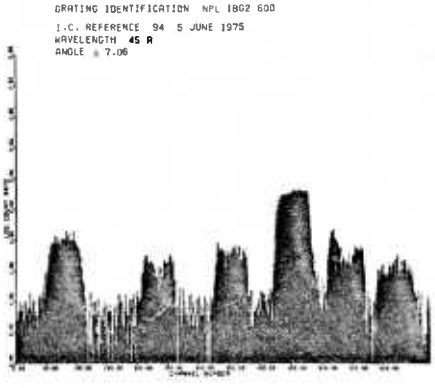
GRATING IDENTIFICATION NPL 1802 600
I.C. REFERENCE 94 5 JUNE 1975
WAVELENGTH 45 A
ANGLE = 7.06

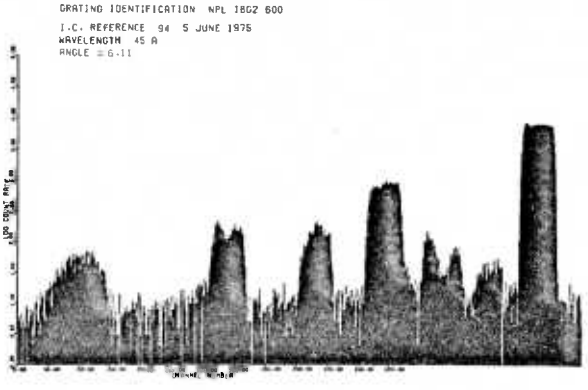
GRATING IDENTIFICATION NPL 1802 600
I.C. REFERENCE 94 5 JUNE 1975
WAVELENGTH 45 A
ANGLE = 8.11

FIG. 117

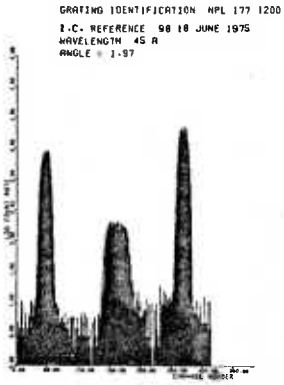
GRATING IDENTIFICATION NPL 177 1200
I.C. REFERENCE 98 18 JUNE 1975
WAVELENGTH 45 A
ANGLE = 1.97

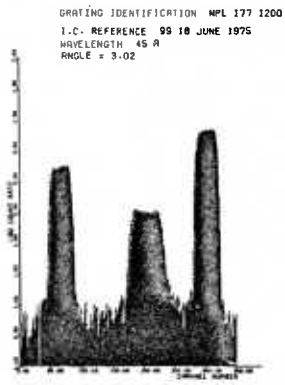
GRATING IDENTIFICATION NPL 177 1200
I.C. REFERENCE 99 18 JUNE 1975
WAVELENGTH 45 A
ANGLE = 3.02

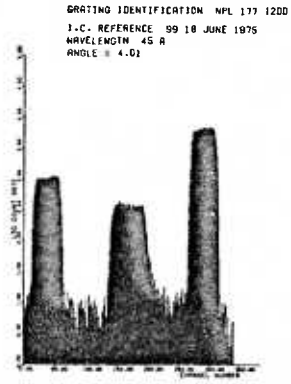
GRATING IDENTIFICATION NPL 177 1200
I.C. REFERENCE 99 18 JUNE 1975
WAVELENGTH 45 A
ANGLE = 4.01

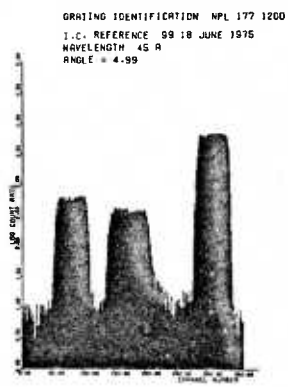
GRATING IDENTIFICATION NPL 177 1200
I.C. REFERENCE 99 18 JUNE 1975
WAVELENGTH 45 A
ANGLE = 4.99

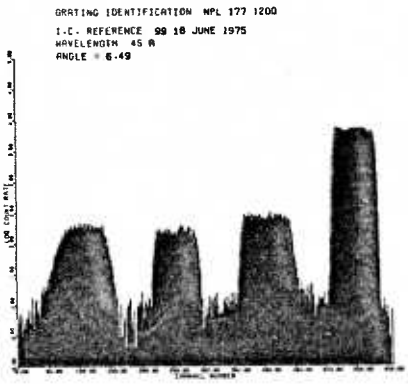
GRATING IDENTIFICATION NPL 177 1200
I.C. REFERENCE 99 18 JUNE 1975
WAVELENGTH 45 A
ANGLE = 6.49

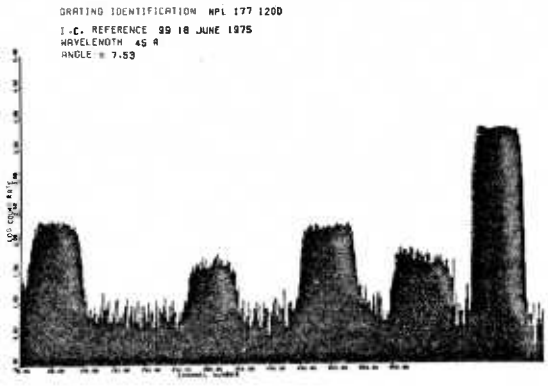
GRATING IDENTIFICATION NPL 177 1200
I.C. REFERENCE 99 18 JUNE 1975
WAVELENGTH 45 A
ANGLE = 7.53

FIG. 118

7.4 PRACTICAL SOFT X-RAY SPECTROSCOPY

The overall aim of the present research programme has been to improve the performance of grazing incidence instruments and spectrographs in the soft x-ray wavelength region. Since soft x-rays are characteristic of plasmas in the 10^6-10^7K temperature range, soft x-ray spectroscopy provides powerful diagnostic methods for the hot plasmas produced in fusion research. Light element x-ray microanalysis has become very popular and it is to be expected that soft x-ray spectroscopy will find increasing applications in chemical analysis. Recently advances have been made in x-ray astronomy and soft x-ray spectroscopy will most probably be very important in this relatively new field. Therefore it is clear that the improvements resulting from the present research programme will have wide application. Naturally, it will take some time for all the results of this research to be applied, however, significant advances have already been made in laboratory emission and absorption spectroscopy and these will be briefly described in this section.

The most fundamental method for increasing the performance of a spectrograph is to increase the efficiency of the diffraction grating by using the most suitable type of grating under the optimum conditions for the application. In many cases use of a better diffraction grating in an existing spectrograph will enable superior spectra to be readily obtained. However, for high resolution soft x-ray spectroscopy the commercially available spectrographs do not provide the features necessary to fully exploit the performance of current diffraction gratings. A new pre-focussed modular 5m spectrograph has been designed by Turner and Speer (116) to take advantage of all the developments in

grazing incidence optics, and this instrument has been used by the author for soft x-ray spectroscopy.

It is difficult to find suitable sources in the soft x-ray region for laboratory spectroscopy. The best source of continuum radiation for absorption spectroscopy is a synchrotron. However, even with such a bright source as a synchrotron inconveniently long exposure times are required for certain applications when using a conventional spectrograph equipped with a shallow blazed grating. This has been found to be the case in the work performed on the absorption spectroscopy of metal vapours at the Physikalisches Institut der Universität Bonn, in collaboration with Imperial College. There have been reports of replica gratings being destroyed when placed directly in a synchrotron radiation beam and usually the vacuum requirements are stringent so that gratings must not out-gas significantly. Since both NPL gratings and the author's gratings are free from organic materials and have high efficiencies, they are most suitable for use in synchrotron experiments.

One of the author's gratings (no. 34) was loaned to the Bonn group to assist them in their work on atomic and molecular absorption spectroscopy. Because of the superior properties of the author's grating new spectra from manganese and chromium have been recorded and will be described by Connerade (138). A typical example, the 3p spectrum of Mn I vapour, is shown in Fig. 119. This work is particularly interesting since it has demonstrated that laminar gratings can be used successfully over a wide wavelength range. The excellent results obtained in this case are indicative of the gains

MANGANESE 3p ABSORPTION SPECTRUM

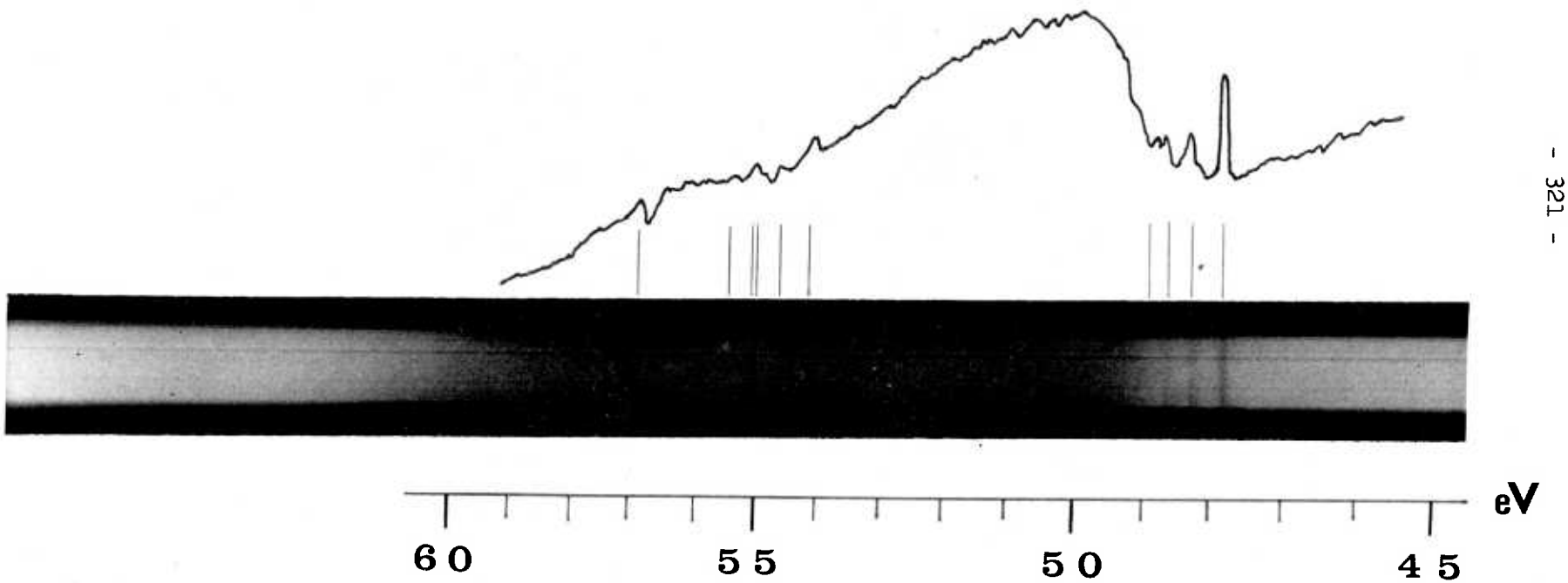

FIG. 119

which can be obtained by using a "state of the art" grating in a conventional spectrograph.

Another source which has been used for laboratory spectroscopy is the BRV source (139) which is essentially a triggered vacuum spark which acts in the same way as a small theta pinch. Since the discharge is small and can move over the anode, alignment can be difficult. In this work a boron nitride capillary was used over the anode to localise the discharge and a special fixture was fabricated to facilitate alignment. The BRV source does not produce a high intensity at short wavelengths so that it is necessary to fire the source repeatedly. The intensity of the source can be increased by employing a larger capacitor but it was found that a 0.5μF capacitor destroyed the boron nitride capillary immediately and better results were obtained with a 0.05μF capacitor. When the source is fired a small quantity of the anode material is ionised and is accelerated under the action of the electric field through the hole in the cathode in the same direction as the electromagnetic radiation. The vaporised anode material can be most troublesome in a windowless system and filters placed directly in front of the source are broken by the combined effects of heating and shock. The use of the boron nitride capillary and a series of baffles in the optical system have reduced the contamination to a satisfactory level in the present system and magnets can also be used to deflect the ionised material.

Two spectra from a BRV source with a Cu anode recorded under identical conditions using a GML 5M spectrograph are shown in

Fig. 120. The upper spectrum was obtained from a ruled laminar grating designed for short wavelength use and the lower spectrum was recorded with one of the author's holographic laminar gratings (no. 21). A complete analysis of these new spectra has yet to be performed but lines from N VI (1s-2p, 28.79 Å), B V (1s-2p, 48.59 Å), B IV (1s-2p, 60.31 Å), Cu XII (56.332 Å) and associated lines can be readily identified. These results show the advantages which can be obtained by using the most suitable grating for the application and also illustrate the excellent spectra which are produced by the GML 5M spectrograph.

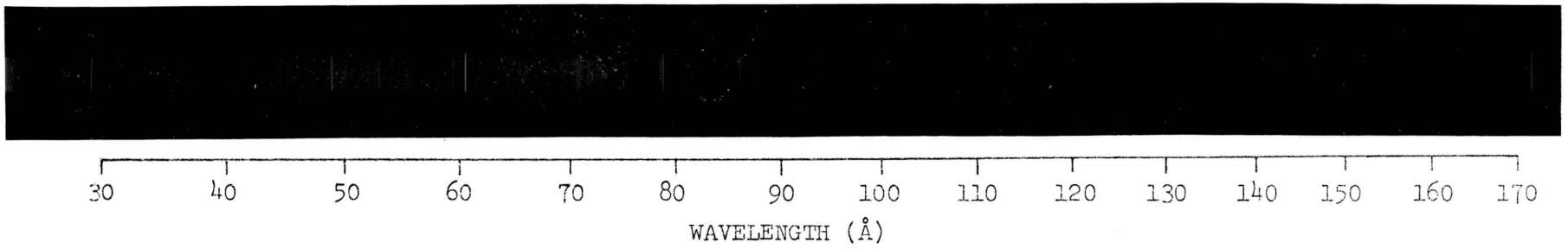

TWO SPECTRA RECORDED UNDER IDENTICAL CONDITIONS FROM A BRV SOURCE WITH A Cu ANODE AND BORON NITRIDE CAPILLARY

UPPER SPECTRUM: RULED LAMINAR GRATING (316 l/mm) - LOWER SPECTRUM: HOLOGRAPHIC LAMINAR GRATING (294 l/mm)

GML 5M Spectrograph, entrance slit 2µm, grazing angle 4°, 1000 shots on BRV source with 0.05µF, 20KV capacitor
Plates developed in D19, 5 min. at 20°C. The plates were contact-printed together.

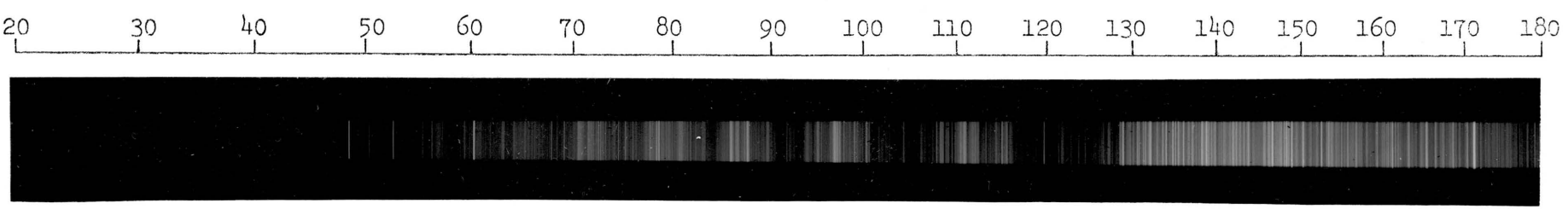

FIG. 120

CONCLUSION

In this thesis the theory of gratings relevant to the soft x-ray region has been reviewed and the properties of spherical, cylindrical, toroidal and elliptical gratings have been analysed by exact ray-tracing. It has been demonstrated for the first time how the astigmatism of the spherical grating at grazing incidence can be removed in practice by using a single toroidal grating. Methods for increasing the resolution and luminosity of spectrometers and monochromators by using elliptical and variable frequency gratings have been described. Finally, an improved simple technique for producing laminar holographic gratings has been devised and this method has been used to make plane, spherical and the first elliptical gratings for use in the soft x-ray region.

The apparatus for measuring the performance of soft x-ray gratings has been extensively redesigned, rebuilt, and partially automated to increase the accuracy and speed of taking measurements. A computer data handling system has been developed which greatly facilitates data evaluation and storage. The apparatus has been used for reflectivity measurements on gold and chromium films and the performance of eighty gratings has been measured.

The results of this work have already been applied to current problems in spectroscopy and have enabled previously unrecorded phenomena to be discovered. Gratings produced by the author are now being used in laboratories at Physikalisches Institut der

Universität Bonn; DESY, Hamburg; Stanford, USA; and in the Spectroscopy Group at Imperial College. Thus, an original contribution has been made in grating science and x-ray instrumentation which is already yielding new results in spectroscopy.

ACKNOWLEDGEMENTS

I should like to express my gratitude to Dr. R.J. Speer, my supervisor over the past three years, for providing the facilities and freedom to pursue the research described in this thesis, and to Professor W.R.S. Garton for the opportunity of working in his laboratory.

I am particularly indebted to Mr. P.W. Ruthven without whose technical assistance it would not have been possible to undertake such an ambitious research programme, and I am very grateful to Mr. D. Turner for advising me on numerous matters.

Mr. H. Yates, Mr. C. Pataky and Mr. T. Dimes of IC Optical Systems receive my special thanks for instructing me in some of the mysteries of optical working.

I am very grateful to Dr. G. Schmahl, Dr. D. Rudolph and Dr. B. Niemann for many interesting and productive discussions, and to Frau Christ for some help in preparing gratings, during my stay at the Universitäts-Sternwarte, Göttingen.

I particularly wish to thank Mr. R. Gavison and Mr. A.P. Jarvis for assistance with computing and the advice, in the early stages of the work on ray-tracing, from Mrs. P.M.J.H. Wormell and Dr. R. Gostick of the Optical Design Section in the Applied Optics Group at Imperial College is gratefully acknowledged. I thank Professor W.T. Welford for several most helpful conversations and Dr. R.C.M. Learner and Mr. D. Turner for reading this thesis.

I am very grateful to Mr. J.F. Verrill and Mr. C.J. Robbie of the NPL for producing the Talystep traces shown in Figs. 70, 71, 104 and 106. I should like to thank Dr. S.J. Peppiatt for producing the transmission electron micrographs shown in Fig. 105, Mr. S. Mrowka and Mr. M.F. Hipkins (74) for Fig. 92, and Dr. J.P. Connerade for Fig. 119.

Finally I should like to express my gratitude to the following organisations: Science Research Council for providing financial support; Bausch and Lomb, USA; National Physical Laboratory, Teddington; and Jobin et Yvon, Paris, for providing some of the gratings examined during this work and for allowing the results to be published; Lockheed, USA, and Grating Measurements Ltd. for providing grating blanks and IC Optical Systems for providing optical working facilities and instruction.

REFERENCES

1. STROKE, G.W., "Diffraction Gratings", Handbuch der Physik, (Springer, Berlin), Vo. XXIX, 426 (1967)
2. MICHELSON, A.A., "Studies in Optics, Phoenix Books, (The University of Chicage Press), 104 (1927)
3. BURCH, J.M., Progress in Optics, Vol. II, 75 (1963)
   BURCH, J.M., and PALMER, D.A., Optica Acta, 8, 73 (1961)
4. RITSCHL, R., and POLZE, S., Optik, 15, 127 (1958)
5. DENISYUK, Yu. N., Sov. Phys. Doklady 7, 543 (1962)
6. LABEYRIE, A., "Quelques Nouvelles Methodes en Holographie. Memoire pour obtenir le Diplôme d'Etude Supérieurs de Sciences Physiques", (University of Paris/Orsay), (1966)
7. RUDOLPH, D., and SCHMAHL, G., Umschau in Wissenschaft und Technik, 67, 225 (1967)
   RUDOLPH, D., and SCHMAHL, G., Mitt. Astron. Ges. 23, 46 (1967)
   Mitt. Astron. Ges. 24, 41 (1968)
8. HAYAT, G.S., and PIEUCHARD, G., Industrial Research, 40, (Aug.1973)
9. SHANKOFF, T.A., U.S. Patent 3,567,444
10. BROOKS, R.E., and HEFLINGER, L.O., U.S. Patent 3,578,845
11. SHERIDON, N.K., Appl. Phys. Letters 12, 316 (1968)
12. SCHMAHL, G., and RUDOLPH, D., Mitt. Astron. Ges. 27, 201-203 (1969)
13. LABEYRIE, A., and FLAMAND, J., Opt. Commun. 1, 5, (1969)
14. RUDOLPH, D., and SCHMAHL, G., Optik 30, 475 (1970)
    RUDOLPH, D., and SCHMAHL, G., Applications of Holography, Proc. International Symposium on Holography, (Université de Besançon) Paper 10-7 (1970)

15. PIEUCHARD, G., FLAMAND, J., CORDELLE, J., and LABEYRIE, A., Applications of Holography, Proc. International Symposium on Holography, (Université de Besançon), paper 10-8 (1970)

16. CORDELLE, J., LAUDE, J.P., PETIT, R., and PIEUCHARD, G., Nouv. Rev. Opt. Appl. 1, 149 (1970)

17. NAMIOKA, T., and HUNTER, W.R., Opt. Commun. 8, 229 (1973)

18. HUTLEY, M.C., Sci. Prog. Oxford, 61, 301 (1974)

19. HUTLEY, M.C., Optica Acta, 22, 1 (1975)

20. HUNTER, W.R., Journal of the Spectroscopical Society of Japan, 24, Suppl. No. 1 (1975)

21. PIEUCHARD, G., Journal of the Spectroscopical Society of Japan, 24, Suppl. No. 1 (1975)

22. DERSHEM, L., and SCHEIN, M., Phys. Rev. 37, 1246 (1931)

23. SCHON, M., Z Physik 58, 165 (1929)

24. COMPTON, A.H., and ALLISON, S.K., X-rays in Theory and Experiment (Van Nostrand, New York), (1935)

25. HENKE, B.L., and DUMOND, J.W.M., J. Appl. Phys. 26, 903 (1955)

26. GROTH, R., Annalen der Physik 2, 380-386 (1959)

27. HENDRICK, R.W., J. Opt. Soc. Amer., 47, 165-71 (1957)

28. JOHNSON, G.L., and WUERKER, R.F., in Third International Symposium on X-ray Optics and Microanalysis, H.H. Pattee, Jr., V.E. Cosslett, and A. Engström, Eds. (Academic Press Inc., New York), 229-239 (1963)

29. STEWARDSON, E.A., and UNDERWOOD, J.H., Brit. J. Appl. Phys., Vol. 16 1877-1884 (1965)

30. BENNETT, J.M., PhD. Thesis London University, 156-9 (1971)

31. LUKIRSKII, A.P., and SAVINOV, E.P., Opt. i. Spektroskopiya 14, 295 (1963); Opt. Spectry. 14, 152 (1963)

32. LUKIRSKII, A.P., SAVINOV, E.P., ERSHOV, O.A., and SHEPELEV, Yu.F., Opt. i Spektroslopiya 16, 310 (1964); Opt. Spectry. 16, 168 (1964)

33. LUKIRSKII, A.P., SAVINOV, E.P., ERSHOV, O.A., FOMICHEV, V.A., and ZHUKOVA, I.I., Opt. i Spektroskopiya 19, 425 (1965); Opt. Spectry 19, 237 (1965)

34. ERSHOV, O.A., BRYTOV, I.A., LUKIRSKII, A.P., Opt. i. Spektroskopiya 22, 127 (1967); Opt. Spectry 22, 66 (1967)

35. SENNETT, R.S., and SCOTT, G.D., J. Opt. Soc. Amer. 40, 203 (1950)

36. HENKE, B.L., Physical Review A, Vol. 6 No. 1, Ultrasoft X-ray Reflection, Refraction and Production of Photoelectrons (100 - 1000 eV Region), (July 1972)

37. MAHAN, I., J. Opt. Soc. Amer. 46, 913 (1956)

38. SMYTHE, W.R., Static and Dynamic Electricity, 3rd ed., (McGraw-Hill Book Co., New York), (1968)

39. ROSENDAHL, G.R., "Contributions to the Optics of Mirror Systems and Gratings with Oblique Incidence. I. Ray Tracing Formulas for the Meridional Plane.", J. Opt. Soc. Am., 51, 1 (1959)

40. WELFORD, W.T., "Tracing Skew Rays Through Concave Diffraction Gratings", Opt. Acta 9, 389 (1962)

41. SPENCER, G.H., and MURTY, M.V.R.K., "General Ray-Tracing Procedure", J. Opt. Soc. Am. 52, 672 (1962)

42. KASTNER, S.O., and NEUPERT, W.M., "Image Construction for Concave Gratings at Grazing Incidence, by Ray Tracing", J. Opt. Soc. Am. 53, 1180 (1963)

43. OFFNER, A., "Ray-Tracing Through a Holographic System", J. Opt. Soc. Am. 56, 1509 (1966)

44. LUDWIG, U.W., "Generalised Grating Ray-Tracing Equations", J. Opt. Soc. Am. 63, 1105 (1973)

45. NODA, H., "The Theory of the Holographic Grating", PhD Thesis Kyoiku University, Japan (1974)

46. NODA, H., NAMIOKA, T., and SEYA, M., "Ray-Tracing Through Holographic Gratings", J. Opt. Soc. Am. 64, 1037 (1974)

47. ROSE, H.W., "Holographic Lens Systems", (Technical Report AFAL-TR-73-101, Wright-Patterson Air Force Base, Ohio 45433, USA), (1973)

48. WELFORD, W.T., "Isoplanatism and Holography", Opt. Commun. 8, 239 (1973)

49. WELFORD, W.T., "A Vector Ray-Tracing Equation for Hologram Lenses of Arbitrary Shape", Opt. Commun. 14, 322 (1975)

50. LATTA, J.N., "Computer-Based Analysis of Holography Using Ray-Tracing", Applied Optics 10, 2698-2710 (1971)

51. ABRAMOWITZ, I.A., Evaluation of Hologram Imaging by Ray-Tracing, Applied Optics 8, 403 (1969)

52. ROWLAND, H.A., Phil. Mag. 35, 397-419 (1893)

53. GLAZEBROOK, R.T., "On Curved Diffraction Gratings - II", Phil. Mag. (1884)

54. KAYSER, H., "Handbuch der Spektroskopie", Vol. I, 450-482 (1900)

55. DANIELSSON, A., and LINDBLOM, P., "Focussing Conditions of the Spherical Concave Grating", Optik 41, 441-451 (1974)

56. BEUTLER, H.G., "The Theory of the Concave Grating", J. Opt. Soc. Am. 35, 311-350 (1945)

57. NAMIOKA, T., "Theory of the Concave Grating", J. Opt. Soc. Am. 49, 446-460 (1958)

58. NAMIOKA, T., "Theory of the Ellipsoidal Concave Grating", J. Opt. Soc. Am. 51, 4-12 (1961)

59. MACK, J.E., STEHN, J.R., and EDLEN, B., "On the Concave Grating Spectrograph, Especially at Large Angles of Incidence", J. Opt. Soc. Am. 22, 245-261 (1932); Addendum J. Opt. Soc. Am. 23, 184 (1933)

60. WELFORD, W.T., "Aberration Theory of Gratings and Grating Mountings" in Progress in Optics, ed. E. Wolf (North-Holland, Amsterdam), Vol. 4, 243-280 (1965)

61. HABER, H., "The Torus Grating", J. Opt. Soc. Am. 40, 153-165 (1950)

62. SAMSON, J.A.R., "Techniques of Vacuum Ultraviolet Spectroscopy", (John Wiley and Sons), (1967)

63. KOZLENKOV, A.I., "The Optics of Reflecting Mirrors"

64. KOZLENKOV, A.I., "Study of Aberrations of a Concave Grating under Defocussing Conditions", Optics and Spectroscopy 8, 365-370 (1960)

65. BOWEN, I.S., "The Aberrations of the Concave Grating at Large Angles of Incidence", J. Opt. Soc. Am. 23, 313-315 (1933)

66. ROWLAND, H.A., "The Physical Papers of Henry Augustus Rowland", The John Hopkins Press, Baltimore, 485, 487, 506, 519, 525, 587 (1902)

67. SORET, J.L., "IV. Über die durch Kreisgitter erzeugten Diffraktionsphänomene", Annalen der Physik und Chemie, Sechste Reihe J.C. Poggendorff Sechster Band, Leipzig, 99-113, (1875)

68. CORNU, A., "V. Über die Diffraction, namentlich über Brennpunktseigenschaften der Gitter", Annalen der Physik und Chemie Sechste Reihe, J.C. Poggendorff, Sechster Band, Leipzig, 114-119 (1875)

69. SIEGEL, B.M., "Studies on the Morphology and Structure of Copper Films Deposited by Vacuum Evaporation", Technical Report No. 9, Document No. AFOSR TN 59-7 ASTIA AD208 303 (December 15, 1958)

70. TURNER, D., "Wide Range High Aperture Scanning Monochrometer Using Grating with Unequally Spaced Lines", to be published.

71. TURNER, D., and BENNETT, J.M., "An Elliptical Reflector Formed by Bending a Cantilever", to be published.

72. TURNER, D., and SPEER, R.J., "Improvements in and Relating to Spectrometers", Patent No. 23688/74 (1974)

73. GALE, B., "The Theory of Variable Spacing Gratings", Optica Acta 13, 41-54, (1966)

74. MROWKA, S., and HIPKINS, M.F., "The Preparation and Examination of Thin Gold Films", unpublished.

75. WERNER, W., "The Geometrical Optical Aberration Theory of Diffraction Gratings", Applied Optics 6, 1691 (1967)

76. MACADAM, D.L., "Focus of a Concave Grating Spectrograph", J. Opt. Soc. Am. 23, 178-181 (1933)

77. RAYLEIGH, Lord, Scientific Papers, (Cambridge University Press) 1, 432-435 (1899)

78. BORN, M. and WOLF, E., "Principles of Optics", (Pergamon 2nd Ed.) (1964)

79. WELFORD, W.T., "Aberrations of the Symmetrical Optical System" Academic Press, London, (1974)

80. FELLNER-FELDEGG, H., "Computer Simulation of the Concave Grazing Incidence Monochromator", University of Uppsala UUIP-857 (March 1974)

81. GREINER and SCHÄFFER, "über den Astigmatismus des Konkavgitters mit sphärischer oder torischer Oberfläche", Optik 16, 288 (1959)

82. SCHÖNHEIT, E., "Ein Seya-Namioka-Monochromator mit torischem Gitter für Photoionisation-Messungen", Optik 23, 305 (1966)

83. STREZHEV, S.A. and ANDREEVA, A.I., "Toroidal Diffraction Gratings for Seya-Namioka Monochromators", Opt. Spect. 28, 426 (1970)

84. RENSE, W.A., and VIOLETT, T., "Solar Emission Lines in the Extreme Ultraviolet", Astrophy J. 130, 954 (1959)

85. CANTU, A.M., and TONDELLO, G., "Continuum Source and a Focussing Technique for the 80-500A Spectral Range: Improvements", Applied Optics 14, 996-998 (1975)

86. ISHII, AITA, ICHIKAWA, and SAGAWA, "Use of a Toroidal Mirror in the Soft X-Ray Optical System", J. Appl. Phys. (Japan) 10, 637-642 (1971)

87. SHCHEPETKIN, Iu. P., Optika i Spectroskopiya 6, 822 (1959) Opt. Spect. 6, 538 (1959)

88. NAMIOKA, T., "Theory of the Ellipsoidal Concave Grating II: Application of the Theory to the Specific Grating Mountings", J. Opt. Soc. Am. 51, 13 (1961)

89. CHASE, R.C., and SILK, J.K., "Ellipsoid-Hyperboloid X-Ray Imaging Instrument for Laser Pellet Diagnostics", Applied Optics 14, 2096-2098 (1975)

90. MURTY, M.V.R.K., "Spherical Zone-Plate Diffraction Grating", J. Opt. Soc. Am. 50, 923 (1960)

91. MURTY, M.V.R.K., and DAS, N.C., "Theory of Certain Diffraction Gratings Produced by the Holographic Method", J. Opt. Soc. Am. 61, 10001-1006 (1971)

92. "Handbook of Diffraction Gratings Ruled and Holographic", JOBIN YVON Optical Systems (1973)

93. LABEYRIE, A., "Holo-Gratings - The New Diffractive Breed", Electro-Optical Systems Design 3, 32-38 (1971)

94. CORDELLE, J., FLAMAND, J., PIEUCHARD, G., and LABEYRIE, A., "Aberration-Corrected Concave Gratings Made Holographically", Optical Instruments and Techniques 1969, Ed. J. Home Dickson (Oriel Press, 1970)

95. WELFORD, W.T., "The Most General Isoplanatism Theorem", Optics Commun. 3, 1-6 (1971)

96. WELFORD, W.T., "Practical Design of an Aplanatic Hologram Lens of Focal Length 50mm and Numerical Aperture 0.5", Optics Commun. 15, 46-49 (1975)

97. NAMIOKA, T., and NODA, H., "Normal Incidence Monochromators Equipped with a Holographic Concave Grating", in Proceedings of International Symposium for Synchrotron Radiation Users, ed G.V. Marr and I.H. Munro (Daresbury, England, 5-7 January, 1973) Daresbury Nuclear Physics Laboratory Report No. 26, 51 (1973)

98. NAMIOKA, T., NODA, H., and SEYA, M., "Possibility of Using the Holographic Concave Grating in Vacuum Monochromators", Sci. Light (Tokyo) 22, 77-99 (1973)

99. NODA, H., "The Theory of the Holographic Grating", Thesis, Kyoiku University (1974)

100. NODA, H., NAMIOKA, T., and SEYA, M., "Geometric Theory of the Grating", J. Opt. Soc. Am. 64, 1031 (1974)

101. NODA, H., NAMIOKA, T., and SEYA, M., "Design of Holographic Concave Gratings for Seya-Namioka Monochromators", J. Opt. Soc. Am. 64, 1043 (1974)

102. NAMIOKA, T., NODA, H., and SEYA, M., "Performance of Aberration-Reduced Holographic Concave Gratings Designed Specifically for Seya-Namioka Monochromators", Proceedings of the Symposium on Diffraction Gratings and Grating Instruments, Tokyo 1974, Journal of the Spectroscopical Society of Japan, Vol. 23, Supplement No. 1 (1974)

103. SAKAYANAGI, Y., "A Stigmatic Concave Grating with Varying Spacing", Sci. Light (Tokyo), 16, 129-137 (1967)

104. GERASIMOV, F.M., YAKOVLEV, E.A., PEISAKHSON, I.V., and KOSHELEV, B.V., "Concave Diffraction Gratings with Variable Spacing", Optics and Spectroscopy 28, 423 (1970)

105. HARADA, T., "Mechanically Ruled Stigmatic Concave Gratings", Preprint I.C.O. Conference on Optical Methods in Scientific and Industrial Measurements Tokyo, 25-30 August 1974

106. WELFORD, W.T., "Aberration Tolerances for Spectrum Line Images", Optica Acta 10, 121 (1963)

107. POUEY, M., "Comparison Between Far Ultraviolet Spectrometers", Optics Commun. 2, 339-342 (1970)

108. SPEER, R.J., Private Communication (1974)

109. PETIT, R., "Electromagnetic Grating Theories: Limitations and Successes", Preprint I.C.O. Conference on Optical Methods in Scientific and Industrial Measurements Tokyo, 25-30 August 1974

110. VAN DEN BERG, P.M., "Diffraction Theory of a Reflection Grating" Appl. Sci. Res. 24, 261-292 (1971)

111. SPRAGUE, G., TOMBOULIAN, D.H., and BEDO, D.E., "Calculations of Grating Efficiency in the Soft X-Ray Region", J. Opt. Soc. Am. 45, 756-761 (1955)

112. LUKIRSKII, A.P., and SAVINOV, E.P., "Use of Diffraction Gratings and Echelettes in the Ultra-Soft X-Ray Region", Opt. i. Spectroskopya, 285-294 (1963), Opt. Spect. 147-151 (1963)

113. SAYCE, L.A., and FRANKS, A., "N.P.L. Gratings for X-Ray Spectroscopy", Proc. Roy. Soc. 282A, 353-357 (1964)

114. NIEMANN, B., "Untersuchungen über Zonenplattenteleskope zum Einsatz für nicht-solare Quellen im Bereich der weichen Röntgenstrahlung", Dissertation, Göttingen (1974)

115. GABRIEL, A.H., SWAIN, J.R., and WALLER, W.A., "A Two-Metre Grazing Incidence Spectrometer for Use in the Range 5-950 A", J. Scient. Inst. 42, 94 (1965)

116. TURNER, D., and SPEER, R.J., to be published; see also T7, Physics Bulletin 26, 504 (1975)

117. SPEER, R.J., "The X-Ray Diffraction Grating", Space Science Instrumentation, Vol. 2, (February 1976), in press

118. SINGH, M., and MAJUMDER, K., "Cylindrical Gratings with Circular Grooves", Sci. Light (Tokyo), 18, 57-71 (1969)

119. WOODGATE, B.E., "Cylindrical and Spherical Gratings", J. Opt. Soc. Am. 64, 654-661 (1974)

120. WOLTER, H., "Spiegelsysteme streifenden Einfalls als abbildende Optiken für Röntgenstrahlen", Ann. Physik 6. Folge, Band 10, 94 (1952)

121. SCHMAHL, G., and RUDOLPH, D., "Holographische Erzeugung von Gittern hoher Teilungsgenauigkeit mit Hilfe rekonstruierter identischer Wellenfronten", Optik 30, 606-609 (1970)

122. FRANKS, A., LINDSEY, K., BENNETT, J.M., SPEER, R.J., TURNER, D., and HUNT, D.J., "The Theory, Manufacture, Structure and Performance of NPL X-Ray Gratings", Phil. Trans. Roy. Soc. 277A, 503-543 (1975)

123. STEDMAN, M., BUTLER, D.W., ENGLISH, T.H., FRANKS, A., GALE, B., HUTLEY, M.C., and STUART, P.R., "Recent Developments in X-Ray Diffraction Gratings at NPL", Space Science Instrumentation Vol. 2, (February 1976), in press

124. STEDMAN, M., and FRANKS, A., "Advances in NPL X-Ray Gratings and Spectrometers", Advance in X-Ray Analysis, Vol. 18 Academic Press (1976)

125. NAGATA, H., and KISHI, M., "Production of Blazed Holographic Gratings by a Simple Optical System", I.C.O. Conference in Optical Methods, Tokyo, 25-30 August 1974

126. SCHMAHL, G., "Holographically Made Diffraction Gratings for the Visible, UV and Soft X-Ray Region", Journal of the Spectroscopical Society of Japan 23, Suppl. No. 1, 3-11 (1974)

127. SCHMAHL, G., and RUDOLPH, D., "Holographic Diffraction Gratings", Progress in Optics (Ed. E. Wolf, Vol. XIV, in press, 1976)

128. LINDSEY, K., "The Production and Topography of X-Ray Optical Components", Proc. X-Ray Optics Symposium, Mullard Space Science Laboratory (April 1973)

129. VERHAEGHE, M.F., "Etude des rugosités des interfaces des couches minches d'or par réflexion diffuse de rayons X sous incidence rasante", Optica Acta 19, 905-940 (1972)

130. EHRENBERG, W., "X-Ray Optics: Imperfections of Optical Flats and Their Effect on the Reflection of X-Rays", J. Opt. Soc. Am. 39, 746-751 (1949)

131. ELLIOTT, S.B., "Effects of Polishing Imperfections on Specular Reflection of X-Rays", in Third International Symposium on X-Ray Optics and Microanalysis, H.H. Pattee, V.E. Cosslett, and A. Engstrom, Eds. (Academic Press Inc., New York 1963), pp. 215-228

132. SCHROEDER, J.B., and KLIMASEWSKI, R.G., "Scatter from X-Ray Reflecting Surfaces", Applied Optics 7, 1921-1927 (1968)

133. WRISTON, R.S., and FROECHTENIGT, J.F., "Soft X-Ray Scattering by Optical Surfaces", Applied Optics 12, 25-28 (1973)

134. RAYLEIGH, Lord, Phil. Mag. 47, 81 (1874)

135. HOBBY, M.G., and PEACOCK, N.J., "Spectrograph Calibration at Soft X-Ray Wavelengths 1: From Grating Diffraction Efficiency and Plate Response Factors", J. Phys. E 6, 854-856 (1973)

136. VERRILL, J.F., "Use of the Talystep in Investigating Diffraction Grating Groove Profiles", J. Phys. E 6, 1199-1201 (1973)

137. HUNTER, W.R., "Diffraction Gratings for the XUV - Conventional vs Holographic", Journal of the Spectroscopical Society of Japan, Vol. 23, Suppl. No. 1, 37-51 (1974)

138. CONNERADE, J.P., and MANSFIELD, M.W.D., "3d Wavefunction Collapse in Inner Shell Absorption Spectra of Elements in the First Long Period", to be presented at 2nd International Conference on Inner Shell Ionization Phenomena, Universität Freiburg, March-April 1976

139. GARTON, W.R.S., CONNERADE, J.P., MANSFIELD, M.W.D., and WHEATON, J.E.G., "Atomic Absorption Spectroscopy in the 100 - 600 A Wavelength Range", Applied Optics 8, 919-924 (1969)

Reprinted from **APPLIED OPTICS**, Vol. 12, page 1731, August 1973

Soft X-Ray Performance of a Plane Reflection Hologram

D. Rudolph, G. Schmahl, R. L. Johnson, and R. J. Speer

The first two authors named are with Universitäts-Sternwarte, Göttingen, Germany; the other authors are with the Physics Department, Imperial College, London, SW7, England.
Received 8 June 1973.
Sponsored by W. R. Hunter, U. S. Naval Research Laboratory.

We have examined the x-ray performance of a plane reflection grating formed holographically. The grating was fabricated at the Universitäts-Sternwarte, Göttingen, and was initially recorded with 457.9-nm laser light in photoresist.[1,2] It was the first prototype designed to be used at grazing incidence and was constructed from interfering plane wavefronts giving 600 fringes/mm over an area of 4 cm × 4 cm. Subsequent development yielded a mask, which, after coating with chromium and subsequent stripping, closely approximated a laminar profile (square wave) of step-height 15.0 nm and grating space 1667 nm with equal land to groove. This profile has the additional scalar property of phase cancellation in the reflected (or zero order) beam at $\lambda \approx 4.4$ nm at grazing angles of incidence within the critical angle for total external reflection of the grating supercoat (Au).

Figure 1 shows the absolute fractions of the incident monochromatic 4.4-nm radiation diffracted into the ±1 orders (right-hand scale). The variable parameter is α the angle of grazing incidence. A minimum is clearly evident in the zero order beam energy (left-hand scale) and correlates in position with the maximum for the sum of the ±1 diffracted energy.

We are able to show theoretically that the effective value of h, the groove height, is given to very good approximation by

$$h = \lambda/(2\Sigma\alpha)$$

where $\Sigma\alpha = {}_{-1}\alpha_{\text{opt}} + {}_{+1}\alpha_{\text{opt}}$ in circular measure. A value of $h = 14 \pm 3$ nm is derived.

The diffraction performance, shown in Fig. 1, has also been measured at 2.3 nm and at both wavelengths is comparable to the highest speed measured to date for gratings produced by classical ruling techniques at this groove frequency.[3] The level of incoherent scatter is also lower. Furthermore, the construction wavefronts need not be plane, and the final reflection hologram contains no photopolymer or other organic material.

We consider our result to have the following consequences:

(1) construction can proceed on spherical surfaces and aspherics with primary focal conditions suited to correct astigmatism or other defects of soft x-ray imagery at grazing incidence;
(2) larger areas may be fabricated limited only by the size of the collimation optics. Such gratings may have applications in x-ray astronomy.

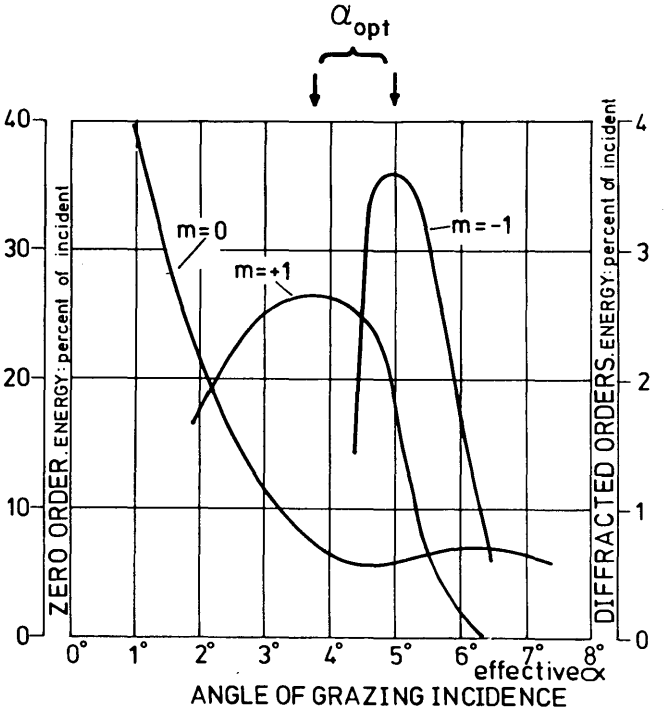

Fig. 1. Absolute fractions of the incident monochromatic 4.4-nm radiation diffracted into the ±1 orders (right-hand scale). The zero order curve (left-hand scale) shows modification due to phase cancellation.

By contrast, the well-known problems associated with diamond positioning, loading, and wear impose severe restrictions on ruled grating design and size for grazing incidence systems involving a single catoptric process.

This work was supported in part by the UKAEA Culham Laboratory and by the Deutsche Forschungsgemeinschaft.

References

1. D. Rudolph and G. Schmahl, Umschau in Wissenschaft und Technik **67**, 225 (1967).
2. D. Rudolph and G. Schmahl, Optik **30**, 475 (1970).
3. R. J. Speer and D. Turner, in *Proceedings of the International Symposium for Synchrotron Radiation Users* (Daresbury Nuclear Physics Laboratory Report No. 26, January 1973, Warrington, Lancashire), pp. 106–114.

Reprinted from APPLIED OPTICS, Vol. 13, page 1258, June 1974

Holographically Formed Grazing-Incidence Reflection Grating with Stigmatic Soft X-Ray Focal Isolation

R. J. Speer, D. Turner, R. L. Johnson, D. Rudolph, and G. Schmahl

The first three authors named are with the Physics Department, Imperial College, London SW7 2BZ, England; the other authors are with the Universitäts-Sternwarte, Göttingen, Germany.
Received 28 March 1974.
Sponsored by W. R. Hunter, U.S. Naval Research Laboratory.

An analysis by Haber[1] has shown that primary astigmatism in Rowland circle mountings can be corrected by a suitable choice of toroidal grating blank radii. For the grazing incidence mounting, the astigmatic line length l, for an in-plane point source at the entrance slit, is given by

$$l = L\sin\beta[(\cos^2\alpha/\sin\alpha) + (\cos^2\beta/\sin\beta)], \quad (1)$$

where L is the length of the rulings, and α and β are the angles of grazing incidence and diffraction, respectively. β is determined for a given α by the usual grating equation:

$$n\lambda = d(\cos\alpha - \cos\beta), \quad (2)$$

where d is the grating constant and n is the order of diffraction. At soft x-ray wavelengths l is normally very large, lying between 1 cm and 20 cm.

A previous communication[2] demonstrated that reflection holograms can now be constructed with lamellar (square wave) profiles at 600 lines/mm in completely metallic form (i.e., without underlying photopolymer) and with absolute diffraction efficiencies at soft x-ray wavelengths competitive with classical ruled gratings[3] of similar size and ruling frequency. The diffraction performances were measured and compared at 23 Å and 44 Å within the range of grazing incidence angles $1° < \alpha < 7°$. We refer to such reflection holograms in subsequent discussion as Type I gratings.

We have now extended this result by forming, in an analogous manner to the Type I construction, a plane reflection hologram on a toroidal substrate. We refer to this construction, in which astigmatism is corrected by substrate curvature, as a Type II grating.

If Ry is the radius of curvature of the grating in the Rowland plane, the orthonormal minor radius Rx of the toroidal substrate is determined from

$$Rx = \sin\alpha\ \sin\beta\ Ry \quad (3)$$

for stigmatism at $\beta(n\lambda_c)$, given α and d.

For our first trial of Type II gratings we have chosen $\alpha = 2°$, $\lambda_c = 44$ Å (Carbon-K), with $n = +1$ and $d = 16667$ Å (600 lines/mm). For the major radius Ry of the substrate we chose 2 m. Equation (2) yielded $\beta = 4.64°$, giving $Rx = 5.65$ mm from Eq. (3). This is a very strong curvature indeed, and a most severe test for our technique at the present state of development.

The toroidal substrate surface measured 45 mm × 8 mm after lapping, and was formed on glass blanks 45 mm × 35 mm × 10 mm to fit the Rank-Hilger E580 grazing incidence spectrograph.

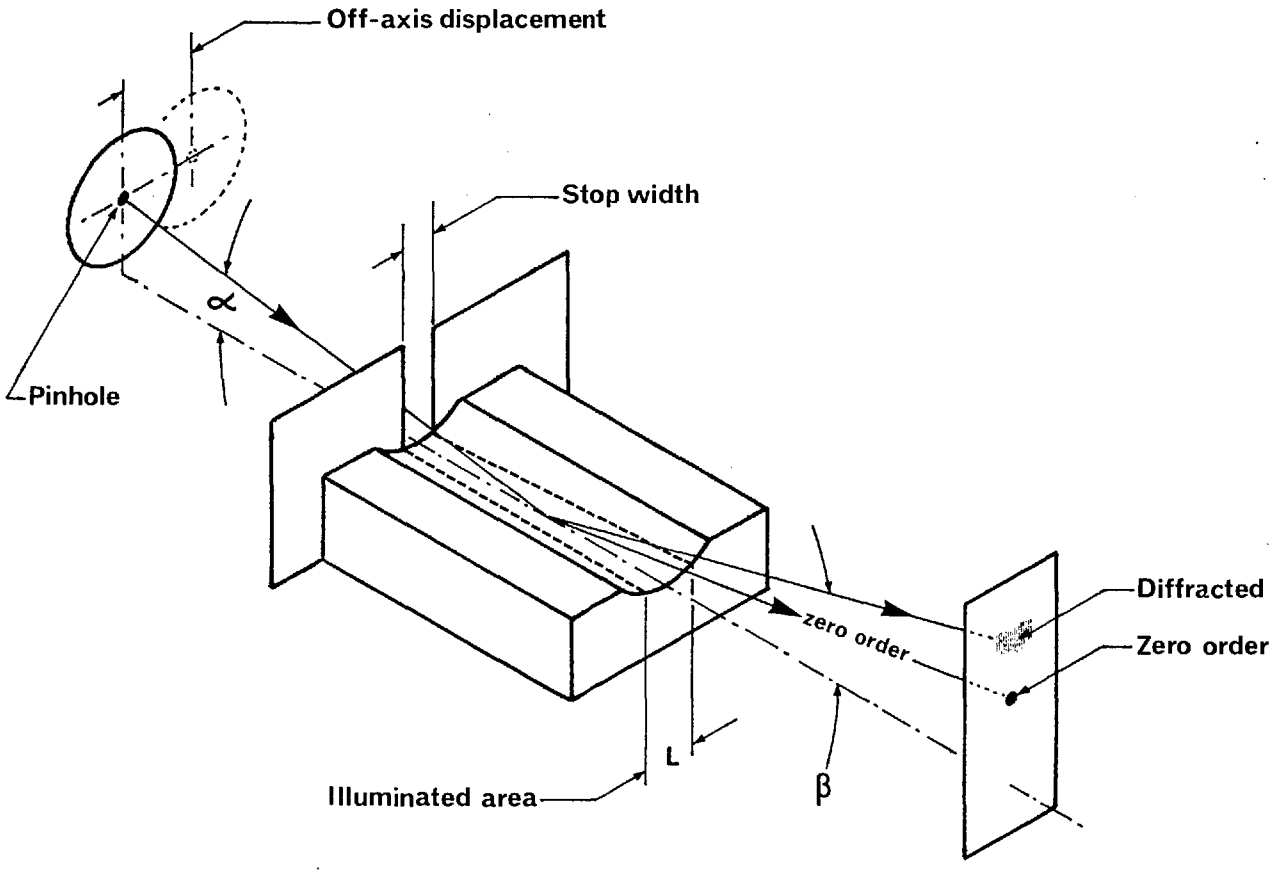

Fig. 1.
Optical arrangement for the recording of white light and x-ray images at grazing incidence.

The substrate was first examined in white light for stigmatism in the specularly reflected beam, as shown in Fig. 1. Under these conditions Eq. (3) may be rewritten:

$$\sin\alpha = (Rx/Ry)^{1/2} \text{ for } \alpha = \beta,$$

yielding $\alpha = 3°$.

The object pinhole and image plane distances from the substrate pole are given in turn by $r_o = Ry \sin\alpha = 10.5$ cm. Figure 2 shows our white light data for these conditions of illumination. The pinhole diameter is ≈ 0.1 mm. Both high aperture and off-axis aberrations are severe for such a small value of Rx, but good correction was obtained at $f/60$ in the Rowland plane with values of L less than 3 mm.

After the grating was formed on the substrate we repeated the test at the same settings, but using 44-Å radiation. The result is reproduced as Fig. 3 (upper). The left-hand image is part of the direct beam passing the edge of the grating. The image at the far right is defocused 44 Å in the first diffracted order. This can be seen stigmatized in Fig. 3 (bottom). For this exposure the illumination conditions are $r = 6.98$ cm, $r' = 16.2$ cm, and $\alpha = 2°$, dictated by the Rowland circle geometry and Eq. (3). In general we achieve stigmatism over the range of wavelengths for which $\sin\alpha \sin\beta\ (\lambda_c) = 2.82 \times 10^{-3}$. We can thus achieve the useful range 20 Å $< \lambda_c <$ 100 Å for $2.5° < \alpha < 1.5°$, despite the fact that this requires α to increase as λ_c decreases.

Figure 4 shows a sequence of images at 0 Å, 23 Å, and 44 Å. Wavelength dispersion changes in each case due to the different values of α and $Ry \sin\beta$, and the images are therefore spaced arbitrarily in the figure.

We have measured the energy returned into the first order image at 44 Å compared to the incident flux and find values lying in the range 2% to 4%. These are very similar to the values obtained with Type I gratings and show convincingly that our method of construction can yield gratings with soft x-ray diffraction performance comparable with that of shallow-blazed classical rulings—but substantially independent of blank curvature. We compute that in the case of the Type II grating described the threshold sensitivity for photographic recording is improved by a factor of ≈ 35, the ratio of the astigmatic line area (classical case) to the corrected image area measured here.

Current work is directed toward the determination of improved holographic construction parameters by tracing exact rays in the wavelength range 10 Å $< \lambda_c <$ 100 Å.

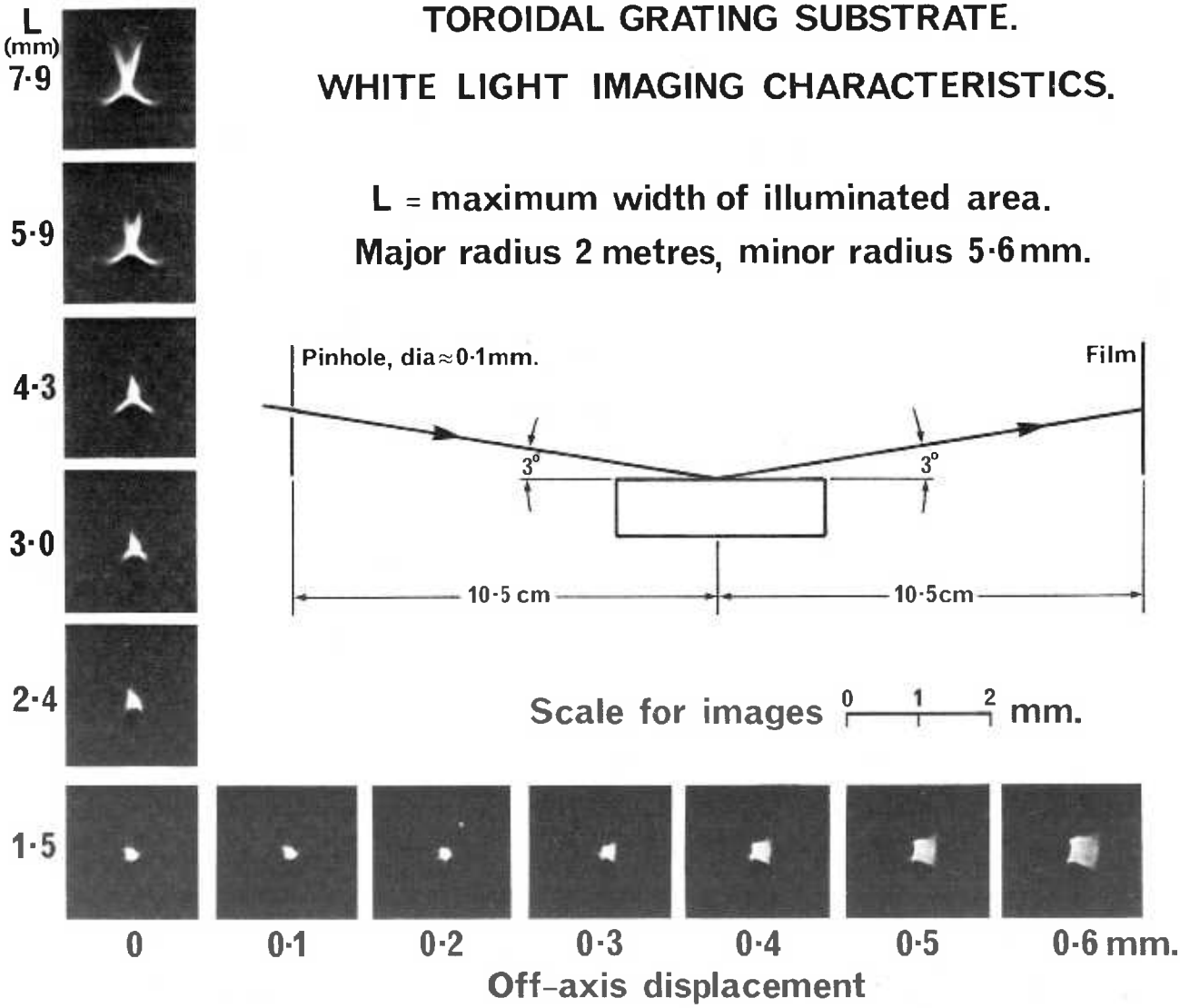

Fig. 2.
White light imaging characteristics of the toroidal grating substrate.

We wish to thank W. T. Welford and P. M. J. H. Wormell, of the Applied Optics Group, Imperial College, for helpful discussions and assistance with ray tracing.

Expert technical support was provided by P. Ruthven of Imperial College.

This work was supported in part by the U.K.A.E.A. (Culham Laboratory) and by the Deutsche Forschungsgemeinschaft. U. K. technical support was funded by the Science Research Council.

Major radius 2 metres. Minor radius 5·6mm. Lamellar profile, 600 lines per mm.

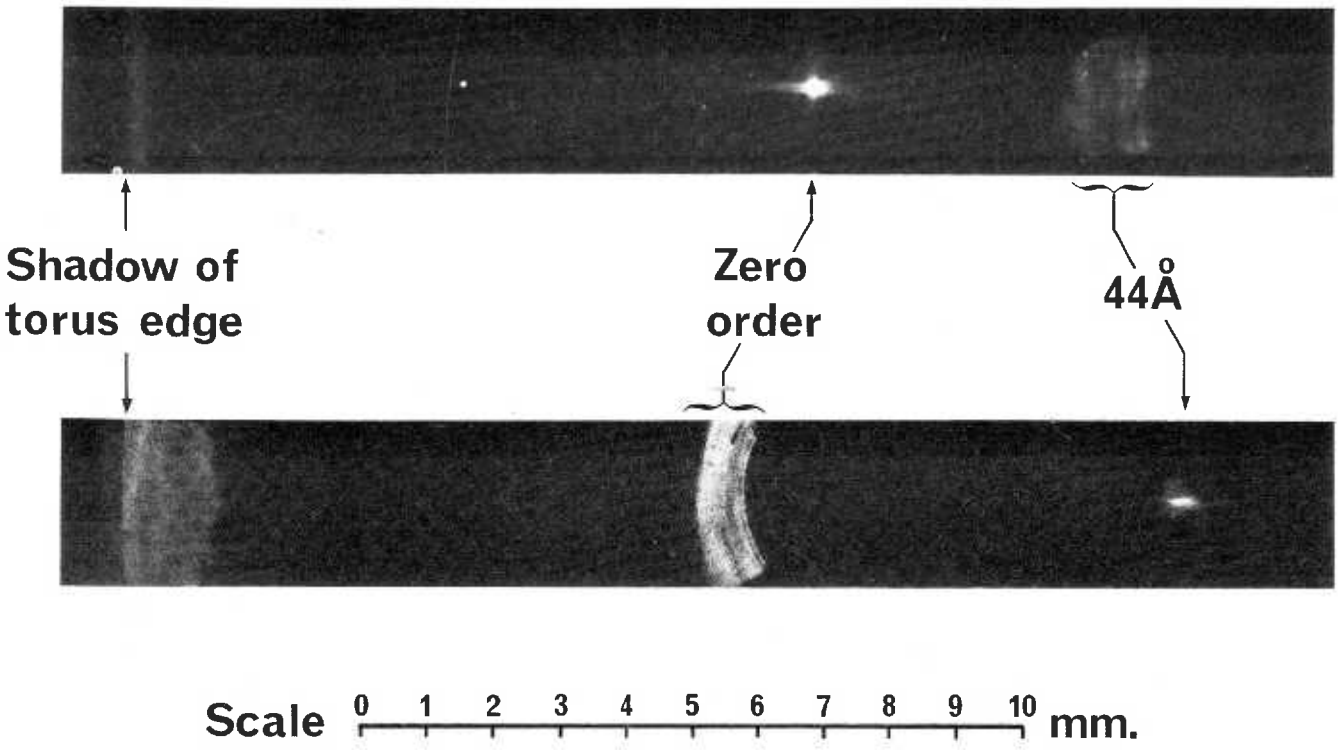

Fig. 3. 44-Å imaging characteristics of the holographically formed grating: *upper:* with zero order focused; *lower:* with first diffracted order focused.

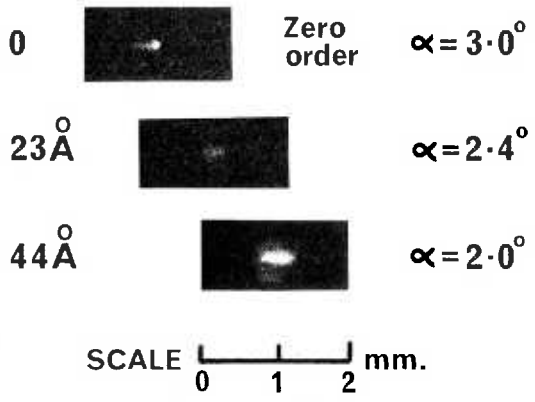

Fig. 4. Soft x-ray focal isolation in the 0–44 Å range.

References

1. H. Haber, J. Opt. Soc. Am. **40,** 153 (1950).
2. D. Rudolph, G. Schmahl, R. L. Johnson, and R. J. Speer, Appl. Opt. **12,** 1731 (1973).
3. R. J. Speer and D. Turner, *Proceedings of the International Symposium for Synchrotron Radiation Users.* Daresbury Nuclear Physics Lab. Rep. No. 26 (Warrington, Lancashire, Jan. 1973), pp. 106–114.